Sediment-hosted base metal deposits

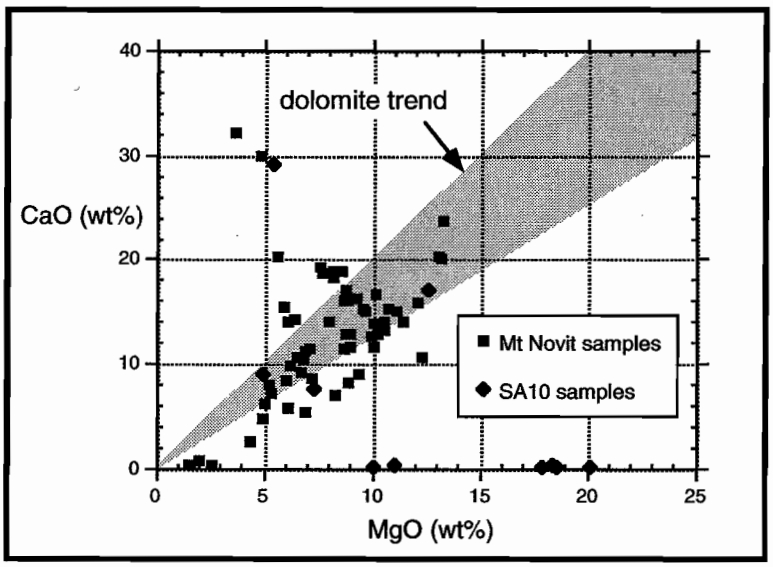

AMIRA/ARC project P384A

Report 2
October 1996

Centre for Ore Deposit and Exploration Studies
University of Tasmania

Contents

Introduction

Project Objectives

1. To determine the primary geological, geochemical and structural controls on the location and timing of base metal mineral deposits in sedimentary basins.

2. To investigate the physical and hydrological processes involved in the evolution and movement of metalliferous fluids in sedimentary basins.

3. To investigate the chemical processes controlling brine compositions and metal sulphide accumulation during fluid movements in sedimentary basins, including the relationships between copper and lead–zinc deposition.

4. To develop geological and geochemical vectors to a variety of styles of sedimentary base metal mineralisation that may be used in the exploration for large tonnage deposits.

Research Framework

This research project is a three-year extension to project P384. The project involves a multi-disciplinary approach using regional geological, geophysical and structural studies, brine chemical modelling and geochemical and isoitopic halo studies to provide a foundation on which to build a network of exploration criteria and ore deposit models for major sediment-hosted base metal deposits.

The project consists of three research modules as outlined below:

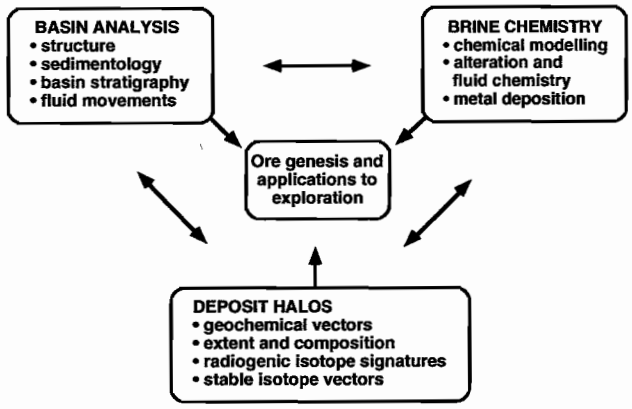

This Report

This is the second progress report for AMIRA Project P384A and covers work carried out during the six months April to October 1996 to be presented at the October meeting, and two outstanding reports from the first meeting. Good progress has been made to date and much of the material covered here results from field work undertaken earlier this year. The reports by Bull, Keele et al. and Duffett distinguish structures that controlled sedimentation on the Lawn Hill Platform during early McNamara Group times, from later (usually more obvious) structures. This early 'grain' was an important control on deformation intensity during later orogeny. Their work has implications for understanding the location of deposits that lack obvious proximal syn-sedimentary structures such as Lady Loretta and Century, and more fundamental implications for understanding the controls on basin scale fluid flow.

The halo studies work at McArthur River has been extended to drill hole Homestead 6 which is

2 km along strike from the HYC orebody. The report by Large and Bull combines this new geochemical and C/O isotope data with results from AMIRA Project P384 to complete the HYC halo model. New C/O isotope data show that C and O isotopes are a powerful method for discriminating MnO_D and AI_3 halos directly related to ore from those that indicate a favourable horizon for Pb-Zn mineralisation.

Geochemical studies of the upper greenschist to lower amphibolite grade metasedimentary hosts to the Mt Novit pyritic mineralisation are described in the report by McGoldrick. This work shows that Mt Novit has a (relatively) weak lithogeochemical vector signature (SedexAI, AI_3, MnO_D and Tl) that is preserved during moderate to high grade metamorphism.

The report by Cooke and Large documents computer modelling of Mn transport in hydrothermal fluids presented at the last meeting, and discusses implications for differences in the genesis of McArthur-type and Broken Hill-type Zn-Pb deposits.

The report by Winefield is a detailed outline of work to be included in his PhD The PhD entitled 'Sedimentology and diagenetic history of late Palaeoproterozoic sequences within the southern McArthur Basin, northern Australia" has logistic support from AMIRA Project P384A.

Also to be presented at the meeting, but not reported here, are a description of the Grevillea prospect and recent sampling for halo studies (McGoldrick and Bull). Cooke will present results of preliminary geochemical modelling of Cu and Fe in hydrothermal solutions. The sampling strategy for illite crystallinity studies of lower McNamara group rocks will be discussed by Keele. Bull and McGoldrick will discuss the outcomes from a recent visit to the Belt Basin and visits to the Sullivan mine (B.C.) and the Sheep Creek prospect in Montana and plans for halo studies on these deposits.

Peter McGoldrick
Project Manager

Sedimentology of the Torpedo Creek Quartzite in the Lady Loretta area: implications for the tectono-sedimentary setting of the Pb–Zn deposit

Stuart W. Bull

The Torpedo Creek Quartzite has been examined in the Lady Loretta region and shown to comprise some or all of three facies: basal pebble-boulder conglomerate (not always present); a lower or middle clean fine- to coarse-grained sandstone and an upper muddy grey quartz sandstone. Palaeocurrent measurements have been made from cross beds in sandstone facies at three localities, and data have a major component indicating palaeoflow to the N/NNE. This interpreted to indicate a palaeoslope inclined away from a basement source being eroded at the time of sedimentation (i.e early McNamara Group times).

The boulder conglomerate facies, interpreted as sourced from underlying Surprise Creek Formation, indicates local growth faults were active at the onset of McNamara Group sedimentation. The dominant N/NNE palaeocurrents suggest ancestral faults to the WNW to NNW structures such as the Leopard and Redie Creek Faults may have been these growth faults. The distribution of Torpedo Creek Quartzite in the area indicates a primary NNE dip direction for the growth faults, and that these structures were subsequently inverted.

The relief responsible for this facies geometry had been subdued well before Lady Loretta Formation times, and the Lady Loretta deposit occurs above the upthrown side of the early McNamara Group growth fault(s). This geometry may have been a fundamental control on mineralising fluid movements during formation of the Lady Loretta deposit. In this respect, Lady Loretta may have an analogous structural setting to the Century deposit; where the Termite Range Fault controlled lower Lawn Hill Formation sedimentation, but was no longer active during deposition of the Century host rocks (Andrews, 1996).

Possible rifting events in the Paradise Creek high strain zone, Lady Loretta region, Mount Isa

Richard A. Keele, S. Bull and M. Duffett

Recent geological and geophysical studies in the N-trending Paradise Creek High Strain Zone, north of Lady Loretta, indicate that this structure may represent a 'soft shoulder' to the underlying Haslingden rift. There is evidence for a second phase of rifting with N-facing fault scarps that formed the margin of a depocentre that lay to the north of Lady Loretta during lower McNamara times. The Lady Annie deposit is located at the intersection of these two rifts. This locus represents an ideal site for thermal anomalism, fluid flow and copper mineralisation.

Manganese transport in sedimentary brines — Chemical controls on McArthur-type and Broken Hill-type sediment-hosted Pb–Zn deposits

David R. Cooke and Ross R. Large

Based on fluid chemistry, Cooke et al. (1995) proposed two classes of stratiform sediment-hosted ("SEDEX") Pb–Zn deposits — ***McArthur-type***, which form from relatively oxidised neutral fluids, and ***Selwyn-type***, which form from reduced, acid fluids. Based on the geochemistry of manganese and on the stability of manganese minerals in equilibrium with hydrothermal solutions, a further distinction is proposed here between McArthur type and ***Broken Hill-type*** (BHT) deposits. Mn-rich BHT deposits form from relatively oxidised, acid fluids derived from dewatering of oxidised clastic, ironstone-bearing, carbonate-depleted sedimentary packages. McArthur-type SEDEX deposits form from relatively oxidised, near-neutral to alkaline fluids that are in equilibrium with thick packages of carbonates and oxidised clastic sediments.

Lithogeochemistry and isotope chemostratigraphy of the Barney Creek Formation, McArthur Basin

Ross R. Large and Stuart Bull

Lithogeochemical studies of the Barney Creek Formation at various localities in the McArthur Basin have confirmed the use of the alteration indices — sedex AI, AI_3 and MnO_D — as vectors to ore, over a distance of about 20 km. It is recommended that these three indices be used in conjunction with Zn, Pb, Tl and ankerite ratio to (a) identify distal horizons favourable for stratiform Pb–Zn mineralisation, and (b) provide vectors for follow-up drilling.

Carbon and oxygen isotope ratios of dolomitic siltstones in the Barney Creek Formation have proved to be a powerful method for discriminating MnO_D and AI_3 haloes directly related to ore, from those which indicate a favourable horizon for Pb–Zn. Anomalies in MnO_D, AI_3 and Zn, Pb associated with ore exhibit $\delta^{18}O > 23‰$ and $\delta^{13}C < -2‰$, whereas anomalies unrelated to ore (or very distal from ore) exhibit $\delta^{18}O < 23‰$ and $\delta^{13}C > -2‰$.

Preliminary research on K–Al silicate relationships in the BCF suggest that the favourable horizon close to ore has a high illite/K-feldspar ratio (i.e. illite dominant) while distal horizons display low illite/K-feldspar ratios (i.e. K-feldspar dominant). Also the barium content of potassium silicates in the HYC Pyritic Shale appears to increase towards ore.

Regional geophysics — Camooweal map sheet

Mark Duffett

Basin structures in the Camooweal region have been more strongly overprinted by Isan Orogeny deformation, particularly E–W compression, than in the previously assessed areas to the north. This has served to obscure earlier structural geometries which may carry information on basin development. However, some areas are less deformed than others. The area between the southern Mount Gordon Fault Zone and Lady Loretta is one example, with the most profound structures being in a WNW orientation, as opposed to sub-N–S to NE–SW grains developed in high strain zones to the east and west (Keele, this report). The WNW structures are considered to have developed concurrently with the basin, and are likely to have controlled sedimentation. Their preservation is evidence that this block has behaved relatively rigidly in relation to others around it. The margins to this block are apparently associated with base metal mineralisation, consistent with an association with both syn-deposition and syn-tectonic bounding structures. Palaeo-basin margins so defined are likely to have been a strong control on syngenetic and epigenetic mineralisation.

Primary dispersion halos associated with the Mount Novit Zn–Pb–Ag mineralisation

Peter McGoldrick

Gossanous ridges between 15 and 20 km south of Mt Isa are the surface expression of a pyritic interval up 25 m thick containing sporadic Zn–Pb–Ag mineralisation. The mineralised sequence is a steep west dipping, fault-bounded package of overturned lower Mount Isa Group sediments (Moondarra Siltstone) lying to the west of the Mount Isa Fault. Metamorphism has reached lower amphibolite grade and a variety of unusual rock textures are thought to reflect deformation at or near, the brittle–ductile transition.

Mineralisation is stratiform (or stratabound) disseminated to massive granular (?recrystallised) pyrite with variable amounts of sphalerite, galena, pyrrhotite and magnetite. More than 15 diamond drill holes have been drilled to test the mineralisation, with a handful of intersections exceed 10% Pb+Zn over thicknesses of more than a metre.

Three drill holes through the mineralisation at about 2 km spacing were systematically sampled to encompass the mineralised interval.

Sixty one samples were analysed for major and trace elements by XRF at the University of Tasmania and the standard set of geochemical vector parameters have been calculated. Ten samples from much lower grade (lower greenschist?) Moondarra Siltstone from diamond drill hole SA10 were also analysed.

The southernmost hole (D496) yields inconclusive results, by contrast, in drill hole F681, AI3, MnOd and Tl are anomalous for tens of metres above and below the ore positon, and in drill hole G880 for the 50 m that includes a (barren) disseminated pyrite zone correlated with mineralisation in the other two holes. None of the Mt Novit geochemical vector signatures approaches the strong response observed in samplers from the mine sequence at Mt Isa, however, patterns resemble those from other significant northern Australian deposits, suggesting the geochemical vectors are preserved during lower amphibolite grade metamorphism.

The weak geochemical vector response at Mt Novit suggests significant Zn–Pb–Ag mineralisation does not exist proximal to the known pyritic mineralisation.

Sedimentology of the Torpedo Creek Quartzite in the Lady Loretta area: implications for the tectono-sedimentary setting of the Pb–Zn deposit

Stuart W. Bull

Centre for Ore Deposit and Exploration Studies, Geology Department, University of Tasmania

Introduction

Recent sedimentological work focused around the Lady Loretta Deposit (Dunster and McConachie, in press) concludes that the host Lady Loretta Formation package in that area is indistinguishable, in terms of character and thickness, from the formation regionally. This observation apparently invalidates prior models for the setting of the Lady Loretta mineralisation, that have proposed a genetic link with the development of a local basinal feature, termed the "Paradise Creek Graben" (Dunnet, 1976), for which various orientations and scales have been proposed (e.g. Large, 1980; Amade, 1986; Lemcke, 1986). Structures interpreted as syn-sedimentary growth faults active during the basin-forming event (e.g. the Carlton Fault; Large, 1980) were envisaged to have been the conduits for mineralising fluids.

In the absence of evidence for syn-sedimentary growth faulting and graben formation during the accumulation of the Lady Loretta Formation, the problem arises as to what were the conduits for the mineralising fluid, which appears to have been introduced to the "trap" sedimentary package during a time of relative tectonic quiescence. In order to address this important question this study was initiated, in conjunction with a detailed structural analysis (Keele, this report), to examine the setting of the Lady Loretta mineralisation in the broader context of its position within the lower McNamara Group package. The basal unit of the McNamara Group, the Torpedo Creek Quartzite, was chosen for initial sedimentological examination because previous studies (eg. of the basal unit of the McArthur Group in the McArthur Basin, the Masterton Sandstone; Bull, 1993), have shown the potential of these basal sandstone units to record the initial tectonic regime of the basin phase in which they occur. Specifically, facies and palaeocurrent data from these clastic units have proved critical in determining which faults were active during sedimentation, because the sedimentary features are preserved even when the original structural and stratigraphic framework has been extensively modified by subsequent tectonic events.

Sedimentology of the Torpedo Creek Quartzite in the Lady Loretta Region

In the Lady Loretta region, the Torpedo Creek Quartzite crops out in four discrete localities to the north of the deposit (Hutton et al., 1985). In each case, the unit occurs as a thin but laterally persistent selvedge adjacent to the northern and/or western edge of blocks of the older Surprise Creek Formation. Three of the four occurrences define anticlinal folds in the Surprise Creek Formation blocks which have north-trending, northerly plunging fold axes (Fig. 1).

Sedimentological examination indicates that the Torpedo Creek Quartzite interval in the Lady Loretta area, which varies in thickness from < 10 m to several tens of metres, can be considered in terms of three constituent facies:

1. A predominantly basal ***pebble–boulder conglomerate*** is not always present but in places reaches a thickness of > 10 m. Clasts are well- to sub-rounded quartz sandstone and are variable in shape from spherical to tabular, however, the largest clasts, which have long axes of > 3 m, are all tabular in shape. In places the sandstone clasts have a distinctive pale pink colour identical to that of the

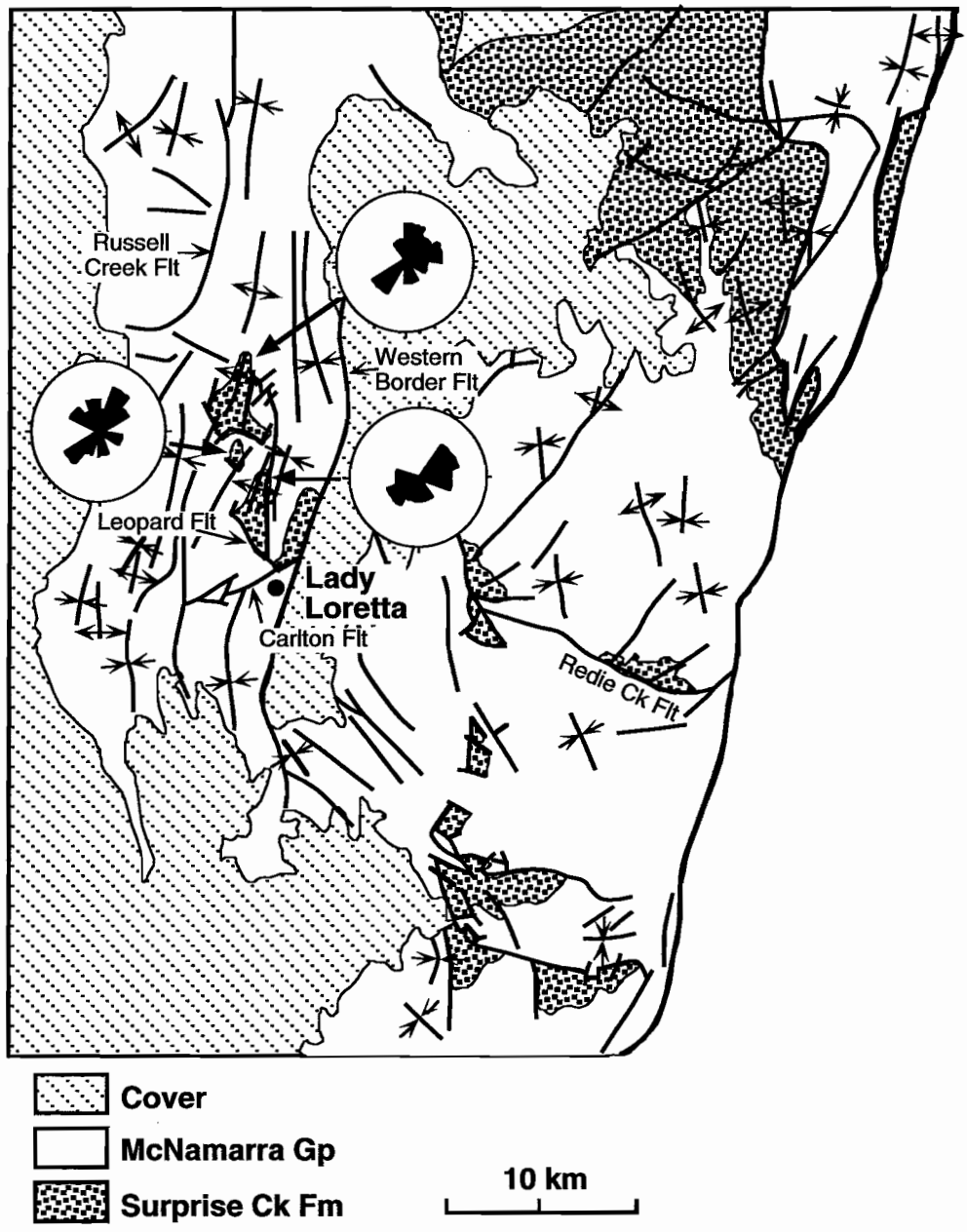

Figure 1 Palaeocurrent data from the sandstone facies of the Torpedo Creek Quartzite north of Lady Loretta. Geology modified after Hutton et al. (1985).

underlying Surprise Creek Formation sandstone. The matrix to the sandstone clasts is a variably muddy medium- to coarse-grained sandstone.

2. A well sorted ***clean fine- to coarse-grained quartz sandstone*** forms the lower to middle part of the unit in all sections. It is up to 20 m thick, is medium- to thinly-bedded, and the predominant sedimentary structures present are planar lamination and small- to medium-scale cross bed sets.
3. A thinly-bedded ***muddy (grey) quartz sandstone*** forms the upper few metres of the Torpedo Creek Quartzite. It has similar sedimentary structures to the underlying well-sorted sandstone, but, in addition, has abundant large symmetrical ripples in some exposures.

In terms of sedimentary environments, the basal Torpedo Creek Quartzite conglomerates are interpreted as debris flows and/or alluvial channel deposits that represent the onset of McNamara Group deposition. The coarse-grained and poorly-sorted nature of these deposits indicates that the McNamara Group depositional cycle was initiated by a relief-forming tectonic event. Their lateral restriction indicates that they accumulated either in erosive channels or as fans sourced from uplifted blocks of Surprise Creek Formation "basement". High-energy (i.e. braided) fluvial systems would have emanated from the toe areas of channels/fans, and as initial relief was subdued by erosion, the clean quartz sandstone facies interpreted to represent these systems became predominant. The uppermost muddy quartz sandstone facies is interpreted to represent the onset of the transgressional event that marks the transition to the Gunpowder Creek Formation throughout the region (Bull, 1996).

Palaeocurrent data were collected from cross-bedding in the sandstone facies of the Torpedo Creek Quartzite at three localities to assist a structural analysis of the area (see below). Unfolded data from the central and northern localities has a major component indicating palaeoflow to the N/NNE (Fig. 1). This is interpreted to represent the major palaeoslope inclined away from a basement source that was being actively eroded at the time of sedimentation. A minor component, recorded mainly in the muddy sandstones that comprise the upper part of the Torpedo Creek Quartzite, indicates palaeoflow to the SW (Fig. 1). This is interpreted to represent onshore palaeoflow (? wave activity) during the onset of the major transgressive event. Additional evidence of wave activity at this level is provided by the symmetrical ripples that occur in this facies. Unfolded data from the southern locality has an equant bimodal pattern indicating palaeoflow to the NE and SW (Fig. 1). The relative strength of the SW (i.e. onshore) component in this case is interpreted to indicate that at the time of deposition, the locality was at a position peripheral to the axis of the main palaeoslope (i.e. in between fan lobes or major channels).

Structural implications of the Torpedo Creek Quartzite sedimentology

Growth fault activity accompanying the onset of McNamara Group sedimentation has previously been proposed by the author, based on facies pattern and thickness changes in drill core intersections from the southern flanks of Kamarga Dome (Bull, 1996). The occurrence of boulder conglomerates, apparently sourced by erosion of the underlying Surprise Creek Formation at the base of the Torpedo Creek Quartzite in the Lady Loretta area is taken as further evidence of growth fault activity at this stratigraphic level. Studies of active graben systems (e.g. Lake Tanganyika; Tiercelin et al., 1992) indicate that such coarse-grained deposits accumulate as clastic wedges, in this case fan-deltas, in piedmont positions on the subsiding hanging wall block immediately adjacent to the border (i.e. growth) fault scarp. Although no data is available from Lake Tanganyika, palaeoflow in the proximal parts of these fan systems would clearly be aligned strongly away from the fault scarp in the elevated footwall block.

In the Lady Loretta area, there are two sets of faults that could be implicated as the syn-depositional structures that controlled Torpedo Creek Quartzite deposition. The most prominent set on 1:100,000 scale geological map patterns trend approximately NNE (e.g. the Western Border and Russell Creek Faults

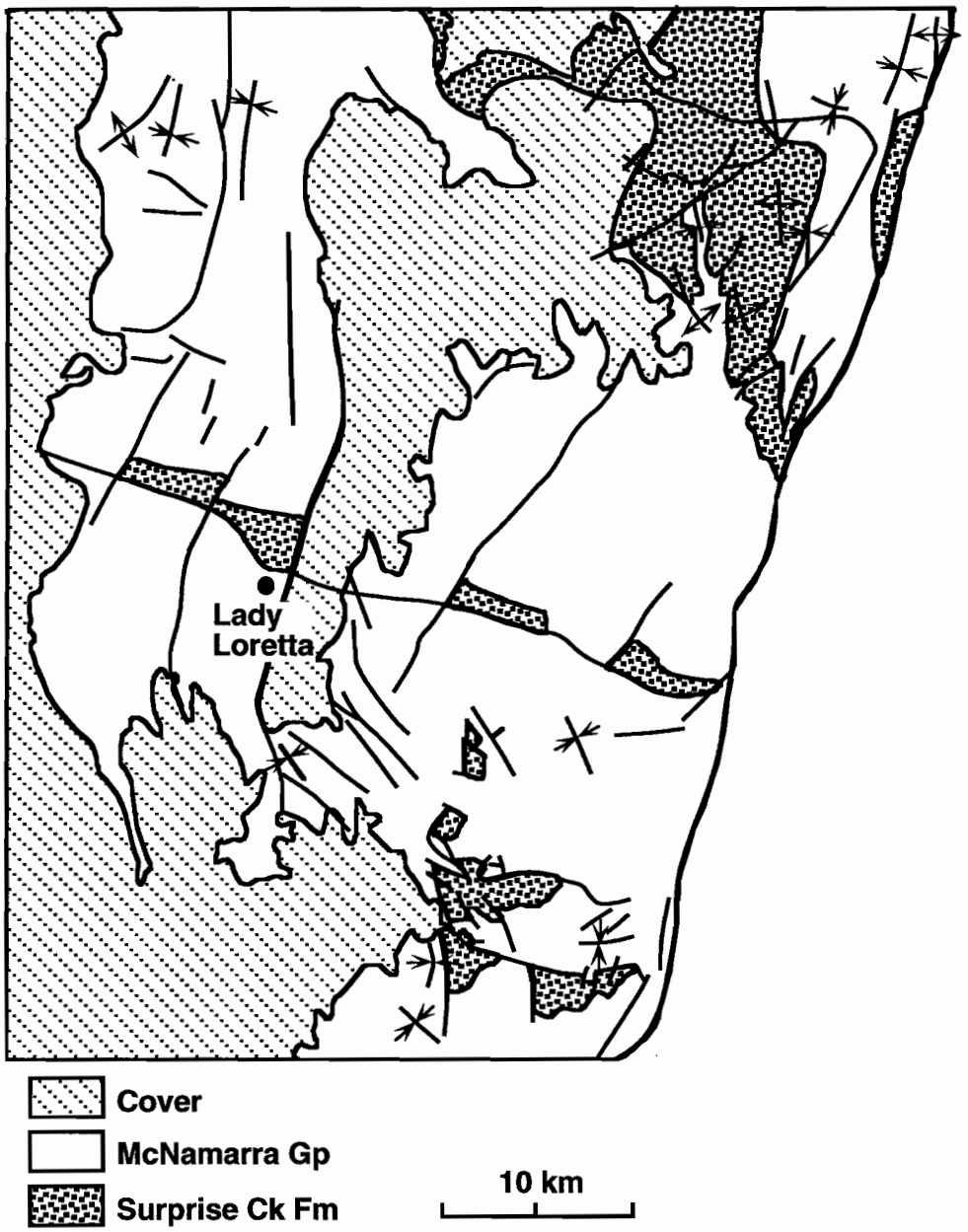

Figure 2 Schematic representation of the structural setting of the Lady Loretta Deposit inferred from a sedimentological analysis of the Torpedo Creek Quartzite .

and parallel unnamed structures in between; Fig. 1). Dips on these structures are poorly constrained, however, data from the Russell Creek Fault indicate that it has operated as a west-side-down normal fault at some point in its history (Keele, this report). A less obvious set of structures trend WNW to NNW (e.g. the Leopard Fault). These faults bound the southern margins of the four en-echelon Surprise Creek Formation blocks (Fig. 1) and surface measurements indicate dips steeply to the south (Keele, this report). Although individual faults in this orientation are partitioned by offset on the more prominent NNE trending structures in the Lady Loretta area, they are parallel to the well developed Redie Creek Fault 20 km along strike to the southeast (Fig. 1, see also Keele, 1994; Fig. 2).

The unfolded palaeocurrent data from the sandstone facies of the Torpedo Creek Quartzite has a major component indicating palaeoflow to the N/NNE at two of the three localities examined. This suggests that the NW-trending structures were N-dipping growth faults at the onset of McNamara Group sedimentation. This accords well with a geophysical interpretation that the Redie Creek Fault dips to the north in the subsurface (Duffet, this report). However, it is somewhat at odds with surface data from both the Leopard and Redie Creek Faults that indicate steep southerly dips (Keele, this report). A possible explanation is that the present day surface dip is the result of post-depositional effects of the Isan Orogeny, which produced relatively intense deformation in the Lady Loretta area as evidenced by the amount of folding present.

Discussion

The geology of the Lady Loretta area has been modified to schematically represent the proposed structural configuration for early McNamara Group times inferred from a sedimentological analysis of the Torpedo Creek Quartzite (Fig. 2). The main point to emphasise is that the Redie Creek Fault trend extended northwest of its present position through the Lady Loretta area, operating as a NNE dipping growth fault that controlled initial sedimentation. The fact that the Torpedo Creek Quartzite is not currently exposed adjacent to the proposed growth faults, but occurs on the northern side of the Surprise Creek Formation blocks, suggests that these structures were subsequently inverted (ie. reactivated as reverse faults).

There is no positive sedimentological evidence that the NNE trending faults present in the area today existed at McNamara Group times as shown, or structural evidence that they were strike slip faults early in their history. However, if this had been the case they could have acted as transfer structures to the NW trending growth faults (Keele, this report). This is an appealing model for two reasons; firstly, given that areas of growth and transfer fault intersections are widely recognised as important sites of hydrothermal activity in modern extensional settings (e.g. Lake Tanganyika; Tiercelin et al., 1992), it could help explain the presence of the Lady Loretta mineralisation; and secondly, if the NNE trending transfer structures were of the right orientation to be extensively re-activated in the Isan Orogeny, their presence could explain the degree of Isan deformation, both folding and faulting, in the Lady Loretta area. This is sufficient to mask the Redie Creek Fault trend in the Lady Loretta area on present day map patterns, even though it is clear in the Redie Creek area to the southeast where there are fewer and smaller scale NNE trending structures. A clear implication of this suggestion is that other areas of comparable McNamara Group structural complexity in the region host the same style of base metal mineralisation.

Drillcore-based studies of the lower McNamara Group in the Kamarga area have indicated that, there at least, the relief generated by the tectonic activity that initiated this depositional cycle was suppressed fairly rapidly (ie. by middle Gunpowder Creek Formation times; Bull, 1996). Poor outcrop of the relevant McNamara Group units precludes an analysis of this kind in the Lady Loretta area, however, the recent proposal of Dunster and McConachie (in press) that there is no evidence of syn-sedimentary structural activity in the Lady Loretta Formation clearly indicates that any tectonically generated relief had been infilled by that time.

In the light of the discussion above, several important points can now be made with regard to the tectono-stratigraphic setting of the Lady Loretta mineralisation:

1. It lies close to a pre-existing growth fault, the main phase of activity of which was over by the time of the deposition of the host sedimentary package.
2. It occurs in an area where the growth fault may have been cut by several relatively closely spaced transfer faults.
3. It is situated over the footwall (ie. relatively uplifted) block, not the hanging wall (i.e. relatively subsided) block.

In some respects, the tectono-stratigraphic position of the Lady Loretta deposit resembles that of the Century mineralisation. Recently published work by Andrews (1996) indicates that although the major NW trending structure adjacent to Century, the Termite Range Fault, did not control deposition of the host sedimentary package (member H4; Fig. 3) , it was a growth fault during the accumulation of the lower members of the Lawn Hill Formation. In fact, the structure has had a long and complex history of syn-sedimentary activity, including operating as a growth fault with the opposite sense of polarity during deposition of the older Riversleigh Siltstone (Andrews, 1996; Fig. 3). The position of the Century deposit adjacent to a growth fault in the subsurface is similar to that proposed for the Lady Loretta deposit. An addition similarity between the two deposit settings, is that published mapping clearly indicates that the Termite Range Fault is cut by several roughly orthogonal structures (?transfers) in the area of the Century mineralisation.

The apparent broad similarities between the tectono-sedimentary settings of the Lady Loretta and

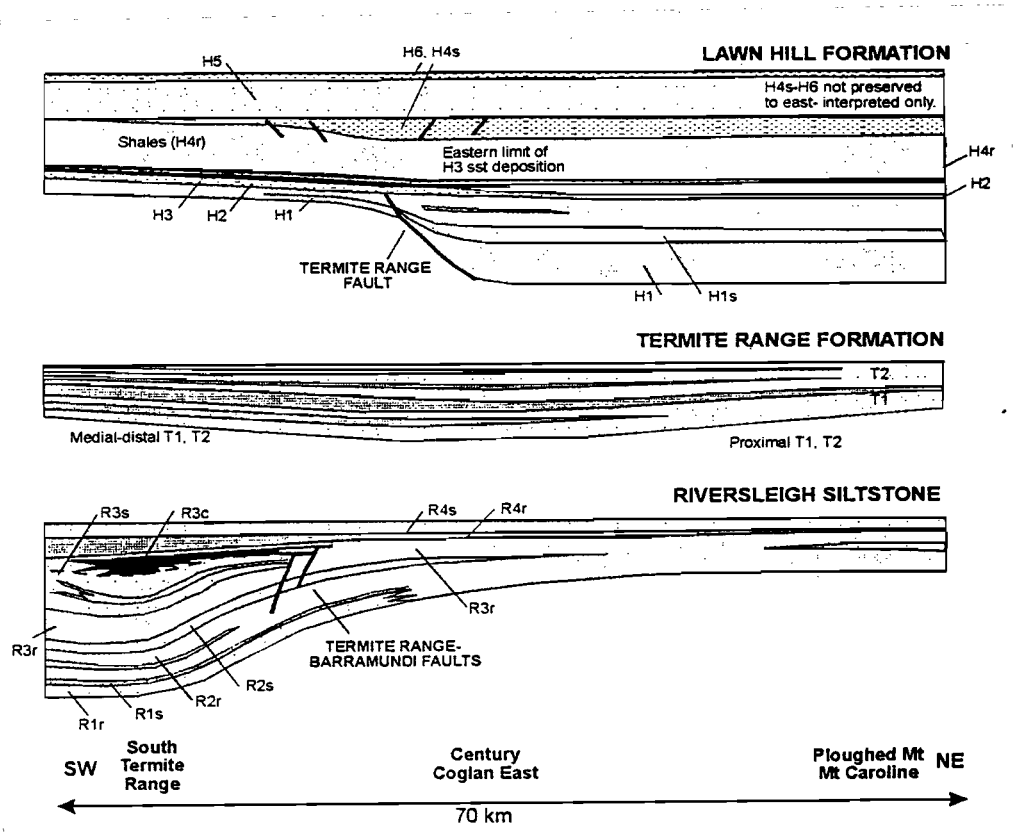

Figure 3 Interpretive cross sections of Upper McNamara Group, Lawn Hill Region (after Andrews, 1996). Note that the Century Deposits is situated in member H4 above the Termite Range Fault.

Century deposits have implications for genetic models for base-metal mineralisation. The relationship between growth and transfer fault intersections and hydrothermal activity and base metal mineralisation has long been recognised. In some cases, for example the HYC deposit in the McArthur Basin, the faults associated with the mineralising event were clearly syn-sedimentary, as evidenced in this case by the abundant inter-ore mass-flow breccias (Large et al., 1996). However, it is apparent from the Lady Loretta and Century deposit settings, that growth faults in the subsurface that were active prior to the deposition of the host stratigraphy for mineralisation can also introduce metal-bearing fluids into the "trap" environment. They may do this via minor faults and/or fracture systems developed above the subsurface growth faults in response to sediment loading during accumulation of the host sedimentary package. Such conduits could be quite subtle and difficult to recognise in mineralised Proterozoic successions, however, possible evidence of this type of activity could include the presence fluid escape pipes or fluidisation breccias, both of which have been described from the Lady Loretta ore zone (McGoldrick, 1993).

A further interesting speculation on genetic models concerns the position of mineralisation with respect to the growth fault (Fig. 4). In the case of the HYC deposit, for which one current model invokes an essentially syn-genetic timing for the mineralisation (Large et al., 1996), the base metals sit at some distance from the syn-sedimentary faults, in the deepest portion of a rapidly subsiding basin. This position accords well with the genetic model in this case, since exhaled dense brine pulses would naturally have ponded in the available topographic depression.

In the case of the Century deposit, however, the mineralisation sits essentially on top of the proposed growth structure, the Termite Range Fault, which affected the units below the host package. It would be difficult to reconcile this position with a syn-genetic exhalative model for the mineralisation because, on the scale of the Andrews (1996) diagram at least, there is no topographic depression in this position to trap exhaled dense brines. However, this limitation does not apply to the current model for the Century mineralisation (Broadbent et al., 1996), which advocates subsurface emplacement of metal into a petroleum reservoir. In fact, the area above a growth fault in the subsurface is a recognised site for the development of fold structures in overlying sedimentary packages during basin inversion. Metal-bearing fluids mobilised during a basin inversion event could use the subsurface fault as conduit into any resultant anticlinal petroleum trap.

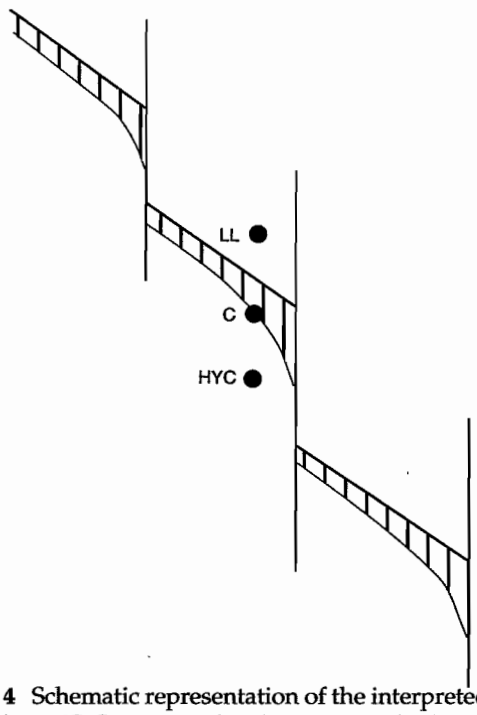

Figure 4 Schematic representation of the interpreted position of the HYC, Century and Lady Loretta orebodies relative to an inferred growth/transfer fault network. Note that the structures are syn-sedimentary with respect to the HYC host package, but in the subsurface with respect to the host packages for the two latter deposits.

Exploration implications of the above discussion are, that where a syn-sedimentary growth fault exists:

1. A syn-genetic model for mineralisation is appropriate where suitable "trap" rocks were accumulating during growth fault activity (e.g. at HYC). In this case, a topographic depression is required to facilitate ponding of exhaled metal-bearing brines. As a result the long envisaged the third order/sub-basin targets that will occur on the downthrown side of the growth fault remain relevant.

2. Given the existence of suitable "trap" lithologies, the adjacent sedimentary package is prospective well above the stratigraphic level/s at which the growth fault was active. An epigenetic model may be more appropriate, in which case the "trap" site for base metal mineralisation need not be restricted to the downthrown side of the associated growth fault.

Conclusions

Sedimentological analysis of the Torpedo Creek Quartzite in the Lady Loretta area indicates that:

1. Although there is no evidence of syn-sedimentary faulting in the Lady Loretta Formation itself, the mineralisation hosted in the unit sits adjacent to a growth fault in the subsurface
2. This structure was a northwestern continuation of the Redie Creek Fault trend, which was active during the onset of McNamara Group deposition as a NE dipping growth fault.
3. The growth fault may have been offset by a number of relatively closely spaced, NNE-trending transfer faults subsequently re-activated during the Isan Orogeny to produce the present day structural complexity of the Lady Loretta area. If this was the case, other areas of equivalent structural complexity on the Lawn Hill Platform may be prospective for base metal mineralisation.
4. The setting of the Lady Loretta and Century Deposits indicates that, given the presence of appropriate reduced "trap" lithologies, the sedimentary packages adjacent to demonstrated syn-sedimentary growth faults are prospective well above the stratigraphic level/s at which the fault was active, on both sides of the structure.

References

Amade, E. 1986. Le gisement exhalatif-sedimentaire de Zn–Pb–Ag de Lady Loretta (Queensland, Australie). *Chronique de la Recherche Miniere* 54/483: 41–63.

Andrews, S. 1996. Stratigraphy and depositional setting of the Upper McNamara Group, Lawn Hill Region. MIC 96 Extended Abstracts, New Developments in Metallogenic Research: The McArthur–Mount Isa–Cloncurry Minerals Province. *EGRU Contribution* 55: 5–9.

Broadbent, G. C., Myers, R. E. and Wright, J. V., 1996. Geology and origin of shale-hosted Zn–Pb–Ag mineralisation at the Century Mine, Northwest Queensland. MIC 96 Extended Abstracts, New Developments in Metallogenic Research: The McArthur–Mount Isa–Cloncurry Minerals Province. *EGRU Contribution* 55: 24–27.

Bull, S. W. 1993. Progress report – Sedimentology and volcanology of the Southern McArthur Basin. AMIRA/ARC Project P. 384, Proterozoic sediment-hosted base metal deposits. Report 4: 33–53.

Bull, S. W. 1996. Progress Report: Sedimentology of the lower McNamara Group, Riversleigh Fold Zone northwestern Queensland. AMIRA/ARC Project P384A, Proterozoic sediment-hosted base metal deposits. Report 1: 1–10.

Duffet, m. This report.

Dunnet, D. 1976. Some aspects of the Panantarctic cratonic margin in Australia. *Philosophical Transactions of the Royal Society* A280: 641–654.

Dunster, J. N. and McConachie B. A., in press. The tectono-sedimentary setting of the Lady Loretta Formation – syn-rift, sag or passive margin?

Hutton, L., Derrick, I. P. and Gallagher, J. 1985. Australia 1:100,000 Geological Special. *GEOLOGY OF THE MAMMOTH MINES REGION, First Edition.*

Keele, R. A. 1994. A preliminary structural analysis of the Riversleigh Fold Belt (formerly Lawn Hill Platform) with special reference to the structures around the Lady Loretta Deposit. AMIRA/ARC Project P. 384, Proterozoic sediment-hosted base metal deposits. Report 7: 37–44.

Keele, R. A. This report.

Large, D. E. 1980. Geological parameters associated with sediment-hosted exhalative Pb–Zn deposits: an empirical model for mineral exploration. *Geologisches Jahrbuch* D 40: 59–129.

Large, R. R. L., Bull, S. W., Cooke, D. C. and McGoldrick, P. 1996. Review of genetic models from the HYC deposits: constraints from sedimentology, alteration halo and fluid chemical modelling. MIC 96 Extended Abstracts, New Developments in Metallogenic Research: The McArthur–Mount Isa–Cloncurry Minerals Province. *EGRU Contribution* 55: 72–74.

Lemcke, D. 1986. Pancontinental–Outokumpu Exploration JV, Lady Loretta area — the Big Syncline: a reappraisal. Unpubl. internal company report.

McGoldrick, P. 1993. Geology of the Lady Loretta Deposit: review, new developments and implications for ore genesis. AMIRA/ARC Project P. 384, Proterozoic sediment-hosted base metal deposits. Report 3: 1–23.

Tiercelin, J-J., Soreghan, M., Cohen, A. S., Lezzar, K-E. and Bourullec, J-L., 1992. Sedimentation in large rift lakes: example from the Middle Pleistocene — modern deposits of the Tanganyika Trough, East African Rift System. *Bulletin, Centre de Recherche Exploration Production Elf Aquitaine* 16(1): 83–111.

Possible rifting events in the Paradise Creek high strain zone, Lady Loretta region, Mount Isa

by Richard A. Keele, S. Bull and M. Duffett
Centre for Ore Deposit and Exploration Studies, Geology Department, University of Tasmania

Summary

Recent geological and geophysical studies in the N-trending Paradise Creek High Strain Zone, north of Lady Loretta, indicate that this structure may represent a 'soft shoulder' to the underlying Haslingden rift. There is evidence for a second phase of rifting with N-facing fault scarps that formed the margin of a depocentre that lay to the north of Lady Loretta during lower McNamara times. The Lady Annie deposit is located at the intersection of these two rifts. This locus represents an ideal site for thermal anomalism, fluid flow and copper mineralisation.

Introduction

Early studies of the Mount Isa Inlier by Dunnet (1976) raised the possibility that the rifting in the Western Fold Belt followed the trend of the WNW-trending Redie Creek Fault system. Dunnet called this particular rift the Paradise graben. This report presents data, including some recent geophysical interpretations by M. Duffet (pers. comm., 1996), which suggests that the N-trending Paradise Creek High Strain Zone may also have been a rift. The fact that the Lady Loretta Zn–Pb and Lady Annie Cu deposits lie at the intersection of the Paradise Creek High Strain Zone (HSZ) and the Paradise rift, begs the question — are the ore occurrences related to these major crustal features in some way?

In a preliminary analysis of part of the Riversleigh Fold Belt, a number of important structures were described (Keele, 1994):

1. The N-trending Lady Loretta high strain zone
2. A WNW-trending structural culmination that transects the Redie Creek Platform and the HSZ; this is defined principally by a change in the plunge of F2 structures
3. An ENE-trending mega shear/kink band.

In this report the Lady Loretta high strain zone is called the Paradise Creek High Strain Zone (HSZ). Studies during the past field season have shown that the second of these structure may be related to a basement high that shed sediment to the north during Torpedo Creek Quartzite times (S. Bull, this volume). Rifting mechanisms lead the author to believe that both the second and third sets of structures may have started life as conjugate accommodation zones developed at the time of the underlying Haslingden rift.

The aims of this study were two-fold:

1. To draw a series of cross-sections and a long section through the HSZ in order to understand the nature of this structure better; the long section was considered crucial in establishing whether the Redie Creek Fault system was a syn-depositional fault active during early McNamara times. It was intended that any N–S section would eventually tie in with the Fiery Creek and Kamarga Domes to the north. To extend the section now would require more field work, as well as a significant geophysical input, neither of which was currently available.
2. To study the regional structural controls to copper mineralisation.

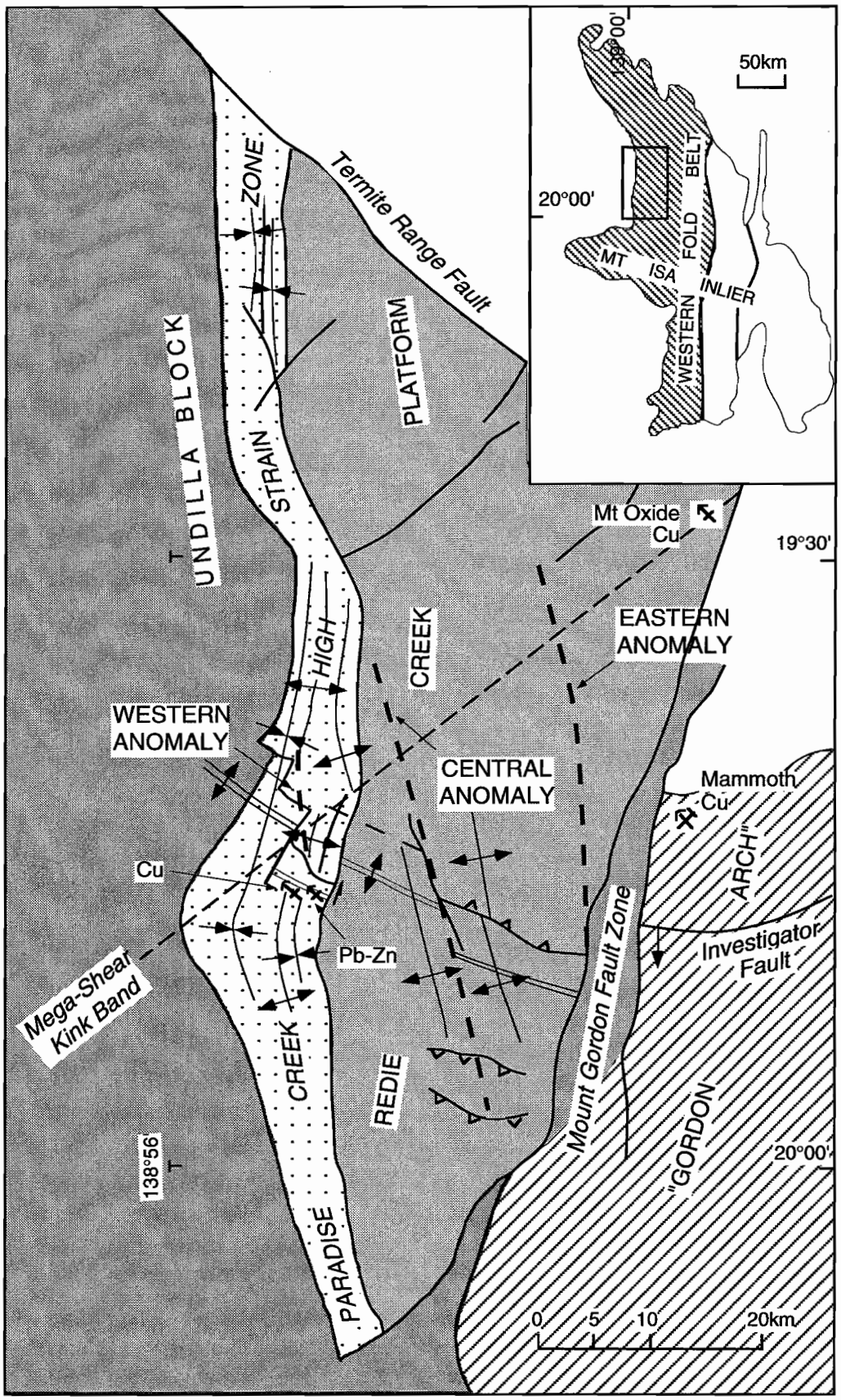

Figure 1 Simplified geological plan of the Lady Loretta region showing main tectonic elements.

Regional structural setting

The Paradise Creek High Strain Zone is a structure that accommodated much of the crustal shortening in the Western Fold Belt during the Isan Orogeny. The effects of the Isan Orogeny (Blake and Stewart, 1992) were for a long time believed to have extended only as far as the Mount Gordon Fault Zone, which is situated some 35 km east of Lady Loretta (Hutton and Wilson, 1984, 1985). The crustal shortening associated with the HSZ (estimated to be approximately 25–30%,) has been transferred away from the Loretta region by movements on the Termite Range Fault. The most likely continuation of the high strains to the north is a region lying between the Kamarga and Fiery Creek Domes (J. Dunster, pers. comm., 1995). E-directed thrusts are present along the Western Border Fault to the north of Loretta (Merrin Jones, Monash University) indicating that eastern side is the 'live' edge to the high strain zone and that some inversion had been taken place. Extensions to the Lady Loretta Ore horizon on the eastern side of the Western Border Fault (Dunster, in prep.) indicates sinistral strike slip movements on the Western Border Fault. The southern termination to the high strain zone is poorly defined due to lack of exposure, however, it appears not to extend south of the Mount Gordon Fault Zone.

Aspects of recent geophysical studies by Duffet (1996) have been integrated with the geological data to take into account the structure of the underlying rift sequence. The results suggest that there may be an early N-trending grain related to a buried volcanic pile.

Studies around the Lady Loretta mine (Hancock and Purvis, 1990) focussed on the significance of the Carlton Fault as a growth fault. This fault, these authors suggested, acted as a fluid conduit for Pb–Zn mineralising fluids. They also recognised a number of fold phases in the vicinity of the Little and Big Synclines that included small-scale F3 folds that cut across the Little Syncline. Keele and Beeson (1994) re-interpreted the Placer/CEC maps and suggested that the plunge reversals in F2 folds were largely due to the presence of early F1 folds that trend in a WNW to WSW direction through the district, recognising at the same time that there were late folds. These authors also recognised an early throughgoing structure — called the "Denmead Suture" after the first geologist to map the Lady Loretta area (Denmead, 1938) — that appears to have a spatial relationship to copper occurrences.

Paradise Creek high strain zone

The Paradise Creek High Strain Zone (formerly the Paradise Creek Graben) is 120 km long by 10–15 km wide and lies along the western flanks of the Western Fold Belt (Fig. 1). It represents a zone of folding, shearing and faulting. The folds are open to close in style and bed dips are generally greater than 30°. In contrast, the less deformed Undilla and Redie Creek Platforms have gentle folds and dips are generally less than 15°.

The Paradise Creek HSZ contains relatively straight forward structures. Major synclines may be traced along the eastern and western sides of the Surprise Creek blocks giving a central fault-bounded anticlinal uplift (horst) with two flanking synclines. Only at its very widest, at the prominent bend in the HSZ, does a second anticline–syncline pair occur to the west (Fig. 1). These relatively simple relationships can be seen in the 1:25,000 map (Fig. 2) and a series cross-sections (A–A', B–B', C–C' D–D' and E–E', Fig. 3).

At a local scale, the characteristic grain and texture of the HSZ is determined by the interplay between ductile and brittle processes. For example, folds, cleavage and shear zones in the siltstones and fine grained dolomitic rocks of the Gunpowder and Paradise Creek Formations wrap around the central rigid blocks of Surprise Creek and Torpedo Creek Formations. Locally, a strong, sub-vertical penetrative cleavage is developed in the siltstones (Figs 5e and 7). In contrast, the rigid sandstones of the TCQ and Surprise Creek Sandstones behaved brittlely during the deformation and have preserved evidence of considerable faulting (Fig. 8). Some faults were clearly re-activated (Fig. 5d). The Redie Creek Platform is different in that no upright penetrative cleavage developed in the fine grained lithologies.

Folding

The folding is open to close in style with inter limb angles varying from 130 to 65° (Fig. 3). The folds on the eastern side of the HSZ are tighter than those on the western side, indicating that the push had been from the east. The folds are classified as close in the high strain domains around Lady Loretta (inter-limb angles of 50° in Lady Loretta Formation). In contrast, the folds are classified as open at the western ends of sections A–A′ and B–B′ (inter-limb angles of 80° in Paradise Creek Formation). This tightness of folds in Lady Loretta Formation is generally maintained along the eastern side of the zone, e.g. the Day View Syncline. From N to S there is also a decrease in inter-limb angle from 140° to 95° in lower McNamara units (Torpedo Creek Quartzite and Gunpowder Formation). This reflects an increase in strain from north to south.

Poles to bedding define a shallow N-plunging fold axis (18/010) (Fig. 7). In contrast, the fold axes and bedding–cleavage intersections give both N- and S-plunging axes. The majority of data points, however, indicate a plunging axis that parallels the pi-pole axis (26/004), with the remainder forming a weak scatter that includes both shallow S-plunges and steep subvertical plunges. Two explanations for this may be suggested. Firstly, the small-scale structures are more susceptible to rotation during shearing: indeed, many of the steep fold plunges come from the Barite Shear Zone where bedding-cleavage intersections are also steep and strike slip movement is inferred (see Fig. 6). Secondly, it is conceivable that the two data sets are biasing different parts of the regional culmination, ie. bedding poles were taken exclusively from the northern side of this regional axis, whilst the small-scale structures included data from the other side of the regional culmination. In fact within the central region of the uplift, S-plunging folds do occur south of the Goat Fault, suggesting that the culmination axis is not a simple structure.

Fault blocks

The regional structure north of Lady Loretta is dominated by a series of uplifted *en-echelon* blocks of Surprise Creek Sandstone (Fig. 2). These blocks stretch over a distance of 12 km and are caused by a combination of folding and faulting; they had their origins near the start of Cover Sequence 4 — the recently re-defined Surprise Creek Formation–McNamara Group sag sequence (O'Dea et al., 1996). The faults controlling these blocks were evidently active during Torpedo Creek Quartzite times (S. Bull, this volume). Two of these blocks have broadly similar dimensions (4 x 1.5 km), whilst a third, sandwiched between the other two, is considerably smaller in size (1.5 x 0.5 km). Each block has a shallow northward tilt and is folded by a series of N to NE trending anticlines and synclines. The Goat and Leopard Faults dip steeply to the S and form steep scarps on the southern edges of these blocks. The faults are folded about a NNE-trending axis during the Isan Orogeny (Fig. 4).

The Goat Fault contains evidence that it was active throughout the deformation. Firstly the fault has been reactivated (at least once) since horizontal dextral striations are overprinted by oblique reverse slip fibres (Fig. 5d). The implication is that the initial movement on the fault pre-dated the Isan Orogeny and was related to a NW–SE compression. Secondly, these faults are folded about F2 fold axes indicating that they pre-dated D2.

Syn-depositional faulting

A number of W- to NW-trending faults form part of a continuous zone of faulting that transects both the Paradise Creek High Strain Zone and the Redie Creek Platform (Figs 1 and 2). Although the Goat and Leopard Faults are probably the same fault, offset along a NNE-trending transfer, there is evidence that a third smaller fault exists (see small block south of the Goat Fault in Fig. 2). It is suggested that these faults were part of an active scarp system that caused streams to run north forming the coarse conglomeratic deposits typically found adjacent to these faults (S. Bull, this volume).

Field measurements along the Goat and Leopard Faults show that they dip steeply S (Fig. 4). The rotation of beds immediately south of the Goat Fault indicates that the final movement on the Goat Fault

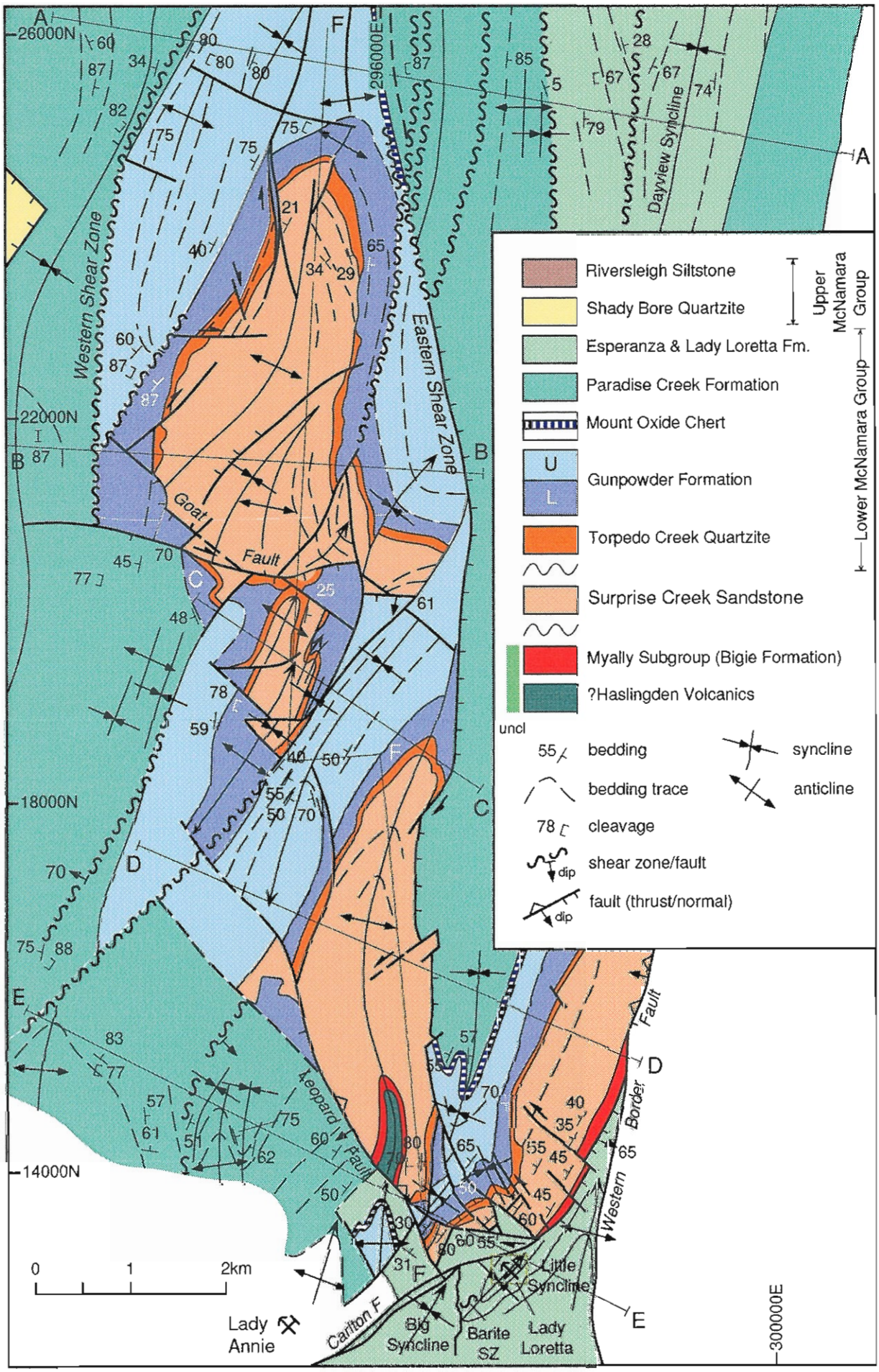

Figure 2 Detailed geological plan of the region north of the Lady Loretta. Data from Hutton and Wilson (1985), Placer/CEC maps and selected traverses done by the author. The positions of the five cross-sections and one longitudinal sectuion are shown.

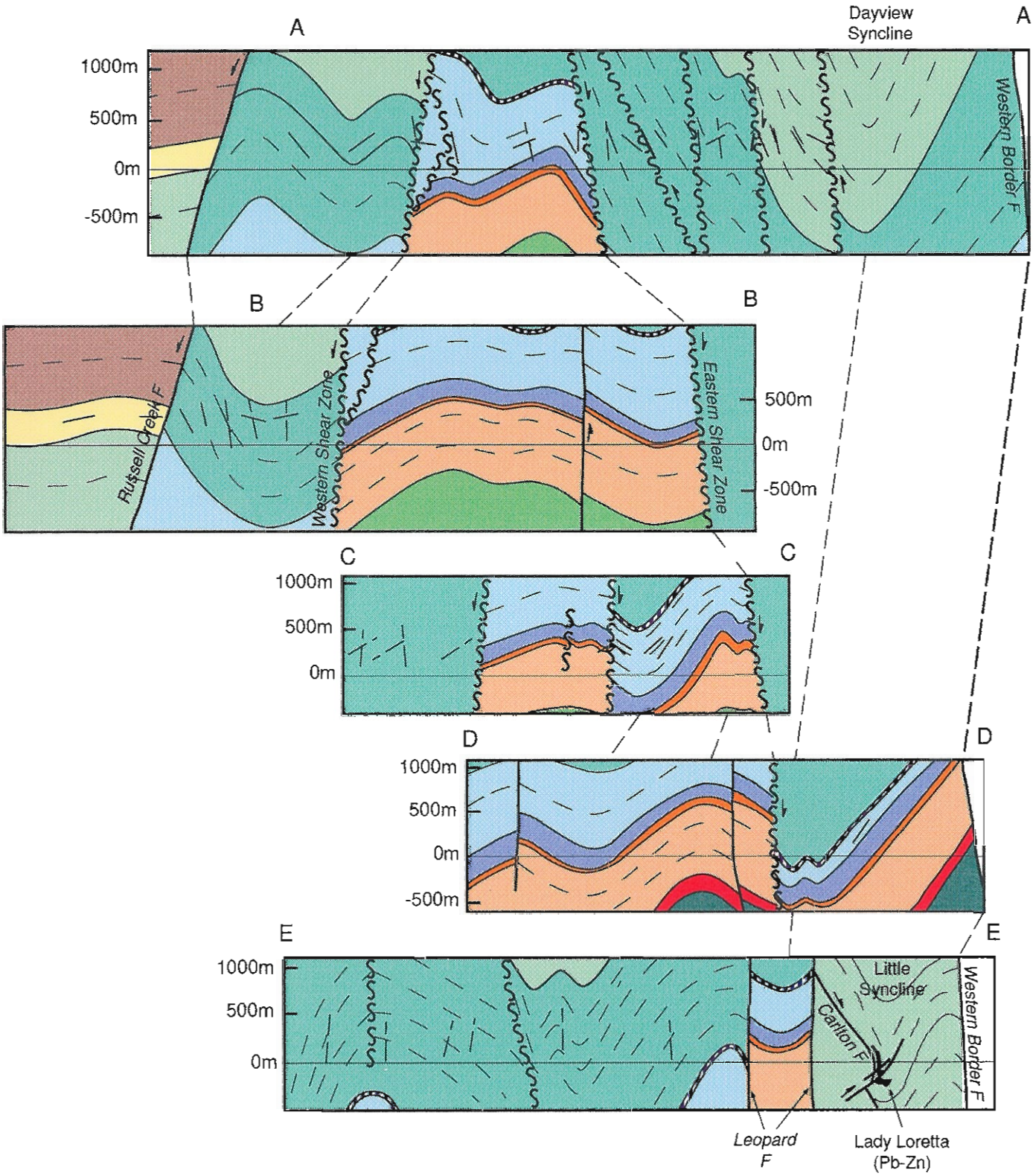

Figure 3 Cross-sections (A–A′, B–B′, C–C′, D–D′ and E–E′) through the area covered by Fig. 2. Horizontal and vertical scales are identical.

was S-block down, or normal. Two models to explain this S-dip, and the apparent normal movement during tectonic inversion, are presented in Figure 4. The basic assumptions used are: (1) movement was N-block-down during TCQ deposition, (2) the fault originally had a vertical dip, and (3) the faults were strongly listric (curved) in shape. A second model has the faults as S-dipping planar domino structures. One of the major differences between the two models is that the first requires a considerable amount of crustal extension, ie. approximately 40–50%, whereas the second requires only small amounts of extension (10–15%).

There is a marked reduction in overall thickness of the Gunpowder Formation across the Eastern Shear Zone. The formation thins from 800m on the western side of the structure, to about half this on the eastern side (see section D–D, Fig. 3). This reduction in thickness of the Gunpowder Formation suggests that the Eastern Shear Zone experienced W-block-down movement during lower McNamara times and formed the edge to a northerly trending depocentre. The structure was inverted during regional compression. The Eastern Shear Zone bends into the Leopard Fault at its southern end indicating a close relationship between the two structures.

The Surprise Creek Sandstone is shown to be thicker north of the Goat Fault (Fig. 4). This shows that the depocentre at the time was located to the north.

Barite Shear Zone

The Barite Shear Zone (BSZ), situated 0.5 km west of the Lady Loretta deposit, is an ENE-trending fault zone that can be traced for several hundred metres on the surface (Fig. 2). It lies on the overturned W-limb of the Little Syncline, between Max's Fault and an unnamed structure to the north, within the barite (or distal) facies of the Lady Loretta Ore Horizon. It is considered to be part of the syncline dividing fault. It shares a common strike with the nearby Carlton Fault Zone (which it probably intersects at depth) and is regionally identified with the mega-shear band that crosses the Paradise Creek HSZ, 5 km north of Lady Annie. This structure was suggested to have developed during late-D2/early-D3 of the Isan orogeny by Keele (1994).

The importance of the BSZ lies in the fact that is accessible, well exposed, and contains the first identifiable F1 folds in the district. The presence of F1 folds, although previously inferred (Keele and Beeson, 1994) had, hitherto, not been identified in outcrop (Fig. 5a). The zone has developed classic shear fabrics more typical of rocks at higher metamorphic grade, eg. upper greenschist/lower amphibolite facies. Clearly, the comparative weakness of barite has much to do with this: the differences in strength between barite and silica are comparable to quartz and felspar at much higher P–T conditions. The excellent 3D exposure gives insights into some of the kinematic processes that occur within such zones. In particular, several movement senses and directions are observed, suggesting that regional kinematic interpretations should be applied to larger structures with caution.

Two generations of folds are recognised in the shear zone. The first are tight to isoclinal F1 folds (without axial plane cleavage) that are obliquely cut by the F2 folds with an axial plane cleavage, resulting in doubly plunging culminations due to D1/D2 interference (Figs. 5a and 6). The early folds, where they can be recognised, have gentler plunges than the later folds; although by far the majority of folds observed in the shear zone are intrafolial or rootless folds developed along and within the intense tectonic fabric. These folds generally parallel the steeply plunging rodding lineation.

The principal kinematic indicators in the BSZ are *shear bands* that indicate both dextral and reverse senses of movement (Figs 5c and 6). As the shear band sites are within meters of each other, it is presumed that the shear zone accommodated the regional flattening during late-D2/early-D3 with two movement senses and directions: the dextral movement is identical to the interpreted regional mega shear that cuts across the HSZ. Whilst the reverse movement caused extension along the western limb of the Little Syncline (e.g. Koff Fault). These movements may have been sequential or they may have been contemporaneous.

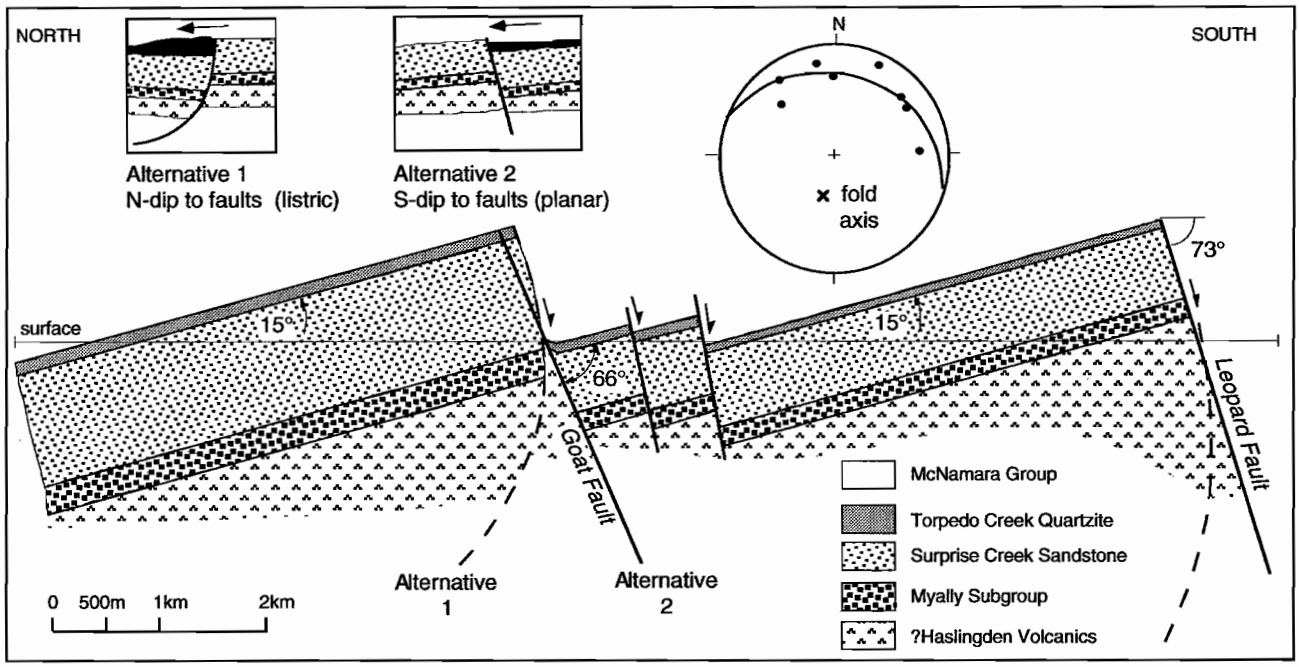

Figure 4 Simplified longitudinal section (F–F') drawn along the length of the uplifted blocks of Surprise Creek Sandstone. Two structural models are proposed to explain the coarse conglomerates at the base of the Torpedo Creek Quartzite (see text for further explanation).

Figure 5 (opposite): Photographs of structures in outcrop: (a) isoclinal F1 fold showing double plunge with S2 transecting both limbs of the fold, from Barite Shear Zone; (b) shear fabric in silica–barite rock; note the intra-shear zone fold on left hand side and strong horizontal fracture cleavage in the silica bands, Barite Shear Zone; (c) reverse shear bands in the Barite Shear Zone; (d) fault re-activation showing early dextral strike slip overprinted by oblique reverse slip movement, Goat Fault; (e) vertically dipping penetrative cleavage in siltstone–shales; note fault in fold hinge and the change in thickness and dip of strongly laminated siltstones across cleavage parallel fracture, bottom right; Gunpowder Formation, loc. 22/23; (f) late fibrous quartz veins cutting early quartz vein; Paradise Creek Formation sandstone, loc 111.

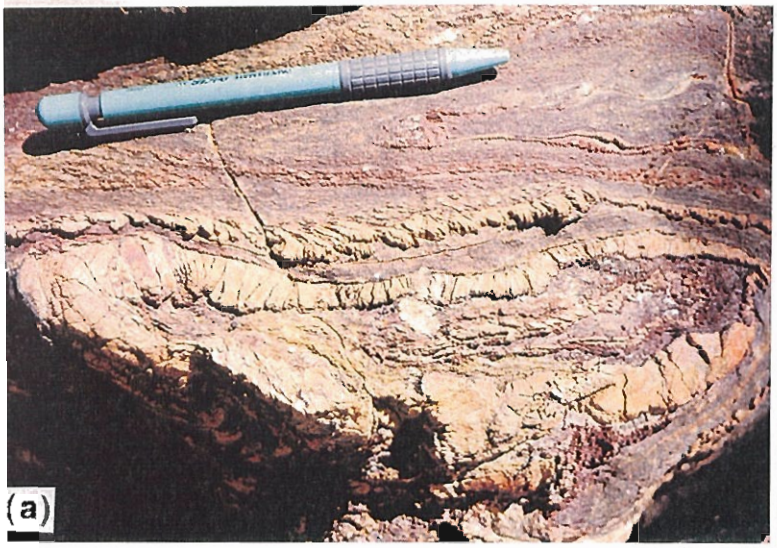
(a)


(b)

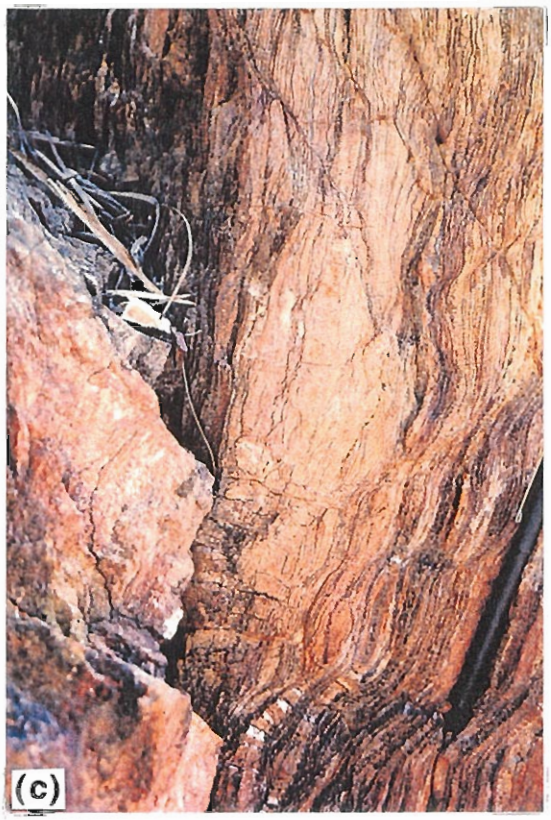
(c)

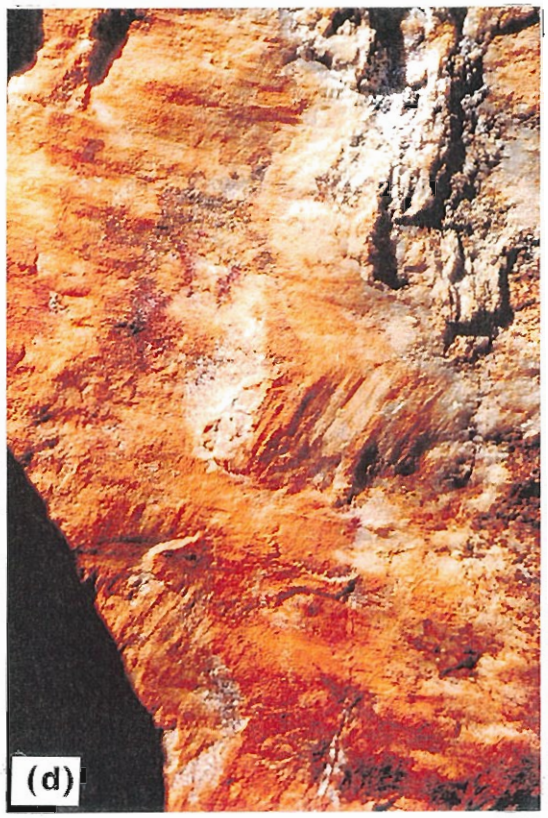
(d)

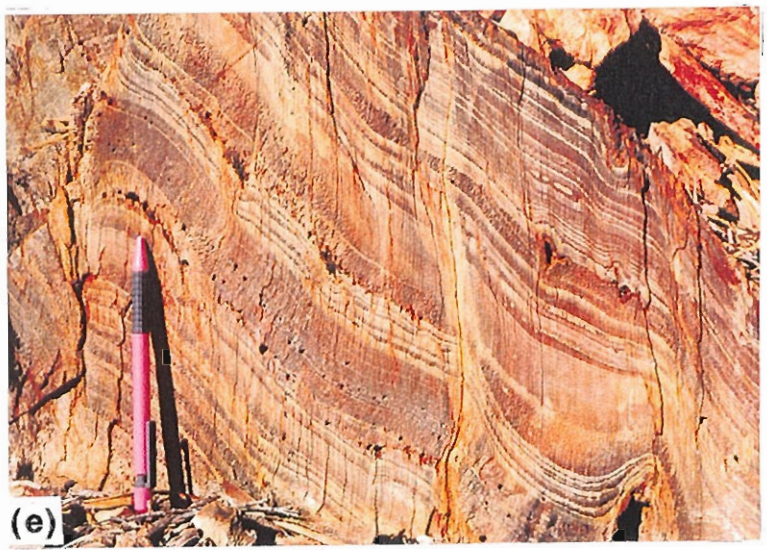
(e)

(f)

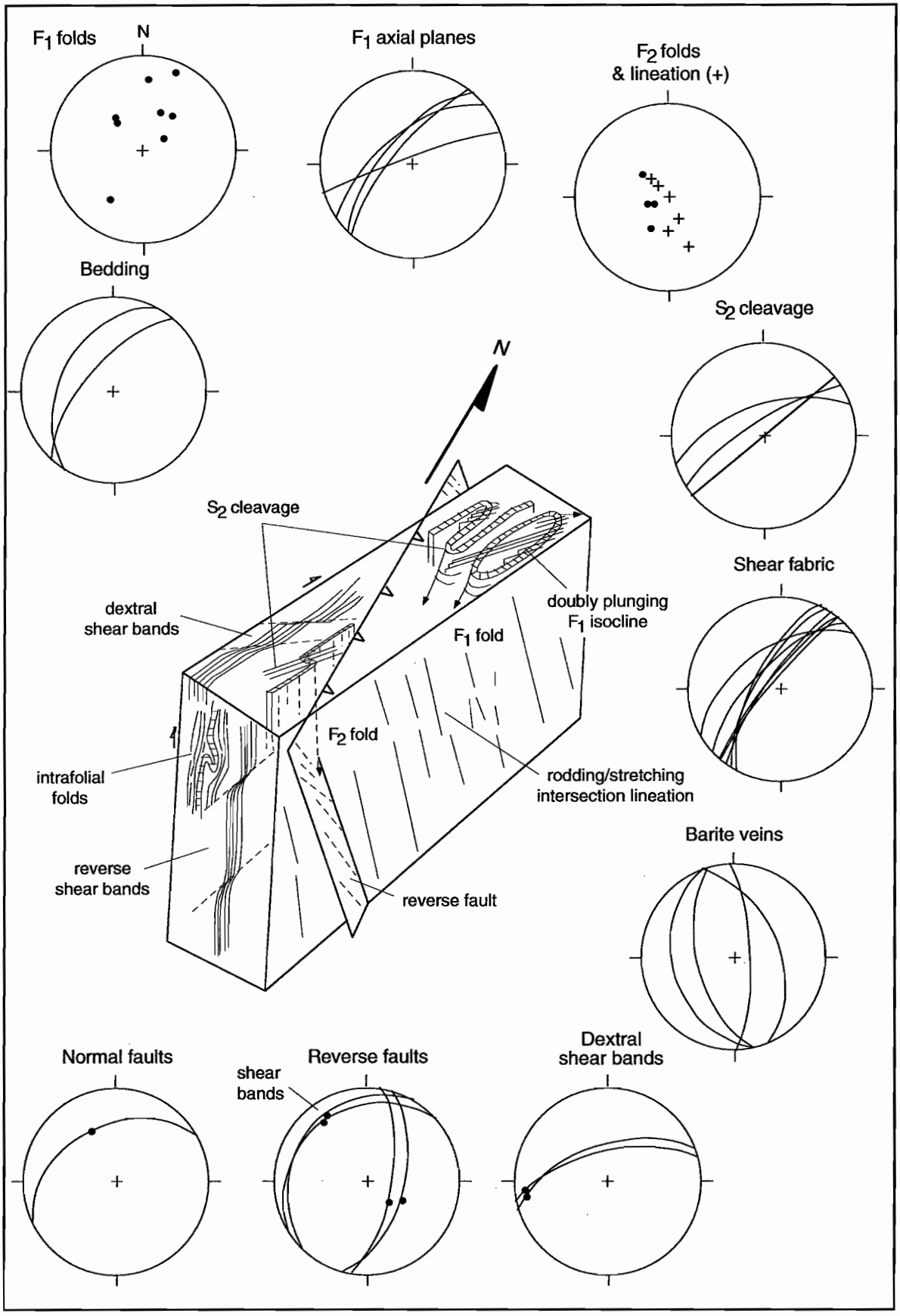

Figure 6 Simplified diagram of structures in the Barite Shear Zone, near Lady Loretta deposit.

Brittle faults in the shear zone are represented by: (1) dip-slip reverse faults that cut across the shear zone and (2) normal faulting N-block-down movement.

Fault striations

Eighty-nine fault striations were measured in the region (63 from the Paradise HSZ and 26 from the Redie Platform). All the following movements were observed: reverse, normal, sinistral and dextral. This wide range of movement senses reflects the dominance of the brittle late-D2–D3 phases of the Isan Orogeny in which E-W compression caused thrusting to be followed by wrenching (Blake and Stewart, 1992). A wide range of strike directions has also been recorded. The results have been analysed and are presented in summary below. They do not materially change the conclusions reached in the first report.

The *reverse* faults have a range of azimuths from WNW to NNE with the majority striking N–S (Fig. 8). Their generally shallow dips reflect the strong control exerted by bedding on this type of faulting. This point is reinforced by the presence of two girdles, one containing the strata folded around the WNW-trending axes in the Redie Platform and the other, the NNE-trending axes in the HSZ. This means that the regional folds were formed by flexural slip along bedding surfaces; however, it does not necessarily mean that they were folded. Consequently, these striation data are interpreted to be due to D1 (NNE–SSW compression) in the Redie Creek Platform and D2 (E–W compression) in the HSZ respectively; subordinate NW–SE and NE–SW compressions are inferred.

The *normal* fault data have a larger spread of poles than the reverse fault data. The striation data are dominated by the Russell Creek Fault on the western side of the HSZ (Fig. 3). Here, NW–SE extension took place on structures striking slightly east of north; this stress field would also imply E-block-down normal movements on steep E-dipping fault surfaces, eg. Eastern Shear Zone and in places, the Western Border Fault.

Poles to faults with *sinistral* movement form a broad NE–SW girdle which is interpreted to mean that sinistral wrenching took place principally along NW–SE striking faults (with a range from W-trending to N-trending). The associated movement directions (striations) occur as inverse to the poles, i.e. they occupy the pole free zone, indicating E–W compression during D3.

The *dextral* strike slip faults have near random strikes with considerable overlap with the sinistral strike slip faults implying fault reactivation or a very unstable direction in the stress field occurred at this time. This is reasonable given the large (up to 32 km) recorded displacements on the NNE-trending dextral wrench faults in the Mt Isa Inlier, of which the Mount Gordon Fault Zone is probably one.

A plot of all wrench and dip-slip striations shows that apart from some minor regions of overlap (ie. between sinistral and dextral movements), the four different movements are reasonably distinct. For the strike-slip data, this can be interpreted two ways: (1) that there was some uncertainty identifying slip directions in the field (this is certainly possible), (2) that there had been reactivation along faults, (3) that the stresses in the D2–D3 event locally resolved around a wide angle (up to 60° or more?). It should be noted that the study area sits at a bend in the HSZ, a fact that might support this particular line of argument.

Twenty-six data collected along the length of the Redie Creek Fault show minor differences to the HSZ data. The WNW-trending reverse faults show N rather than S-dips, indicating that the Redie Creek Fault probably dips steeply to the north, instead of south. The sinistral faults trend sub E–W suggestive of a NE–SW component to the principal stress tensor, in addition to the main E–W compression. The dextral striations are dominated by the NNE trending strike slip motions such as might be inferred on the Mount Gordon Fault Zone.

Correlations with magnetics

The western edge of the Paradise Creek HSZ corresponds to the edge of the Haslingden Group volcanic pile. This is because the character of the magnetic terrain west of the Russell Creek Fault excludes any volcanics at depth (M. Duffet, pers.

comm., 1996). The fault is, therefore, an older deeper structure that was reactivated during the Isan Orogeny (see section A–A in Fig. 2).

Three broad linear magnetic anomalies, associated with buried Eastern Creek Volcanics, are recognised trending in a northerly direction (Fig. 1):

1. The *western* anomaly occurs in the centre of the HSZ and correlates well with individually uplifted, tilted and folded Surprise Creek blocks indicating that the source of the anomaly is close to the surface (Duffet, pers. com. 1996)
2. The *central* anomaly trends slightly west of north and lies at the western end of the Redie Creek Fault; it lines up with a conspicuous left-hand bend in the HSZ which would be due to interference between the HSZ and the F2 Isan folds, or an intersection of primary rift trends in the underlying Haslingden Group.
3. The *eastern* anomaly also trends slightly west of north and terminates against the Mount Gordon Fault.

The *central* and *eastern* anomalies are spaced about 18 km apart and are more diffuse than their western counterpart (with the exception of the Mt Kelly area). They lie almost, but not precisely, along the anticlinal fold hinges. This has led Mark Duffet and Richard Keele to believe that the volcanics are a deeply buried substrate that is magnetically detectable only where it comes close to the surface, either by the processes of uplift or folding. It is, however, likely that these linear anomalies represent rift-related features (e.g. half-grabens) that controlled the thicker portions of the volcanics: as such the flanking volcanic units may not only be thinner, but also more deeply buried than the graben fill, making them difficult to detect.

The mega-shear/kink band crosses obliquely across the HSZ north of the Lady Annie and Loretta deposits (Fig. 1). The significance of this structure lies in the fact that, although active late in the Isan Orogeny, it may have originated as an accommodation zone during initial rifting. The Barite Shear Zone is one of a family of such structures. The mega shear may also be traced as a discontinuity in the magnetics across the Redie Creek Platform where it affects the *central* anomaly and coincides with a dextral offset on the *eastern* anomaly. Of significance from an exploration point of view, is that it passes through the Mount Oxide deposit (Mark Duffet, pers. comm.).

Regional quartz veins

The reason for studying the quartz veins are two-fold: firstly, geothermometric data on fluid inclusions provides a useful check on illite crystallinity data, and secondly, intended vein paragenetic studies (eg. at Lady Annie) can be put into a regional context. This will aid exploration by identifying those faults that are associated with copper-bearing fluids. For example, initial studies have shown an early generation of pyritic quartz veins that is related to wrenching along E–W faults.

The regional quartz veins can be divided into two major groups, according to their orientation and timing. At present, the two groups are loosely related to each other; however, further work should make it possible to relate them to each other in a more systematic way.

Type 1 veins

Type 1 veins comprise E- and W-dipping sets that parallel bedding in the fold limbs of the HSZ (Fig. 7). Identical angles between the pole maxima for bedding and veins (87 and 88° respectively) reflect the fact that the veins are mostly bedding parallel and that the sequence is folded; however, this does not necessarily mean that the veins themselves were folded. If the plot of quartz fibres is compared to the normal pole to veins plot, there are small differences. For instance, the type 1 veins evidently dilated obliquely, i.e. in a sub-vertical direction, rather than perpendicular to bedding. This is consistent with a vertical sigma 3 direction inferred to accompany thrusting (i.e. late D2).

Type 2 veins

Type 2 veins are subvertically dipping and form a conjugate set trending NW and NE. The near horizontal fibres indicate that they are related to the wrenching event (D3); fibres are coincident with poles

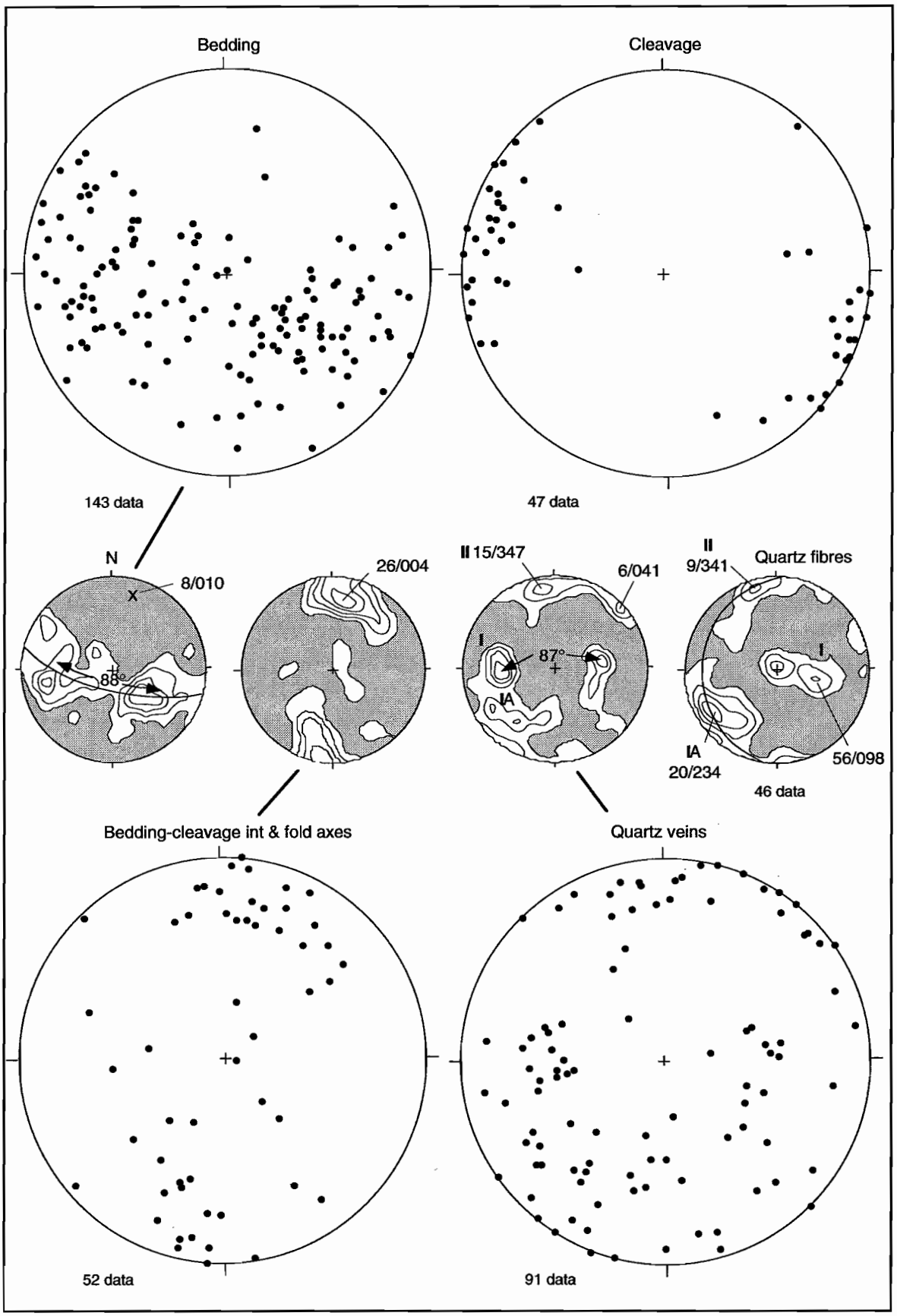

Figure 7 Structural data from the Paradise Creek High Strain Zone (Study area 1).

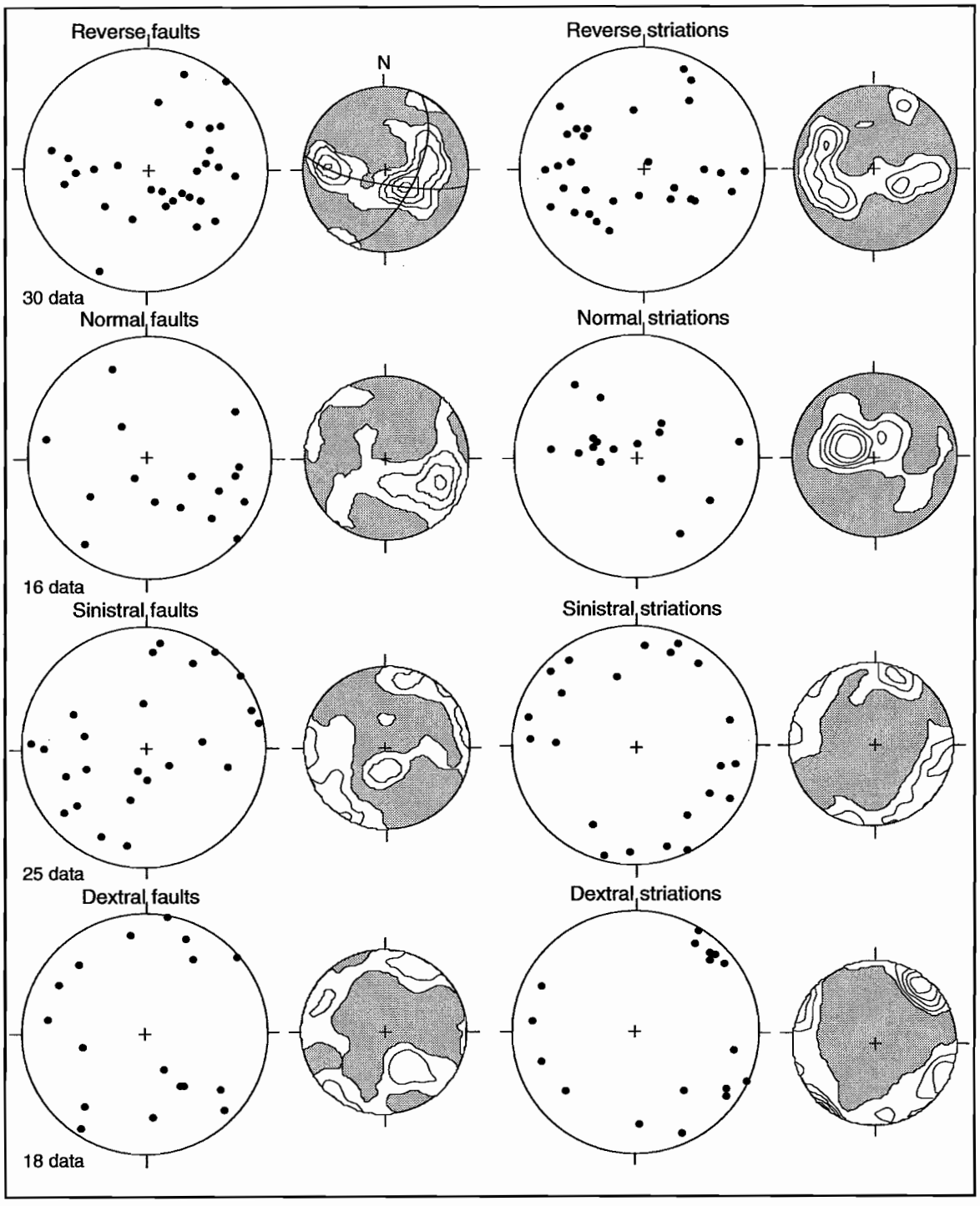

Figure 8 Fault data from the Paradise Creek HSZ (study area 1) and The Redie Creek Platform (study area 2). The poles to faults are shown on the left hand side of the diagram. Striations are shown on the right.

suggesting that insignificant rotational displacements were associated with this event.

The second group has two types, one that formed early in the deformation and another that formed late. The early veins are fault-related, vuggy and have carbonate ± pyrite associated with them. The late veins are more widespread and comprise fibrous quartz-only veins that are rarely vuggy; they are related to peak P–T conditions during the Isan Orogeny and probably correspond to maximum burial conditions. Overprinting relationships between the two types are common (Fig. 5f). The displacement vectors — as indicated by the quartz fibres — are consistent with them having formed during wrench fault movements and compression during the Isan Orogeny.

Regional controls to copper mineralisation

Following an earlier investigation into copper in the region (van Dijk, 1991), this brief study takes a look at the significance of the break-up unconformity at the end of Surprise Creek times (McConachie and J. Dunster, pers. comm.) and its possible relationship to mineralisation. An inferred low-angle northward tilt to the units below the Torpedo Creek Quartzite unconformity surface suggests that escaping brines would have moved *away* from a depocentre which is inferred to lie to the north. Implications for Mammoth-style Cu is that such deposits would tend to be sited on the basin-ward facing slopes of uplifted blocks.

Mount Gordon Arch

The Mount Gordon Arch, which divides the Leichhardt Fault Trough into two smaller second-order basins, commenced life as an uplift during the Fiery Creek deformation and continued through until the middle of the Paradise Creek Formation (Plumb et al., 1980; Derrick, 1982). It has been described as a zone of complex uplift and deformation 250 km long stretching from south of Mount Isa to Mammoth mines (Derrick, 1982). Although some controversy surrounds the existence of this structure, it is clear that uplift exposed Myally sub-Group rocks to erosion prior to deposition of the Torpedo Creek Quartzite. This was particularly so on the eastern side of Mount Gordon Fault (Fig. 9). A number of E–W structures acted as important growth faults during the latter part of the basin history (e.g. Investigator and Mammoth Faults).

This uplift, however, was variable: for example, the Pickwick Basalts appears to have been uplifted along NE trending structures, whilst the Cromwell Basalts were exhumed along the Mount Isa Fault. This indicates maximum uplift was in the east and south. The distribution of Leander and Lena Quartzites, however, are near to random in their distribution indicating that whilst some of the uplift may have been fault related much of it may have been due to isostasy and intra-rift flexure.

The Torpedo Creek Quartzite rapidly thins eastward onto the Myally sub-Group block (from data by Hutton et al., 1985), indicating that uplift on the Mount Gordon Arch continued at least until lower McNamara Group times. The Investigator Fault probably did not exist in Haslingden times, although it became important during lower McNamara Group times, especially during deposition of the Gunpowder Creek Formation when it was an active growth fault (Derrick, 1982).

Carters Bore Rhyolite

The Carters Bore Rhyolite has its thickest development in the region of the Sybella Granite (Fig. 9). It approximates a N–S trending fault-bound caldera in shape and is some 15 x 20 km in dimensions. If uplift is controlled by sub surface granites, then the existence of a second much smaller area of rhyolite (2 x 6 km) at southern end of the Mount Gordon Fault Zone, implies the existence of granite here as well.

Mammoth Mines

The regional dip of the Surprise Creek beds west of the Mount Gordon Arch is very shallow to the north (i.e. away from the Sybella Granite). Although there are minor interruptions to this trend, the implied migration direction of escaping basinal brines is from north to south. For this reason the location of the

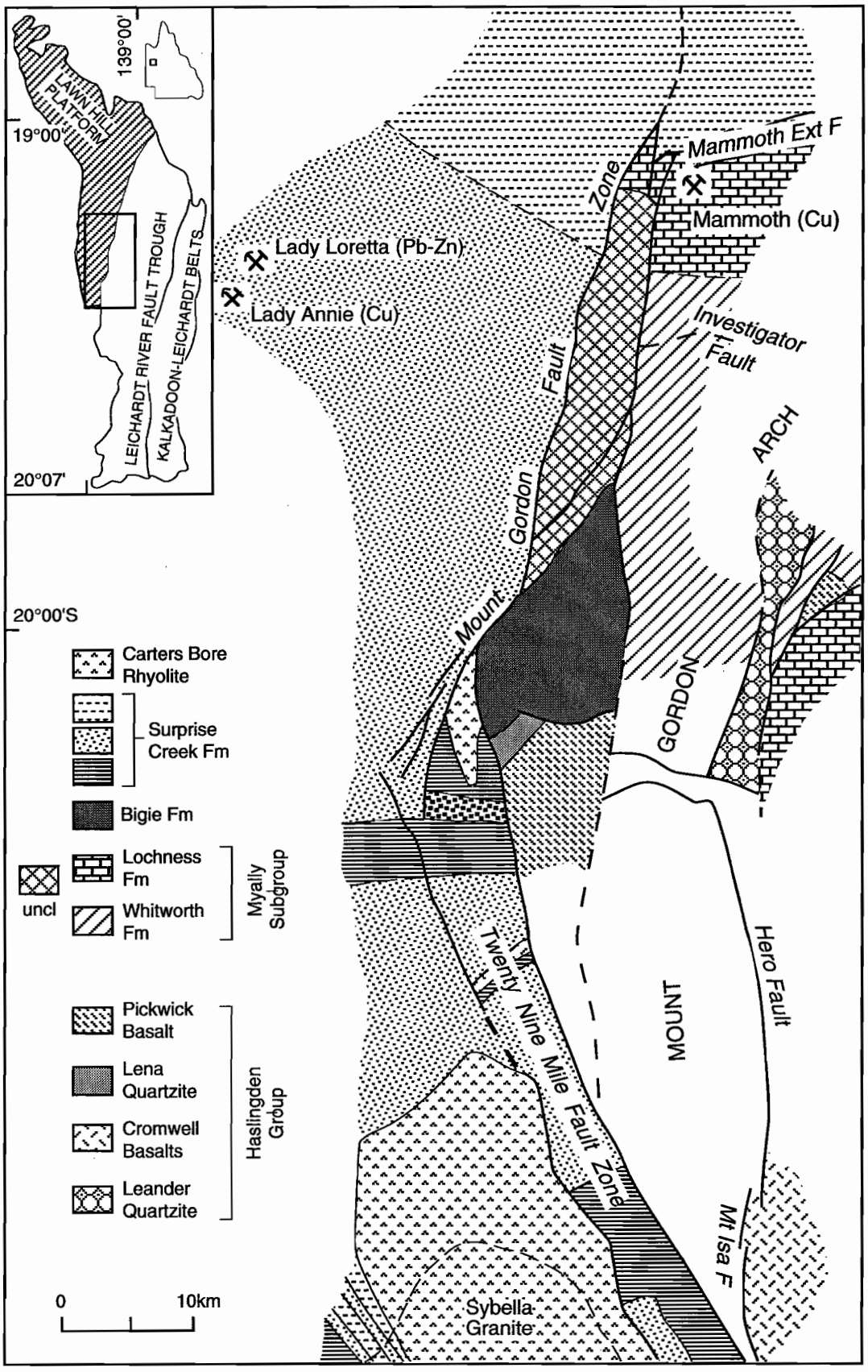

Figure 9 Interpreted geological plan of the sub-Torpedo Creek Quartzite unconformity in the Mammoth and Kennedy Gap region, (data from Hutton et al. 1985). The inferred uplift along the western margin of the Mount Gordon Arch is interpreted to be fault controlled.

Mammoth mine becomes significant because it lies (1) on the basinward side of an uplift feature buried beneath an unconformity surface, an ideal place for fluids to be trapped, (2) at a fault intersection, and (3) adjacent to carbonate rocks of the Loch Ness Formation would have been a suitably reactive host (Fig. 10). One aspect to this model is that the preferred aquifer — the middle sandstone unit of the Surprise Creek Formation — lies beneath the upper flaggy siltstone unit which would have been an aquaclude. Note that the siltstone/sandstone boundary is predicted (from Fig. 9) to lie at depth beneath the deposit, thus the fluids would have needed to travel up the fault to the present site of deposition. The copper deposits occur in brecciated sandstones of the Myally Subgroup, rather than the McNamara or Mt Isa Groups (Williams, 1980). The E–W Mammoth Extended and the N–S Portal Faults were clearly important in controlling mineralisation (Mitchell and Moore, 1975). The source of the copper is suggested to be the nearby Eastern Creek Volcanics, i.e., Pickwick Basalts (Scott and Taylor, 1982).

The northward continuation of the Mount Gordon Fault beyond Mammoth is a later propagation of the fault during the Isan Orogeny. The implication for mineralisation is that the fluid conduits were established at the beginning of McNamara Group times. Consequently the mineralisation could have been as early as this although a later age is not precluded; it does, however, suggest that the D3 age for the copper at the Hilton mine (Valenta, 1994) may not necessarily apply to this deposit, because many of the pre-conditions for ore deposition were set in place well before the orogeny.

Nature of the rifts

Early rifting in the basin was probably oblique rather than orthogonal. The presence of a basement grain that trends NNW and the N–S trend of the rift margin itself strongly suggests that the rift vector lay at angle of 15–20° to a line drawn perpendicular to the edge of the basement rift zone. A second phase of rifting, with a rotation of the direction of extension, might be inferred for the sub E–W trending Redie Creek Fault system at the start of McNamara times. One possible explanation, therefore, is a rotation of about 50° from azimuth 065 to 020 in the extension axis. An alternate explanation, and one which simplifies matters, is that the Redie Creek trend is an accommodation zone or zone of complex structural development within the rift. Recent analogue modelling experiments on rifts (McClay, 1996) display a number of features that may relate directly to the Paradise Creek High Strain Zone. They are:

1. The intra rift faults are segmented and lie at a high angle to the extension direction, whereas the rift border fault systems are parallel to the underlying zone of basement stretching.

2. Oblique accommodation zones, formed by conjugate fault arrays that separate the individual depocentres, tend to lie in pairs at acute angles (<45°) to the basement rift zone. Note that one of these accommodation zones lies parallel to the extension vector (Fig. 11).

A second rifting event is postulated (Dunnet 1976, S Bull, this volume) with extension approximately in a NNE–SSW direction at during Surprise Creek Formation/basal McNamara Group times. This rift would be an orthogonal rift (McClay, 1996).

The significance of these results is:

- the Eastern Shear Zone may be an intra-rift fault that controlled the eastern edge of a N–S depocentre at least until Gunpowder Creek times. Note that the intra-rift faults (and depocentres) lie slightly west of north, a feature already noted in relation to the magnetic anomalies.

- The Western Border Fault (perhaps more appropriately called the Eastern Border Fault!) is made up of a combination of intra-rift and rift border faults. The large bend north of Lady Loretta may be the point where the character of this fault changes from intra-rift to rift border.

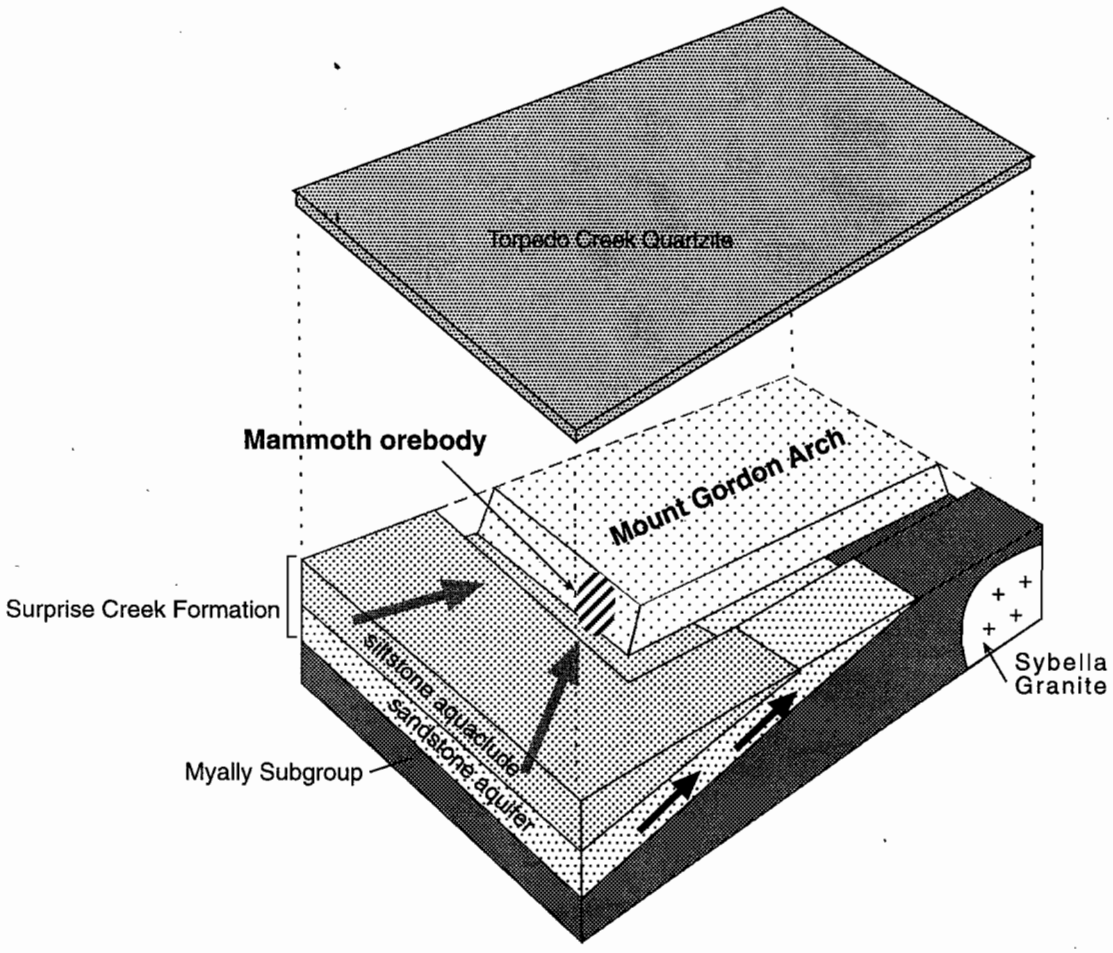

Figure 10 Block diagram showing the focussing of basinal fluids towards the northwest corner of the Mount Gordon Arch. The Surprise Creek Formation units dip very shallowly to the north underneath the TCQ unconformity and comprises a lower sandstone aquifer and an upper siltstone aquaclude.

- The Redie Creek Fault trend and the mega-shear/kink band may follow the trace of two of these accommodation zones. In this case, there would be no need to advocate a second phase of extension at the base of the McNamara Group (see conclusions of Betts et al. (1996) for the Termite Range Fault region).

- It is interesting to note that recent studies of the Jean D'Arc Basin off Newfoundland (Sinclair, 1995) show that a shift in the extension direction of 90° (from NW–SE to NE–SW) actually results in inversion of parts of the basin. Clearly, further work is required to discriminate between one rifting event with a constant direction of extension and episodic rifting with a change in the extension direction.

- **The** Lady Annie deposit is unique because it lies at the intersection of two important crustal features: (1) the N-trending Paradise Creek High Strain Zone which is inferred to be an expression of the underlying "Haslingden rift" and (2) the WNW-trending structural axis or basement high that is an expression of the Paradise rift. This location is an ideal one for maximising the potential for thermal anomalism, fluid flow and mineralisation.

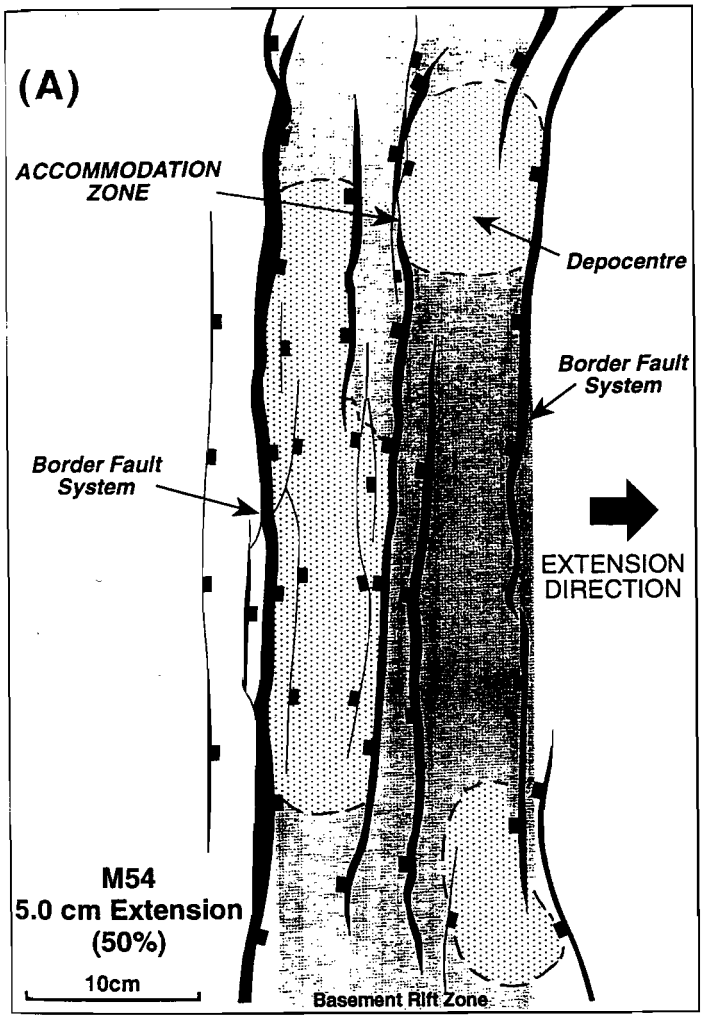

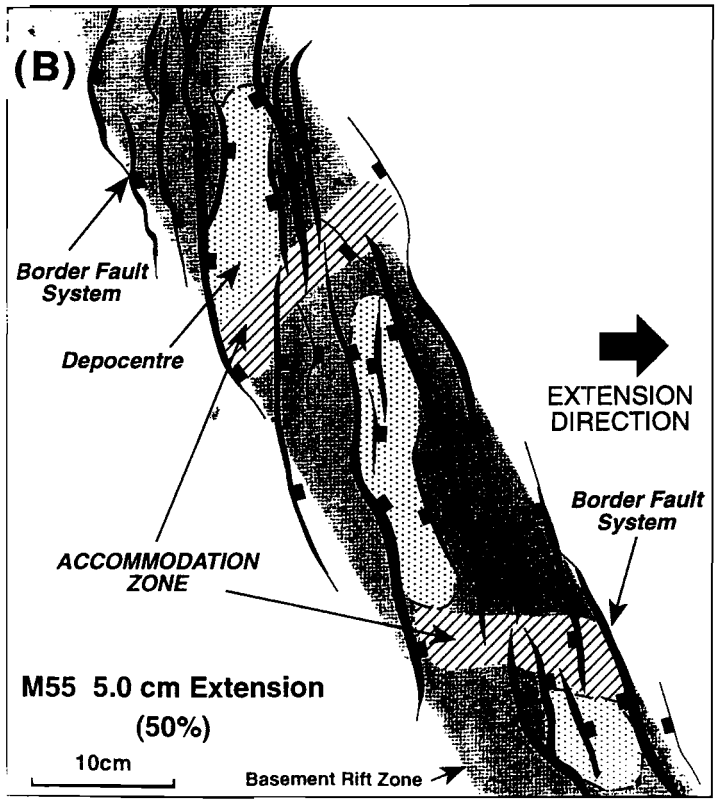

Figure 11 The nature of (A) orthogonal rifting (B) oblique rifting from model experiments by McClay (1996). If the reverse view of the orthogonal rift is taken (C) a number of features may be directly related to the inferred rift beneath the Paradise Creek High Strain Zone (see text for further discussion).

Conclusions

- The Paradise Creek High Strain Zone is the western edge or 'soft shoulder' to the Haslingden Rift. The Russel Creek Fault is a normal fault that had been re-activated with W-block down movement during the Isan Orogeny. During earlier times, its progenitor probably faced in towards the rift.

- The Leopard and Goat Faults may be reconciled with N-dipping syn-depositional fault model if they were strongly listric, i.e. they dipped vertically at surface and flattened off markedly at depth.

- The Lady Annie copper deposit lies at the intersection of the central uplift of the HSZ with a structural culmination that trends in a WNW direction across the Redie Creek Platform and Paradise Creek HSZ. This confluence of structures, suggested to be the intersection of two rifts, would provide ideal conditions for focussing of basinal fluids during tectonic inversions.

- An oblique rifting model for the underlying Haslingden Group is able to explain a number of features in the Paradise Creek HSZ.

Further work

1. Illite crystallinity studies should be carried out to map the extent depth of individual depocentres in the region. Current studies indicate a depocentre existed north of Lady Loretta in Lower McNamara times.

2. Thermometric studies on regional quartz veins in the Paradise Creek HSZ provide useful checks on illite crystallinity data. Early observations suggest that there is a set pyrite-bearing quartz veins which pre-date a set of ubiquitous syn-metamorphic fibre veins. The relationship of these veins to copper mineralisation should be investigated.

3. Detailed studies of a copper prospect to provide timing relationships of mineralisation with respect to tectonic events (eg. rifting, inversion, orogeny).

Acknowledgements

Buka Minerals provided accommodation and support in the field. J. Dunster is thanked for providing some data and for the many useful discussions.

References

Betts, P., Pound, K. and Lister, G., 1996. Episodic rift-sag sequences in cover sequence three, north western Mount Isa inlier. *Geological Society of Australia Abstracts* 41: 32.

Blake, D.H. and Stewart, A.J., 1992. Stratigraphic and tectonic framework, Mount Isa Inlier. *In* A.J. Stewart & D.H. Blake (Eds): *DETAILED STUDIES OF THE MOUNT ISA INLIER. AGSO Bulletin* 243: 1–11.

Denmead, A.K., 1938. Sketch map of Paradise Valley. 1"=150' geological plan. Mines Dept, Brisbane.

Derrick, G.M., 1982. A Proterozoic rift zone at Mount Isa, Queensland, and implications for mineralisation. *BMR Journal of Australian Geology and Geophysics* 7: 81–92.

van Dijk, P.M., 1991. Regional syn-deformational copper mineralisation in the Western Mount Isa Block, Australia. *Economic Geology* 86: 278–301.

Duffet, M.L., 1996. Geophysical environment of the Lady Loretta Pb–Zn deposit. *In* T. Baker, J. Rotherham, J. Richmond, G. Mark and P. Williams (Eds): *NEW DEVELOPMENTS IN METALLOGENIC RESEARCH: THE MCARTHUR, MT ISA, CLONCURRY MINERALS PROVINCE. EGRU Contrib.* 55: 45–46.

Dunnet, D., 1976. Some aspects of the Panantarctic cratonic margin in Australia. *Philosophical Transactions of the Royal Society* A280: 641–654.

Dunster, J.D., 1996. Sedimentology of the Lady Loretta Formation – a comparison of the regional setting to that of the Lady Loretta ore body. *In* T. Baker, J. Rotherham, J. Richmond, G. Mark and P. Williams (Eds): *NEW DEVELOPMENTS IN METALLOGENIC RESEARCH: THE MCARTHUR, MT ISA, CLONCURRY MINERALS PROVINCE. EGRU Contrib.* 55: 45–46.

Hancock, M.C. and Purvis, A.H., 1990. Lady Loretta silver–lead–zinc deposit. *In* F.E. Hughes (Ed.): *GEOLOGY OF THE MINERAL DEPOSITS OF AUSTRALIA AND PAPUA NEW GUINEA.* The Australian Institute of Mining and Metallurgy: Melbourne: 943–948.

Hutton, L.J. and Wilson, I.H., 1984. Mount Oxide Region. 1:100,00 geological map commentary. Bureau of Mineral Resources, Geology and Geophysics.

Hutton, L., Derrick, G.M. and Gallagher, J., 1985. Geology of the Mammoth Mine region. Explanatory notes and map. BMR & GSQ.

Keele, R.A., 1994. A preliminary structural analysis of the Riversleigh Fold Belt (formerly Lawn Hill Platform) with special reference to structures around the Lady Loretta deposit. CODES:AMIRA/ARC Project P.384 Proterozoic sediment-hosted base metal deposits: 37–44.

Keele, R.A. and Beeson, J., 1994. Exploration model for Lady Annie Copper Mineralisation, NW Queensland. Unpubl. report to Pancontinental Mining Ltd: 12 pp.

O'Dea, M. G., Lister, G. S., MacReady, T., Betts, P., Oliver, N.H.S., Pound, K.S., Huang, W. and Valenta, R.K., in press. Geodynamic evolution of the Proterozoic Mount Isa terrain. *In* J.P. Burg & M. Ford (Eds): *OROGENY THROUGH TIME. Special Publication of the Geological Society of London.*

McClay, K.R., 1996. Recent advances in analogue modelling: uses in section interpretation and validation. *In* P.G. Buchanan, and D.A. Nieuwland (Eds): *MODERN DEVELOPMENTS IN STRUCTURAL INTERPRETATION, VALIDATION*

AND MODELLING. Geological Society Special Publication 99: 201–225.

Mitchell, J.W and Moore, G.P., 1975. Mammoth Copper Deposit. *In* C.L. Knight (Ed.): *ECONOMIC GEOLOGY OF AUSTRALIAN AND PAPUA NEW-GUINEA, vol. 1.* Australian Institute of Mining and Metallurgy: Melbourne: 383–389.

*Plumb K.A., Derrick G.M. and Wilson I.H., 1980. Precambrian geology of the McArthur River–Mount Isa region, northern Australia. *In* R.A. Henderson and P.J. Stephenson (Eds):

Scott, K.M. and Taylor, G.F., 1982. Eastern Creek Volcanics as the source of copper at the Mammoth mine, northwest Queensland. *BMR Journal of Australian Geology and Geophysics* 7: 93–98.

Sinclair, I.K., 1995. Transpressional inversion due to episodic rotation of extensional stresses in Jeanna d'Arc Basin, offshore Newfoudland. *In J.G.* Buchanan and P.G. Buchanan (Eds): *BASIN INVERSION. Geological Society Special Publication 88*: 249–271.

*Williams, N., 1980. Precambrian mineralisation in the McArthur–Cloncurry region, with special reference to stratiform lead–zinc deposits. In R.A. Henderson and P.J.

Manganese transport in sedimentary brines — Chemical controls on McArthur-type and Broken Hill-type sediment-hosted Pb–Zn deposits

David R. Cooke and Ross R. Large
Centre for Ore Deposit and Exploration Studies, Geology Department, University of Tasmania

Summary

Based on fluid chemistry, Cooke et al. (1995) proposed two classes of stratiform sediment-hosted ("SEDEX") Pb–Zn deposits — ***McArthur-type***, which form from relatively oxidised neutral fluids, and ***Selwyn-type***, which form from reduced, acid fluids. Based on the geochemistry of manganese and on the stability of manganese minerals in equilibrium with hydrothermal solutions, a further distinction is proposed here between McArthur type and ***Broken Hill-type*** (BHT) deposits. Mn-rich BHT deposits form from relatively oxidised, acid fluids derived from dewatering of oxidised clastic, ironstone-bearing, carbonate-depleted sedimentary packages. McArthur-type SEDEX deposits form from relatively oxidised, near-neutral to alkaline fluids that are in equilibrium with thick packages of carbonates and oxidised clastic sediments.

Introduction

Manganese is enriched in sedimentary lithologies that underlie HYC and other Australian Proterozoic SEDEX deposits, and is inferred to be (at least in part) a product of hydrothermal activity (i.e. an alteration halo). This reports discusses the geochemistry of manganese in 150°–250° hydrothermal solutions, and comments on the implications for SEDEX genesis. Because manganese enrichment can occur by 'normal' sedimentary and diagenetic processes in sedimentary lithologies, this report begins with a brief review of manganese enrichment in black shales.

Manganese in black shales

Redox processes are important for Mn transport and deposition in surface waters and low-T groundwaters. Manganese is generally enriched in black shales, and this has been attributed to chemical precipitation of manganese oxides or carbonates under highly oxidised or reducing conditions respectively. Calvert and Pedersen (1996) summarised the hypothesised mechanisms for manganese carbonate deposition in black shales as follows:

(i) deposition in anoxic or oxygen-deficient bottom waters
(ii) deposition in mixing zones between shallow oxygenated and deeper anoxic or dysaerobic waters
(iii) deposition in 'anoxic' sediments

For point (iii), it is worth noting that black shales can form at any water depth, in oxic to anoxic conditions, and in fresh to estuarine to marine waters (Quinby-Hunt and Wilde, 1996). Black shale formation relates to the surface productivity of organic material (e.g., plankton), with high settling rates favouring black shale formation, as oxygen is consumed by organic decay in the sediment pile (Calvert and Pedersen, 1996). Figure 1 illustrates some of the redox transitions associated with progressive oxygen consumption by decay of organic matter within the sediment pile (from Drever, 1984).

Quinby-Hunt and Wilde (1993) summarised the possible nature of redox zonation within black shales based on the Eh–pH conditions of sediment deposition (Figure 1). In each field shown in Figure 2, manganese and iron solubilities and mineralogies vary as follows:

I Mn, Fe insoluble (high concentrations of Fe and Mn as oxides in black shales)

IIa Mn soluble, Fe insoluble (high concentrations of Fe as oxides, low concentrations of Mn as carbonates in black shales)

IIb Mn and Fe soluble (low concentrations of Fe and Mn in black shales); sulfides absent due to relatively oxidised Eh conditions

III Mn soluble, Fe insoluble (high concentrations of Fe as sulfides, low concentrations of Mn as carbonates in black shales)

IV Mn and Fe soluble (low concentrations of Fe and Mn in black shales); sulfides present due to reduced Eh conditions.

Based on these relationships, Quinby-Hunt and Wilde (1996) have proposed that the Mn and Fe chemistry and mineralogy of black shales can be used as indicators of the depositional environment.

Manganese in hydrothermal solutions

Mn occurs naturally in a variety of oxidation states (Mn^{II}, Mn^{III}, Mn^{IV}, Mn^{VI}, Mn^{VII})

High temperature thermodynamic data is available for the following Mn-bearing aqueous species:

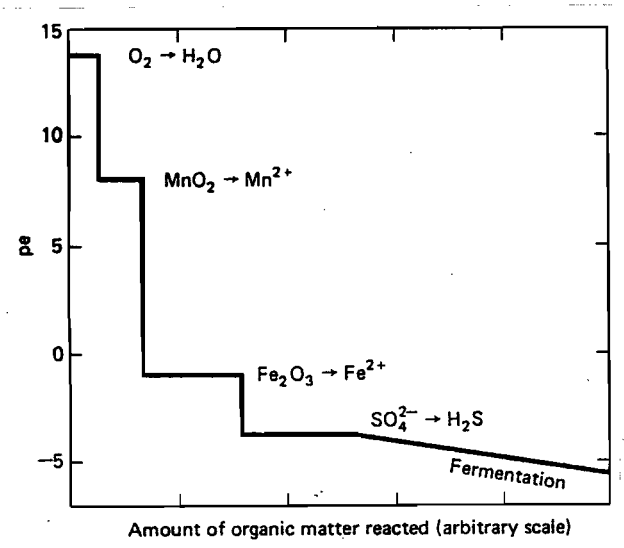

Figure 1 Change in pe of a fresh water in contact with sediment as a function of the amount of organic matter decomposed. The lengths of the various horizontal segments are arbitrary, depending on the amounts of specific solid phases available for reaction. pH is assumed constant at 7.0. (Drever, 1984)

Manganous Species (Mn^{II}: +2 valence state)

- Manganous ion: Mn^{+2}
- Chloride: $MnCl^+$, $MnCl_{2\,(aq)}$, $MnCl_3^-$
- Hydroxide: $MnOH^+$, $Mn(OH)_{2\,(aq)}$, $Mn(OH)_3^-$, $Mn(OH)_4^{-2}$
- Carbonate: $MnCO_{3\,(aq)}$, $MnHCO_3^-$
- Sulfate: $MnSO_{4\,(aq)}$

Manganate Species (Mn^{VI}: +6 valence state)

- Manganate ion: MnO_4^{-2}

Permanganate Species (Mn^{VII}: +7 valence state)

- Permanganate ion: MnO_4^-

For 10 eq. wt % NaCl brines that contain 1 wt % $CO_{2\,(aq)}$ and $\Sigma S = 0.001$ molal, distribution of species calculations have shown that $MnCl_3^-$ and $Mn(OH)_4^{-2}$ are the predominant aqueous manganese species at

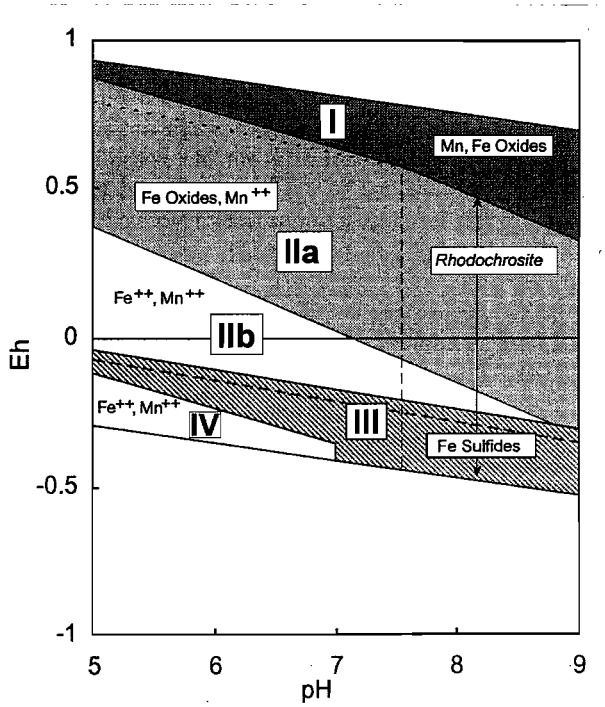

Figure 2 Combination pH–Eh diagram showing redox zonation of black shales based on mineral dissolution (from Quinby-Hunt and Wilde, 1963). Boundaries are based on dissolution of minerals from concentrations observed in oxic seawater. Reduction of NO_3^- to N_2 (indicated by the line of short dashes) is usually considered the boundary between oxic and anoxic conditions. Reduction of SO_4^{2-} to H_2S and HS^- (long dashes) roughly marks the boundary between oxic and sulfidic species. Note that the correspondence is not exact — pyrite can appear within the sulfate stability zone.

150°C (Fig. 3) and 250°C (Fig. 4). Furthermore, $Mn(OH)_4^{-2}$ is only predominant under extremely alkaline conditions (pH > 10), indicating that $MnCl_3^-$ will be the dominant Mn species in saline brines at these temperatures and compositions.

Manganese-bearing minerals

As for the aqueous Mn-bearing species, manganese can occur in a variety of oxidation states within common rock-forming minerals. Examples include:

Mn^{II} (+2 valence state)

- Rhodochrosite: $MnCO_3$
- Rhodonite: $MnSiO_3$
- Alabandite: MnS
- Manganosite: MnO

Mn^{III} (+3 valence state)

- Manganite: MnO(OH)

Mn^{VI} (+4 valence state)

- Pyrolusite: MnO_2

High temperature thermodynamic data is only available for the manganous (+2 valence state) minerals, although Figure 2 illustrates how pyrolusite (the most common Mn-bearing mineral that contains Mn in the +4 valence state) is only stable in equilibrium with highly oxygenated surface waters. Oxygen contents of sediments removed from contact with the atmosphere are too low for pyrolusite to be stable. Consequently, Mn is present as Mn^{II} in minerals formed within the hydrothermal environment.

Figures 5 and 6 illustrate how rhodochrosite ± rhodonite can be precipitated from alkaline to neutral brines at 150° and 250°C respectively. Rhodochrosite is stable at lower pH values than rhodonite, resulting in it being the most common Mn-bearing mineral formed in the hydrothermal environment (e.g. abundant rhodochrosite in some low sulfidation epithermal deposits, which form from near-neutral pH fluids). Rhodonite will be stabilised in preference to rhodochrosite at low $a_{(CO2)}$. Alabandite (MnS) is extremely unlikely to form in the hydrothermal

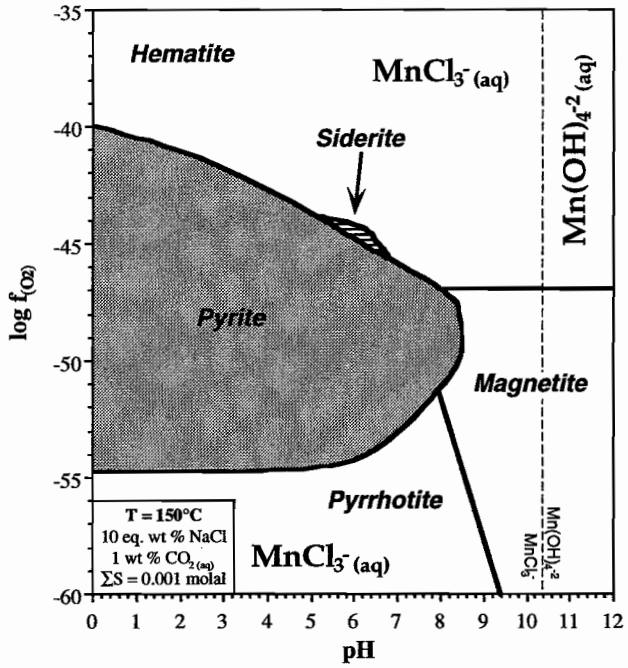

Figure 3 Log fO_2-pH diagram at 150°C showing the predominance fields for aqueous Mn species, together with the stability fields for pyrite, pyrrhotite, hematite, magnetite and siderite. This diagram, and Figures 4 to 8 have been constructed for 10 eq. wt % NaCl solutions that contain 0.001 molal ΣS, 0.256 molal ΣC (≈ 1 wt. % $CO_{2\,(aq)}$), 1 wt. % $CaCl_2$ and 36 ppm Mg^{+2}.

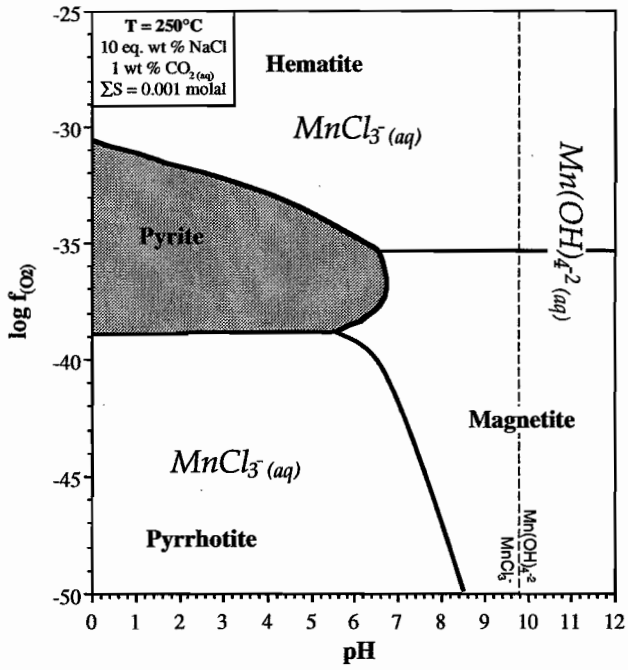

Figure 4 Log fO_2-pH diagram at 250°C showing the predominance fields for aqueous Mn species, together with the stability fields for pyrite, pyrrhotite, hematite, magnetite and siderite. See Figure 3 for the parameters used to construct this diagram.

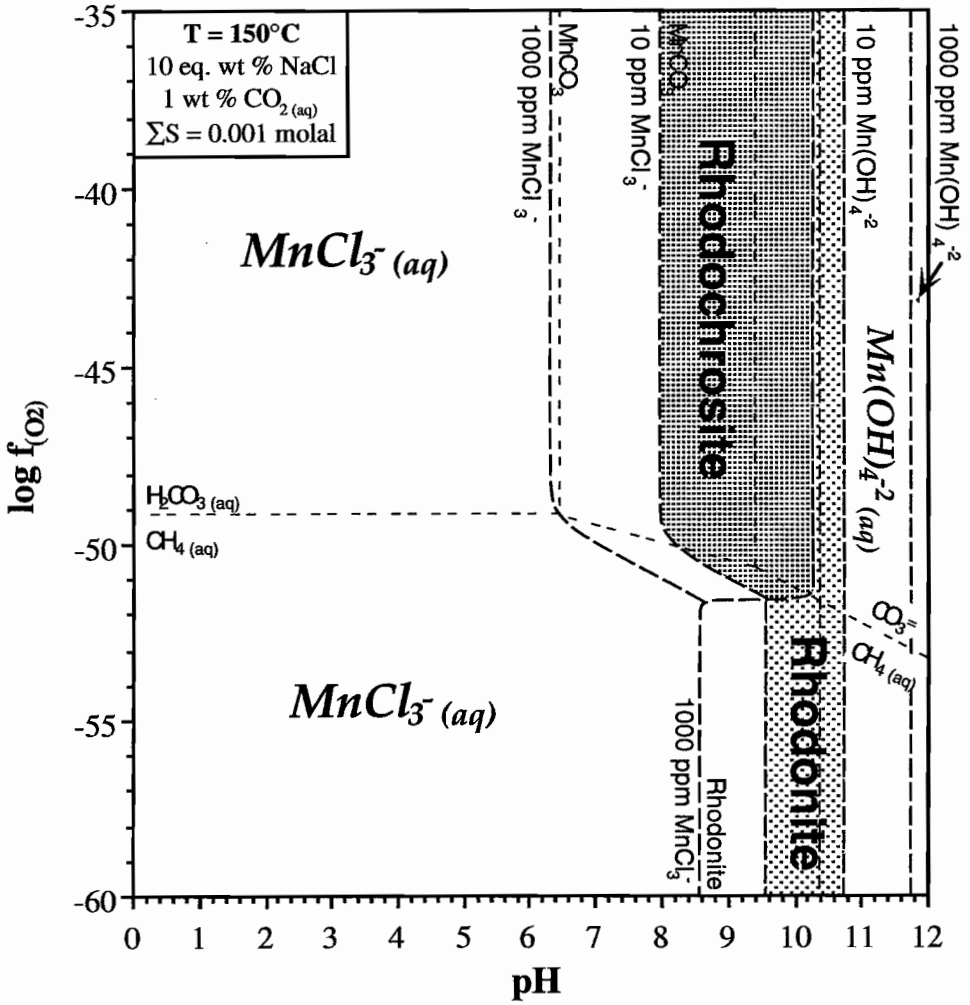

Figure 5 Log fO_2–pH diagram at 150°C showing the predominance fields for aqueous Mn species, together with the stability fields for pyrite, pyrrhotite, hematite, magnetite and siderite, solubility contours for rhodochrosite and rhodonite at Mn^{+2} concentrations of 10 ppm and 1000 ppm. See Figure 3 for the parameters used to construct this diagram.

environment, requiring high ΣS concentrations and/or extremely alkaline (pH > 12) reduced fluids.

At HYC, Mn occurs within dolomite, rather than as a discrete Mn-mineral. Mn substitution into other carbonates can occur at lower pH values than illustrated on Figures 5 and 6. For $a_{(MnCO3)} = 0.1$, the $MnCO_3$–$MnCl_3^-$ solubility contours shift by 0.5 pH units to the left on Figures 5 and 6. The low Mn contents of hydrothermal carbonates at HYC are consistent with deposition from near-neutral, rather than alkaline fluids.

Based on the relationships illustrated in Figures 5 and 6, temperature, pH and salinity control rhodochrosite and rhodonite solubilities in hydrothermal solutions:

$$MnCl_3^- + H_2CO_{3\,(aq)} \Leftrightarrow MnCO_{3\,(s)} + 2\,H^+ + 3\,Cl^-$$

$$MnCl_3^- + H_2O + SiO_{2\,(s,\,aq)} \Leftrightarrow MnSiO_{3\,(s)} + 2\,H^+ + 3\,Cl^-$$

Rhodochrosite and rhodonite will precipitate via pH increase and/or dilution. If alabandite ever became saturated in a sedimentary brine due to high ΣS concentrations, precipitation would occur via pH increase, sulfur loss and/or dilution from highly reduced and alkaline fluids:

$$MnCl_3^- + HS^- \Leftrightarrow MnS_{(s)} + H^+ + 3\,Cl^-$$

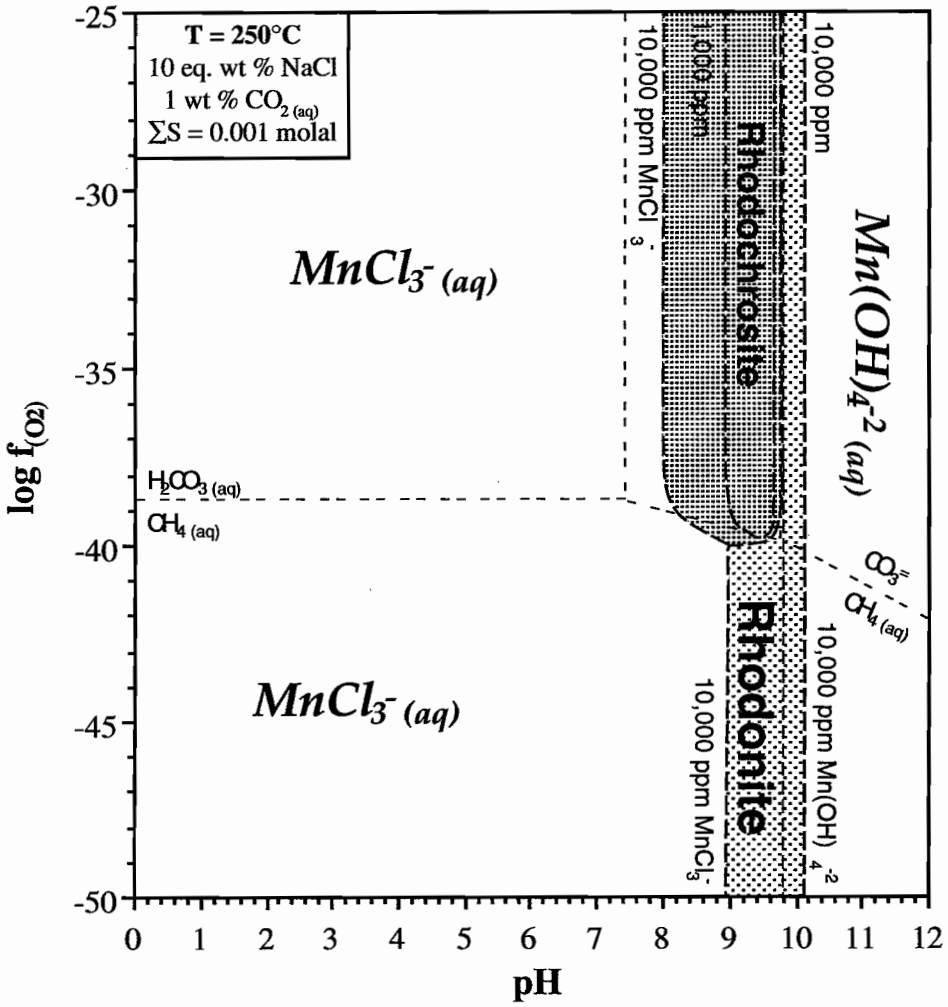

Figure 6 Log fO_2–pH diagram at 250°C showing the predominance fields for aqueous Mn species, together with the stability fields for pyrite, pyrrhotite, hematite, magnetite and siderite, solubility contours for rhodochrosite and rhodonite at Mn^{+2} concentrations of 10 ppm and 1000 ppm. See Figure 3 for the parameters used to construct this diagram.

Implications for sediment-hosted Pb–Zn mineralisation

Figures 7 and 8 illustrate rhodochrosite, rhodonite, galena and sphalerite solubility contours, together with the stability fields for the common iron oxides and sulfides at 150° and 250°C respectively. Figure 8 illustrates how at 250°C, Mn can be transported in large quantities (> 1000 ppm) by reduced and oxidised brines over a pH range of 0 to 6. Consequently, Mn is highly soluble in acid fluids, and is difficult to precipitate at 250°C

At 150°C, Mn can be transported by reduced, acid brines (Region 1), oxidised, acid to neutral brines (Region 2a), and reduced, neutral to alkaline brines (Region 3a). Mn solubilities are low in Region 2b (oxidised, neutral to alkaline brines), with the exact amount of Mn able to be transported in solution depending on the amount of dissolved CO2 in solution, and on the amount of Mn substitution into carbonate minerals.

Region 1 corresponds to the type of fluids Cooke et al. (1995) inferred were responsible for the formation of *Selwyn-type* SEDEX deposits. Based on the calculations presented here, Mn is predicted to be enriched in the ore position sediments, as exhalation of Mn-rich mineralising brines onto the basin floor will cause enrichment of Mn in seawater, and possibly Mn deposition in the sediments

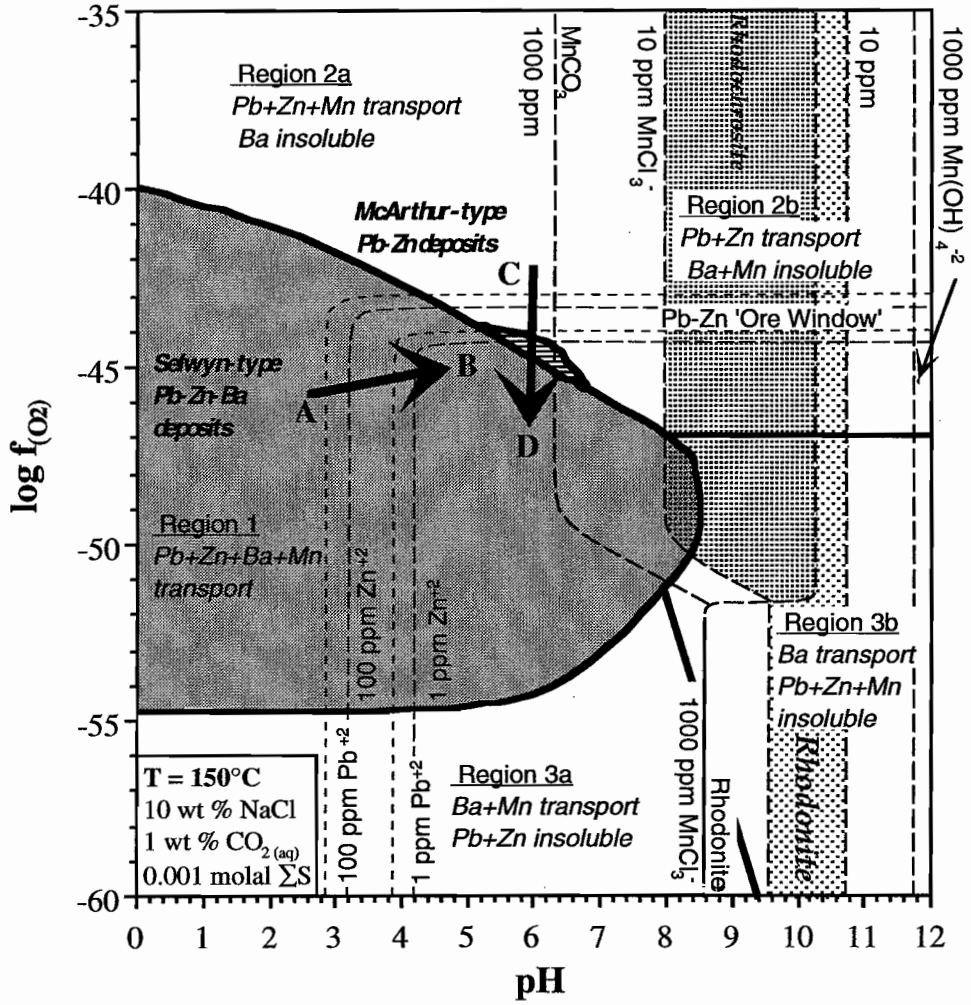

Figure 7 Log fO_2–pH diagram at 150°C. See Figure 3 for the parameters used to construct this diagram. Selwyn-type sediment-hosted Pb–Zn–Ba deposits form from reduced, acidic fluids (region 1) that can carry significant Pb, Zn and Ba in solution. Pb and Zn deposition occurs in response to T decrease, pH increase (A–B), dilution and/or increasing m(H_2S). Barite deposition occurs in response to oxidation via mixing with seawater. McArthur-type sediment-hosted Pb–Zn deposits form from oxidised, carbonate-stable, near-neutral fluids (region 2b) that can carry significant Pb and Zn, no Ba, and low but variable amounts of Mn. Pb and Zn deposition occurs in response to T decrease, reduction (C–D), dilution and/or increased m(H2S). BHT deposits probably form from fluids that have compositions capable of transporting significant Pb, Zn and Mn, but no Ba (region 2a). Depositional mechanisms will be similar to the McArthur-type deposits. Barite-only deposition occurs in region 3 (see Cooke et al., 1995, for further details), from fluids that can transport Ba(± Mn) but no Pb or Zn.

(depending on the redox potential of the basin waters).

The subdivision of region 2 (previously assigned to *McArthur-type* deposits by Cooke et al., 1995) based on the ability of oxidised hydrothermal solutions to transport Mn, has some interesting implications for the relationships of BHT deposits to SEDEX deposits. Although BHT deposits occur in highly metamorphosed environments (preventing determination of original mineralogies), they are characterised by high Mn contents which is reflected in the metamorphic mineralogies (manganiferous garnets, rhodochrosite, rhodonite, etc.). Assuming that no Mn addition occurred during metamorphism, BHT deposits contain significantly more Mn than McArthur-type SEDEX deposits. This appears to be consistent with the basinal environments that the two deposit types formed in. Mn-rich BHT deposits are inferred to have formed in sedimentary basins rich in oxidised clastic sediments and ironstones, but devoid of carbonates (conditions favourable for acid, oxidised fluids and high Mn solubilities; Region 2a

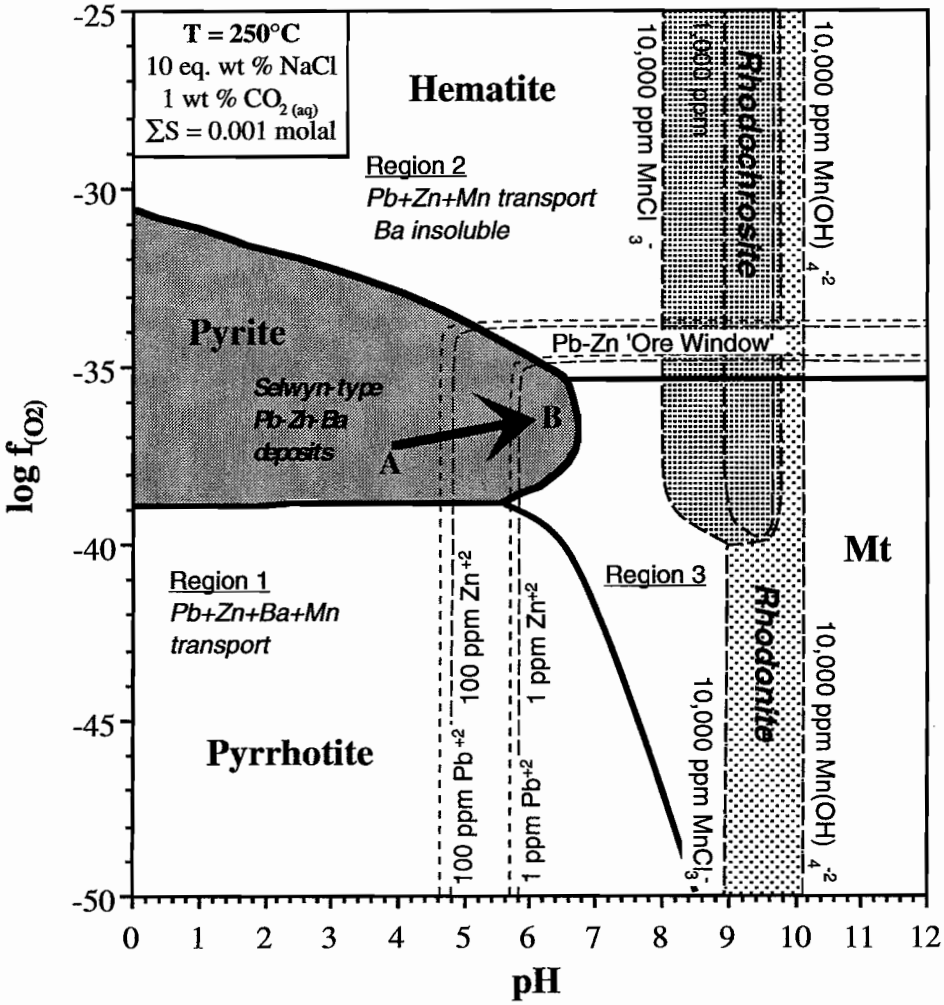

Figure 8 Log fO_2–pH diagram at 250°C. See Figure 3 for the parameters used to construct this diagram. Selwyn-type sediment-hosted Pb–Zn–Ba deposits form from reduced, acidic fluids (region 1) that can carry significant Pb, Zn and Ba in solution. Pb and Zn deposition occurs in response to T decrease, pH increase (A–B), dilution and/or increasing m(H_2S). Barite deposition occurs in response to oxidation via mixing with seawater. McArthur-type sediment-hosted Pb–Zn deposits probably do not form at these temperatures, due to the very high solubilities of Pb and Zn in high temperature, oxidised, saline brines.

of Figure 7). McArthur-type SEDEX deposits are inferred to form from relatively oxidised, near-neutral to alkaline fluids (Region 2b of Fig. 7). that are in equilibrium with thick packages of carbonates and oxidised clastic sediments (Cooke et al., 1995). The BHT and McArthur-type Proterozoic sediment-hosted Pb–Zn deposits are therefore concluded to have formed in different types of oxidised sedimentary basins (those rich in oxidised clastic and carbonate sediments respectively), which has resulted in different fluid chemistries, and different gangue mineral assemblages and alteration minerals.

Depositional processes

Based on the change in rhodochrosite stability from 250° to 150°C (compare Figures 8 and 7), rhodochrosite will be less soluble in lower temperature hydrothermal fluids (at constant $a_{(CO2)}$). Mn is insoluble in oxygenated surface waters, where it occurs in the +4 valence state. Pyrolusite (rather than rhodochrosite) will be stable at these conditions. Consequently, Mn can be precipitated from hydrothermal solutions as rhodochrosite or manganiferous carbonates at 150°C by pH increase, dilution, cooling and/or mixing with cold, oxygenated groundwaters.

Mixing of hydrothermal fluids with seawater can cause pH increase, dilution, cooling, and oxygenation, all of which would favour Mn deposition from a sedimentary brine, and may have been important for Mn enrichment around BHT (and McArthur-type?) deposits. Sub-surface carbonate replacement should also cause pH increase and cooling, favouring Mn deposition (important for Mn halos around McArthur-type deposits?). The relative efficiency of these two processes for Mn precipitation needs to be assessed further, as do controls on Mn substitution in dolomite.

References

Calvert, S.E., and Pedersen, T.F., 1996. Sedimentary geochemistry of manganese: implications for the environment of formation of manganiferous black shales. Economic Geology, 91, 36–47.

Cooke, D.R., Large, R.R., McGoldrick, P.J., and Bull, S.W., 1995. Two classes of sediment-hosted Pb–Zn deposits. AMIRA/ARC p.384, Final Report, 345–370.

Drever, J.I., 1984. The geochemistry of natural waters. Prentice-Hall, N.J.,p. 234.

Quinby-Hunt, M.S., and Wilde, P., 1993. Thermodynamic zonation in the black shale facies based on iron–manganese–vanadium content. Chemical Geology, 113, 297–317.

Quinby-Hunt, M.S., and Wilde, P., 1996. Chemical depositional environments of calcic marine black shales. Economic Geology, 91, 4–13.

Lithogeochemistry and isotope chemostratigraphy of the Barney Creek Formation, McArthur Basin

Ross R. Large and Stuart Bull
Centre for Ore Deposit and Exploration Studies, Geology Department, University of Tasmania

Summary

Lithogeochemical studies of the Barney Creek Formation at various localities in the McArthur Basin have confirmed the use of the alteration indices — sedex AI, AI_3 and MnO_D — as vectors to ore, over a distance of about 20 km. It is recommended that these three indices be used in conjunction with Zn, Pb, Tl and ankerite ratio to (a) identify distal horizons favourable for stratiform Pb–Zn mineralisation, and (b) provide vectors for follow-up drilling.

Carbon and oxygen isotope ratios of dolomitic siltstones in the Barney Creek Formation have proved to be a powerful method for discriminating MnO_D and AI_3 haloes directly related to ore, from those which indicate a favourable horizon for Pb–Zn. Anomalies in MnO_D, AI_3 and Zn, Pb associated with ore exhibit $\delta^{18}O > 23‰$ and $\delta^{13}C < -2‰$, whereas anomalies unrelated to ore (or very distal from ore) exhibit $\delta^{18}O < 23‰$ and $\delta^{13}C > -2‰$.

Preliminary research on K–Al silicate relationships in the BCF suggest that the favourable horizon close to ore has a high illite/K-feldspar ratio (i.e. illite dominant) while distal horizons display low illite/K-feldspar ratios (i.e. K-feldspar dominant). Also the barium content of potassium silicates in the HYC Pyritic Shale appears to increase towards ore.

Introduction

Systematic sampling of the Barney Creek Formation, host to the HYC ore deposit, has been undertaken at a number of localities throughout the McArthur Basin (Fig. 1). The purpose of this investigation has been:

- to determine the sedimentological environment of the Barney Creek Formation
- to study the geochemistry of sediments distal to the HYC deposit
- to characterise the nature and extent of the lithochemical and mineralogical halo surrounding the HYC deposit
- to study isotope (C/O) chemostratigraphy of the Barney Creek Formation and determine whether an isotope halo surrounds the ore deposit
- to develop a basket of indices which can be applied to locate favourable horizons for stratiform Pb–Zn mineralisation
- to develop direct vectors to ore

This research commenced in AMIRA Project P384 and is on-going in Project P384A.

Previous work on AMIRA Project P384

Results of our previous work on geochemical halos and vectors to the HYC deposit are summarised in the P384A Project Outcomes Report (June 1995: 16) and repeated below.

Published data on the HYC geochemistry (Lambert and Scott, 1973) was initially compared with the halo model developed for Lady Loretta (Report 3: 91–126). This comparison revealed remarkable similarity between the Lady Loretta halo and HYC halo. However, the HYC manganese halo was found to be far more extensive (up to 23 km along strike) and siderite was lacking from the district. The geochemical vectors (AI and MnO_D) developed

at Lady Loretta were found to be directly applicable to HYC. For example, MnO_D in the footwall sediments increases systematically towards the favourable horizon from a background of 0.5 wt % up to 1–12 wt % MnO_D over about 50 m. AI_3 increases along strike towards the deposit, over 25 km, from values of 30–40 to 70–100. Factors contributing to the alteration index were studied in a series of mixing models (Report 7: 45–68) which reproduced the trends shown in the HYC ores and wall rocks.

Further sampling and sedimentological studies of DDH BMR 2 and DDH Barney 3 in the McArthur Basin showed a relationship between sedimentary facies and the alteration indices (Report 7: 99–114; Final Report: 159–182) which allowed the formulation of a relationship between sedimentary facies and mineralising events (Final Report: 371–408). Microprobe analyses of carbonates from DDH BMR 2 (Final Report: 283–288) confirmed that the whole-rock calculations of MnO_D were justified and closely correlate with the microprobe analyses of mineral chemistry. Studies utilising the XPLOR® program enabled the distinction between dolomite and ankerite in the HYC drill holes, and showed the presence of an extensive halo of ankerite-bearing sediment surrounding HYC (Final Report: 273–282). Although the MnO_D, AI_3, ankerite and zinc halos at HYC overlap, they have important spatial and chemical differences which all contribute to the overall halo model and alteration vectors developed for HYC (Fig. 2).

This report

Sampling and geochemical analyses have now been completed on two further drill holes (Homestead 6 and Barney Creek 3), in addition to the ground traverse at Top Crossing. Results from these three localities are reported here and compared to the previous studies on DDH BMR 2 (Bull, 1995; Bull & Large, 1995). Results of the isotope chemostratigraphy are reviewed and a basket of vectors to ore is developed from the lithochemistry and isotope studies.

DDH Barney Creek 3

Diamond drill hole Barney Creek 3 is located 15 km southwest of the HYC deposit. It was collared in Reward Dolomite and intersected a 184 m section of HYC Pyritic Shale followed by 42 m of the W-Fold Shale Member (Fig. 3).

Sedimentological summary of DDH Barney Creek 3

W-Fold Shale Member

Thickness — >41.7 m (311 m to the bottom of the hole at 352.7m; Fig. 3).

Description — interbedded thinly-bedded to laminated, pale grey, recrystallised dolomite and black carbonaceous siltstone/shale (Shannon et al., 1981) which is locally brecciated (?stylo-brecciated).

Contact with undifferentiated Barney Creek Formation — sharply marked at 311 m by an abrupt upsection change from interbedded dolomite and shale to massive pyritic mudstone, the core of which is extensively disaggregated.

Undifferentiated Barney Creek Formation

Thickness — 184 m (127–311 m)

Description — much of the core of this interval, particularly towards the base, is extensively disaggregated due to pervasive internal fracturing making sedimentary facies determination difficult in places. Overall it appears that at least the lowermost 46 m (which is more extensively fractured than the remainder), and possibly the lowermost 100 m, comprises the massive carbonaceous ± pyritic mudstone facies. The overlying 80–138 m appears to be dominated by the thinly-bedded dolomitic sandstone/siltstone/mudstone facies. It is interesting that the relative deepening event recorded in the upper part of the undifferentiated Barney Creek Formation in DDH BMR McArthur 2 (Bull, 1995) is not clear on the facies log. However, a distinct kick in TOC values at this level (Fig. 3) is regarded as evidence of the deepening event in this intersection.

Contact with Reward Dolomite — gradational over 7 m (from 120–127 m) characterised by an upsection increase in the proportion of recrystallised grey

dolomite and resultant decrease in the proportion of grey to black siltstone/shale.

Lithochemistry and alteration vectors

Twenty-six samples collected at regular intervals down the drill hole were analysed for major and selected trace elements at the Geology Department, University of Tasmania. Results are tabulated in Appendix 1 and plotted as a series of downhole plots in Figures 3 and 5.

Zinc (Fig. 3) — The maximum zinc values (> 1000 ppm) occur in the base of the HYC Pyritic Shale 260–290 m downhole. This corresponds with the ore position at HYC. An anomalous spike at 165 m downhole may represent the position of the hanging wall zinc marker at HYC. The lower zinc anomaly confirms that the zinc halo surrounding the HYC deposit extends at least 15 km south west of HYC. However, the zinc halo was not detected in DDH BMR2, 23 km southwest of HYC.

Alteration Index Mark 3 (Fig. 3) —

$$AI_3 = \frac{(10Mn) + FeO) \times 100}{(FeO + 10MnO = MgO + Al_2O_3)}$$

This index was established to respond to changes in (a) the composition of carbonate, (b) the shale/dolomite ratio and (c) pyrite content of the sediments; all of which show systematic trends in proximity to stratiform Pb–Zn deposits (Large, 1994c)

AI_3 values greater than 30 are considered anomalous (Large, 1994c). AI_3 reaches a maximum at the base of the HYC Pyritic Shale and top of the W-Fold Shale. Five values of > 30 are recorded in this zone (270–330 m). A second anomaly (AI_3 = 25 to 30) occurs at a depth of 150 m down hole, toward the top of the HYC Pyritic Shale.

Manganese content of dolomite (MnO_D) — Maximum values of 1.5 to 2.0 wt % MnO in dolomite occur in the W-Fold Shale at the bottom of the drill hole. The concentration of MnO in dolomite immediately below the base of the HYC Pyritic Shale (equivalent to the ore position at HYC) is similar to that recorded in drill holes at HYC (Large & McGoldrick, 1993) and DDH BMR 2 (Bull & Large, 1995).

Thallium (Fig. 3) — Peak values of 9 and 25 ppm occur toward the base of the HYC Pyritic Shale in the equivalent ore position. Background values of less than 4 ppm, occur through the middle to upper HYC Pyritic Shale, W-Fold Shale and the Reward Dolomite.

Dolomite distribution and composition: — The variation in dolomite content of the BCF sediments, calculated from the CaO and CO_2 whole rock values is shown in Figure 4. A systematic increase in dolomite is apparent from the pyritic base of the HYC Pyritic Shale (2–20% dolomite) to the top of the member and across the gradational contact with the Reward dolomite (50–60 % dolomite). The plot of CaO vs CO_2 in Figure 5 shows that dolomite/ankerite is the dominant carbonate mineral in the Barney Creek 3 drill hole. Neither siderite nor calcite are present in significant amounts. Previous studies by Large & Duhig (1995) indicate that the dolomite composition varies systematically downhole with the more ankeritic carbonate [(Fe + Mn)/Mg molar ratio > 0.25)] occurring at the base of the HYC Pyritic Shale (ore position) and the top of W-Fold Shale. The lack of ankerite in DDH BMR 2, indicates that DDH Barney 3 intersects the outer zone of the ankerite halo to HYC (Fig. 6)

Assessment of geochemical vectors for Barney Creek 3

The relationship between zinc and AI_3 shown in Figure 7a indicates a positive trend extending from the background region toward the ore zone. On the MnO_D vs AI_3 plot (Fig. 7b)only one sample (4% of data) occurs in the priority 2 zone, and four samples (15% of data) fall in the priority 3 zone.

Summary of Barney Creek 3 geochemistry

- At a distance of 15 km from HYC, the favourable horizon (ore position) is clearly indicated by the anomalies in AI_3, MnO_D, Zn, Pb, Tl and pyrite over the zone 250–300 m downhole
- this zone also corresponds with an increase in the Fe content of dolomite sufficient to form ankerite
- At 15 km from ore, the data indicate a priority rating for follow-up of: priority 2 (4% of data), and priority 3 (15% of data)

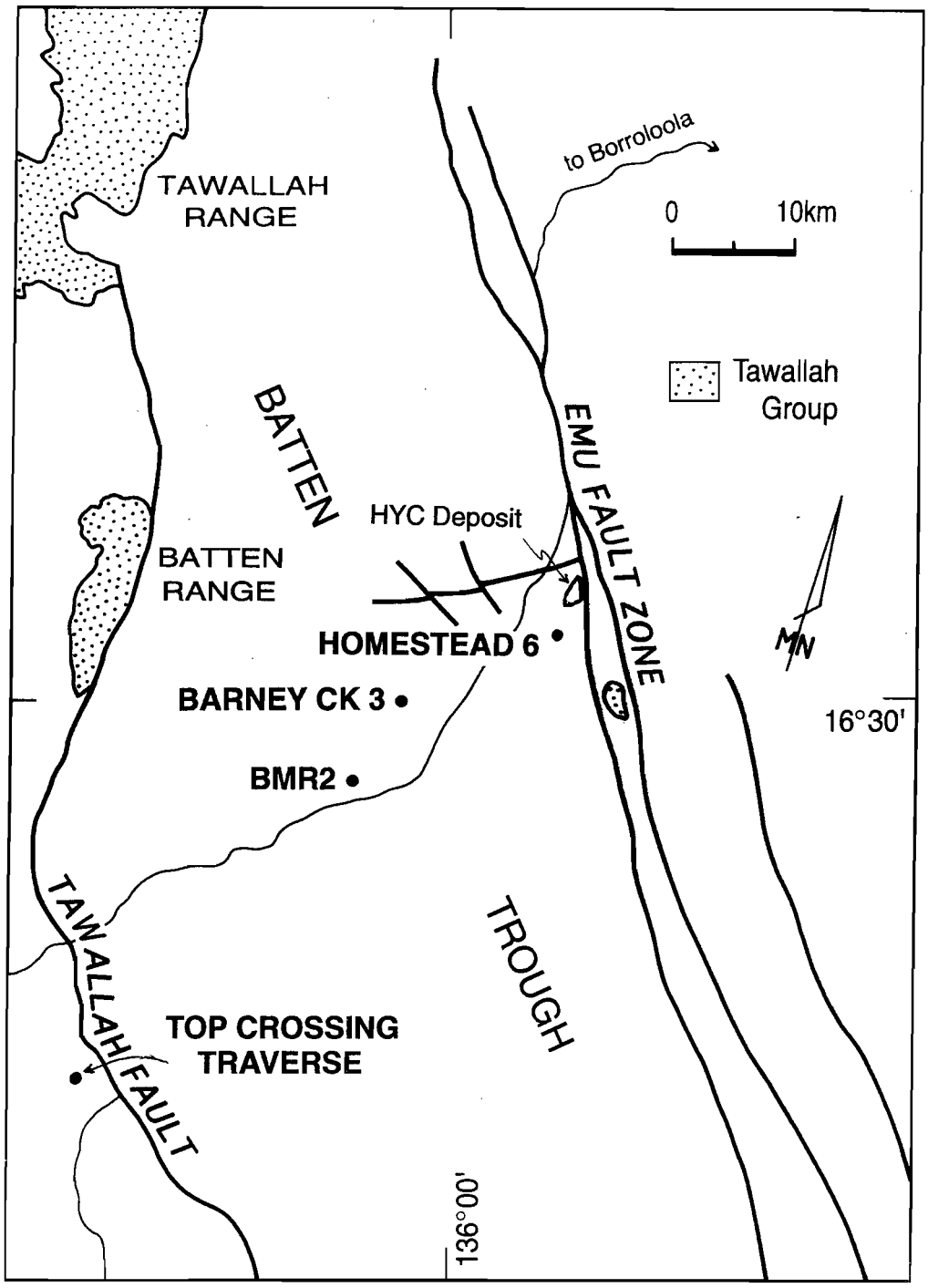

Figure 1 Locality diagram showing position of drill holes and traverses sampled in this study.

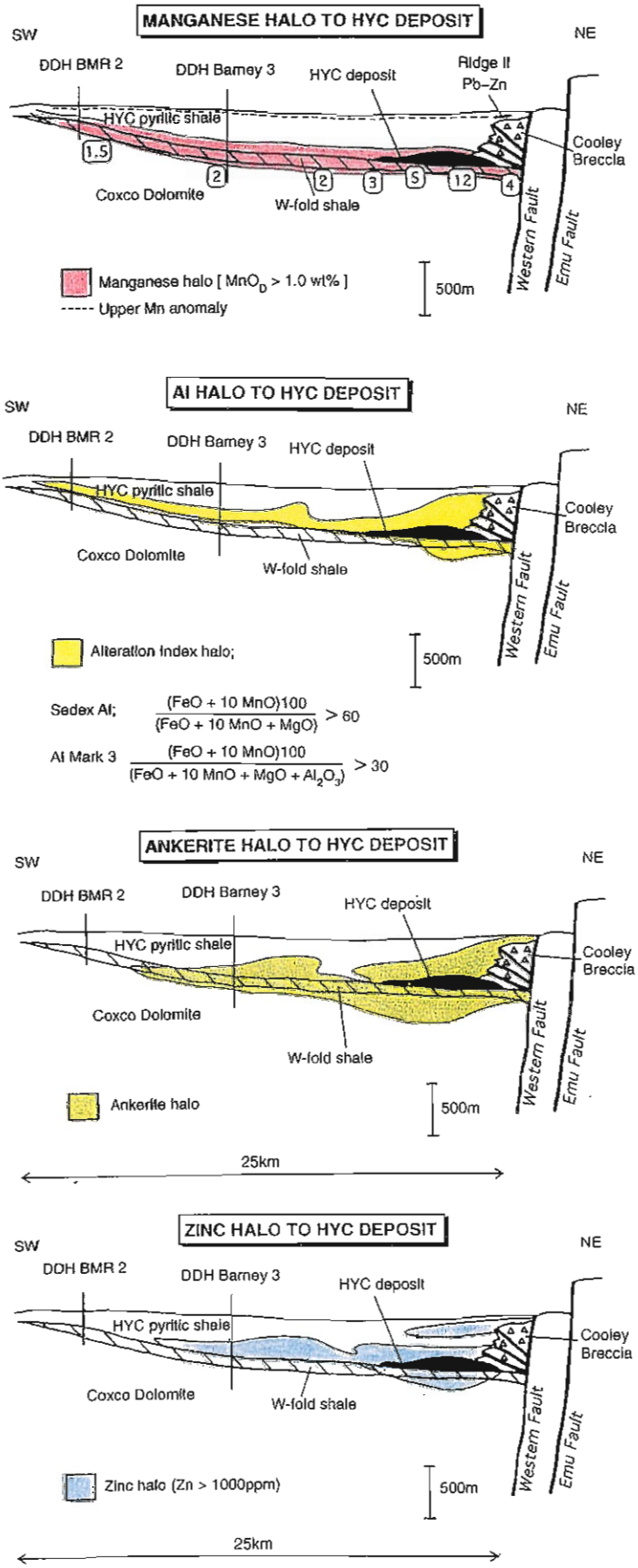

Figure 2 Halo model for the HYV deposit, McArthur Basin (from P 384 Project Outcomes Report, 1995).

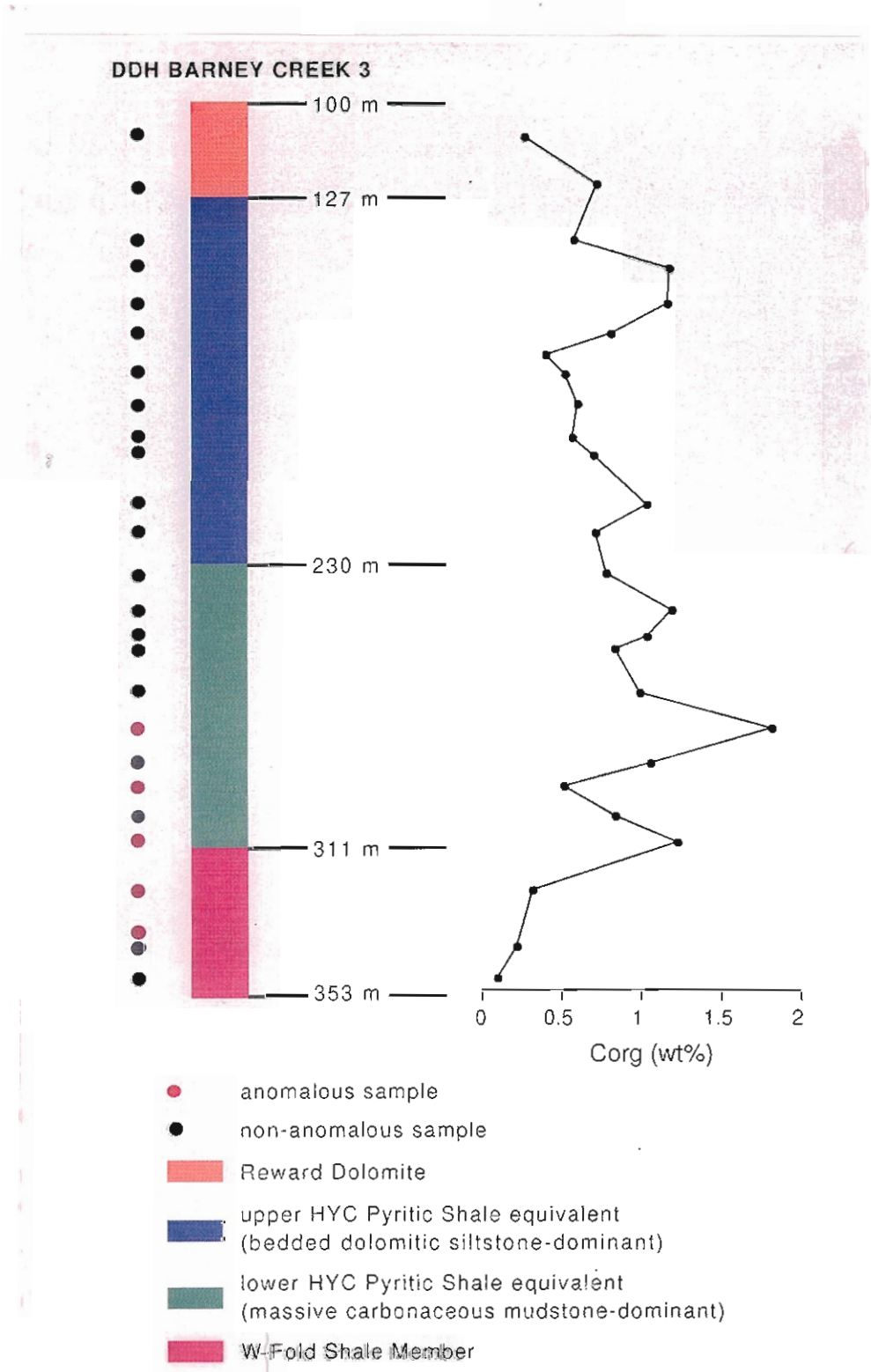

Figure 3 Sedimentology summary log, sample locations and organic carbon content of DDH Barney Creek 3.

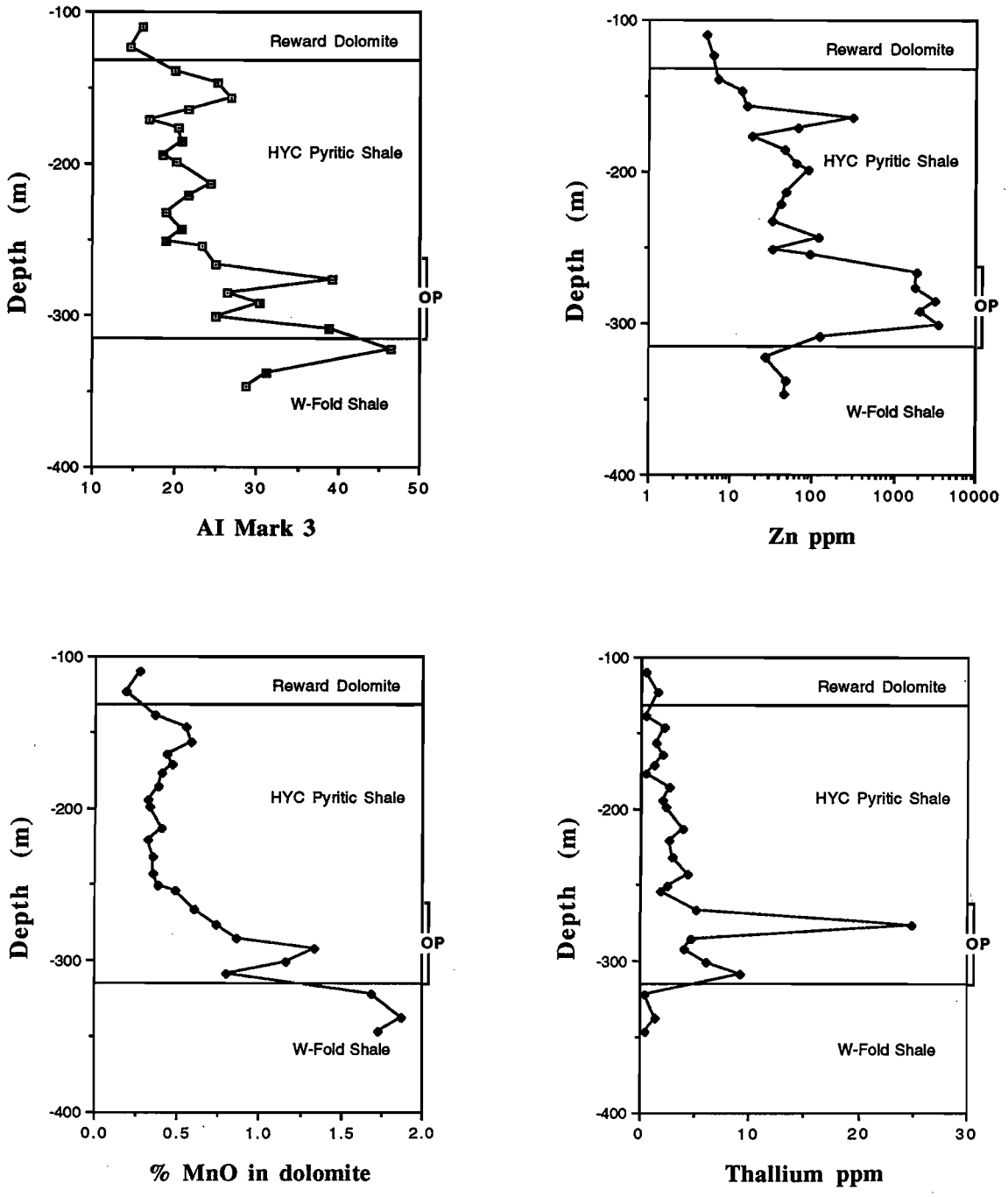

Figure 4 DDH Barney Creek 3; downhole variation in AI_3, Zn, MnO_D and thallium

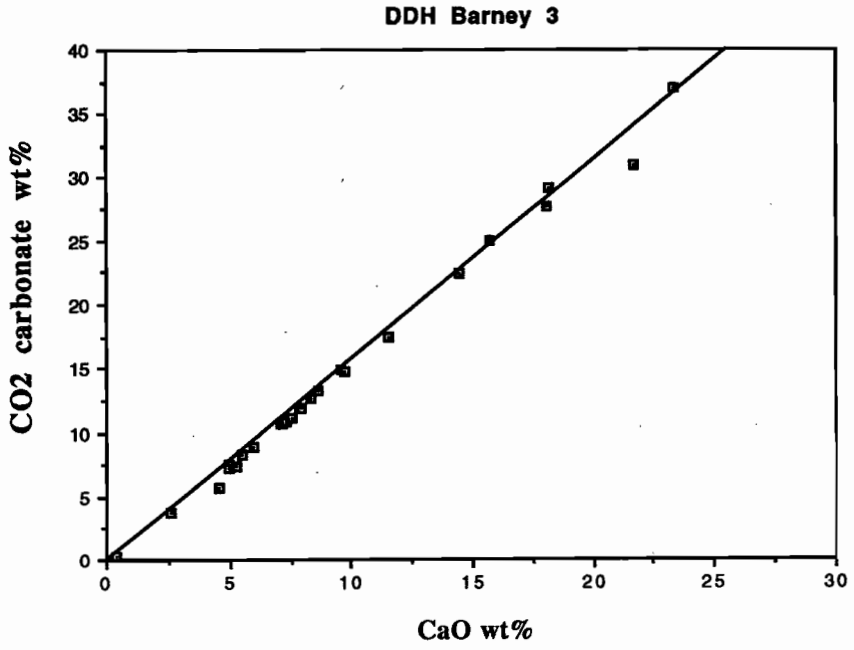

Figure 5 CaO vs CO_2 for samples from Barney Creek 3, showing that all data fall close to the pure dolomite line. There is no evidence of significant siderite or calcite in the sample set.

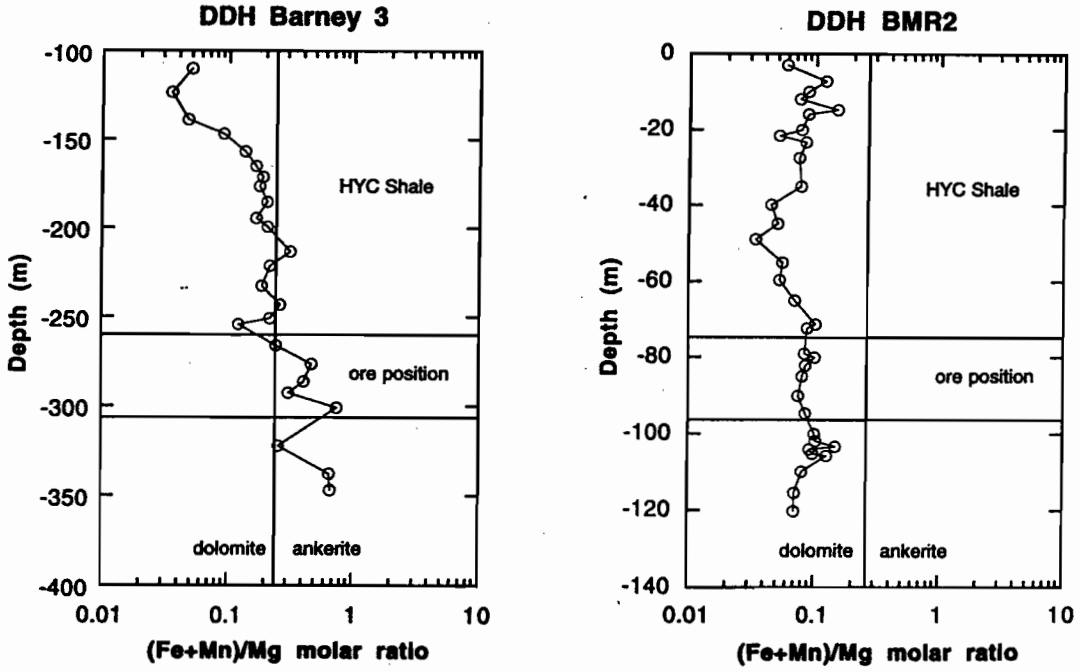

Figure 6 Variation in ankerite ratio; [(Fe + Mn)/Mg] molar ratio, in DDH Barney Creek 3 (from Large and Duhig, 1995).

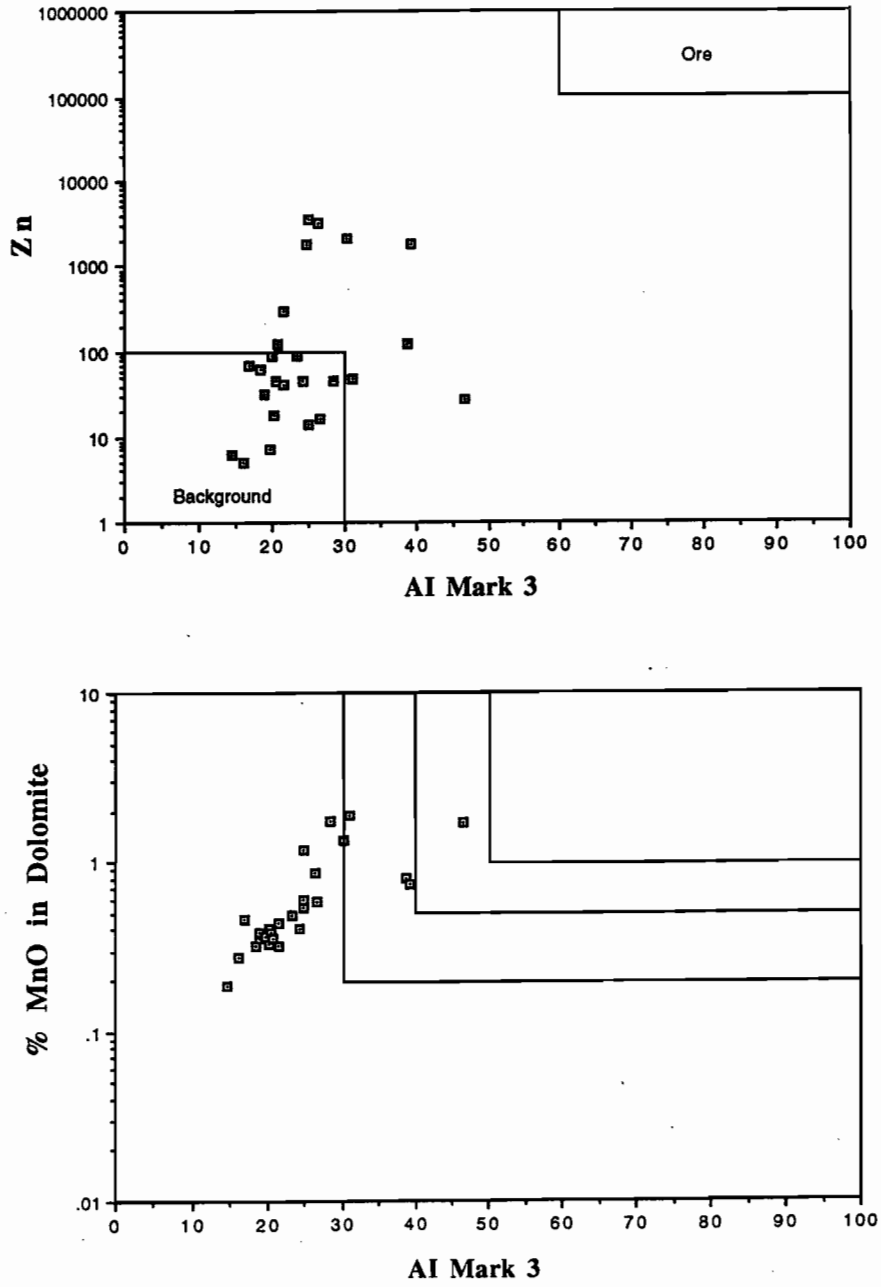

Figure 7 (a) Zn vs AI_3 for DDH Barney Creek 3 samples; (b) AI_3 vs MnO_D with priority boxes marked. Only one sample (4% of data) falls in the priority 2 zone.

DDH Homestead 6

This diamond drill hole was collared 1.9 km south of the southwestern margin of the HYC deposit (Fig. 1). The hole intersected a sequence of strongly pyritic black dolomitic mudstones of the Barney Creek Formation and provides an ideal opportunity to examine the lithochemistry of the host sedimentary package close to HYC.

The condition of the drill core is very poor and it was not possible to undertake sedimentological studies on the hole. The geochemical data indicate that the hole intersected 175 m of HYC Pyritic Shale, followed by 50 m of W-Fold Shale. Twenty samples were collected at roughly 10 m intervals over the section from 43 to 225 m. Analytical data for the samples are given in appendix 1 and selected downhole plots are provided in Figures 8 and 9.

Zinc (Fig. 8) — Anomalous zinc values of 1100–7560 ppm occur throughout the HYC Pyritic Shale intersected in the drill hole. Sediments interpreted to be W-Fold Shale (Based on MnO_D values) exhibit zinc values of less than 25 ppm.

Alteration Index Mark 3 (AI_3) — Peak values greater than 50 occur over the interval from 40 to 125 m downhole. Unlike the pattern in the orebody (e.g. DDH Te 115) and for DDH Barney Creek 3 (Fig. 5), the AI_3 shows a marked low at the base of the HYC Pyritic Shale.

Manganese content of dolomite (MnO_D) — MnO content of dolomite increases systematically from the base of the drill hole (225 m) up to 192 m where a peak value of 1.8% MnO_D occurs. This position is interpreted to correspond to the top of the W-Fold Shale. MnO_D values in the HYC Pyritic Shale range from 0.4 to 1.0% similar to those recorded in the ore zone (e.g. DDH O 123, Large & McGoldrick, 1993: 99).

Thallium — All 15 samples through the HYC Pyritic Shale exhibit anomalous thallium values (> 4 ppm) reaching a peak of 118 ppm at 90 m downhole.

Priority rating based on alteration vectors — The Zn vs AI_3 plot (Fig. 10a) shows two distinct trends. The low zinc sediments show a linear flat trend extending out of the background box, which is separate from the high zinc sediments which show a similar range of AI_3 values from 20–60. This suggests that the sphalerite in the high zinc samples may be present as remobilised veins rather than stratiform layers. Petrographic studies are planned to resolve this problem.

On the priority diagram of MnO_D vs AI_3 (Fig. 10b) 50% of the samples plot in the priority 2 zone and a further 25% plot in the priority 3 zone. No samples plot in the priority 1 zone, even though this drill hole is less than 2 km from a major stratiform Pb–Zn deposit.

Summary of Homestead 6 geochemistry

- At a distance of 1.9 km from ore, all the vector indicators show strong anomalies within the host sediment package:
  - Zn 1000–7000 ppm
  - Tl 20–120 ppm
  - AI_3 40–65
  - Pb 200–800 ppm
- MnO_D shows a characteristic increase in the footwall of the favourable horizon reaching values of 1.8 wt % MnO_D.
- Pyrite content of the host package is considerably increased, varying from 10 to 30 wt % throughout the favourable horizon
- However, no samples gained a priority 1 rating on the MnOD vs AI_3 diagram; 50% rated priority 2 and a further 25% rated priority 3.

Top Crossing traverse

The Top Crossing area was selected for lithochemical study as it represents a well-exposed section of the Barney Creek Formation distal from known mineralisation. Previous geochemical studies by Brown et al. (1969) had indicated the presence of anomalous manganese-bearing sediments in the BCF at this locality. The traverse selected for sampling at Top Crossing is located 60 km southwest of the HYC deposit and 3 km west of the Twallah Fault, a regional fault striking roughly parallel to the Emu Fault (Fig. 1). Twenty-six samples of the BCF were collected along a NW-trending traverse line extending from the base to the top of the BCF over a stratigraphic thickness of 120 m. Analytical results are presented

in Appendix 1, and selected plots are given in Figures 11, 12 and 13.

Discussion of lithochemistry and alteration vectors

All samples along the traverse contain less than 30 ppm Zn and less than 3 ppm Tl. No anomalous zones are indicated for these elements. A distinct AI_3 and MnO_D anomaly occurs in the interval 40–60 m stratigraphically above the base of the BCF. These alteration vectors indicate the presence of an horizon favourable to stratiform Pb–Zn mineralisation.

Priority rating

On the Zn vs AI_3 plot only two samples, representing 8% of the data, fall outside the background (Fig 13a). In Figure 13b, one sample (4% of data) lies in the priority 2 zone and a further two samples (8% of data) lie in the priority 3 zone.

Summary of Top Crossing geochemistry

- AI_3 and MnO_D anomalies define a favourable horizon for stratiform Pb–Zn mineralisation in the lower BCF at Top Crossing
- Background Zn and Tl values indicate no mineralisation on this horizon in the vicinity of Top Crosing
- Alteration vector plots indicate a very low priority for follow-up, with only 4% of samples in priority 2

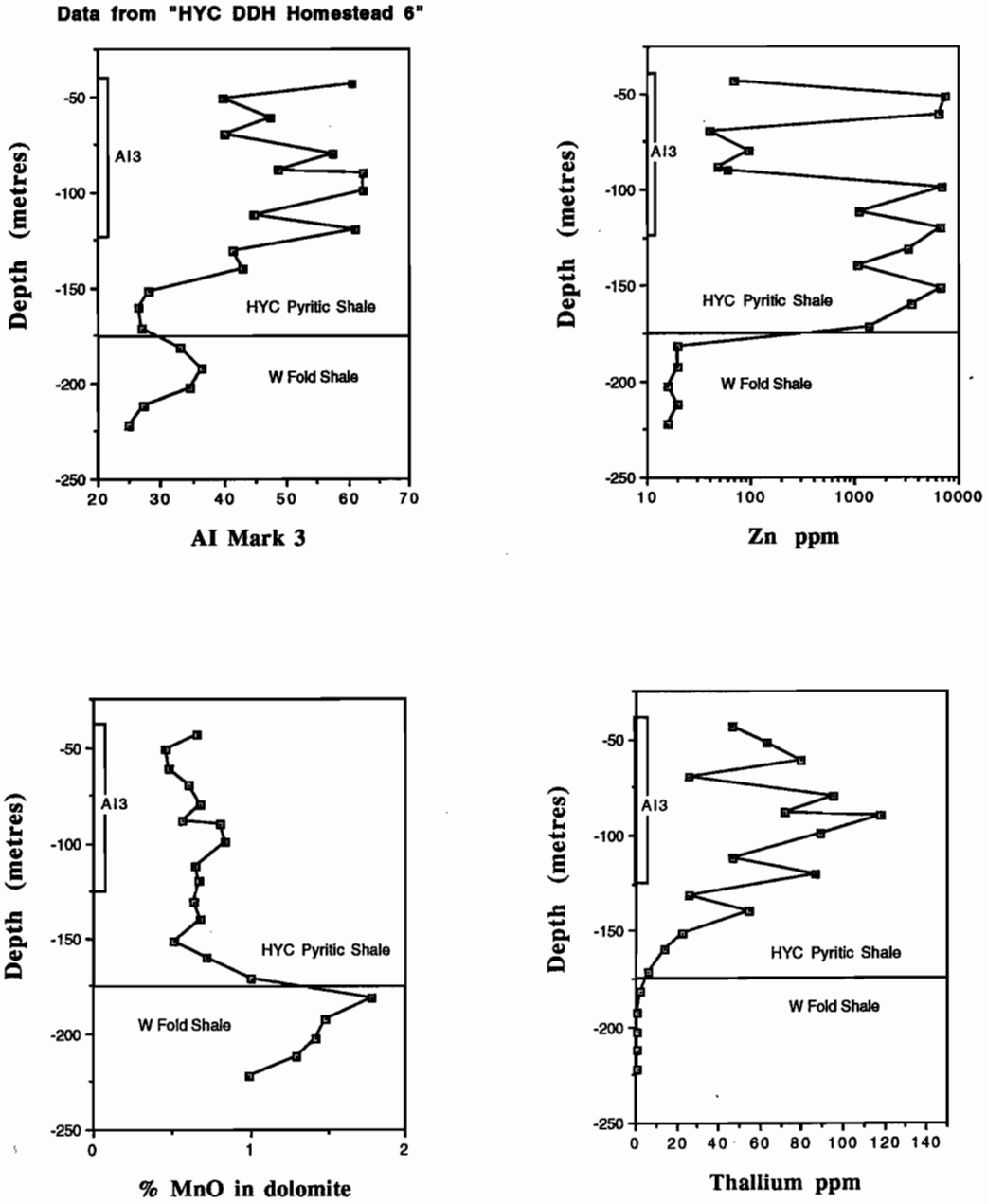

Figure 8 DDH Homestead 6; downhole variation in Al_y, Zn, MnO_D and thallium.

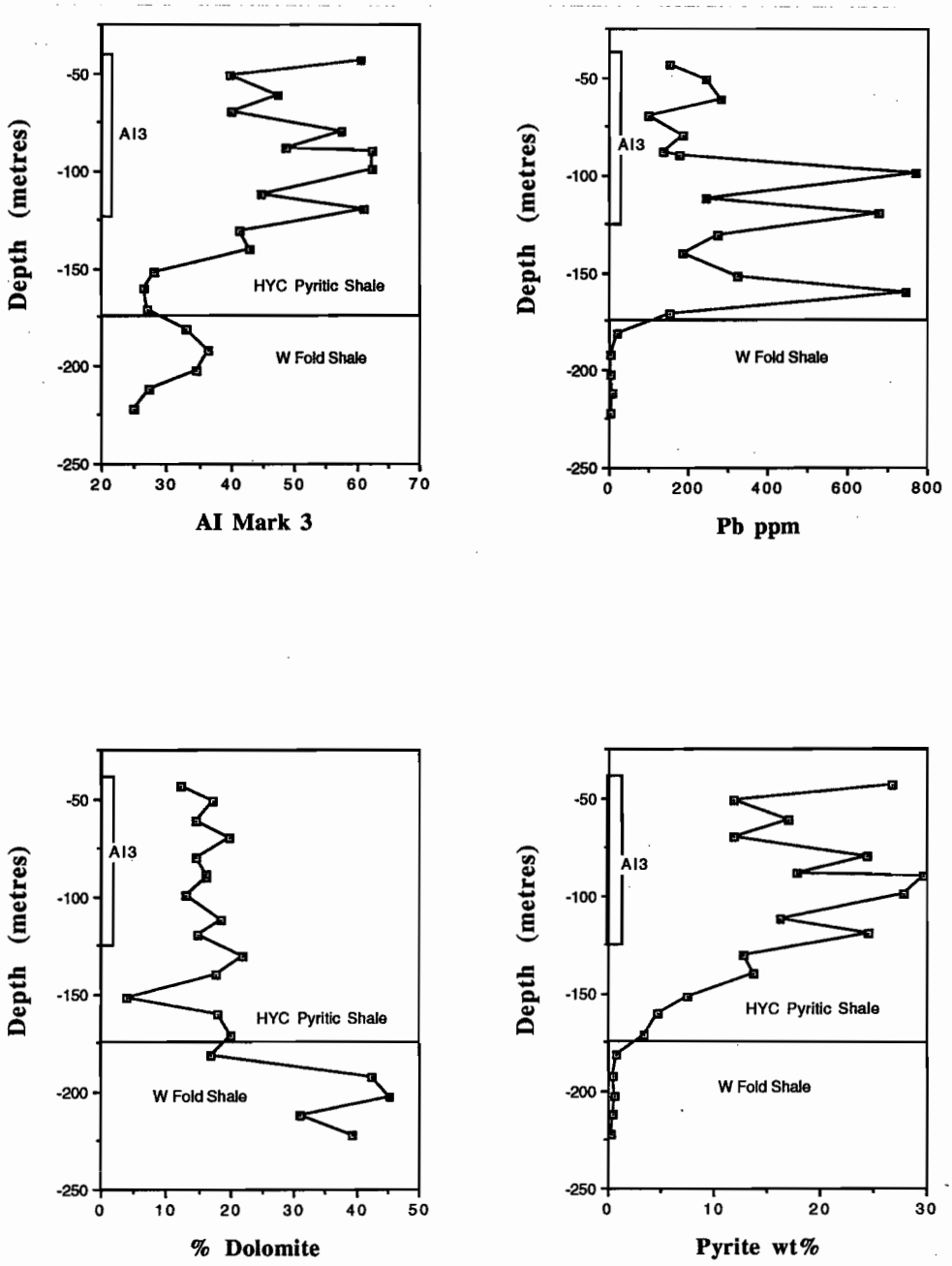

Figure 9 DDH Homestead 6; downhole variation in Al_3, Pb, calculated dolomite content and calculated pyrite content.

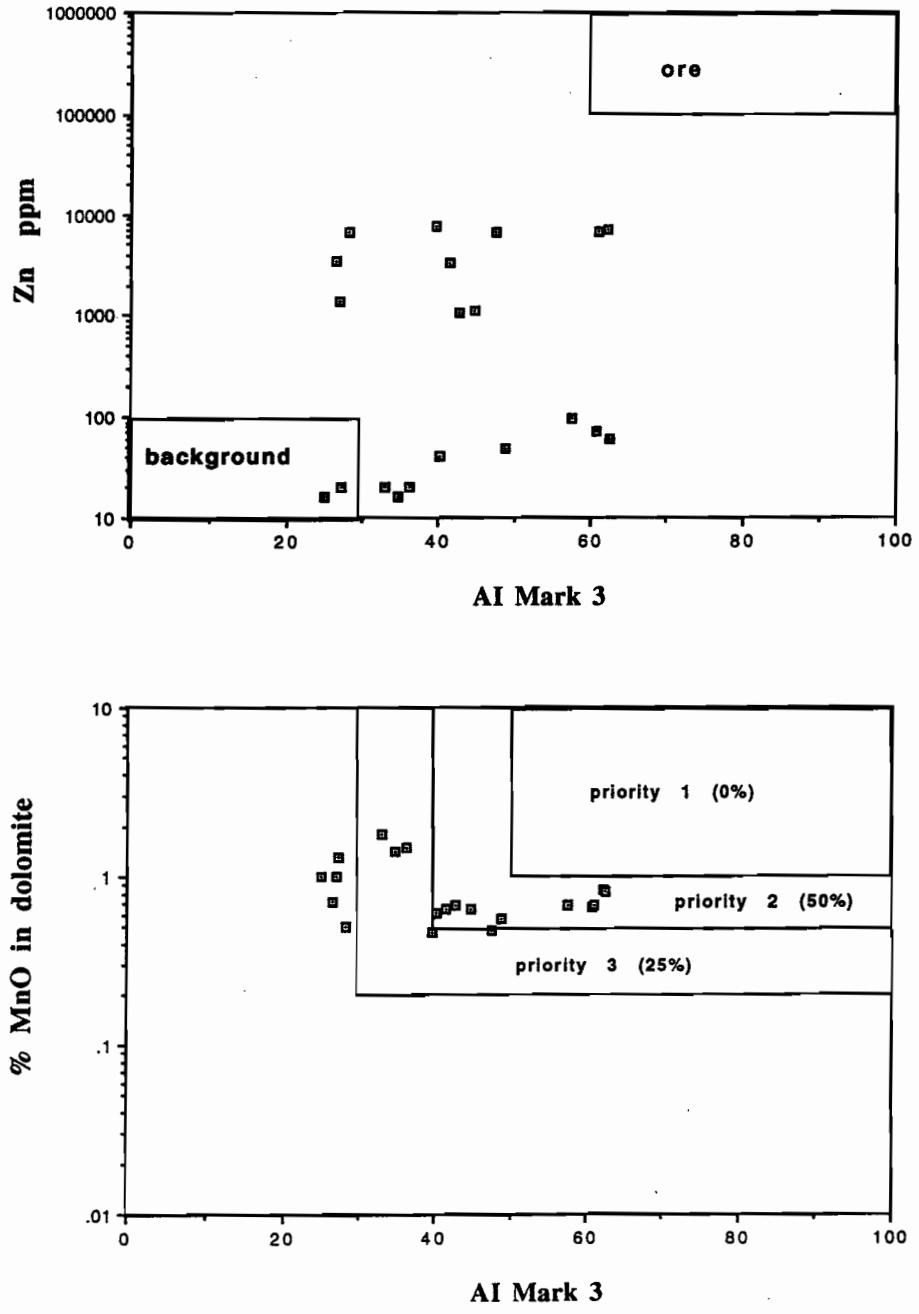

Figure 10 (a) AI_3 vs Zn for DDH Homestead 6 samples; (b) AI_3 vs MnO_D; 50% of samples fall in the Priority 2 zone.

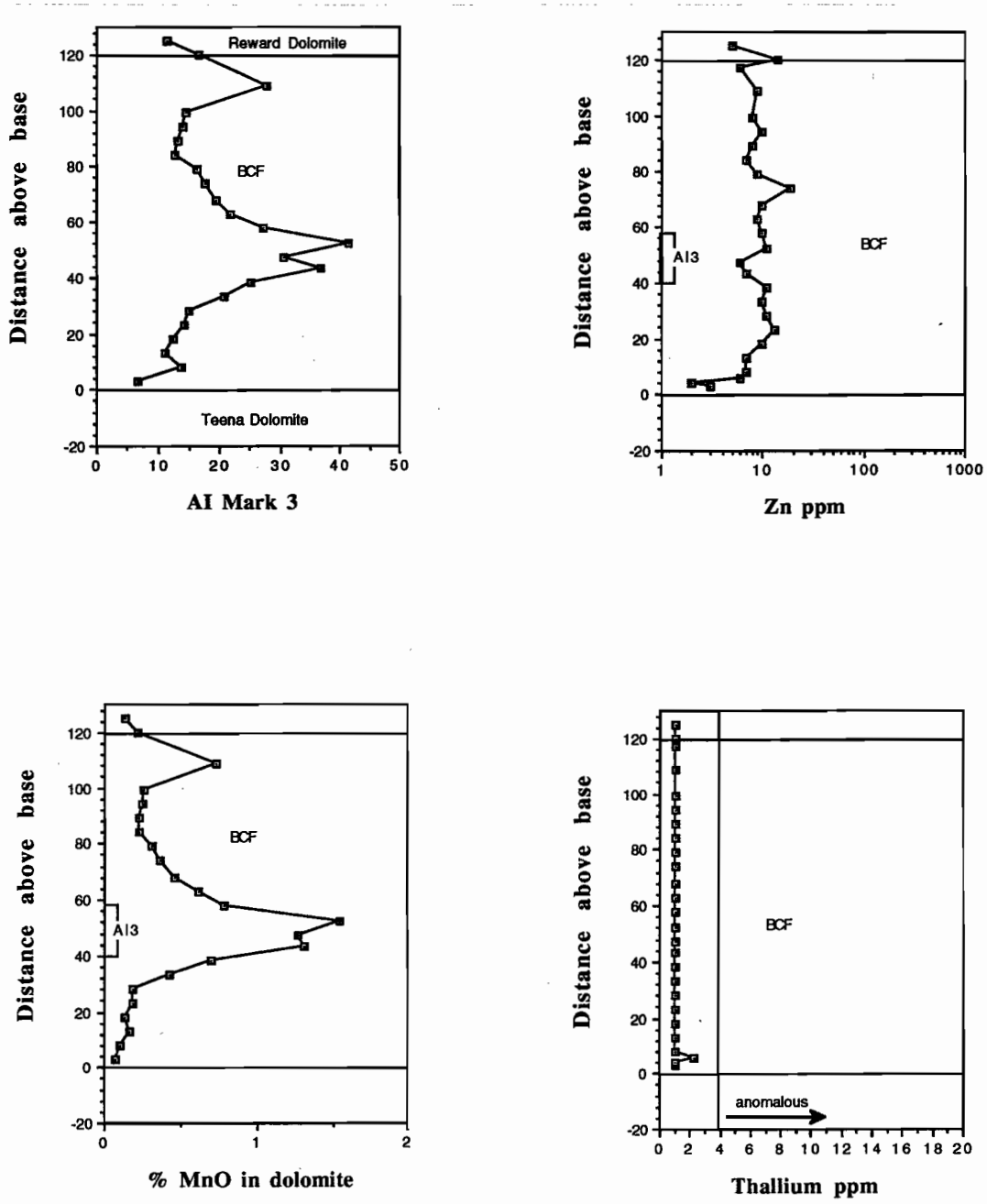

Figure 11 Top Crossing traverse; variation in Al_3, Zn, MnO_D and Thallium plotted against stratigraphic distance above the base of the BCF.

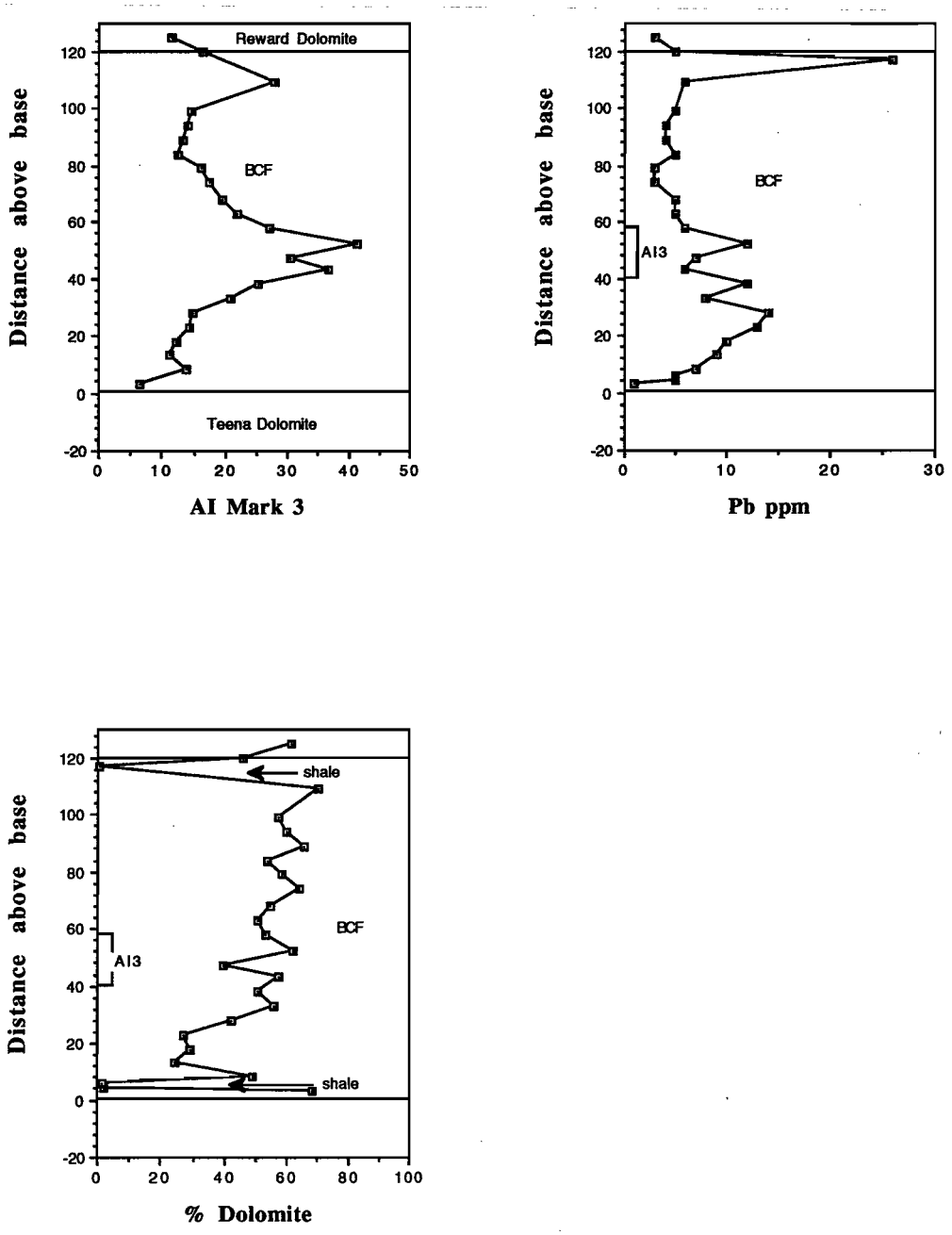

Figure 12 Top Crossing Traverse; variation in AI_3, Pb and calculated dolomite content.

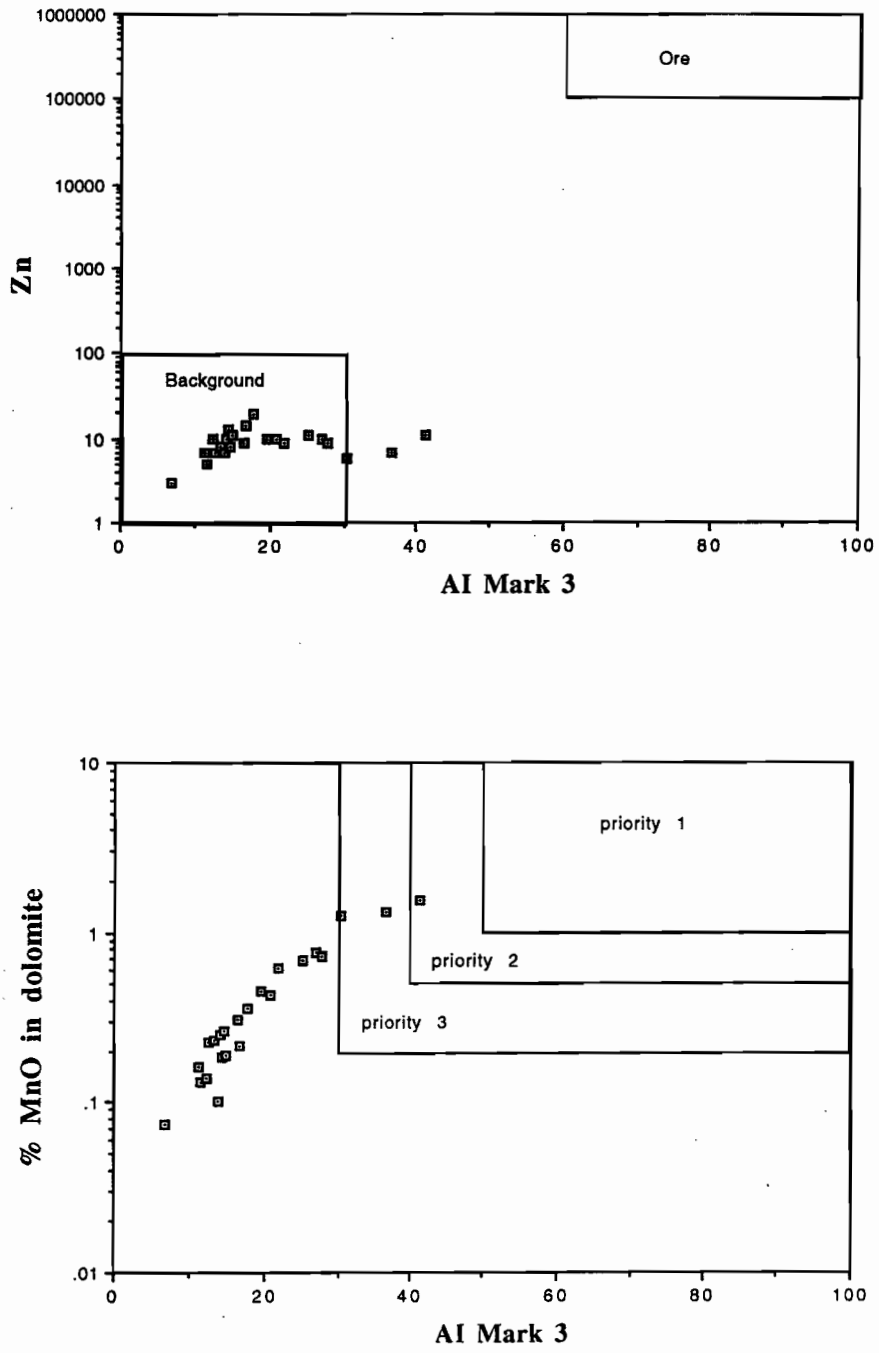

Figure 13 (a) AI_3 vs Zn for Top Crossing samples; (b) AI_3 vs MnO_D showing 1 sample (4% of data) in the priority 2 zone.

Oxygen and carbon-isotope chemostratigraphy

Previous research by Large et al. (1995) indicated the presence of an oxygen isotope halo surrounding the Lady Loretta deposit, coincident with a zone of siderite development in the sediments. Studies were subsequently undertaken on the McArthur Basin sediments from DDH BMR 2, Top Crossing, DDH Barney Creek 3 and DDH Homestead 6 to evaluate the stratigraphic variation in C/O isotope in the BCF and to investigate the potential for an isotopic halo surrounding the HYC deposit.

DDH BMR 2

Bull & Large (1995) reported the $\delta^{18}O$ and $\delta^{13}C$ variation in sedimentary carbonates from DDH BMR 2, 23 km south west of HYC. Downhole plots are produced here in Figure 14. No correlation is apparent between the isotopic values in the carbonates and the alteration vectors AI_3 and MnO_D. A comparison of the C/O isotopes in the BMR 2 dolomites with dolomite microbands in the HYC orebody (from Rye & Williams, 1981) indicate that the HYC ore dolomite is generally heavier in $\delta^{18}O$ and lighter in $\delta^{13}C$ compared to the BMR 2 sedimentary dolomite (Fig. 15). It was concluded by Bull & Large (1995) that if an isotopic halo exists at HYC, then it does not extend as far as DDH BMR2.

DDH Barney Creek 3

Dolomite sediments in Barney Creek 3 show an increase in $\delta^{18}O$ values from 22 to 27‰ downhole from towards the top of the HYC Pyritic Shale into the W-Fold Shale (Fig. 16). The trend of increasing $\delta^{18}O$ is accompanied by a decrease in $\delta^{13}C$ over the same interval from about –1 to –3‰ (Fig. 16). A comparison of the isotopic chemostratigraphy in DDH Barney 3 and DDH BMR 2 (Fig. 16) indicates the distinctly anomalous trend in the former hole. [Note: the low $\delta^{13}C$ value at 300 m is considered to be in error due to the high SO_2 content of this run.] The heaviest $\delta^{18}O$ values and lightest $\delta^{13}C$ values in dolomite correspond to the zone from 250 to 350 m downhole where MnO_D and AI_3 values also reach a maximum (Fig. 3). This correlation of C/O isotopes with alteration indicies suggests that the increase in $\delta^{18}O$ and decrease in $\delta^{13}C$ may represent an isotopic halo to the HYC deposit.

On a $\delta^{18}O$ vs $\delta^{13}C$ diagram (Fig. 17) there is considerable scatter in the dolomitic sediments from DDH Barney Creek 3. However, it is apparent that many of the samples overlap the field of HYC stratiform ore, while other samples show transitional isotopic values close to the field of the BMR 2 sediments. This plot suggests that the lower BCF stratigraphy intersected in DDH Barney Creek 3 may lie with the isotopic halo to the HYC deposit.

Top Crossing Traverse

Dolomitic sediments from Top Crossing (60 km SW of HYC) have C/O isotopes which overlap with the sediments from DDH BMR 2 (Fig.18). These values are considered to be typical of BCF dolomitic shales uneffected by the stratiform Pb–Zn forming event. The downhole plot of $\delta^{18}O$ indicates a possible negative correlation with AI_3 (Fig. 19). This pattern is the reverse of that seen in DDH Barney Creek 3, and indicates a different fluid is involved in the isotopic fractionation. For example, low salinity meteoric fluids may have caused the ^{18}O depletion in the Top Crossing area, while high salinity connate fluids (related to mineralisation) are probably responsible for the ^{18}O enrichmnent in the Barney Creek 3 drill hole.

DDH Homestead 6

Dolomitic pyritic shales of the BCF in Homestead 6 are distinctly heavier in oxygen (mostly 24 to 26‰) and lighter in carbon (mostly –2 to –3‰) than the corresponding sediments from DDH BMR 2 and the Top Crossing area (Fig. 20).

The downhole plots (Fig. 20) show that anomalous $\delta^{18}O$ values of greater than 23‰, occur throughout the drill hole. The HYC Pyritic Shale section from 60 to 200 m downhole also shows anomalous $\delta^{13}C$ values (< –2‰) with background values recorded for the bottom few samples of the hole in the W-Fold Shale section (Fig. 20).

In Figure 21, the Homestead 6 sediments form a tight cluster which overlaps the data collected from

the HYC orebody. This grouping with values of $\delta^{18}O$ = 23 to 26‰ and $\delta^{13}C$ = –1.5 to –3‰ is interpreted to represent the ore and halo signature of the HYC deposit.

HYC ore C/O isotope values

Previous studies by Rye & Williams (1981) indicate that the carbonate siltstone horizons in the stratiform Pb–Zn ore at HYC show a linear C/O isotope variation (Fig. 15) with $\delta^{18}O$ = 21 to 25‰ and $\delta^{13}C$ = –1.9 to –3.2‰. They interpreted the C/O linear trend to be due to carbonate deposition over the temperature range ~ 120°C (heavy $\delta^{18}O$) to 170°C (light $\delta^{18}O$). Additional C/O analyses on samples from the HYC no. 2 orebody were conducted as part of this study to compare with the previous Rye & Williams data. Nine samples were drilled out, using a fine dentist drill, from thin micro-bands of carbonate silt (3–15 mm thick) within the laminated Pb–Zn ore. The data forms a tight grouping (Fig. 22) with a variation of $\delta^{18}O$ = 23.1 to 25.2‰, $\delta^{13}C$ = –2.1 to -2.8‰. These data overlap the previous data of Rye & Williams (1981) but do not show the linear trend to lighter $\delta^{18}O$ and $\delta^{13}C$ values.

Isotope discrimination matrix

By combining MnO_D and $\delta^{18}O$ carbonate in the one diagram it may be possible to discriminate MnO_D anomalies related to stratiform Pb–Zn deposits from those which identify favourable host rocks only. In Figure 20 three fields are defined:

- Field 1 — Background:
  $MnO_D < 0.5$, $\delta^{18}O < 23‰$
- Field 2 — potential ore horizon (distal):
  $MnO_D > 0.5$, $\delta^{18}O < 23‰$
- Field 3 — halo to stratiform Pb–Zn ore:
  $MnO_D > 0.5$, $\delta^{18}O > 23‰$

Summary of C/O Isotopes McArthur Basin

- Background dolomitic sediments in the BCF, McArthur Basin, have $\delta^{18}O$ = 20 to 23 ‰ and $\delta^{13}C$ = 0 to –2 ‰
- Dolomitic siltstone samples in the HYC orebody and surrounding halo collected in ths study display heavier oxgyen isotope ratios and lighter carbon isotope ratios with the range:
  $\delta^{18}O$ = 23 to 26‰ and $\delta^{13}C$ = –2 to –3.5‰
- The C/O isotope halo extends throughout the lower BCF, including DDH Homestead 6 (2 km distant) and DDH Barney 3 (15 km distant).
- C/O isotopes provide a powerful method of discriminating MnO_D and AI_3 anomalies directly related to stratiform Pn–Zn mineralisation
  - anomalies associated with ore exhibit heavy $\delta^{18}O$ > 23‰ and light δ13C < –2‰
  - anomalies unrelated to ore (or very distal from ore) exhibit $\delta^{18}O$ < 23‰ and $\delta^{13}C$ > -2‰.
- A discrimination matrix combining MnO_D and $\delta^{18}O$ carbonate provides an effective way to positively identify the halo to stratiform Pb–Zn deposits of the HYC and Lady Loretta type.

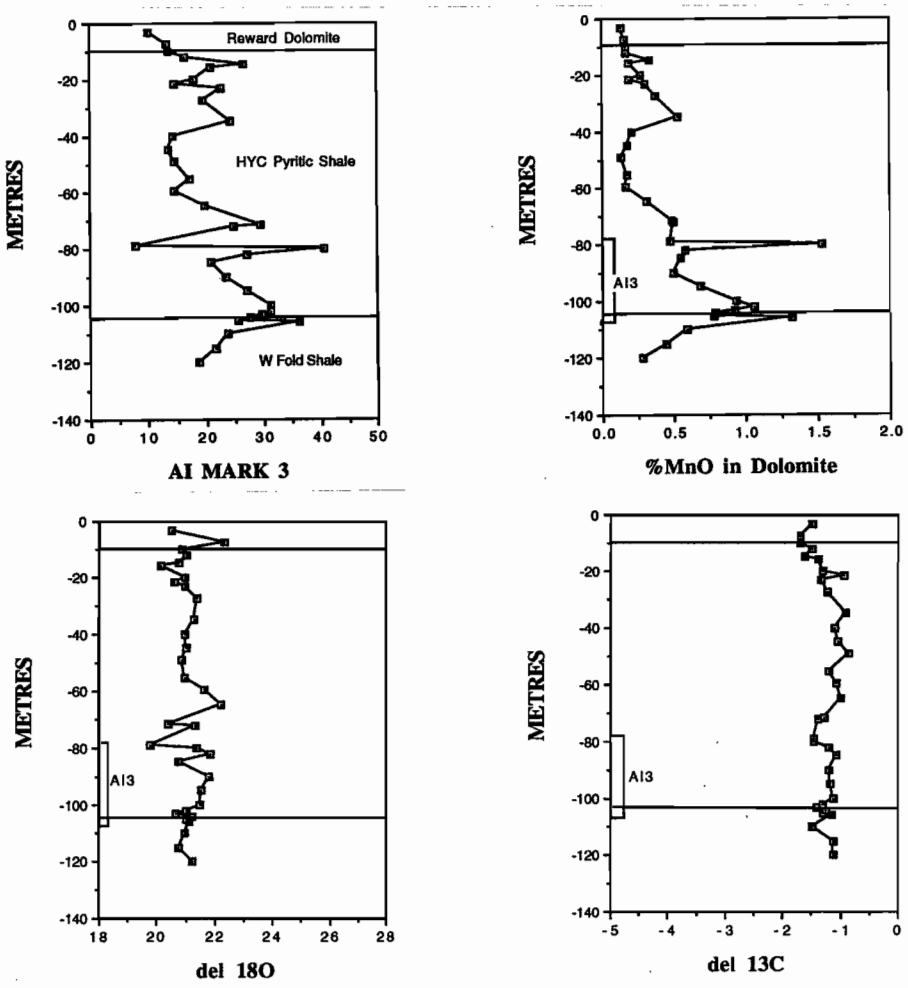

Figure 14 Downhole plots of $\delta^{18}O$ (SMOW) and $\delta^{13}O$ (PDB) compared with AI_3 and MnO_D.

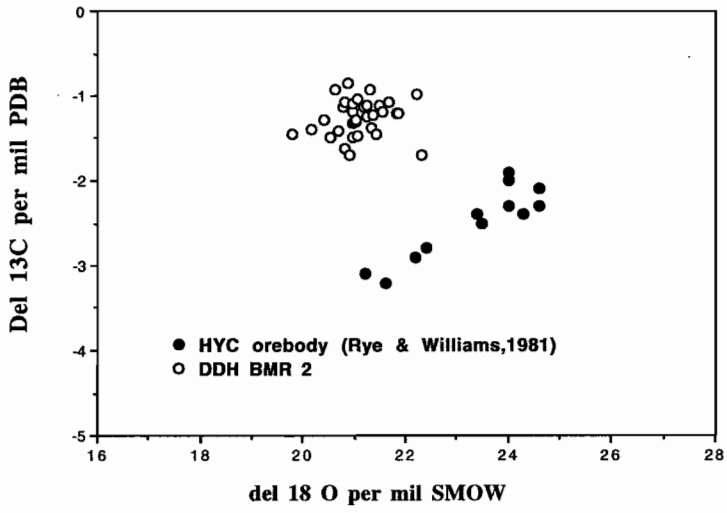

Figure 15 Comparison of C/O isotopes in sedimentary carbonates from DDH BMR2 compared to those reported for the HYC ore zone by Rye and Williams (1981).

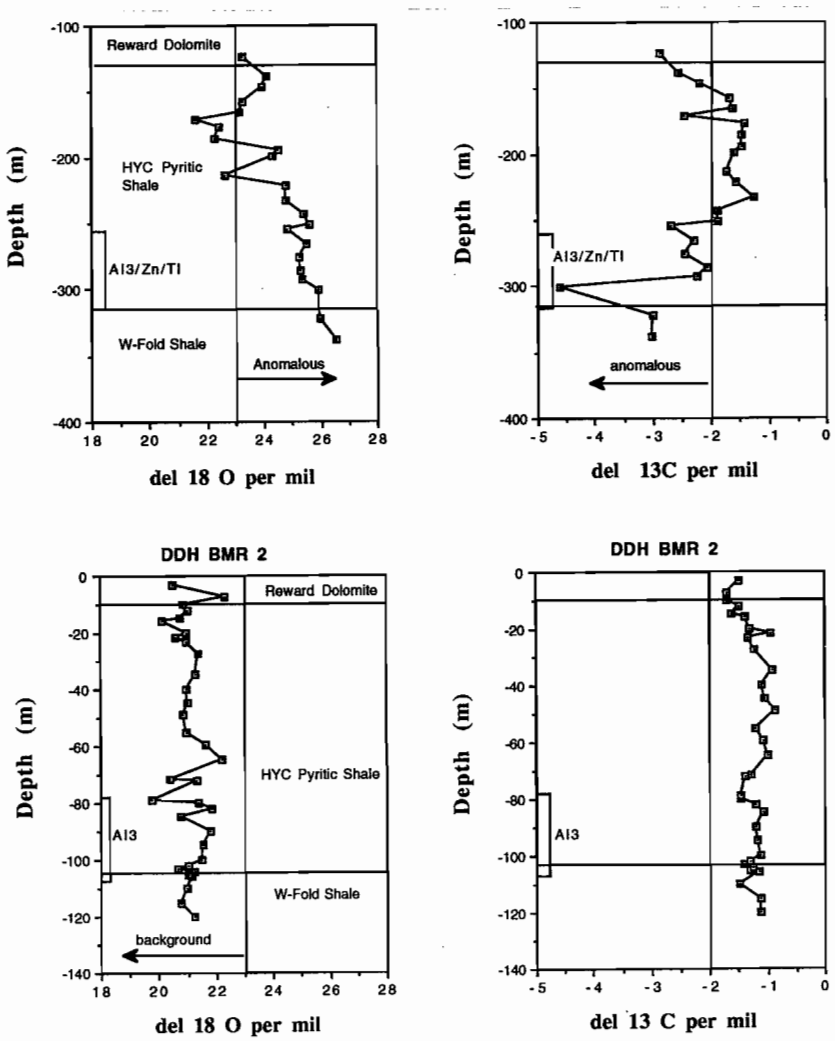

Figure 16 Comparison of C/O isotope chemostratigraphy in DDH Barney 3 with DDH BMR 2.

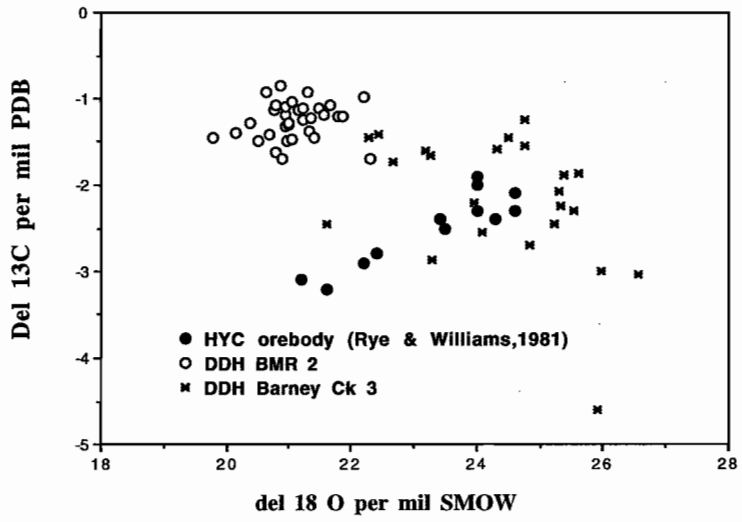

Figure 17 Sedimentary carbonates from DDH Barney Creek 3 compared to data from DDH BMR2 (very remote from ore) and HYC.

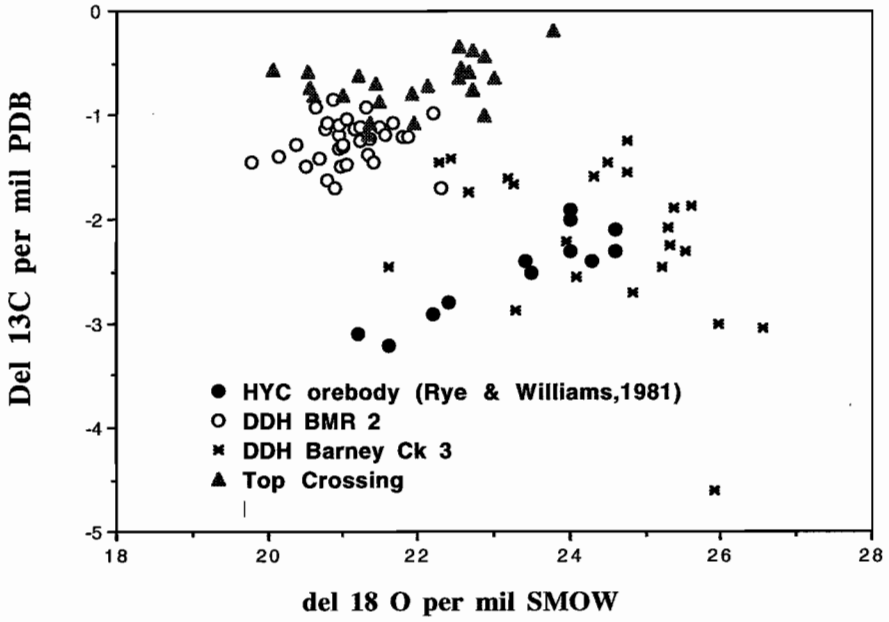

Figure 18 C/O isotope plot showing that the Top crossing dolomite sediments overlap with the BMR2 data and form a coherent group considered to represent normal background sedimentary dolomite in the BCF. By comparison the samples from DDH Barney Creek 3 show anomalous values that overlap the ore signature.

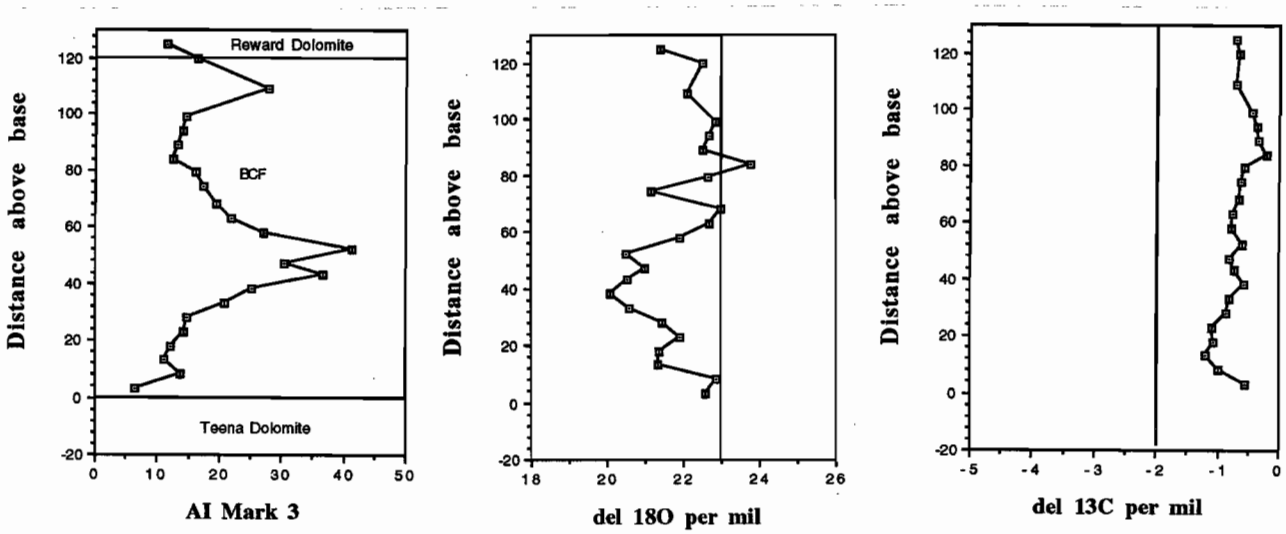

Figure 19 Comparison of alteration index variation (AI_3) with C/O isotope variation in the Top Crossing area. Note that the AI_3 anomaly between 40–60 m above base is associated with depletion in $\delta^{18}O$ in the dolomite.

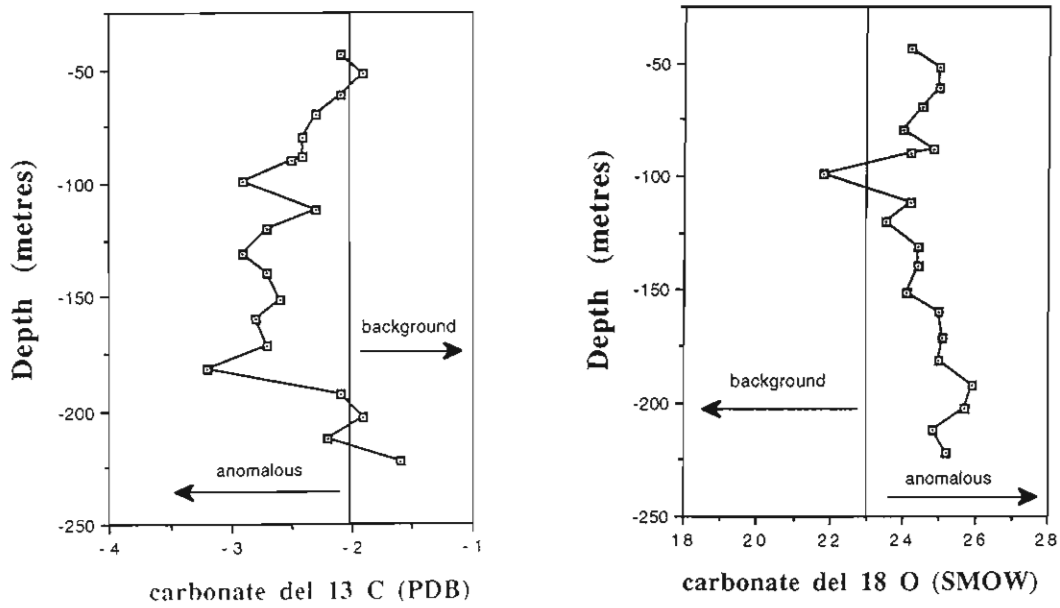

Figure 20 Isotope chemostratigraphy for dolomitic sediments of the BCF in DDH Homestead 6. Most of the samples have enriched $\delta^{18}O$ values (>23‰) and depleted $\delta^{13}O$ values (< –2‰) compared with the regional sediments in BMR2 and Top Crossing.

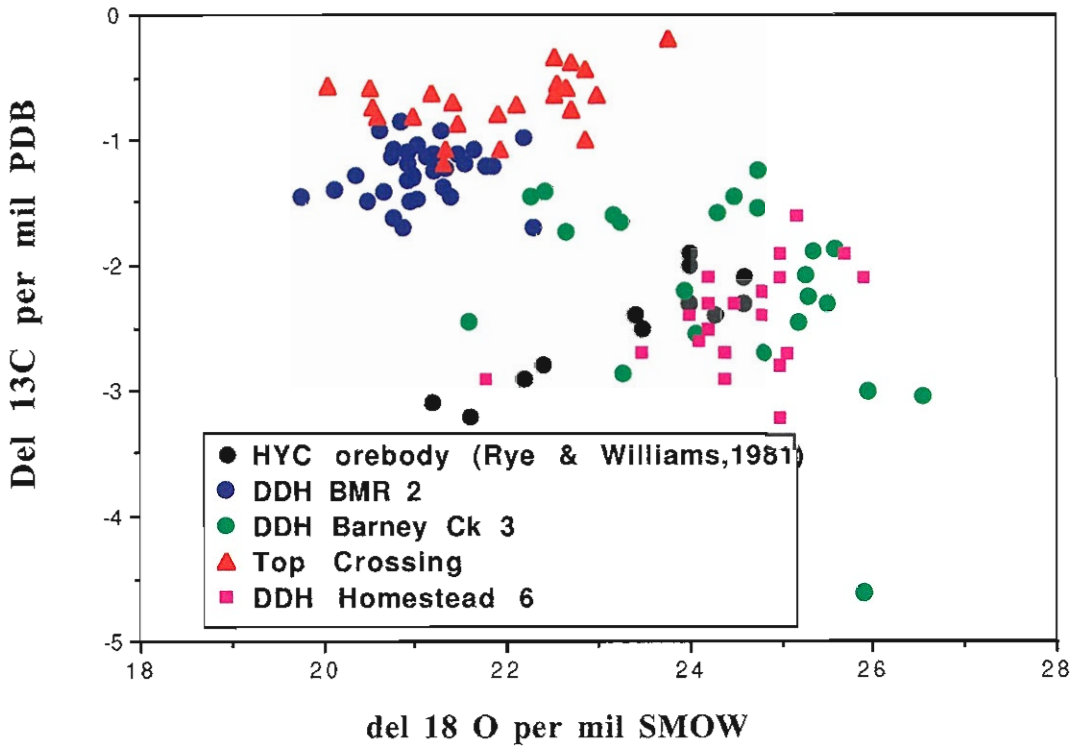

Figure 21 C/O isotope plot for all data collected in this study in the McArthur Basin. Two groupings are indicated; background sedimentary carbonates (DDH BMR2 and Top Crossing) generally have heavier $\delta^{13}C$ and lighter $\delta^{18}O$ than the ore and halo carbonates (HYC, DDH Homestead 6 and most data from DDH Barney Creek 3).

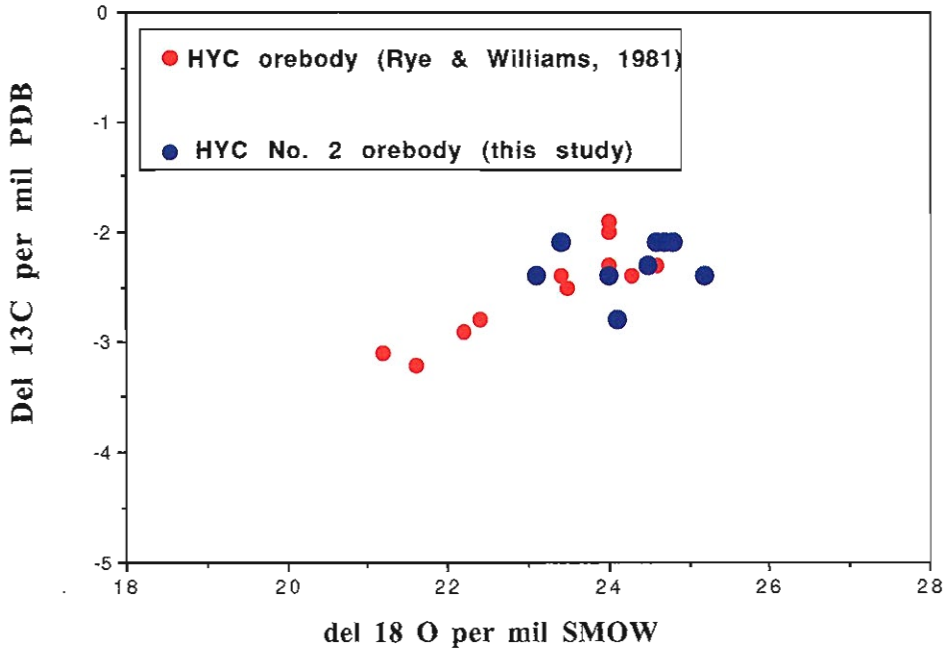

Figure 22 C/O isotope plot comparing data from the stratiform HYC orebody reported by Rye and Williams (1981) with samples analysed as part of this study.

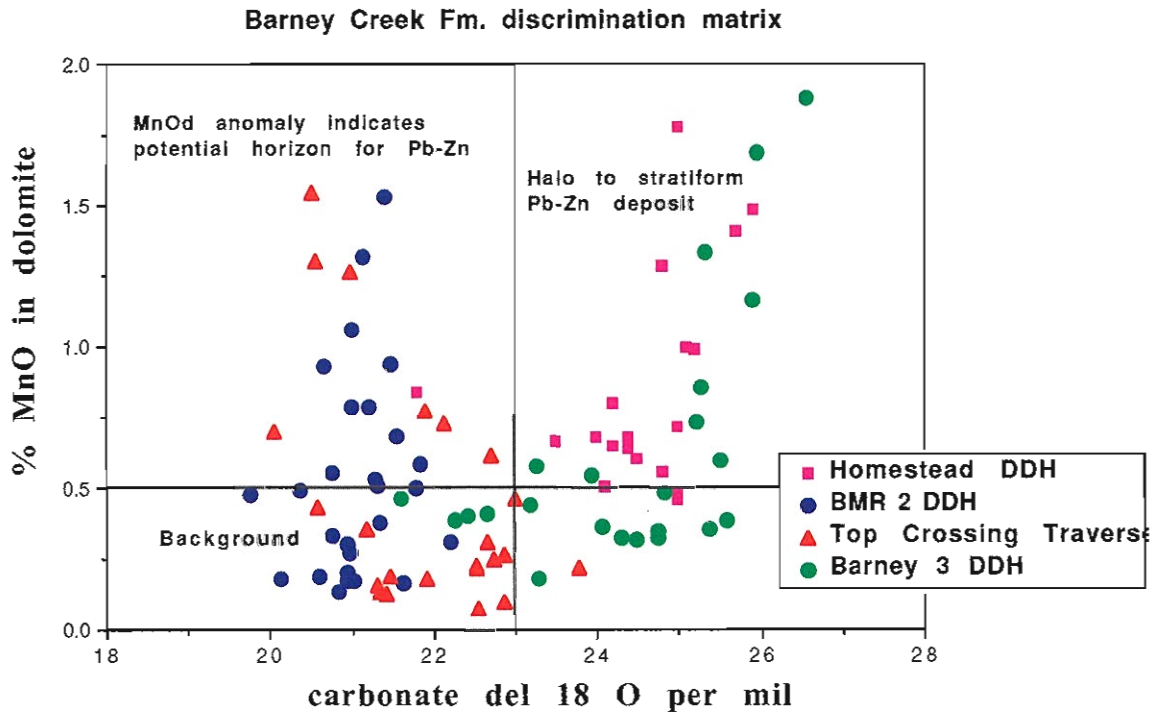

Figure 23 $\delta^{18}O$–MnO_D discrimination diagram showing samples from DDH Homestead 6, DDH BMR2, DDH Barney Creek 3 and the Top Crossing traverse. Samples containing greater than 0.5% MnO_D and 23‰ $\delta^{18}O$ fall within the halo of stratiform Pb–Zn mineralisation.

Illite and K-feldspar relationships

Petrographic studies indicate a wide range in the illite and K-feldspar content of dolomitic shales of the Barney Creek Formation throughout the McArthur Basin. Utilising the whole rock K_2O and Al_2O_3 analyses, a preliminary study of illite/K-feldspar distribution has been undertaken to investigate any relationships to stratiform Pb–Zn mineralisation. This is made possible because illite and K-feldspar are the only major minerals in the sediments which contain both K_2O and Al_2O_3. Other aluminium silicates such as albite and chlorite occur in insignificant amounts in the samples studied to date.

In Figure 22 it is apparent that samples remote from HYC, at Top Crossing and DDH BMR2, contain significantly higher K_2O/Al_2O_3 ratios than samples close to HYC (DDH Homestead 6) and within the deposit (DDH Te 115). This is interpreted to indicate that K-feldspar is the dominant potassium silicate in the sediments remote from HYC, while illite or phengite is the dominant mineral in the HYC Pyritic Shales close to the ore deposit. Preliminary petrographic studies have confirmed this interpretation.

Downhole plots of the Al_2O_3/K_2O ratio provide an estimate of the balance between K-feldspar and illite through the Barney Creek Formation at HYC, Homestead 6, Barney Creek 3 and BMR2 (Fig. 23). In Te 115 through the HYC deposit, the illite/K-feldspar ratio increases upwards through the W-Fold Shale reaching a maximum in the base of the ore zone. K-feldspar becomes progressively more important toward the top of the ore zone, followed by a second cycle of illite enrichment in the upper HYC Pyrite Shale.

Homestead 6, 1.9 km south of HYC, displays a constant Al_2O_3/K_2O ratio of about 2.0 through the HYC Pyrite Shale indicating an assemblage containing about equal portions of illite and K-feldspar. In DDH Barney 3 the gradual increase in Al_2O_3/K_2O downhole, indicates a maximum illite/K-feldspar ratio at the base of the HYC Pyrite Shale corresponding to the favourable horizon.

In DDH BMR2 (Fig. 23) the low Al_2O_3/K_2O ratio of 1 to 1.5 indicates that K-feldspar is the dominant phase throughout the drill hole.

Barium content of K-silicates

Barium is present in only trace amounts in the HYC environment, with sediments and ore typically containing 100 to 500 ppm Ba. Unlike Lady Loretta no barite has been reported from the ores or surrounding host sediments.

Barium shows no correlation with base metals or sulphur, however a linear relationship between Ba and K_2O (Fig. 24) indicates that the barium is present within the lattice of the potassium silicates; illite and K-feldspar.

Of considerable interest is the observation in Figure 23 that the Ba/K_2O ratio increases with proximity to HYC. This suggests a vector of increasing barium in K-silicates towards ore. Note however that DDH Barney 3 (15 km from HYC) has a higher Ba/K_2O ratio than DDH Homestead 6 (2 km from HYC). Mean Ba/K_2O contents for the four drill holes are:

	$(Ba/K_2O) * 10^4$
HYC ore (Te 115)	110
DDH Barney Creek 3	84
DDH Homestead	60
DDH BMR 2	37

Microprobe analysis of the barium content of illite and K-feldspar is required to confirm this pattern.

Basket of exploration vectors

This study has enabled the development of a basket of exploration vectors which may be used together to:

1. Identify favourable horizons for stratiform Pb–Zn.
2. Place priorities on weak Pb–Zn anomalies in dolomite sediments.
3. Indicate proximity to mineralisation and direction of follow-up drilling.

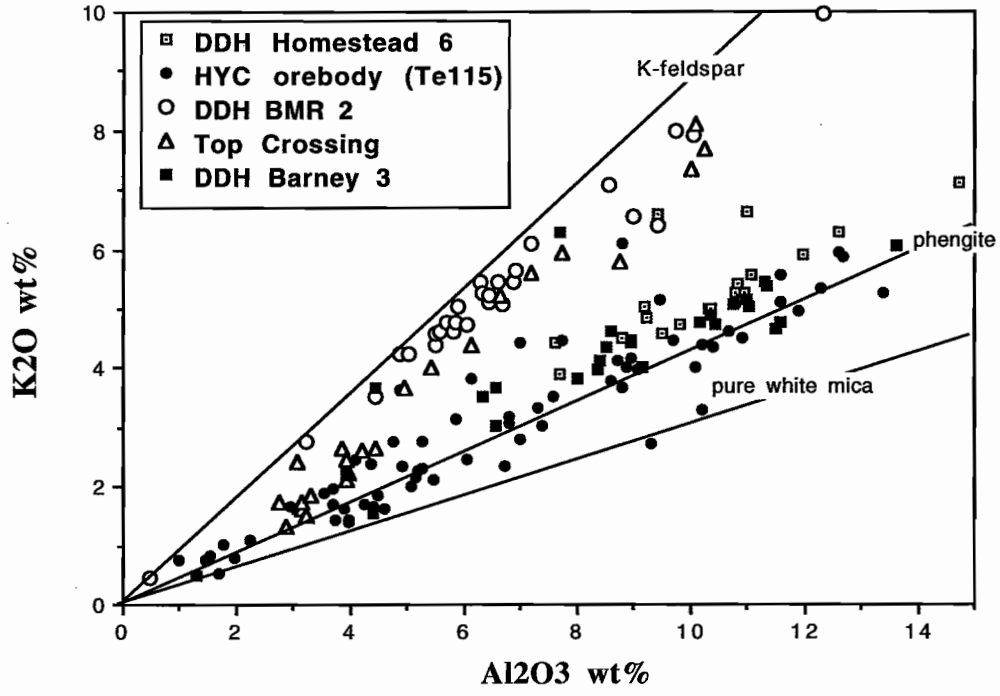

Figure 24 Linear trends on this Al_2O_3–K_2O diagram indicate the dominant K-A1 silicate mineral for each given locality. Sample sets remote from mineralisation (BMR2 and Top Crossing) are K-feldspar dominant, while samples close to mineralisation (Te 115, and Homestead 6) are illite/phengite dominant.

The basket of vectors includes the following:

1. Sedex Alteration Index:

$$\text{Sedex AI} = \frac{(10MnO + FeO)\ 100}{(10MnO + FeO + MgO)}$$

2. Alteration Index Mark 3:

$$AI_3 = \frac{10MnO + FeO)\ 100}{(10MnO + FeO + MgO + Al_2O_3)}$$

3. MnO content in dolomite

$$MnO_D = \frac{MnO \times 30.4)}{CaO}$$

4. Thallium: Tl ppm

5. Ankerite Ratio

$$\frac{(Fe + Mn)}{Mg} \text{ molar ratio in carbonates}$$

6. AI_3 vs MnO_D plot; provides a priority rating as the percentage of samples in Priority 1, Priority 2 or Priority 3.

7. Oxygen isotopes in carbonate; $\delta^{18}O$ carbonate

8. Carbon isotopes in carbonates; $\delta^{13}O$ carbonate

9. Illite/K-feldspar ratio; Al_2O_3/K_2O

10. Barium content of K-silicates; $(Ba/K_2O) * 10^4$

Table 1 provides the range of values for each vector at varying distances from the HYC deposit.

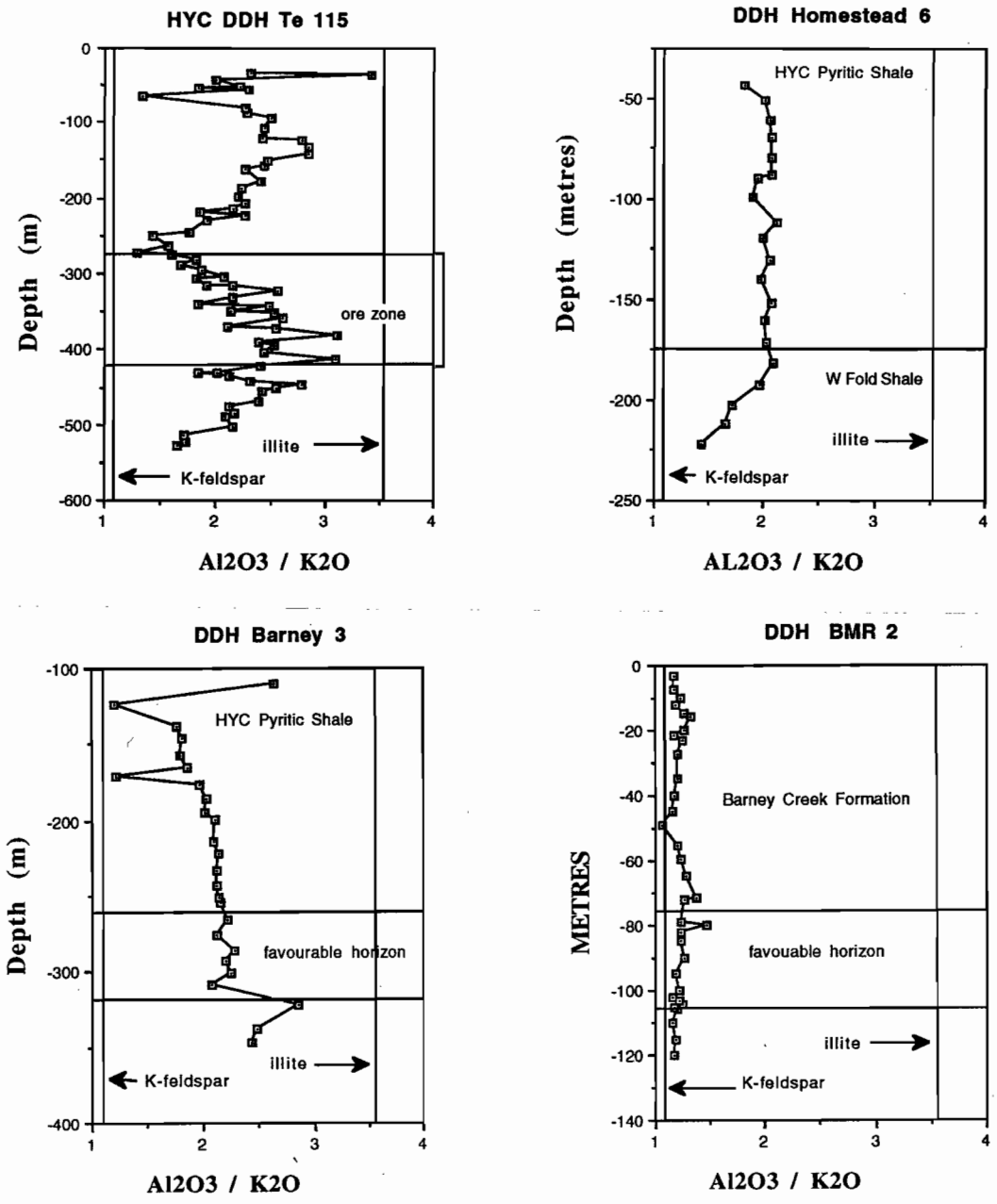

Figure 25 Downhole plots of Al_2O_3/K_2O ratio indicating the balance between K-feldspar and illite through the BCF stratigraphy.

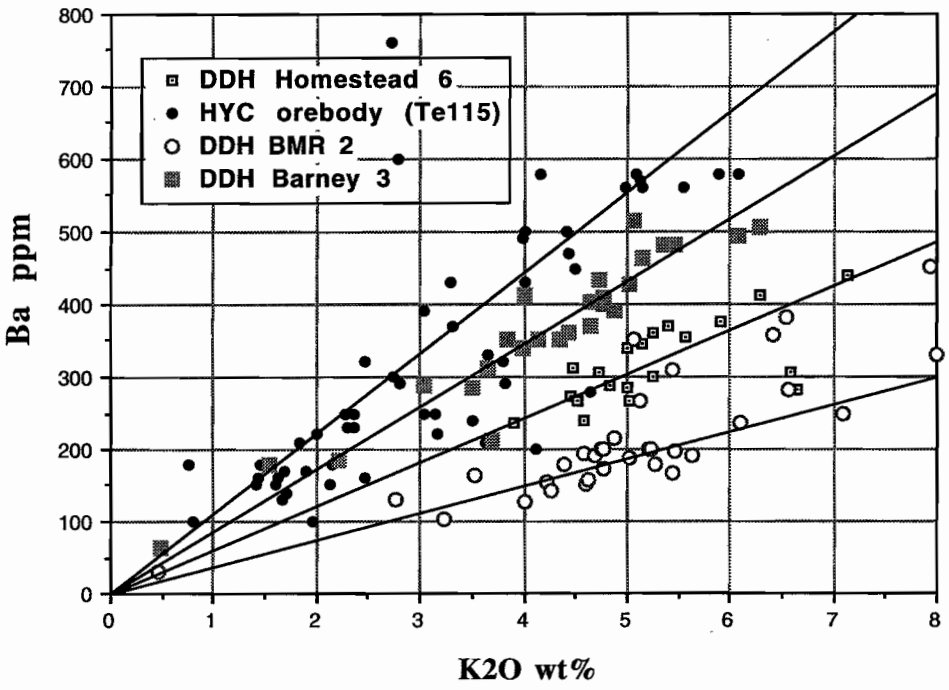

Figure 26 Linear trends on a Ba vs K_2O plot for sample sets from the McArthur basin. This data indicates a variation in the Ba content of K-silicates (feldspar and white mica) which may relate to proximity to mineralisation.

Table 1 Range of values for the Basket of Vectors in the favourable horizon at varying distances from HYC.

Vector		Orebody	Close Proximity ~ 2 km	Distal from ore 5–25 km	Very remote > 25 km
1	Zn ppm	>100,000	1000–10,000	10–3,000	< 20
2	Pb ppm	> 10,000	50–1000	20–1,000	< 30
3	Sedex AI	50–100	50–90	40–75	20–50
4	AI3	60–95	50–90	20–50	20–40
5	MnOD wt%	2–12	1.0–2.0	1.0–2.0	0.5–1.5
6	Thallium ppm	200–900	20–120	4–25	1–2
7	Ankerite Ratio	0.2–10	0.2–1.0	0.1–1.0	< 0.2
8	AI3 v MnOD	26% Priority 1	50% Priority 2	4% Priority 2	4% Priority 2
	Priority rating	20% Priority 2	25% Priority 3	15% Priority 3	8% Priority 3
9	$\delta^{18}O‰$	23–26	22–26	20–26	20–23
10	$\delta^{13}O‰$	–2 to –3.5	–2 to –3.5	–1 to –3.5	0 to –2
11	Al_2O_3/K_2O	2–3	~ 2	1–2	1–1.4
12	$(Ba/K_2O) * 10^4$	~ 110	~ 60	30–90	no data

References

Brown, M.C., Claxton, C.W. & Plumb, K.A., 1969. The Proterozoic Barney Creek Formation and some associated carbonate units of the McArthur Group, NT. *BMR Record* 145: 59 pp.

Bull, S.W., 1994. Depositional attributes of the Barney Creek Formation in DDH BMR2. AMIRA P384 — Proterozoic sediment-hosted base metal deposits. Report 7: 97–114.

Bull, S.W., 1995. Towards a regional depositional model for the Palaeoproterozoic Barney Creek Formation, southern McArthur Basin, NT. AMIRA/ARC Project P384 — Proterozoic sediment-hosted base metal deposits. Final Report: 133–159.

Bull, S.W. & Large, R.R., 1995. Sedimentology, Geochemistry, alteration patterns and C/O isotope chemostratigraphy, DDH BMR2, McArthur Basin, NT. AMIRA P384, Proterozoic sediment-hosted base metal deposits. Final Report: 159–182.

Duhig, N., 1975. A microprobe study of carbonates from DDH BMR2. AMIRA P384 — Proterozoic sediment-hosted base metal deposits. Final Report: 283–288.

Lambert, L.B. & Scott, K.M., 1973. Implications of geochemical investigations of sedimentary rocks within and around the McArthur zinc–lead–silver deposit, Northern Territory. *J. Geochem. Explor.* 2: 307–330.

Large, R.R. & McGoldrick, P., 1993. Primary Geochemical halos related to Proterozoic sediment hosted Pb–Zn deposits and applications to exploration. AMIRA P384, Proterozoic sediment-hosted base metal deposits. Report 3: 63–126.

Large, R.R., 1994a. Background data on Sedex AI and MnO_D for McArthur Basin sediments. AMIRA P384 — Proterozoic sediment-hosted base metal deposits. Proterozoic sediment-hosted base metal deposits. Report 5: 7–24.

Large, R.R., 1994b. Case Studies: application of the alteration index to selected areas in the McArthur Basin. AMIRA P384 — Proterozoic sediment-hosted base metal deposits. Report 5: 25–40.

Large, R.R., 1994c. Modelling the relationship between sedimentary facies and alteration index, and resolution of the "shale factor". AMIRA P384 — Proterozoic sediment-hosted base metal deposits. Report 7: 45–68.

Large, R.R. & Duhig, N., 1995. Ankerite halo to the HYC deposit. AMIRA P384, Final Report: 273–282.

Large, R.R., Kitto, P.A. & McGoldrick, P.J., 1995. Variation of carbon and oxygen isotopes in the alteration halo to the Lady Loretta deposit — implications for exploration and ore genesis. AMIRA P384, Final Report: 89–302.

Rye, D.M. & Williams, N., 1981. Studies of base metal sulfide deposits at McArthur River, Northern Territory, Australia. III: The stable isotope geochemistry of the HYC, Ridge and Cooley deposits. *Econ. Geol.* 76: 1–26.

Shannon, C.H.C., Lafferty, S. & Kneale, C.M. 1980. Annual report on exploration, EL1203, 7/9/78 to 6/9/79. A. O. (Australia) Pty Ltd. Northern Territory Department of Mines and Energy. Unpubl. open file company report 80/19.

Appendix 1

Analytical results for drill holes Barney Creek 3, Homestead 6 and the Top Crossing traverse

- Major and trace element analyses by Phil Robsinson, Geology Department, University of Tasmania
- Carbon and oxygen isotope analyses by Mike Power, Central Science Laboratory, University of Tasmania
- Organic carbon and CO_2 analyses by Leco at the Central Science Laboratory, University of Tasmania
- All major element in % and trace elements in ppm.

DDH Barney Ck 3

	Depth (m)	del 13C per	del 18O per mil	SiO2	TiO2	AL2O3	Fe2O3	FeO*	MnO
1	-109.80			20.54	0.06	1.29	1.69	1.536	0.21
2	-123.30	-2.87	23.28	30.69	0.18	4.42	1.97	1.791	0.11
3	-138.90	-2.54	24.08	23.46	0.16	3.91	2.00	1.818	0.26
4	-146.80	-2.20	23.95	36.75	0.26	6.34	3.19	2.900	0.26
5	-157.00	-1.66	23.27	45.22	0.25	6.54	3.44	3.127	0.22
6	-165.00	-1.61	23.18	47.55	0.34	8.58	3.29	2.991	0.14
7	-171.20	-2.46	21.60	58.40	0.16	7.70	1.54	1.400	0.12
8	-176.40	-1.41	22.43	52.64	0.34	8.52	3.08	2.800	0.11
9	-185.20	-1.45	22.28	54.47	0.32	8.41	3.20	2.909	0.10
10	-194.50	-1.45	24.49	47.74	0.36	8.94	3.06	2.782	0.10
11	-199.40	-1.59	24.31	55.68	0.34	8.35	3.22	2.927	0.08
12	-213.40	-1.73	22.66	61.55	0.31	8.00	3.76	3.418	0.07
13	-221.30	-1.55	24.75	50.65	0.42	10.38	4.28	3.891	0.08
14	-232.70	-1.24	24.75	48.31	0.42	10.16	3.38	3.073	0.10
15	-243.20	-1.88	25.38	52.45	0.45	11.34	4.15	3.773	0.07
16	-250.70	-1.87	25.60	50.83	0.46	11.00	3.50	3.182	0.09
17	-254.20	-2.69	24.83	33.15	0.30	6.56	3.26	2.964	0.25
18	-266.20	-2.30	25.52	50.26	0.48	10.46	4.59	4.173	0.14
19	-276.50	-2.46	25.22	49.22	0.46	10.74	9.41	8.555	0.11
20	-286.10	-2.07	25.29	60.71	0.37	9.13	3.86	3.509	0.14
21	-292.70	-2.25	25.33	49.72	0.45	11.02	4.71	4.282	0.32
22	-300.90	-4.60	25.90	58.30	0.55	13.62	5.22	4.745	0.10
23	-308.40			61.87	0.46	11.30	8.96	8.145	0.01
24	-322.20	-3.00	25.96	28.16	0.20	4.41	5.48	4.982	1.01
25	-337.60	-3.03	26.56	55.51	0.48	11.51	4.67	4.245	0.34
26	-346.80			57.56	0.47	11.59	4.27	3.882	0.28

DDH Barney Ck 3

	Depth	MgO	CaO	Na2O	K2O	P2O5	Loss	Sum	S %
1	-109.8	17.69	23.31	0.12	0.49	0.03	36.08	101.51	0.19
2	-123.3	12.48	18.09	0.11	3.69	0.11	27.82	99.66	1.06
3	-138.9	13.92	21.69	0.13	2.22	1.60	30.91	100.26	0.89
4	-146.8	10.11	14.48	0.13	3.51	0.19	24.80	100.01	1.55
5	-157.0	8.07	11.56	0.12	3.66	0.16	20.77	100.01	1.55
6	-165.0	7.42	9.74	0.12	4.64	0.13	17.84	99.81	1.22
7	-171.2	5.10	7.84	0.08	6.30	0.06	12.88	100.19	0.33
8	-176.4	6.72	8.31	0.12	4.34	0.12	15.64	99.93	1.12
9	-185.2	6.58	7.91	0.10	4.14	0.12	14.89	100.24	1.03
10	-194.5	7.71	9.56	0.12	4.43	0.12	17.59	99.75	0.88
11	-199.4	6.39	7.45	0.13	3.98	0.13	14.37	100.11	1.09
12	-213.4	4.76	5.25	0.11	3.84	0.12	11.64	99.40	1.58
13	-221.3	6.67	7.52	0.12	4.88	0.15	15.28	100.42	1.75
14	-232.7	7.31	8.65	0.14	4.78	0.15	16.88	100.27	1.07
15	-243.2	5.63	5.97	0.13	5.36	0.20	13.83	99.57	1.75
16	-250.7	6.40	7.10	0.13	5.14	0.20	14.91	99.74	1.23
17	-254.2	11.37	15.71	0.11	3.04	0.11	26.50	100.39	0.88
18	-266.2	6.35	7.14	0.12	4.72	0.20	15.28	99.92	2.06
19	-276.5	4.16	4.54	0.13	5.06	0.48	14.66	99.15	6.04
20	-286.1	4.57	4.96	0.09	4.02	0.25	11.16	99.60	1.56
21	-292.7	6.20	7.28	0.14	5.03	0.17	14.95	100.20	1.95
22	-300.9	3.66	2.61	0.11	6.07	0.25	8.92	99.77	2.31
23	-308.4	1.68	0.38	0.05	5.46	0.25			5.73
24	-322.2	12.89	18.16	0.09	1.55	0.13			0.47
25	-337.6	5.47	5.50	0.13	4.65	0.31	11.19	99.77	0.10
26	-346.8	5.08	4.91	0.12	4.77	0.29	10.38	99.71	0.08

DDH Barney Ck 3

	Depth	Rb	Pb	Zn	Cu	As	Tl	Ba	Sr
1	109.8	9	11	5	4	5	0.5	63	110
2	123.3	55	34	6	11	23	1.6	213	38
3	138.9	61	33	7	9	27	0.5	186	48
4	146.8	105	38	14	13	31	2.1	284	41
5	157	109	31	16	10	23	1.4	313	36
6	165	146	25	304	18	21	2.0	370	38
7	171.2	70	8	68	3	<3	1.2	506	32
8	176.4	144	21	18	12	11	0.5	351	36
9	185.2	141	20	45	13	13	2.6	350	34
10	194.5	156	24	63	20	20	2.0	362	42
11	199.4	142	26	88	16	13	2.3	339	36
12	213.4	133	39	47	15	21	3.9	350	31
13	221.3	179	39	41	15	60	2.7	392	39
14	232.7	175	29	32	13	30	2.9	408	41
15	243.2	193	47	120	23	25	4.4	481	41
16	250.7	186	36	32	21	31	2.5	464	40
17	254.2	106	36	91	18	33	1.8	288	35
18	266.2	174	259	1840	36	59	5.1	434	39
19	276.5	175	445	1780	49	326	24.9	514	35
20	286.1	142	488	3200	44	38	4.7	411	32
21	292.9	183	1101	2090	65	97	4.1	428	42
22	300.9	216	541	3580	77	93	6.0	495	36
23	308.4	167	221	122	75	548	9.1	482	22
24	322.2	39	33	27	4	22	0.5	180	17
25	337.6	184	247	48	5	6	1.4	402	39
26	346.8	192	13	46	6	<3	0.5	401	38

DDH Barney Ck 3

	Al Mark 3	METRES	% MnO D	% Dolomite	DOP	CO2carb	%CO2 total	%	% C organic
1	16.08	-109.8	0.27	58.27	0.14	37.01	38.03	0.36	0.28
2	14.61	-123.3	0.18	45.22	0.66	27.73	30.41	1.98	0.73
3	19.86	-138.9	0.36	54.23	0.55	30.93	33.09	1.67	0.59
4	25.06	-146.8	0.55	36.20	0.60	22.43	26.78	2.90	1.19
5	26.72	-157.0	0.58	28.90	0.56	17.40	21.73	2.90	1.18
6	21.53	-165.0	0.44	24.35	0.46	14.69	17.70	2.28	0.82
7	16.88	-171.2	0.47	19.60	0.26	11.95	13.45	0.62	0.41
8	20.38	-176.4	0.40	20.78	0.45	12.59	14.55	2.10	0.53
9	20.68	-185.2	0.38	19.77	0.40	11.86	14.11	1.93	0.61
10	18.51	-194.5	0.32	23.90	0.35	14.94	17.07	1.65	0.58
11	20.18	-199.4	0.33	18.62	0.42	11.06	13.67	2.04	0.71
12	24.40	-213.4	0.41	13.12	0.52	7.41	11.21	2.96	1.04
13	21.58	-221.3	0.32	18.80	0.50	11.13	13.78	3.27	0.72
14	18.91	-232.7	0.35	21.62	0.39	13.21	16.09	2.00	0.79
15	20.86	-243.2	0.36	14.92	0.52	8.81	13.19	3.27	1.20
16	19.00	-250.7	0.39	17.75	0.43	10.67	14.51	2.30	1.05
17	23.36	-254.2	0.48	39.28	0.33	24.93	28.03	1.65	0.85
18	24.90	-266.2	0.60	17.85	0.55	10.65	14.33	3.85	1.00
19	39.32	-276.5	0.74	11.35	0.79	5.74	12.42	11.30	1.82
20	26.38	-286.1	0.86	12.40	0.50	7.16	11.07	2.92	1.07
21	30.29	-292.7	1.34	18.20	0.51	10.86	12.75	3.65	0.52
22	24.95	-300.9	1.17	6.52	0.55	3.72	6.82	4.32	0.85
23	38.85	-308.4	0.80	0.95	0.79	0.26	4.76	10.72	1.23
24	46.57	-322.2	1.69	45.40	0.11	29.11	30.30	0.88	0.32
25	31.05	-337.6	1.88	13.75	0.03	8.22	9.01	0.19	0.22
26	28.61	-346.8	1.73	12.27	0.02	7.45	7.80	0.15	0.10

DDH Homestead 6

	Depth	del 13 C	del 18 O	SiO2	TiO2	Al2O3	Fe2O3	FeO	MnO
1	-43.9	-2.1	24.2	39.28	0.45	9.19	20.72	18.667	0.08
2	-51.6	-1.9	25.0	46.04	0.48	10.84	10.50	9.459	0.08
3	-61.2	-2.1	25.0	42.97	0.48	10.78	14.09	12.694	0.07
4	-70.0	-2.3	24.5	44.99	0.54	10.94	10.53	9.486	0.12
5	-80.0	-2.4	24.0	38.95	0.45	9.51	18.88	17.009	0.10
6	-88.2	-2.4	24.8	43.77	0.44	10.36	14.22	12.811	0.09
7	-90.0	-2.5	24.2	34.81	0.40	8.81	21.86	19.694	0.13
8	-99.1	-2.9	21.8	36.06	0.37	9.21	21.54	19.405	0.11
9	-112.0	-2.3	24.2	41.00	0.46	10.93	12.70	11.441	0.12
10	-120.0	-2.7	23.5	34.83	0.37	8.95	20.93	18.856	0.10
11	-131.0	-2.9	24.4	43.45	0.43	10.31	10.60	9.550	0.14
12	-140.0	-2.7	24.4	45.68	0.47	11.06	11.51	10.369	0.12
13	-151.7	-2.6	24.1	56.77	0.59	14.73	7.25	6.532	0.02
14	-160.0	-2.8	25.0	50.48	0.51	12.59	5.58	5.027	0.13
15	-171.7	-2.7	25.1	51.03	0.50	11.97	4.91	4.423	0.20
16	-181.9	-3.2	25.0	59.45	0.38	9.83	4.63	4.171	0.30
17	-192.6	-2.1	25.9	39.64	0.30	7.68	3.93	3.541	0.63
18	-202.9	-1.9	25.7	37.18	0.32	7.60	3.21	2.892	0.64
19	-211.9	-2.2	24.8	45.26	0.41	10.99	3.18	2.865	0.40
20	-222.5	-1.6	25.2	40.78	0.35	9.44	2.27	2.045	0.39

DDH Homestead 6

	Depth	MgO	CaO	Na2O	K2O	P2O5	Loss(inc.S-)	Total	S
1	-43.9	3.44	3.72	0.09	5.03	0.15	17.34	99.50	14.33
2	-51.6	4.65	5.26	0.13	5.40	0.17	14.71	99.19	6.70
3	-61.2	4.08	4.41	0.12	5.26	0.21	15.98	99.25	9.42
4	-70.0	5.00	6.04	0.13	5.26	0.17	15.95	99.67	6.32
5	-80.0	3.85	4.47	0.09	4.58	0.22	18.30	99.40	13.08
6	-88.2	4.08	4.87	0.10	5.00	0.27	16.00	99.21	9.49
7	-90.0	3.80	4.91	0.11	4.52	0.27	20.49	100.12	15.87
8	-99.1	3.18	3.99	0.04	4.83	0.24	20.12	100.54	15.19
9	-112.0	4.65	5.62	0.14	5.14	0.20	18.58	99.69	8.77
10	-120.0	3.68	4.54	0.15	4.48	0.28	21.21	100.35	13.44
11	-131.0	5.17	6.65	0.13	5.01	0.31	17.23	99.85	7.03
12	-140.0	4.37	5.35	0.12	5.58	0.30	15.22	99.91	7.39
13	-151.7	2.47	1.20	0.08	7.13	0.32	8.19	99.59	4.37
14	-160.0	5.00	5.49	0.15	6.28	0.20	12.73	99.59	2.69
15	-171.7	5.35	6.09	0.15	5.92	0.22	12.72	99.22	1.89
16	-181.9	4.79	5.12	0.12	4.72	0.24	9.63	99.20	0.45
17	-192.6	9.59	12.92	0.11	3.91	0.23	20.61	99.55	0.21
18	-202.9	9.92	13.78	0.15	4.45	0.25	22.36	99.84	0.32
19	-211.9	7.39	9.45	0.10	6.64	0.32	15.36	99.49	0.23
20	-222.5	8.47	11.98	0.12	6.58	0.31	18.30	98.99	0.17

DDH Homestead 6

	Rb	Depth	Pb	As	Zn ppm	Cu	Sr	Ba	Tl
1	160	-43.9	155	451	71	76	22	267	47.0
2	201	-51.6	244	353	7560	56	31	371	63.0
3	196	-61.2	283	751	6590	71	29	299	80.0
4	202	-70.0	99	168	40	26	33	361	26.0
5	165	-80.0	188	332	97	48	25	240	95.0
6	188	-88.2	137	304	48	46	33	286	72.0
7	156	-90.0	180	474	61	83	27	267	118.0
8	177	-99.1	772	577	6980	70	27	287	89.0
9	202	-112.0	246	339	1100	45	38	346	47.0
10	168	-120.0	681	569	6690	65	28	312	87.0
11	189	-131.0	277	207	3290	38	35	338	26.0
12	204	-140.0	189	239	1085	42	34	356	55.0
13	257	-151.7	324	166	6750	90	39	438	23.0
14	227	-160.0	747	84	3490	84	38	411	14.0
15	211	-171.7	155	201	1360	37	36	375	6.2
16	161	-181.9	21	42	20	192	26	307	2.4
17	131	-192.6	4	4	20	7	29	237	0.5
18	114	-202.9	6	48	16	3	26	273	0.5
19	174	-211.9	10	2	20	10	25	281	0.5
20	131	-222.5	4	4	16	3	24	307	0.5

DDH Homestead 6

	Sedex Al	Al Mark 3	Depth	% MnOD	% Dolomite	C org %	CO2 wt%
1	85.0	60.7	-43.9	0.7	12.2	0.47	4.49
2	68.8	39.8	-51.6	0.5	17.3	0.58	6.53
3	76.7	47.4	-61.2	0.5	14.5	0.72	5.22
4	68.1	40.1	-70.0	0.6	19.9	0.49	7.83
5	82.4	57.4	-80.0	0.7	14.7	0.74	5.65
6	77.1	48.7	-88.2	0.6	16.0	0.59	6.15
7	84.7	62.5	-90.0	0.8	16.2	0.89	6.67
8	86.6	62.3	-99.1	0.8	13.1	3.28	5.29
9	73.1	44.8	-112.0	0.6	18.5	1.81	7.64
10	84.4	61.1	-120.0	0.7	14.9	3.15	6.48
11	67.9	41.4	-131.0	0.6	21.9	1.01	9.32
12	72.6	42.9	-140.0	0.7	17.6	0.88	6.61
13	73.2	28.1	-151.7	0.5	3.9	0.95	1.17
14	55.9	26.5	-160.0	0.7	18.1	0.52	7.68
15	54.6	27.1	-171.7	1.0	20.0	0.52	8.75
16	60.0	32.9	-181.9	1.8	16.8	0.04	7.54
17	50.6	36.3	-192.6	1.5	42.5	0.06	19.51
18	48.4	34.7	-202.9	1.4	45.3	0.02	20.94
19	48.2	27.2	-211.9	1.3	31.1	0.05	13.96
20	41.2	24.9	-222.5	1.0	39.4	0.01	18.24

Top Crossing traverse

	sample no.	m above base	distance (m)	SiO2	TiO2	Al2O3	Fe2O3	FeO	MgO	CaO	MnO
1	Pmq80	3	50	26.04	0.07	3.05	0.27	0.49	14.28	20.74	0.05
2	Pmq81	4	100	63.04	0.20	17.68	1.17	0.16	0.20	0.67	-0.01
3	Pmq82	6	150	64.29	0.16	17.46	0.35	0.02	0.24	0.41	-0.01
4	Pmq83	8	200	35.48	0.34	7.20	1.05	1.24	9.59	14.88	0.05
5	Pmq84	13	250	54.43	0.42	10.09	0.89	0.70	4.94	7.48	0.04
6	Pmq85	18	300	50.50	0.39	10.02	1.19	0.80	6.16	8.86	0.04
7	Pmq86	23	350	50.65	0.39	10.25	1.68	0.66	5.81	8.28	0.05
8	Pmq87	28	400	41.40	0.30	7.75	1.20	0.95	8.41	12.87	0.08
9	Pmq88	33	450	32.81	0.21	5.40	1.00	1.06	11.17	17.01	0.24
10	Pmq89	38	500	36.24	0.24	6.14	1.08	0.98	10.11	15.35	0.35
11	Pmq90	43	550	32.37	0.17	4.93	0.61	1.26	11.12	17.46	0.75
12	Pmq91	47	600	46.45	0.19	6.63	0.49	0.88	7.79	11.99	0.50
13	Pmq92	52	650	29.26	0.13	3.83	0.87	0.91	12.20	18.87	0.96
14	Pmq93	58	700	38.65	0.15	3.94	0.84	0.66	10.88	16.10	0.41
15	Pmq94	63	750	40.58	0.16	4.43	0.60	0.65	10.90	15.30	0.31
16	Pmq95	68	800	36.58	0.14	3.93	0.78	0.59	11.75	16.56	0.25
17	Pmq96	74	850	29.56	0.09	3.14	0.67	0.62	13.40	19.47	0.23
18	Pmq97	79	900	35.71	0.10	3.16	0.62	0.62	12.21	17.67	0.18
19	Pmq98	84	950	38.43	0.14	4.19	0.55	0.57	11.54	16.37	0.12
20	Pmq99	89	1000	27.37	0.08	3.21	0.58	0.62	14.25	19.88	0.15
21	Pmq100	94	1050	33.34	0.11	3.12	0.50	0.63	12.80	18.28	0.15
22	Pmq101	99	1100	36.05	0.12	3.30	0.75	0.48	12.19	17.34	0.15
23	Pmq102	109	1150	22.21	0.07	2.85	0.83	0.94	14.77	21.36	0.51
24	Pmq103	117	1200	76.62	0.38	8.77	4.68	0.07	0.33	0.13	0.01
25	Pmq104	120	1250	44.17	0.15	3.95	1.22	0.69	10.19	13.97	0.10
26	Pmq105	125	1300	32.63	0.10	2.75	0.50	0.75	12.60	18.74	0.08

Top Crossing traverse

	m above base	Na2O	K2O	P2O5	LOI	TOTAL	H2O	CO2	As
1	3	0.13	2.41	0.10	3.45	99.91	0.53	28.30	-4
2	4	0.14	15.40	0.10	0.10	99.88	0.54	0.48	-4
3	6	0.15	16.16	0.06	0.09	100.19	0.32	0.48	5
4	8	0.17	5.62	0.09	-0.48	99.49	1.06	23.20	8
5	13	0.18	8.11	0.23	-0.11	100.02	1.12	11.50	-4
6	18	0.17	7.33	0.18	-0.96	99.80	1.52	13.60	7
7	23	0.14	7.70	0.15	-0.18	100.21	1.53	13.10	15
8	28	0.13	5.95	0.10	-2.77	99.81	0.94	22.50	30
9	33	0.15	4.03	0.06	-2.56	99.92	0.84	28.50	6
10	38	0.15	4.38	0.10	-2.90	99.51	1.00	26.30	13
11	43	0.16	3.66	0.10	-2.62	99.92	0.65	29.30	4
12	47	0.12	5.22	0.07	1.39	99.50	0.68	17.10	4
13	52	0.14	2.64	0.07	-5.29	99.48	0.99	33.90	7
14	58	0.13	2.47	0.06	1.36	99.74	1.19	22.90	4
15	63	0.13	2.66	0.07	1.31	100.07	1.27	21.70	-4
16	68	0.12	2.14	0.06	3.11	99.21	1.50	21.70	4
17	74	0.13	1.64	0.05	-2.52	99.50	1.32	31.70	-4
18	79	0.11	1.76	0.04	3.36	99.94	1.20	23.20	-4
19	84	0.17	2.61	0.05	1.87	99.98	1.28	22.10	-4
20	89	0.11	1.53	0.04	-3.44	99.24	1.56	33.30	4
21	94	0.14	1.66	0.05	-3.99	99.61	1.33	31.50	4
22	99	0.15	1.86	0.04	2.24	99.71	1.24	23.80	8
23	109	0.14	1.34	0.04	-4.42	98.92	1.48	36.80	8
24	117	0.10	5.81	0.03	-0.88	99.68	2.27	1.36	50
25	120	0.09	2.25	0.05	4.41	99.48	1.34	16.90	6
26	125	0.12	1.75	0.04	6.07	99.36	0.53	22.70	-4

Top Crossing traverse

	Cu	m above base	Pb	Rb	Sr	Tl	Zn	Al Mark 3	% MnOD
1	2	3	1	28	25	1	3	6.6	0.1
2	9	4	5	148	10	1	2		
3	8	6	5	146	18	2	6		
4	20	8	7	90	43	1	7	13.8	0.1
5	2	13	9	124	33	1	7	11.2	0.2
6	15	18	10	131	36	1	10	12.3	0.1
7	22	23	13	136	34	1	13	14.3	0.2
8	15	28	14	102	39	1	11	14.9	0.2
9	11	33	8	75	24	1	10	20.8	0.4
10	11	38	12	89	27	1	11	25.1	0.7
11	9	43	6	68	23	1	7	36.7	1.3
12	9	47	7	84	21	1	6	30.5	1.3
13	6	52	12	56	26	1	11	41.3	1.5
14	10	58	6	58	32	1	10	27.1	0.8
15	8	63	5	66	34	1	9	21.9	0.6
16	7	68	5	58	38	1	10	19.5	0.5
17	5	74	3	44	34	1	19	17.6	0.4
18	6	79	3	45	31	1	9	16.2	0.3
19	4	84	5	58	37	1	7	12.6	0.2
20	7	89	4	42	36	1	8	13.2	0.2
21	4	94	4	45	33	1	10	14.0	0.2
22	3	99	5	49	35	1	8	14.6	0.3
23	5	109	6	37	40	1	9	27.8	0.7
24	25	117	26	122	26	1	6		
25	11	120	5	60	34	1	14	16.5	0.2
26	4	125	3	44	29	1	5	11.5	0.1

Top Crossing traverse

	m above base	% Dolomite	del 13C per mil	del 18O per mil
1	3	68.2	-0.5	22.6
2	4	2.2		
3	6	1.3		
4	8	49.0	-1.0	22.9
5	13	24.6	-1.2	21.3
6	18	29.1	-1.1	21.4
7	23	27.2	-1.1	21.9
8	28	42.3	-0.9	21.5
9	33	56.0	-0.8	20.6
10	38	50.5	-0.6	20.1
11	43	57.4	-0.7	20.6
12	47	39.4	-0.8	21.0
13	52	62.1	-0.6	20.5
14	58	53.0	-0.8	21.9
15	63	50.3	-0.8	22.7
16	68	54.5	-0.6	23.0
17	74	64.1	-0.6	21.2
18	79	58.1	-0.6	22.7
19	84	53.9	-0.2	23.8
20	89	65.4	-0.3	22.5
21	94	60.1	-0.4	22.7
22	99	57.0	-0.4	22.9
23	109	70.3	-0.7	22.1
24	117	0.4		
25	120	46.0	-0.6	22.5
26	125	61.7	-0.7	21.4

Regional geophysics — Camooweal map sheet

Mark Duffett
Centre for Ore Deposit and Exploration Studies, Geology Department, University of Tasmania

Introduction

This report presents preliminary analysis of gravity and magnetic data from the Camooweal 1:250,000 map sheet. This area overlaps parts of three major geological provinces — the Cloncurry Orogen (McConachie et al, 1993), in particular the Leichhardt Rift of O'Dea and Lister (1995); the southern portion of the Riversleigh Fold Zone; and the northeastern portion of the Georgina Basin. The interpretation follows from the work of Leaman (1992–94) and employs the same methodology (Leaman, 1993b, 1994a, c). However, there are a number of inconsistencies between this work and that of Leaman which are yet to be resolved. This is expanded upon in the 'Interpretation' section.

Geology

Significant Palaeoproterozoic outcrop over a substantial proportion of the Camooweal sheet (Fig. 1), in particular the eastern third, enforces stringent controls on the overall analysis. Siliciclastic sediments and voluminous mafic volcanics of the Haslingden Group ('Cover sequence 2' of Blake, 1987) dominate the area east of the Mount Gordon Fault Zone. The oldest exposed unit is the Leander Quartzite in the southeast corner of the map sheet, though still older rocks (Ewen Granite, Leichhardt Volcanics) outcrop just off the eastern edge of the area. The Haslingden Group sequence generally youngs northwards, though this trend is interrupted and repeated by a series of E–W striking faults.

West of the Mount Gordon Fault Zone, both the exposed structural level and structural style change markedly. Dolomites, dolomitic siltstones and shales of the McNamara Group are the dominant exposed lithology, overlying siliciclastics and minor bimodal volcanics (Surprise Creek Formation, Bigie Formation, Fiery Creek Volcanics) which in turn lie unconformably on the Haslingden Group and Quilalar Formation. The Quilalar Formation, a mixed carbonate/siliciclastic sequence correlated with the sag or thermal subsidence phase of Blake's cover sequence 2 (op cit.), only appears in the northern half of the region.

The dominant structural style is one of basin-and-dome folding with wavelengths up to many kilometres, though Keele (this volume) believes the structuring to be somewhat more brittle. The gross sense of regional plunge is reversed to that of the Leichhardt Rift, with older units generally becoming more prevalent northwards. An overall N–S tectonic grain was imposed on the region during E–W shortening (D2) of the Isa Orogeny. Isan Orogeny deformation appears to be accentuated in a north-trending 'high strain zone' bounded by the Russell Creek and Western Border Faults (Keele, this report).

Mineralisation

Locations of base metal mineralisation are depicted in Figure 1. The only notable stratiform sediment-hosted Pb–Zn deposit amongst these is the Lady Loretta Pb–Zn–Ag orebody. More detailed information on Lady Loretta and its setting within carbonaceous and dolomitic shales of the Lady Loretta Formation (middle McNamara Group) may be found in McGoldrick et al. (1996) and Dunster (1996).

All other base metal mineralisation is dominated by copper occurrences; the largest of these being the stratabound Mammoth orebodies. Mammoth Cu is hosted by the Whitworth Quartzite of the Myally Subgroup, and is thought to have been sourced from the Eastern Creek Volcanics via fluids which migrated up the Mammoth Extended and associated faults (Scott and Taylor, 1982). As with Lady Loretta, it is currently considered marginally economic. Other notable copper deposits in the Camooweal area include Mount Oxide (Hutton and Sweet, 1982), Mount Kelly (Bampton et al., 1977) and Lady Annie, near Lady Loretta (Lewis, 1975).

Geophysical data

As with previous geophysical analyses presented in the course of this project (Leaman 1992–4), AGSO regional gravity and magnetic data compilations are the mainstay of the interpretation. The AGSO gravity data (generally at 11 km spacing) have been thoroughly checked, and stations apparently in error (rare) removed. Aeromagnetic data are from four separate AGSO surveys on Camooweal and adjoining 1:250,000 map sheets. The rectangular 'hole' in the southwestern corner of the magnetic map (Fig. 3) denotes missing data on a number of flight lines from the Camooweal survey as received from AGSO. Both the Dobbyn and Cloncurry surveys (east and southeast of Camooweal, respectively) have a line spacing of 1500 m; the older Camooweal and Mount Isa surveys have flight lines approximately 3000 m (2 miles) apart. All have been merged using ECS AGP software, with the survey flown most recently (Dobbyn,1985) used as the datum for the grid joining algorithm. The resulting unified aeromagnetic map is a residual (IGRF removed), with a dc shift of 5000 added.

Regional reconnaissance data have been integrated with more detailed datasets, as this analysis is also to become part of the author's PhD thesis. One-kilometre-spaced gravity traverses have been observed in the southeastern quadrant of the Camooweal 1:250,000 sheet by the author and the Geological Survey of Queensland (B. Stockill, pers. comm.). Data from more detailed surveys centred on Lady Loretta (Duffett, 1996) and Mount Kelly (C. Stegman/CRA, pers. comm.) have also been incorporated, though their presence is not apparent at this scale of gridding and interpretation. An additional aeromagnetic dataset flown in 1987 by Ashton Mining over the Mammoth Mines 1:100,000 map sheet (southeastern corner of Camooweal) with much closer line spacing (250 m) has also been included in the joined regional aeromagnetic map after upward continuation to the nominal terrain clearance of the AGSO surveys (150 m.).

Both gravity and magnetic data are dominated by NNW to NNE oriented features, though sub E–W trends are also apparent. Among the most prominent features in the combined gravity (Fig. 2) and magnetic (Fig. 3) data are coincident gravity and magnetic highs associated with the Eastern Creek Volcanics either in outcrop or at shallow depths in the Cloncurry Orogen (east of the Mount Gordon Fault Zone). High frequency trends within the volcanics define the position and orientation of intercalated siliciclastic sedimentary layers. N–S trending dolerite dykes, clearly less magnetic than the volcanics which they intrude (Myally Subgroup sediments are also intruded) are visible as prominent magnetic lows, and may even be reversely magnetised.

Over most of the map area the gravity field slopes gently down to the west, with an abrupt steepening resulting in quite low Bouguer values in the western quarter of the area. Magnetic data mimics this apparent major tectonic boundary only moderately, with a high amplitude, long wavelength magnetic anomaly partly coincident with the gravity low.

A NE–SW oriented coincident gravity and magnetic low is clearly associated with the Weberra Granite. Emplacement of the granite beneath the Fiery Creek Dome and further to the southwest is evidently implied. The geophysical data also provide confirmation that the Weberra Granite and Fiery Creek Volcanics are co-magmatic, as seen in the relationship of the gravity and magnetic low to the most extensive outcrops of Fiery Creek Volcanics.

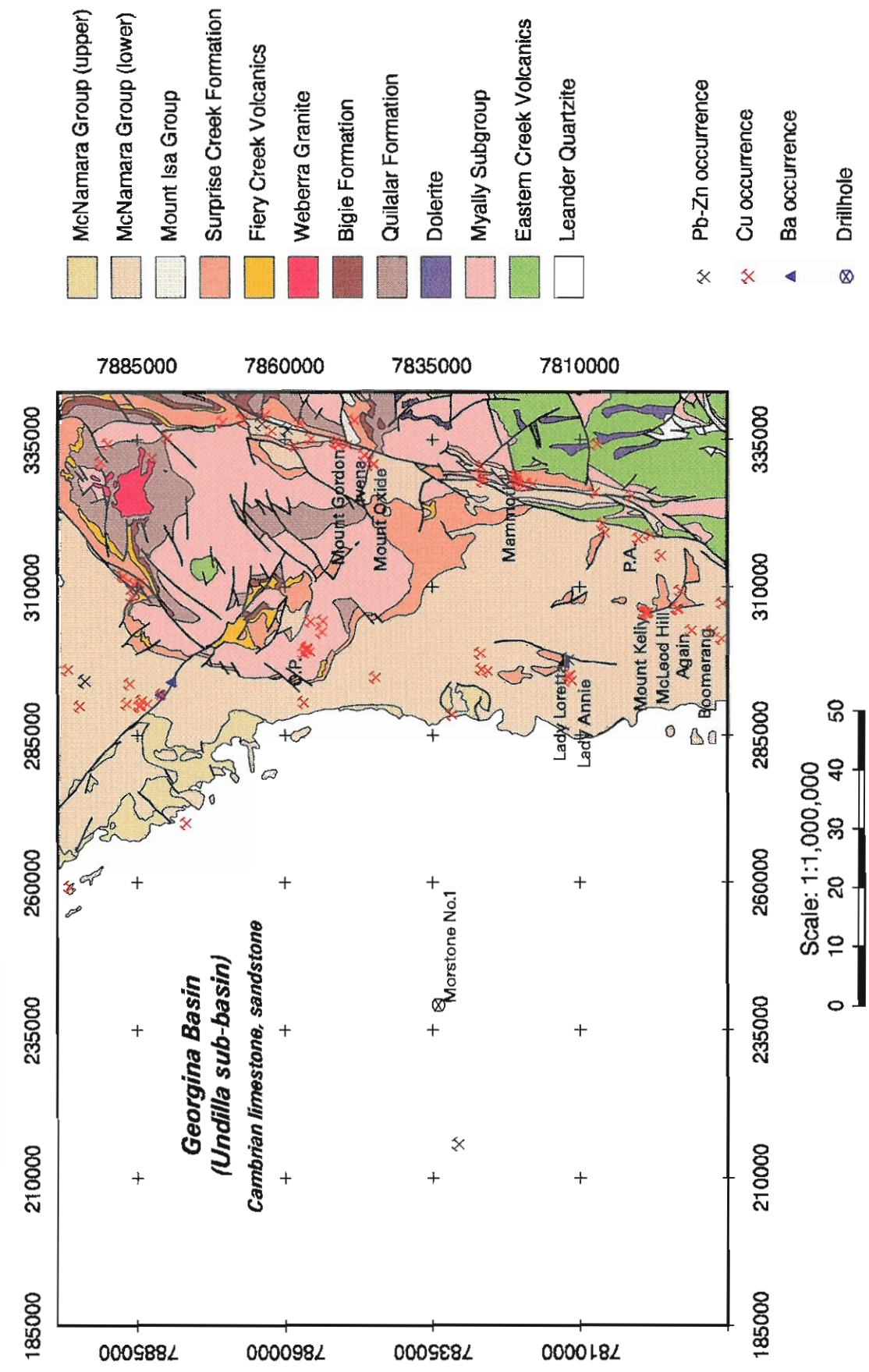

Figure 1 Camooweal geology and mineral occurrences (extracted from AGSO Mount Isa GIS — Wyborn et al., 1993)

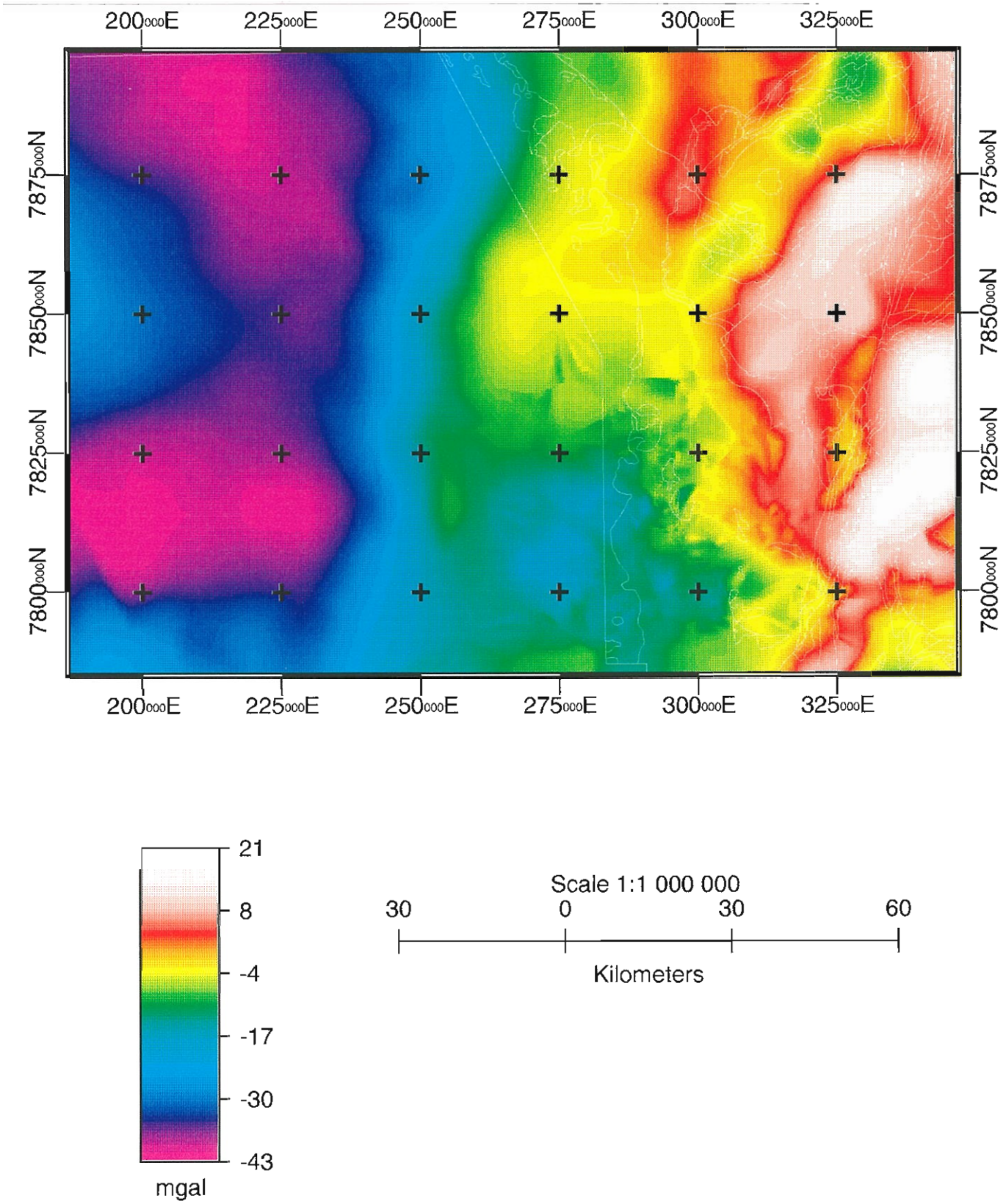

Figure 2 Camooweal Bouguer gravity with geology overlay

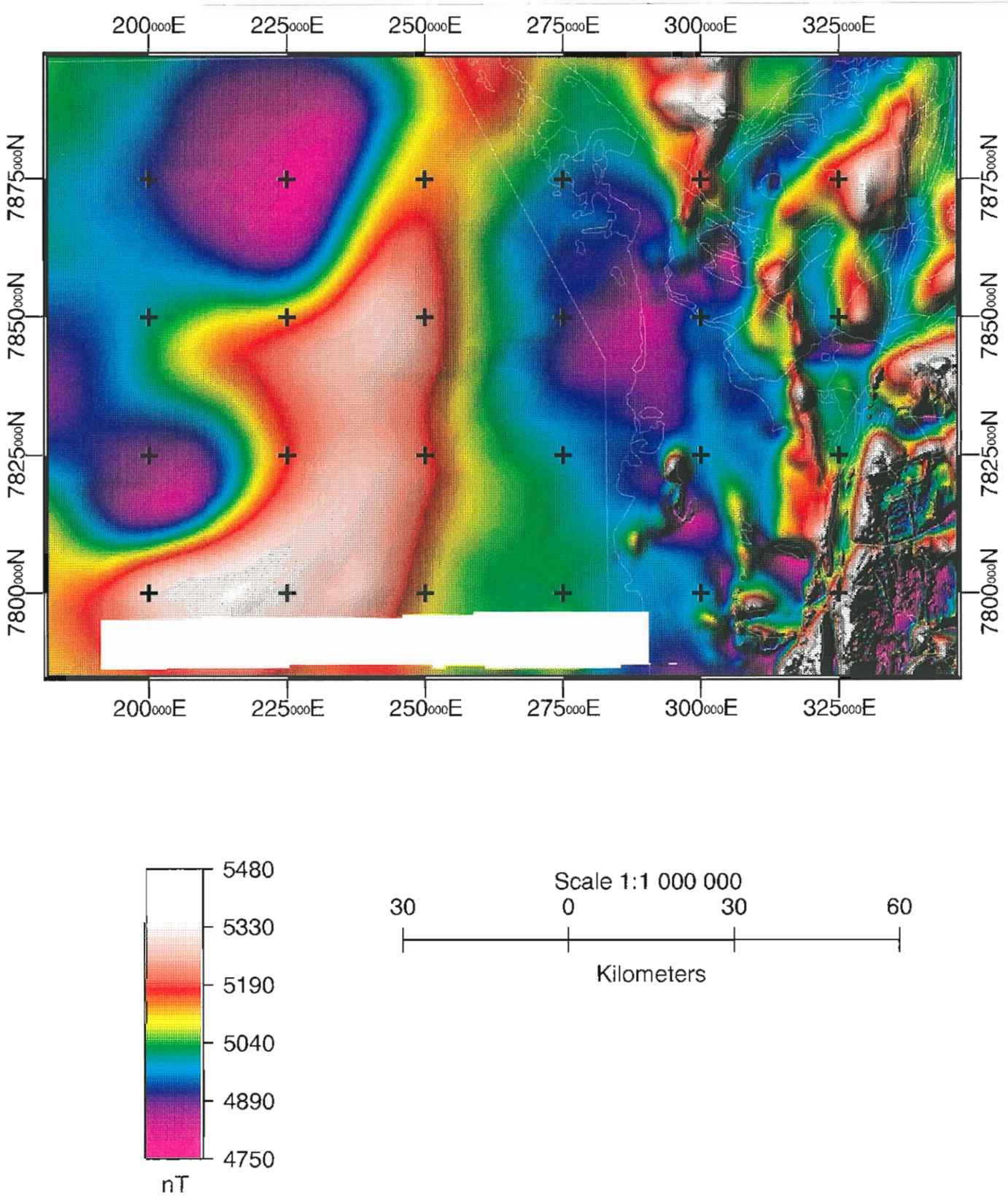

Figure 3 Camooweal aeromagnetic data compilation with geology overlay

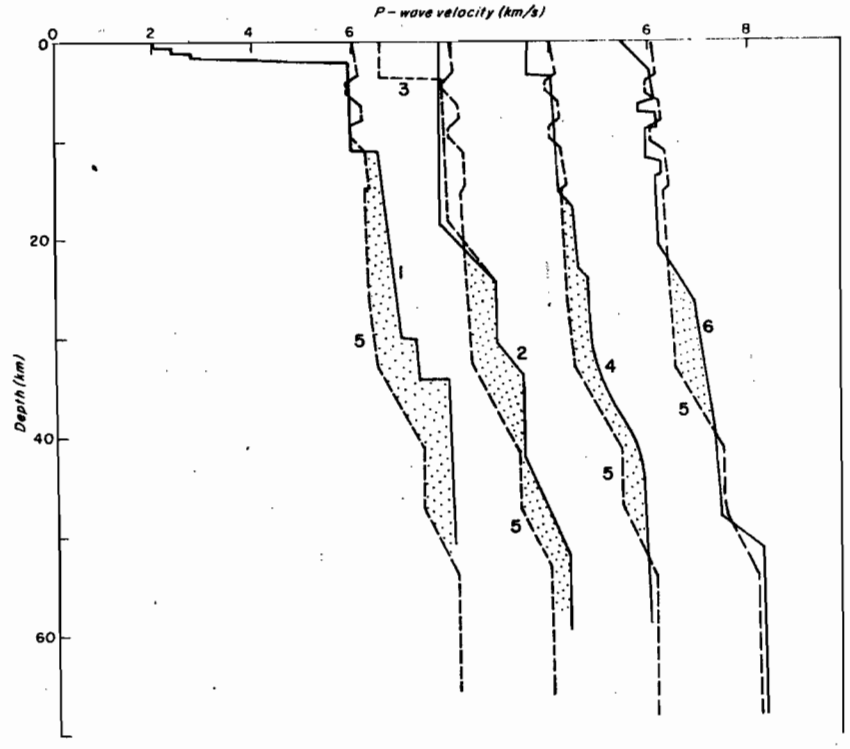

Figure 4 Seismic P wave velocity–depth profiles from the north Australian Proterozoic, after Finlayson (1982; his Fig. 6): 1, West Arafura Sea; 2 and 3, west McArthur Basin; 4, east McArthur Basin; 5, North Australian Craton – Mount Isa; 6, North Australian Craton – Tennant Creek. Note the relatively low velocity in the (western) Mount Isa region over a substantial range of crustal depths (stippled area).

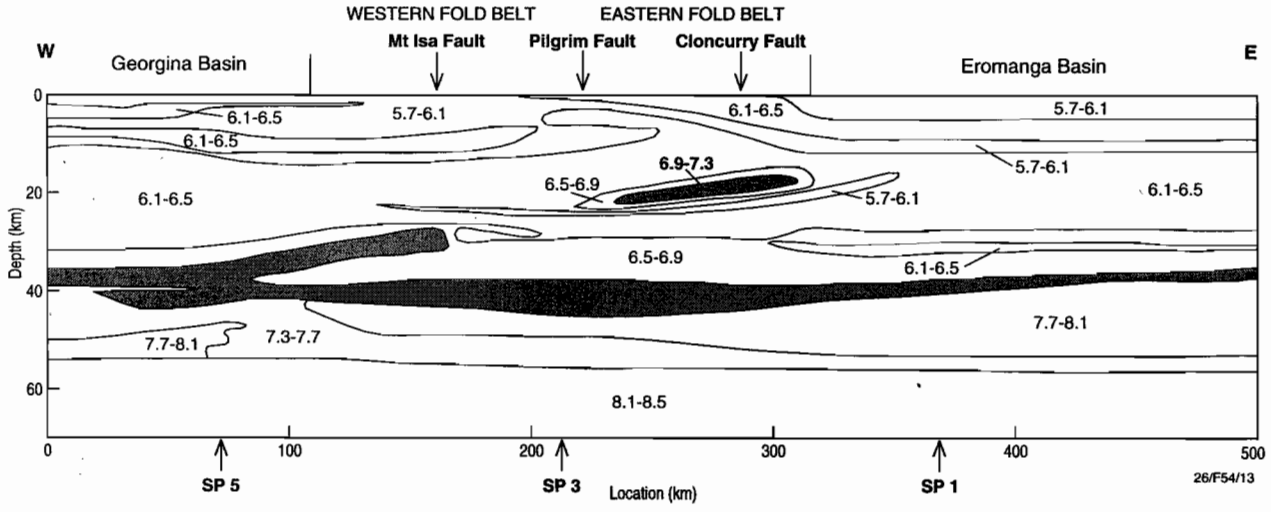

Figure 5 Seismic velocity distribution along the AGCRC Mount Isa geodynamic transect. After Goncharov et al. (1996).

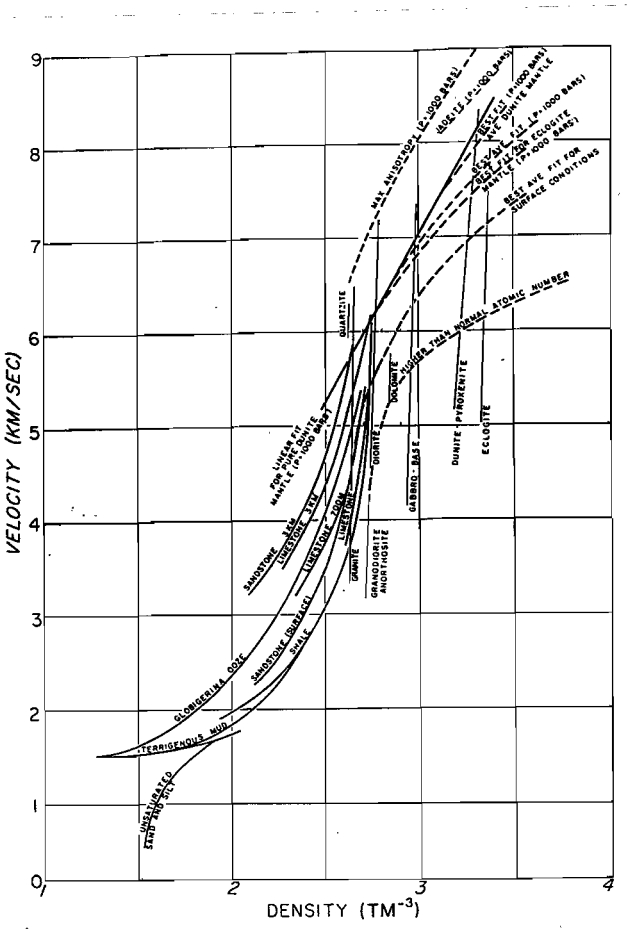

Figure 6 Velocity–density relationships for various lithologies. After Woollard (1962).

Previous work

Some interpretation of AGSO regional geophysical data has been undertaken previously in the region of the Camooweal sheet, but this has generally been only semi-quantitative at best. Wellman (1992a,b) has subdivided the Mount Isa province of the Carpentaria Superbasin ('Mount Isa Geophysical Domain') into a number of zones based on qualitative assessments of gravity and magnetics. The western boundary of the 'Mount Isa Domain' was fixed *east* of outcropping Riversleigh Fold Zone rocks based on truncation of structures in the data, though a discrepancy between indications from gravity and magnetic data was noted in the Camooweal region. Wellman suggested that the 'geophysical boundary' might be 'gradational' in this area. He also observed the Mount Isa region to be a relative high on continental Bouguer and free-air gravity maps, and ascribed this to the 'Mount Isa Domain' crust being of relatively high density.

Control of the regional gravity field by relief on the Moho has been postulated by a number of authors. Crustal thinning from 40 km to 38 km coincident with outcrop and subsurface extensions of the Cloncurry Orogen was interpreted principally from regional gravity by Shirley (1979), however this work did not adequately define crustal thickness on the western margin of the Carpentaria Superbasin. Variations in crustal thickness ranging from 33 to over 35 km were invoked to account for regional Bouguer gravity gradients by Tucker et al. (1979) in their regional gravity and magnetic study of the Georgina Basin, though the possibility of gross lateral density changes in the crust contributing to the regional gravity field was also canvassed.

A combined sedimentary accumulation of up to 13 km including 5000 m of 'Adelaidean' sediments (probably equivalent to the South Nicholson Group) and 8000 m of 'Carpentarian Lawn Hill Formation'

was modelled to fit a gravity low in the area corresponding to the western third of the Camooweal sheet by Tucker et al. (1979). Marked basement shallowing over a distance of a few tens of kilometres from 13 km depth to less than 200 m beneath subcrop of Carpentaria Superbasin rocks was thereby implied. This basement was inferred to composed of rocks with affinities to the Hatches Creek Group and Warramunga Group of the Tennant Creek Inlier. The boundary between these units ('Aljawarra Craton') and the 'Mount Isa Orogen' was placed 20 km east of the wildcat hydrocarbon exploration drillhole Morstone No.1 by Tucker et al (op. cit.).

Seismic refraction data provide some information on upper crustal geology in the Camooweal region. Finlayson (1987) quoted a Moho depth of between 51 and 54 km for the region between Tennant Creek and Mount Isa; this should be compared with a crustal thickness of 44 km in the eastern McArthur Basin (Collins, 1983). Low velocity zones (5.9–6.25 km/s) were attributed to 'Leichhardt Metamorphics with interspersed granites', and interpreted to persist to depths of at least 15 km (Finlayson, 1982). Lower velocities persist to greater (middle-lower crustal; 25–35 km) depths at Mount Isa compared to other Proterozoic cratonic areas in northern Australia (Fig. 4), implying relatively lower crustal density in the Camooweal region. Finlayson (1987) noted unusually thick high velocity layers in the lower crust beneath fold belt provinces such as the Cloncurry Orogen/Riversleigh Fold Zone compared to surrounding intracratonic basins. Such features are likely to be a significant control on regional gravity gradients.

Crustal seismic velocity models for the south-western portion of the Carpentaria Superbasin (west of Mount Isa) have been refined in the course of the AGSO seismic reflection/refraction traverse across the Riversleigh Fold Zone and Cloncurry Orogen (Goncharov et al., 1996). Crustal thickness was assessed at 50–55 km, though this was at the base of a transitional layer up to 15 km thick (Goleby et al., 1996). Velocities west of Mount Isa are seen to be generally relatively lower at upper to lower-mid crustal depths in comparison to the central Cloncurry Orogen (Fig. 5). The improved seismic refraction model, still essentially consistent with the velocity model of Finlayson (1982), can be used as evidence for gross crustal density changes (see Fig. 6) as well as possible crustal thickness increases controlling the observed regional gravity decrease to the west.

A seismic reflection survey (Robertson, 1963; quoted in Tucker et al., 1979) conducted in the Undilla region near Morstone No. 1 was only partially successful, obtaining reflections from a maximum depth of 3000 m. This provides partial support for Tucker et al.'s (1979) hypothesis of a massive sedimentary accumulation below this part of the Georgina Basin.

The discrepancy between seismically-derived crustal thickness values (50–55 km) and those derived from gravity (33–40 km) probably arises from differences in definition of the Moho, which can in turn be traced to the transitional nature of the crust-mantle boundary in this region. Gravity methods have tended to pick a depth corresponding to the top of the transitional layer as the base of the crust, while seismic methods place the boundary beneath the transitional layer. Whatever the semantic definition, lateral density variations at all levels within and at the base of the crust defined by previous regional gravity and seismic studies are likely to form a significant component of regional gravity gradients. Crustal-scale components will therefore be required in gravity models.

Rock properties

A number of petrophysical data sets exist for lithostratigraphic units of the Camooweal region. Data from Hone et al. (1987) and Emerson (1995) is summarised in Figure 7, and may be compared with values adopted by Leaman in previous AMIRA reports (Fig. 8). Additional data have been collated from Clark (1980), Shirley (1976), Neumann (1964), Gibb (1957), J. Dunster (pers. comm.) and values quoted in Leaman (1991). In spite of this plethora of sources; of the units observed or inferred to occur in the Camooweal region, only the Eastern Creek Volcanics, Myally Subgroup and Mount Isa Group are considered to be well characterised petro-

physically. This is due to the large number of samples obtained from below the weathering surface in studies associated with the Mount Isa Mine. Other data sets, particularly that of Hone et al. (1987), contain a large proportion of samples obtained from outcrop, and thus bulk property estimations based on simple arithmetic means, especially of density, are likely to be too low.

The majority of McNamara Group samples shown in Figure 7 are black shales (Emerson, 1995). Nearly all can be considered slightly magnetic to non-magnetic. Two populations are discernible within the data, essentially differentiated on density; one centred near 2.65 t/m^3 and the other near 2.75 t/m^3. The high-density, slightly magnetic 'tail' on the second population is due to an increasing sulphidic component, possibly including traces of pyrrhotite (Emerson, 1995).

There are however many other volumetrically significant lithological components of the McNamara Group, including dolostones, siltstones and sandstones. Additionally, these lithologies are not evenly distributed through the McNamara Group, lower siliciclastics (Torpedo Creek Quartzite, Gunpowder Creek Formation) giving way to dolostone-dominated units higher up (Paradise Creek Formation, Lady Loretta Formation). Consequently the Emerson (1995) data set on its own does not petrophysically define the whole McNamara Group adequately. Values derived from the correlative Mount Isa Group (Leaman, 1991) have thus been primarily employed in modelling the McNamara Group. It is probable that gravity methods may distinguish siliciclastic and dolostone/shale formations within the McNamara Group, however this is beyond the scope of the current study.

Siliciclastic-dominated sediment packages underlying the McNamara Group (Surprise Creek Formation, Bigie Formation, Myally Subgroup) are likely to be indistinguishable in their bulk physical properties, and have been modelled as a single package. This package is likely to include the basal siliciclastic McNamara Group in many places.

Physical properties measured on the older felsic volcanic units are the most problematic so far as their characterisation for geophysical modelling is concerned. The majority of samples (all from Hone et al., 1987) have a density less than 2.70 t/m^3, and magnetic susceptibility is highly variable. Note also the low density of the Fiery Creek Volcanics — a younger 'felsic volcanic' unit. This should be compared with the 2.79 t/m^3 density and 3.8x10^{-3} SI magnetic susceptibility adopted for 'felsics' by Leaman (previous AMIRA reports). A value of 2.74 t/m^3 has been adopted for the density of lower felsic volcanic units in this report. All petrophysical properties used in modelling are summarised in the table below. Reference density employed in modelling is the standard average crustal density of 2.67 t/m^3.

Unit	Density range (t/m^3)	Magnetic susceptibility (x10^{-3} SI)
Phanerozoic sediments	2.50	0
South Nicholson Group	2.59	0.20
McNamara Group (upper)	2.67	0.28
McNamara Group (lower)	2.70–2.77 (2.74)*	0.25
Mount Isa Group	2.73	0.63
Surprise Ck/Bigie/Quilalar Fm.	2.60–2.65 (2.62)	0.20–0.30
Fiery Creek Volcanics	2.55	0.34
Weberra Granite	2.60	0.08
Myally Subgroup	2.60	0.05
Eastern Creek Volcanics	2.85	63
Leander Quartzite	2.60	0.20
'Felsics'	2.74	38
'Basement' granites, metamorphics	2.62–2.74 (2.62)	0.10

* most commonly used value in brackets

Figure 7 **Petrophysical Measurements, Mount Isa Region**

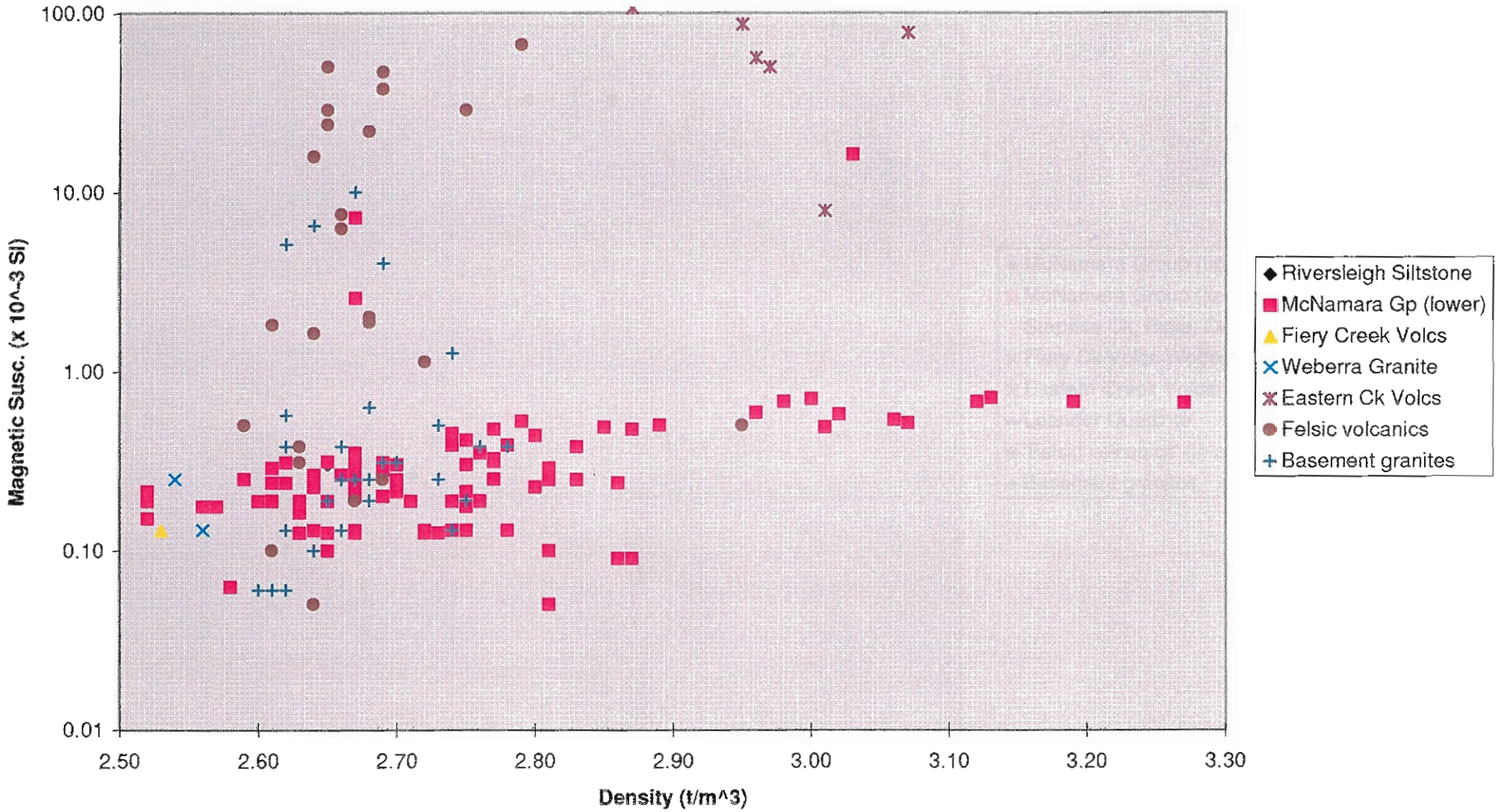

Data from Hone et al. (1987) and Emerson (1995)

Figure 8 **Petrophysical Properties Used in Modelling**

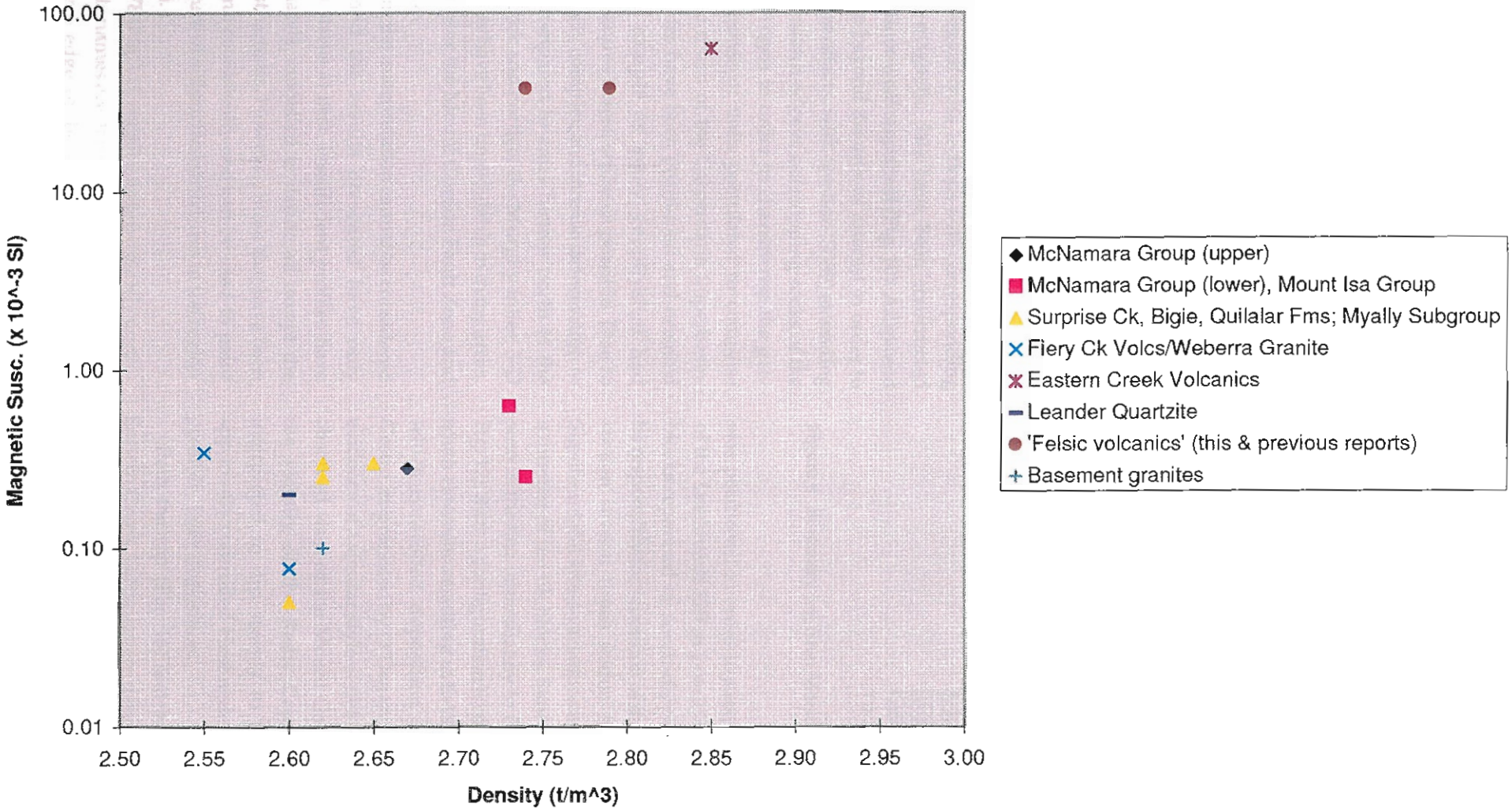

These rock properties, along with geological constraints on modelling and previous geophysical work, form the basis for interpretation. The only other notable geological data available is from the borehole Morstone No.1 (Fig. 9), drilled to test the hydrocarbon potential of the northeastern Georgina Basin. It intersected little more than 300 m of Cambrian Georgina Basin sediments, but then continued on through another several hundred metres of alternating sandstones and siltstones, which are tentatively correlated with the Constance Sandstone or Mullera Formation of the Mesoproterozoic South Nicholson Group (post-McNamara Group siliciclastic sediments).

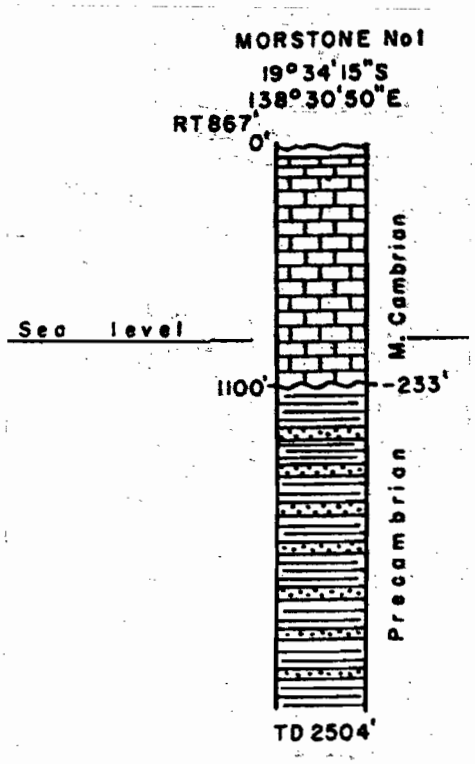

Figure 9 Summary log from Morstone No.1 drillhole

Interpretation

Twelve geological cross sections with corresponding gravity and magnetic data have been constructed across the Camooweal map sheet (Fig. 10). All extend at least 25 km beyond the area of interest in order to eliminate edge effects, with one line (S089) extending beyond the eastern edge of outcropping rocks of the Cloncurry Orogen in order to characterise the geophysical response of units postulated to comprise 'basement' to much of the Carpentaria Superbasin. The 2D profiles have been positioned and oriented in order to sample as many geophysical and geological features across strike as possible. Due to the increasingly complex and intense deformation in this region compared to areas further north in the Bowthorn Block and north of the Murphy Inlier, 3-D (off line) effects have been unavoidable in many areas, particularly near the Mount Gordon Fault Zone and Lady Loretta.

At present the interpretation cannot be considered complete, and the results presented have only preliminary status at best. Insufficient profiles have been adequately modelled to define all except the most gross structures. However, those that have been modelled link consistently and can be used to paint a broad picture of subsurface structures in the region (Figs 16–18).

Profile 178 (Fig. 11), running approximately north–south (profile names are derived from their bearings) on the eastern edge of the Camooweal map sheet, was positioned in order to sample as many features of the Leichhardt Rift as possible. Northward-tilting blocks separated by south-dipping faults are seen to be responsible for repetition of the Haslingden Group section several times within the Leichhardt Rift. Significant thickness variations are apparent between a number of the tilt blocks. Similar structures can be seen in the line immediately to the west (Profile 175, Fig. 12). Such a configuration is consistent with north–south extension resulting in E–W oriented structures which controlled deposition of the Haslingden Group, as proposed by O'Dea and Lister (1995). Some evidence of a similar style of deformation can also be observed west of the Mount Gordon Fault Zone in the vicinity of the Redie Creek Fault, which is interpreted to dip steeply to the north and has apparently controlled Haslingden Group as well as, possibly, later deposition.

Both the top (Fig. 16) and base (Fig. 17) of the Eastern Creek Volcanics are depressed in the central eastern part of the region (around northing 7840000), rising gently towards exposure as Kamarga Volcanics

in the Kamarga Dome to the north. These features might be interpreted as peripheral foreland and forebulge structures which developed post-Eastern Creek Volcanics eruption, probably during deposition of the McNamara Group.

The Haslingden Group is interpreted to thicken considerably from north to south. The most pronounced development of the depression which hosts the Haslingden Group may have been in the area south and east of Gunpowder and east of the Mount Gordon Fault Zone, as this area contains the greatest accumulation of Eastern Creek Volcanics and Leander Quartzite, though the former has been largely removed by erosion in the southeastern corner of the map area.

Conclusions about structures which may have controlled deposition of Carpentaria Superbasin sediments including the McNamara Group are difficult to draw due to the moderately intense deformation apparent in many areas. An example of this is seen in the apparent thickening of Eastern Creek Volcanics associated with the southern Mount Gordon Fault Zone and the Investigator Fault. While at least some of this may be 'real', syn-depositional thickening, a component of it is undoubtedly due to steepening of the sequence into near-vertical dips, resulting in increased apparent thickness. It should be emphasised that the 'thickness' map (Fig. 18) is of isochores, representing apparent (vertical) thickness, not isopachs (true thickness).

In spite of this effect, original thickness changes across the Mount Gordon Fault Zone may still be inferred from the isochore map presented. The Mount Gordon Fault may have acted as an accommodation zone controlling development of the Leichhardt Rift, foreshadowing its role as a major wrench fault during the latter stages of the Isan Orogeny. Its activity over a substantial period during basin development is likely to have been a significant control on the migration of mineralising fluids which resulted in the many base metal accumulations such as the Mammoth and Mount Oxide Cu deposits observed in close spatial association with the fault zone.

The unit most dominating both gravity and magnetic response in the forward models in the Eastern Creek Volcanics. Extensive outcrops of this unit east of the Mount Gordon Fault Zone place tight constraints on interpretation, and generally confirm the petrophysical properties assigned (see above). A thickness of up to 7 km of Eastern Creek Volcanics is demanded by the magnetic data (see for example profile 178). This would normally also imply a large positive Bouguer anomaly, however at most only small (in absolute terms) positive Bouguer gravity values are observed. A great volume of rock with compensating negative density contrast is therefore implied. Possible candidates for such material include the Myally Subgroup/Surprise Creek Formation siliciclastics (above the Eastern Creek Volcanics), Leander Quartzite and basement granites, however there are problems finding sufficient space for such units in many profiles. In order to account for the overall negative Bouguer anomaly values in this region, a vast volume of granitic rock is modelled as 'basement' to the Carpentaria Superbasin sequence, but even this is not enough to account for some of the lower Bouguer gravity values coincident with significant volumes of mafic volcanics (assuming a root depth of 15 km).

For this reason, gross changes in crustal thickness have been invoked in order to explain changes in the regional gravity field. There is some precedent for this step in the work of Shirley (1976) and Tucker et al. (1979; see above), and the crustal thickness changes proposed by Tucker (op cit.) have been used as a starting point for this interpretation. Relief of up to 3 km on the Moho has been used principally to explain Bouguer gravity values as low as –50 mgal in the western half of the Camooweal map sheet. Following Shirley (1976) and Tucker et al. (1979), a crust/mantle density contrast of 0.5 t/m3 has been employed.

The region west of Lady Loretta (termed the Undilla Block in this report) is highly problematic, and not solely because of the substantial Bouguer gravity low partially underlying it. The gravity low is partly coincident with a long-wavelength magnetic high of a similar magnitude to that created by the outcropping Eastern Creek Volcanics east of the Mount Gordon Fault Zone, and a body of similar dimensions and magnetic properties is required to

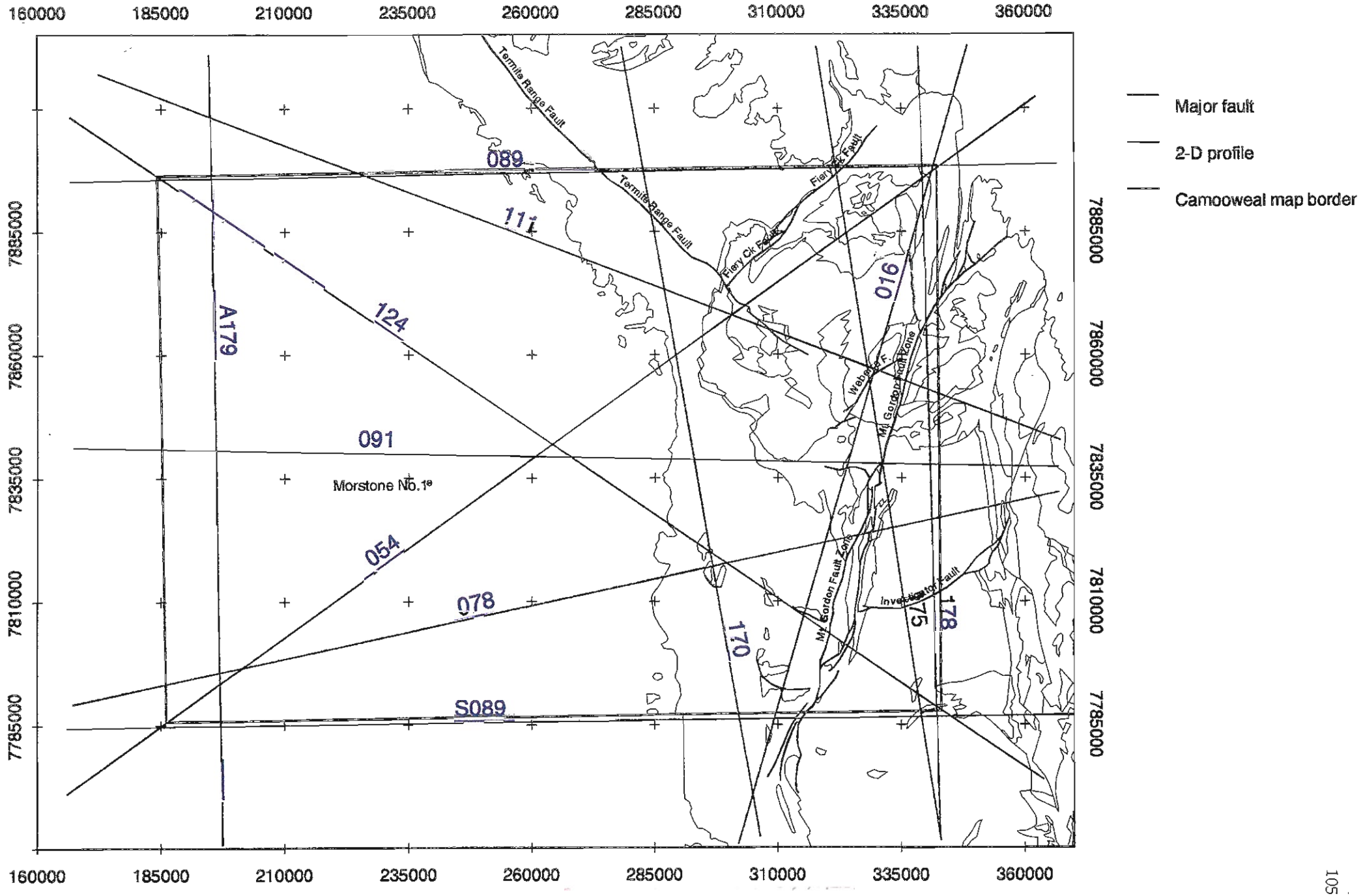

Figure 10 Locations of 2D profiles in relation to geology and major structures

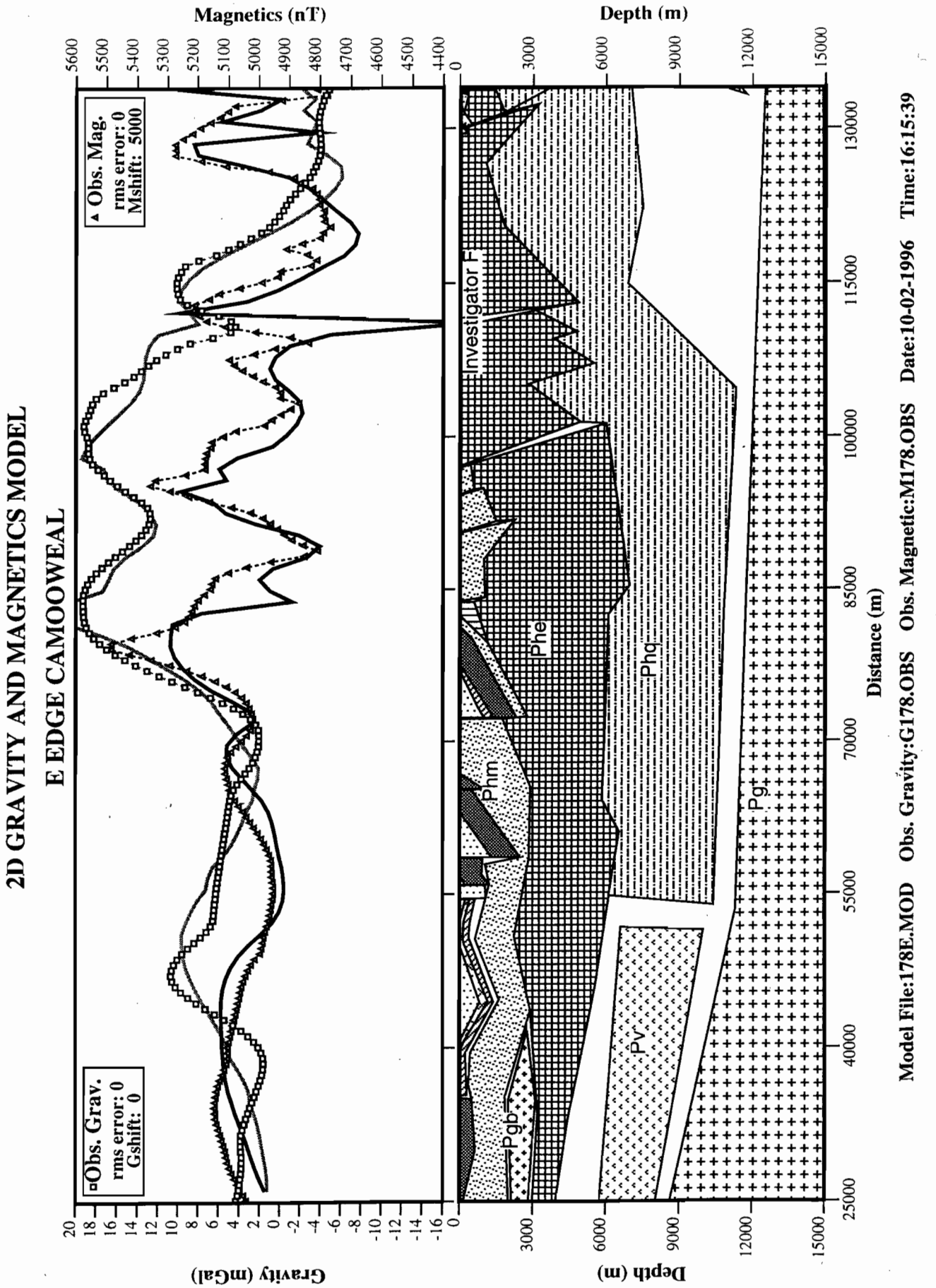

Figure 11 2D profile 178

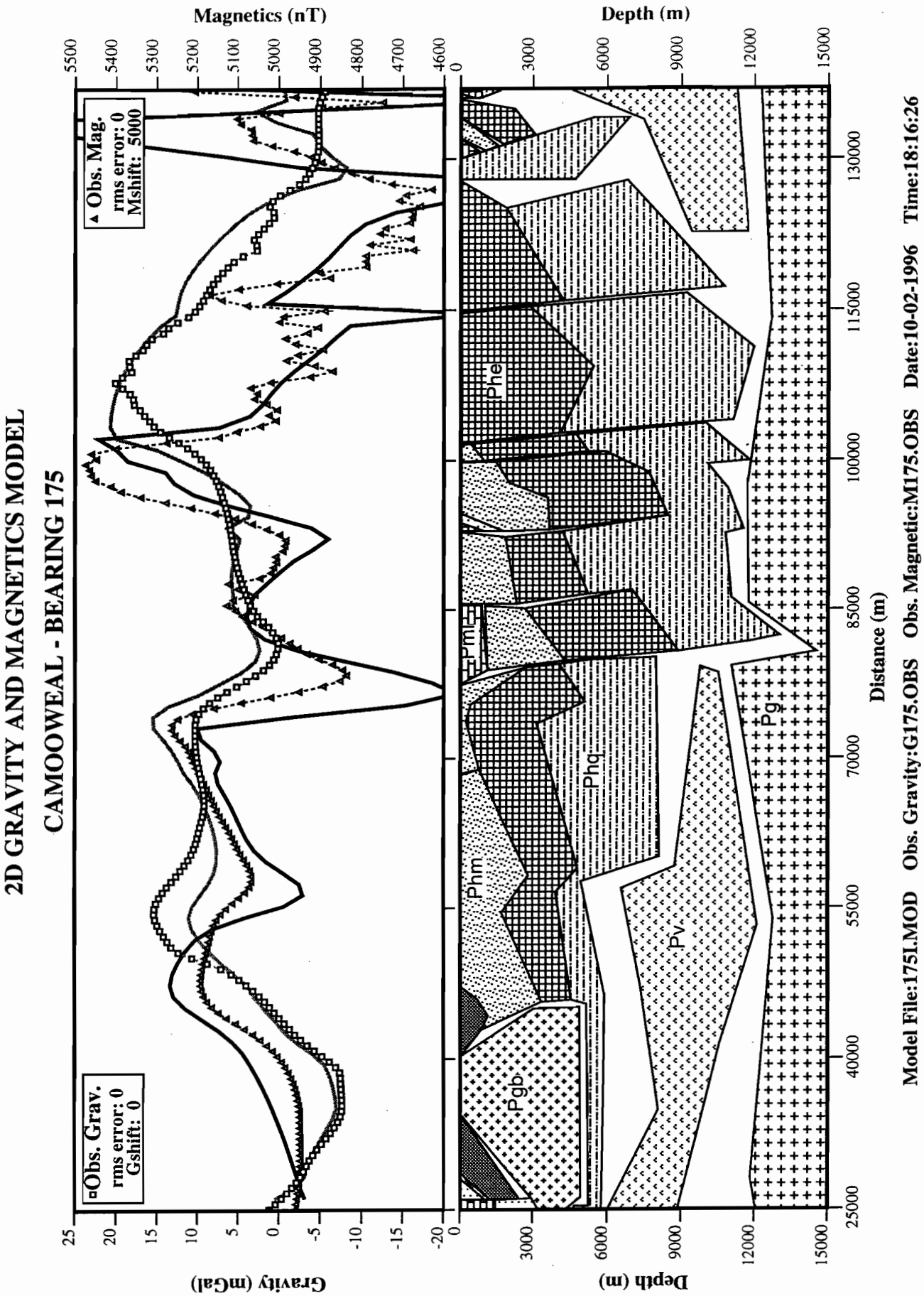

Figure 12 2D profile 175

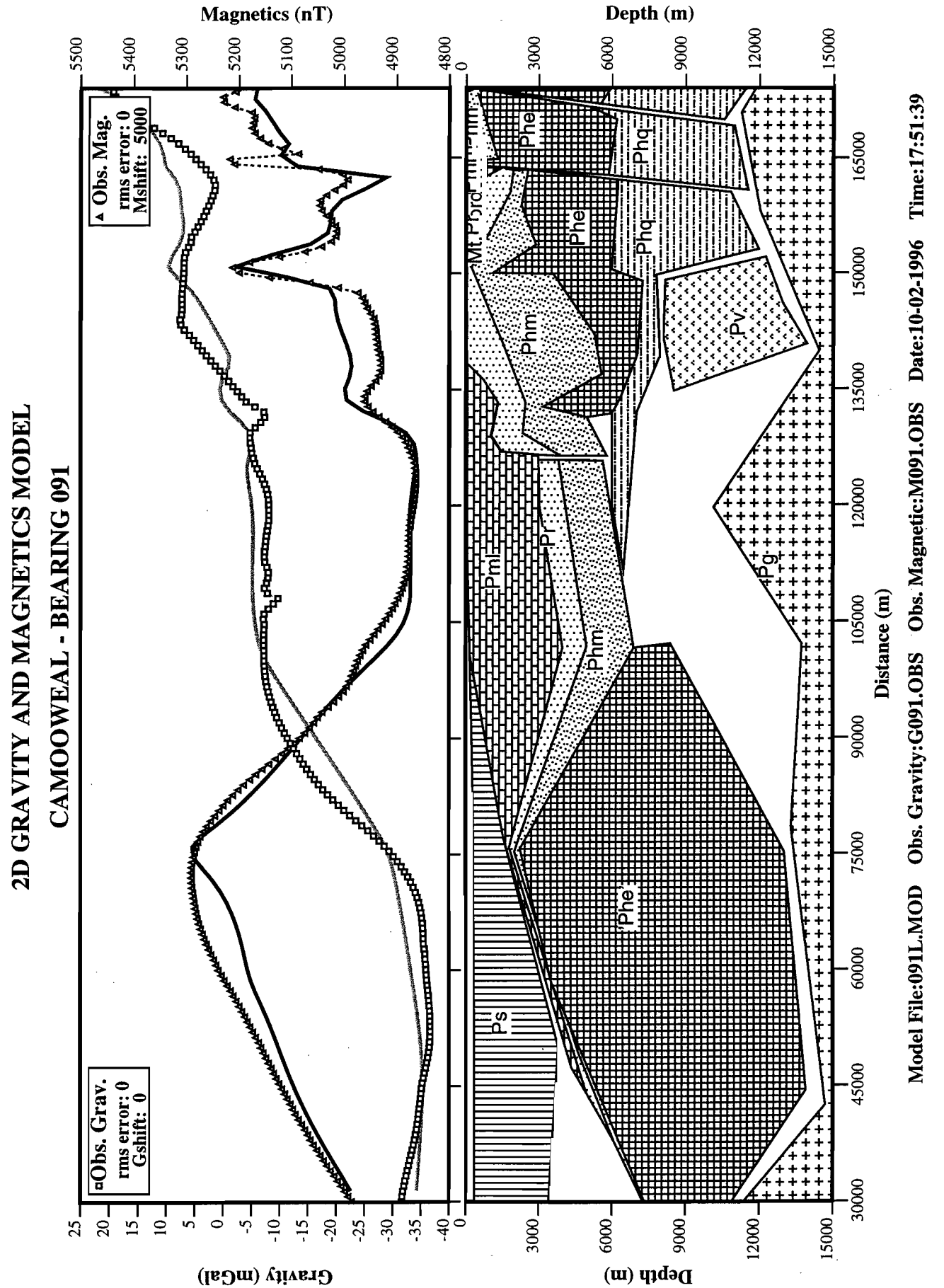

Figure 13 2D profile 091. To fit the data, the ëPheí body has magnetic susceptibility equivalent to that used for the Eastern Creek Volcanics, but has a density of 2.62 t/m³ — completely unrealistic for the Eastern Creek Volcanics.

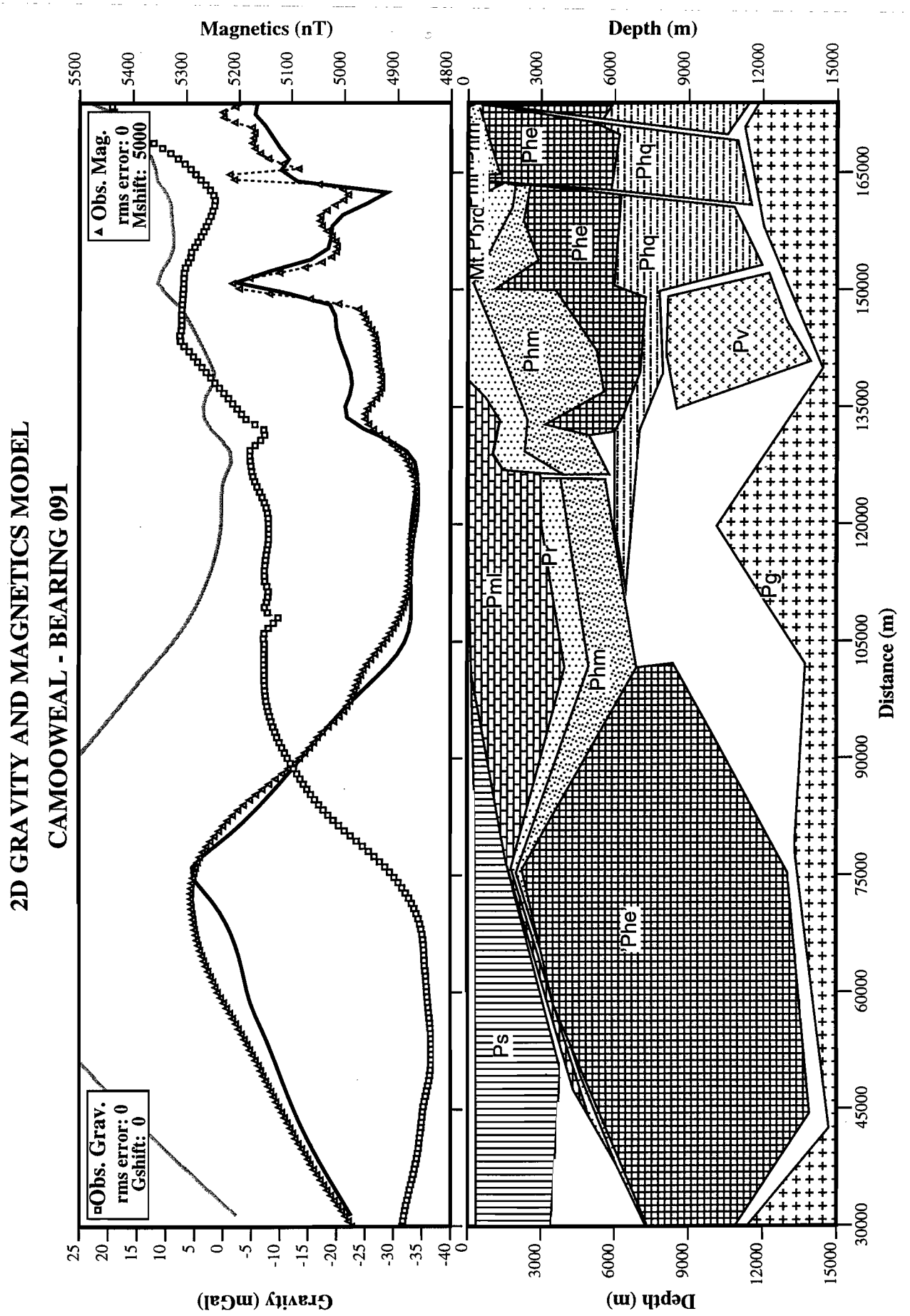

Figure 14 2D profile 091x. This profile demonstrates the impossibility of fitting the gravity data with a body of anything approaching the density of the Eastern Creek Volcanics.

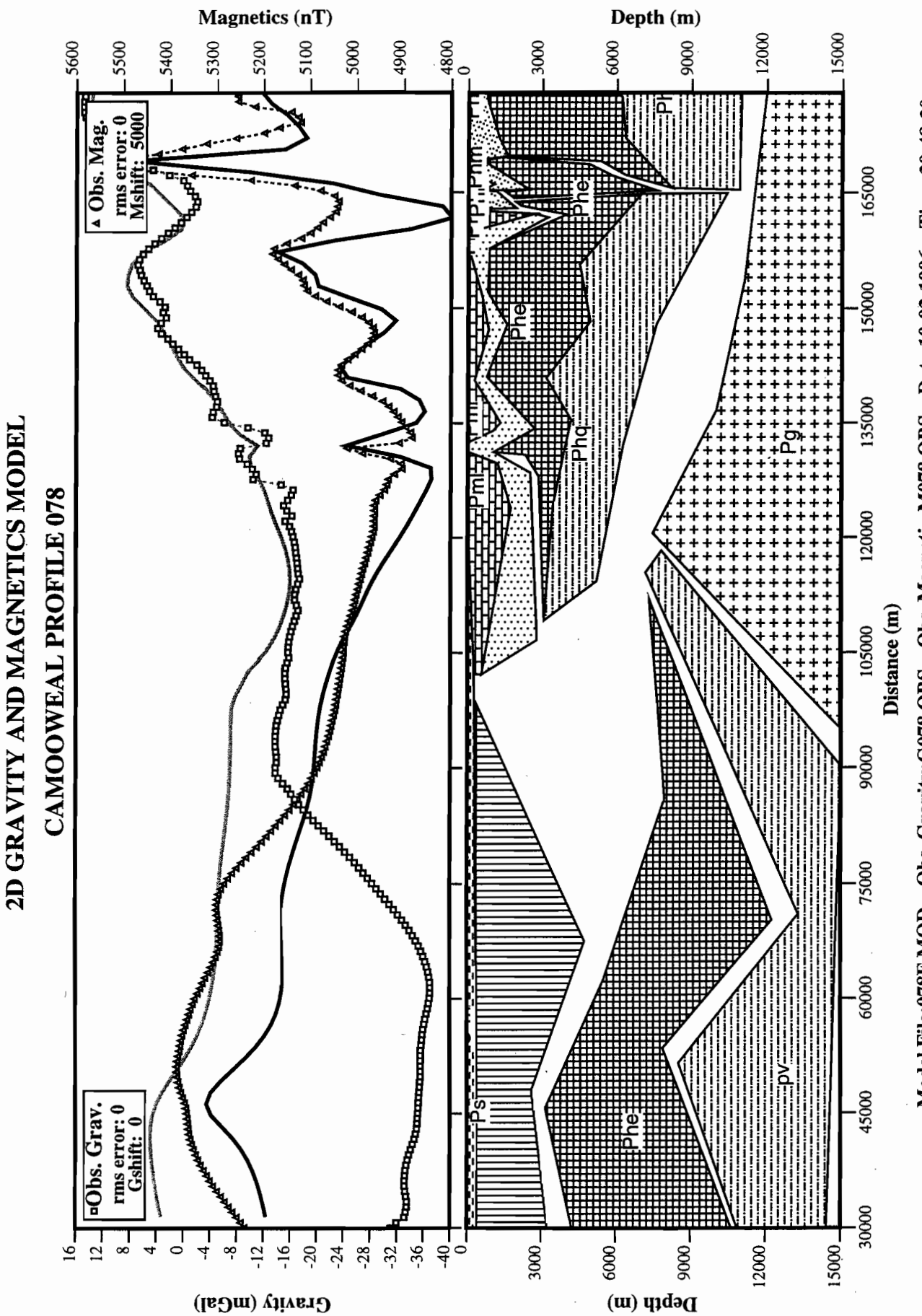

Figure 15 2D profile 078. As with profile 091, this line illustrates the difficulty in fitting both the magnetic and gravity features of the Undilla Block, even using more geologically realistic geometries. The existence of a major geological discontinuity immediately west of Lady Loretta is nonetheless confirmed.

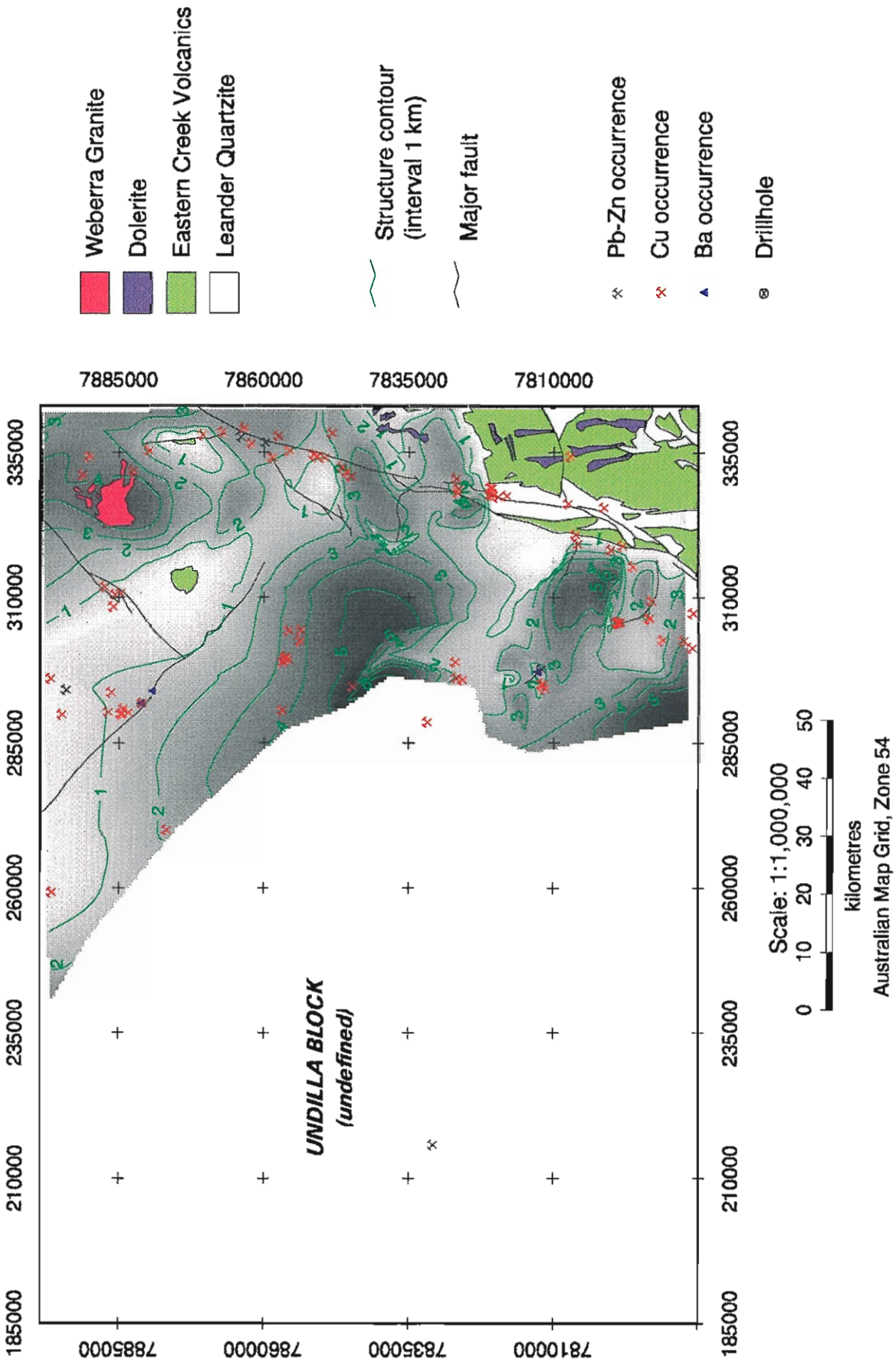

Figure 16 Interpreted upper surface of Eastern Creek Volcanics, with mineral deposit locations added for comparison.

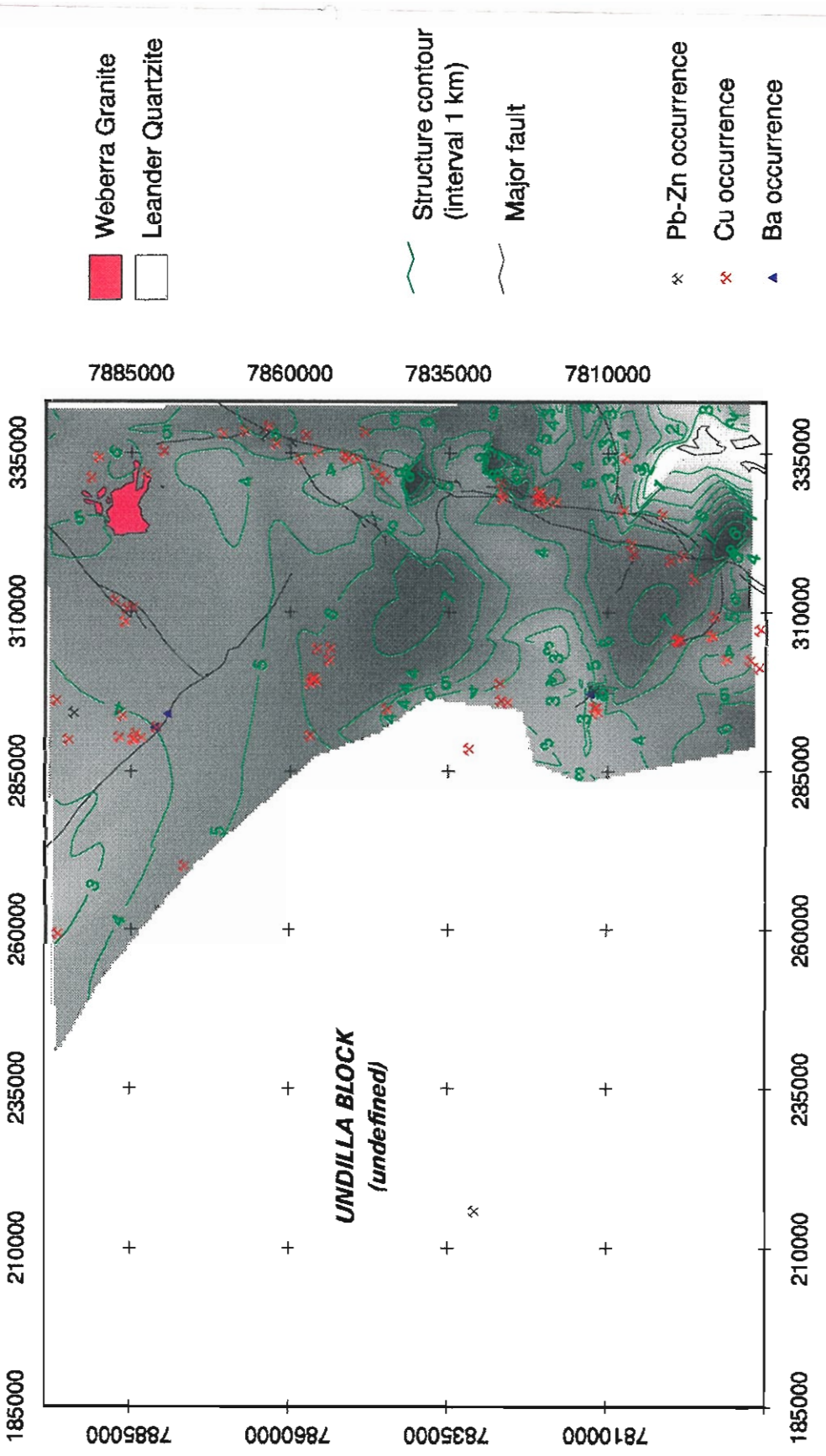

Figure 17 Interpreted basal surface of Eastern Creek Volcanics. Mineral deposits overlaid.

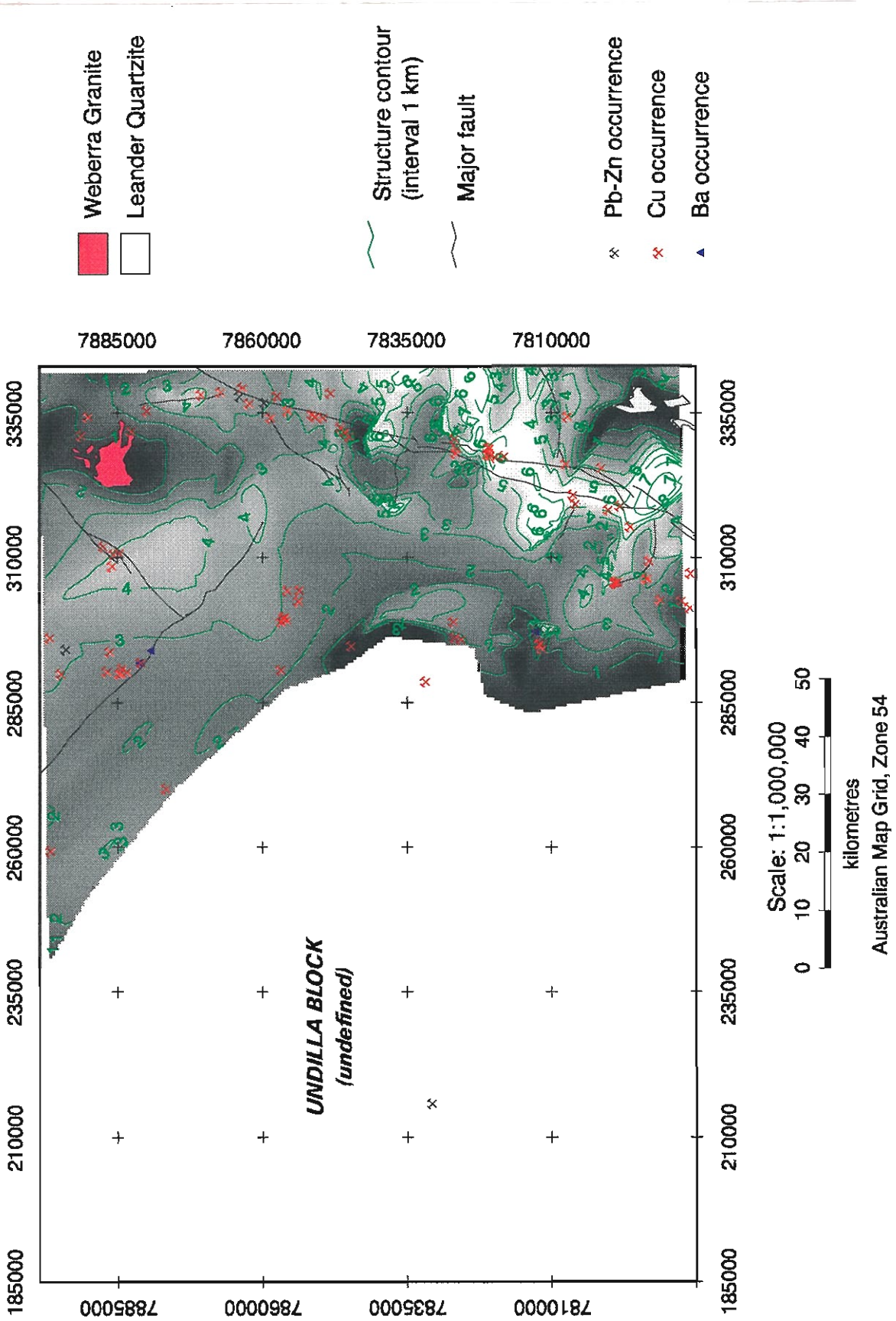

Figure 18 Interpreted preserved thickness of Eastern Creek Volcanics, expressed as isochores. Base metal mineralization locations overlaid.

model anything like the observed magnetic signature (Fig. 13, profile 091). Such a body would have to be quite shallow, however depth to its top is constrained beneath about 600 m depth by the lack of any significant magnetic units in Morstone No. 1.

There would be nothing wrong per se with a concept of a Leichhardt Rift equivalent filled with Eastern Creek Volcanics in the Undilla Block, were it not for the large gravity low. It is impossible to explain the Undilla magnetic anomaly with a body as dense as the Eastern Creek Volcanics and still successfully model the steep negative gravity gradient to the west (Figs 14 and 15, profiles 091, 078).

It is possible that some of the original assumptions made about the source magnetic data may be in error. An increase in residual magnetic base level of the order of 130 nT may be helpful in modelling the Undilla magnetic anomaly (D. Leaman, pers. comm.), however no such universal base shift is obviously implied throughout the remainder of the interpretation. A modification of this magnitude to the magnetic data would have profound effects. A further though more remote possibility is of more fundamental errors in both source data sets. Both magnetic and gravity data in this area date from the mid 1960s or before. In spite of these possible problems, and though the full implications of base level shifts are yet to be adequately explored, the null hypothesis (that the base level derived over the remainder of the region is the correct one, and that the data are essentially correct) is still preferred at this stage.

A major tectonic break is therefore proposed between the western edge of the Carpentaria Superbasin and the Undilla Block. The Eastern Creek Volcanics are interpreted to terminate at or near the western edge of outcropping Palaeoproterozoic units, though they continue in the central north and northeast through to their equivalent outcropping mafic volcanics in the Carrara Range Group and Kamarga Dome (Kamarga Volcanics). The sub-Georgina/South Nicholson geology of the Undilla Block is believed to be of different affinity, possibly to the Arunta Block, and is not yet resolved.

The absence of any significant discussion of the major felsic volcanic units interpreted by Leaman (1992–94) will have been noted by readers of previous CODES/AMIRA project reports. This omission is deliberate, and reflects uncertainties in the interpretation. Most of this uncertainty arises from doubts about the physical properties of the 'felsic volcanics' as defined by Leaman, in particular their density. Gravity data place severe restrictions on the possible volume of any felsic volcanics with a putative density of 2.79 t/m3. Even with the lower density preferred in this report (2.74 t/m^3), only relatively small thicknesses of felsic volcanics are permitted by the gravity data, and these must occur at great depth (constrained by modelled thickness of younger sediments and volcanics). Consequently, any such felsic volcanic accumulation deep in the basin has only minor (in terms of amplitude) effects on the magnetic field, and such long wavelength effects that they do have are obscured by the signal from the shallower, more magnetic and generally voluminous Eastern Creek Volcanics. A corollary to this is that the felsic volcanics' geometry is very poorly defined, to the point where presentation of structure contour and isopach maps purporting to depict their form is not considered justified at this stage in the interpretation.

Of course, this does not necessarily mean that major piles of felsic volcanics do not exist at depth in the Camooweal region. Felsic magmas, whether extrusive or not, probably form a substantial proportion of the large volumes of undifferentiated, non-magnetic 'basement' at the reference density of 2.67 t/m^3 modelled in many profiles. All that can be said is that at most only a small proportion of these possess the distinctive moderate to high magnetic susceptibility and density which characterise the substantial accumulations of felsic volcanics hypothesised to occur further north, and which are correlated with the Scrutton and Cliffdale Volcanics. Such a mixture of low to moderately high densities, and low to very high magnetic susceptibilities, is consistent with lithologies and observed physical properties of possible correlative units to the east (Leichhardt Volcanics, Argylla Formation, Bottletree Formation).

Summary and implications for mineralisation

Basin structures in the Camooweal region have been more strongly overprinted by Isan Orogeny deformation, particularly E–W compression, than in the previously assessed areas to the north. This has served to obscure earlier structural geometries which may carry information on basin development. However, some areas are less deformed than others. The area between the southern Mount Gordon Fault Zone and Lady Loretta is one example, with the most profound structures being in a WNW orientation, as opposed to sub-N–S to NE–SW grains developed in high strain zones to the east and west (Keele, this report). The WNW structures are considered to have developed concurrently with the basin, and are likely to have controlled sedimentation. Their preservation is evidence that this block has behaved relatively rigidly in relation to others around it. The margins to this block are apparently associated with base metal mineralisation, consistent with an association with both syn-deposition and syn-tectonic bounding structures. Palaeo-basin margins so defined are likely to have been a strong control on syngenetic and epigenetic mineralisation.

Acknowledgements

Advice and assistance from David Leaman and Michael Roach is gratefully acknowledged.

References

Blake, D.H., 1987. Geology of the Mount Isa Inlier and environs, Queensland and the Northern Territory. *BMR Bulletin* 225.

Bampton, K.F., Collins, A.R., Glasson, K.R. and Guy, B.B., 1977. Geochemical indications of concealed copper mineralization in an area northwest of Mount Isa, Queensland, Australia. *Journal of Geochemical Exploration* 8: 169–188.

Clark, D.A., 1980. Magnetic properties of rocks from the Mount Isa area. *Restricted Investigation Report* 1149R. CSIRO Division of Mineral Physics.

Collins, C.D.N., 1983. Crustal structure of the southern McArthur Basin from deep seismic sounding. *BMR Journal of Australian Geology and Geophysics* 8: 19–34.

Duffett, M.L., 1996. Geophysical environment of the Lady Loretta Pb–Zn deposit. In Baker, T. et al (eds.), MIC '96: The McArthur, Mt Isa, Cloncurry Minerals Province - New Developments in Metallogenic Research, Extended Conference Abstracts. *EGRU Contribution* 55: 45–46.

Dunster, J.N., 1996. Sedimentology of the Lady Loretta Formation - a comparison of the regional setting to that of the Lady Loretta orebody. In Baker, T. et al (eds.), MIC '96: The McArthur, Mt Isa, Cloncurry Minerals Province - New Developments in Metallogenic Research, Extended Conference Abstracts. *EGRU Contribution* 55: 47–50.

Emerson, D.W., 1995. Black shale conductivities, McNamara Group, NW Qld.; Petrophysical study for Aberfoyle Resources Ltd. Systems Exploration (NSW) Pty Ltd. (unpubl.). Used with permission.

Finlayson, D.M., 1982. Seismic crustal structure of the Proterozoic North Australian Craton between Tennant Creek and Mount Isa. *Journal of Geophysical Research* 87B: 10569–10578.

Finlayson, D.M., 1987. Seismic features of Proterozoic crust in northern Australia and their evolution. In Kroner, A. (ed.), Proterozoic Lithospheric Evolution. *Geodynamics Series* 17: 99–113. American Geophysical Union, Washington D.C..

Gibb, R.A., 1967. Western Queensland reconnaissance gravity surveys, 1957–1961. *Bureau of Mineral Resources, Australia, Report* 129.

Goleby, B.R., Drummond, B.J., MacCready, T. and Goncharov, A., 1996. The Mount Isa deep seismic transect. In Baker, T. et al (eds.), MIC '96: The McArthur, Mt Isa, Cloncurry Minerals Province - New Developments in Metallogenic Research, Extended Conference Abstracts. *EGRU Contribution* 55: 51–55.

Goncharov, A.G., Collins, C.D.N., Goleby, B.R., Drummond, B.J. and MacCready, T., 1996. The Mount Isa geodynamic transect: Implications of the seismic refraction model. *AGSO Research Newsletter* 24: 9–10.

Hone, I.G., Carberry, V.P. and Reith, H.G., 1987. Physical property measurements on rock samples from the Mount Isa Inlier, northwest Queensland. *Bureau of Mineral Resources, Australia, Report* 265. 30pp.

Hutton, L.J. and Sweet, I.P., 1982. Geological evolution, tectonic style and economic potential of the Lawn Hill Platform cover, Northwest Queensland. *BMR Journal of Australian Geology and Geophysics* 7: 125–134.

Leaman, D.E., 1991. Geophysical constraints on structure and alteration of the Eastern Creek Volcanics, Mt Isa, Queensland. *Australian Journal of Earth Sciences* 38: 457–472.

Leaman, D.E., 1992. Regional geophysics-basin architecture: 1. Batten Trough region. CODES AMIRA/ARC Project P384 Report 1: 1–34 (unpubl.).

Leaman, D.E., 1993a. Regional geophysics-basin architecture: 2. Batten Trough region - update and further analysis. CODES AMIRA/ARC Project P384 Report 2: 1–25 (unpubl.).

Leaman, D.E., 1993b. Issues in interpretation - McArthur Basin: Do volcanic piles really exist? CODES AMIRA/ARC Project P384 Report 2: 27–46 (unpubl.).

Leaman, D.E., 1993c. Regional geophysics-basin architecture: 3. The Wearyan Shelf and Murphy Inlier. CODES AMIRA/ARC Project P384 Report 2: 65–99.

Leaman, D.E., 1993d. Issues: Basin correlations and overall architecture. CODES AMIRA/ARC Project P384 Report 2: 101–113.

Leaman, D.E., 1993e. Regional geophysics-basin architecture: 4. The Bauhinia Shelf. CODES AMIRA/ARC Project P384 Report 4: 1–15.

Leaman, D.E., 1994a. Criteria for evaluation of potential field interpretations. *First Break* 12: 181–191.

Leaman, D.E., 1994b. Regional geophysics - basin architecture 5. The Lawn Hill Platform. CODES AMIRA/ARC Project P384 Report 7: 1–35.

Leaman, D.E., 1994c. Application of magnetics to basin structures. CODES AMIRA/ARC Project P384 Report appendix (unpaginated).

Lewis, R.W., 1975. Lady Annie secondary copper deposit. *In* Knight, C.L. (Ed.), Economic geology of Australia and Papua New Guinea; 1, Metals. *Australasian Institute Mining. Metallurgy, Monograph Series* 5: 1023–1033.

McConachie, B.A., Barlow, M.G., Dunster, J.N., Meaney, R.A. and Schaap, A.D., 1993. The Mount Isa Basin - Definition, structure and petroleum geology. *APEA Journal* 33: 237–257.

McGoldrick, P., Dunster, J., Cooke, D. and Aheimer, M., 1996. New observations from the Lady Loretta Zn–Pb–Ag deposit: towards a new genetic model. In Baker, T. et al (eds.), MIC '96: The McArthur, Mt Isa, Cloncurry Minerals Province - New Developments in Metallogenic Research, Extended Conference Abstracts. *EGRU Contribution* 55: 81–84.

Neumann, F.J.G., 1964. Normanton to Daly Waters reconnaissance gravity survey, Queensland, N.T. 1959–60. *BMR Record* 1964/131 (unpubl.).

O'Dea, M.G. and Lister, G.S., 1995. The role of ductility contrast and basement architecture in the structural evolution of the Crystal Creek block, Mount Isa Inlier, NW Queensland, Australia. *Journal of Structural Geology* 17: 949–960.

Robertson, C.S., 1963. Undilla Basin seismic survey, Queensland, 1961. *Bureau of Mineral Resources Record* 1963/63.

Scott, K.M. and Taylor, G.F., 1982. Eastern Creek Volcanics as the source of copper at the Mammoth mine, northwest Queensland. *BMR Journal of Australian Geology and Geophysics* 7: 93–98.

Shirley, J.E., 1976. Deep Crustal Structure of North Queensland. Ph.D. thesis, University of Tasmania (unpubl.).

Shirley, J.E., 1979. Crustal structure of north Queensland from gravity anomalies. *BMR Journal of Australian Geology and Geophysics* 4: 309–321.

Tucker, D.H., Wyatt, B.W., Druce, E.C., Mathur, S.P. and Harrison, P.L., 1979. The upper crustal geology of the Georgina Basin region. *BMR Journal of Australian Geology and Geophysics* 4: 209–226.

Wellman, P., 1992a. Structure of the Mount Isa region inferred from gravity and magnetic anomalies. In Stewart, A.J. and Blake, D.H. (Eds.), Detailed studies of the Mount Isa Inlier. *BMR Bulletin* 243: 15–27.

Wellman, P., 1992b. Structure of the Mount Isa region inferred from gravity and magnetic anomalies. *Exploration Geophysics* 23: 417–422.

Woollard, G.P., 1962. The relation of gravity anomalies to surface elevation, crustal structure and geology. Research Report 62-9 December 1962. University of Wisconsin Geophysical and Polar Research Center (unpubl.).

Sedimentology and diagenetic history of late Palaeoproterozoic carbonate sequences within the southern McArthur Basin, northern Australia: PhD thesis outline

Peter R. Winefield
Centre for Ore Deposit and Exploration Studies, Geology Department, University of Tasmania

Supervisors: Stuart Bull, Peter McGoldrick & Malcolm Wallace (University of Melbourne)

Introduction

The McArthur Basin extends along the southern and western margins of the Gulf of Carpenteria in Northern Australia (Fig. 1). It forms an extensive Proterozoic sedimentary system whose regional stratigraphy consists of four groups (in ascending order): the Tawallah Group (quartz sandstones, lesser conglomerate and carbonate, and mafic and felsic volcanics); the ***McArthur Group*** (dominated by carbonate and evaporitic facies with lesser sandstone; Fig. 2); the Nathan Group (mainly carbonate with lesser sandstone; and the Roper Group (quartz sandstones).

The McArthur Group is one of the world's best preserved (and unmetamorphosed) late Palaeoproterozoic carbonate-dominated sequences. It is best exposed in the southern McArthur Basin and is host to the world-class Pb–Zn–Ag McArthur River deposit, as well as several smaller non-economic mineral deposits. The discovery of the large McArthur River (or HYC) deposit in the 1950s prompted a long and continuing history of exploration and research in the southern McArthur Basin. Regional mapping has been conducted at the 1:100,000 scale by AGSO (Jackson et al., 1987) and the NTGS (Pietsch et al., 1991a,b). Together with earlier studies (e.g. Brown et al., 1969), this forms an excellent starting point for more detailed sedimentological and diagenetic research to be conducted on carbonate sequences deposited in the McArthur River area.

Significance

This research will be significant because:

- relatively few studies have been conducted on Proterozoic carbonates, especially those involving diagenetic and geochemical aspects. The chance exists to gain a better understanding of ancient carbonate facies, if/how Proterozoic carbonates differ from Phanerozoic and modern carbonates, and whether they are primary dolomites or early dolomitised limestones. This would/will have implications as to how we interpret the Proterozoic climate and atmosphere as well as depositional environment;

- recognition and analysis of diagenetic processes is fundamental to the understanding and modelling of ore-forming processes. Diagenetic changes in sediments recorded by different cement generations and porosity changes, exert a major control (together with tectonics, which are now relatively well understood) on fluid movements. This in turn is a major factor in the localisation and style of mineral deposits (as well as petroleum accumulations). The application of cement stratigraphy as part of this study will hopefully allow a regional diagenetic history to be constructed which can be then related to events within the southern McArthur basin;

- the results from work conducted on the sedimentology, diagenesis and geochemistry of

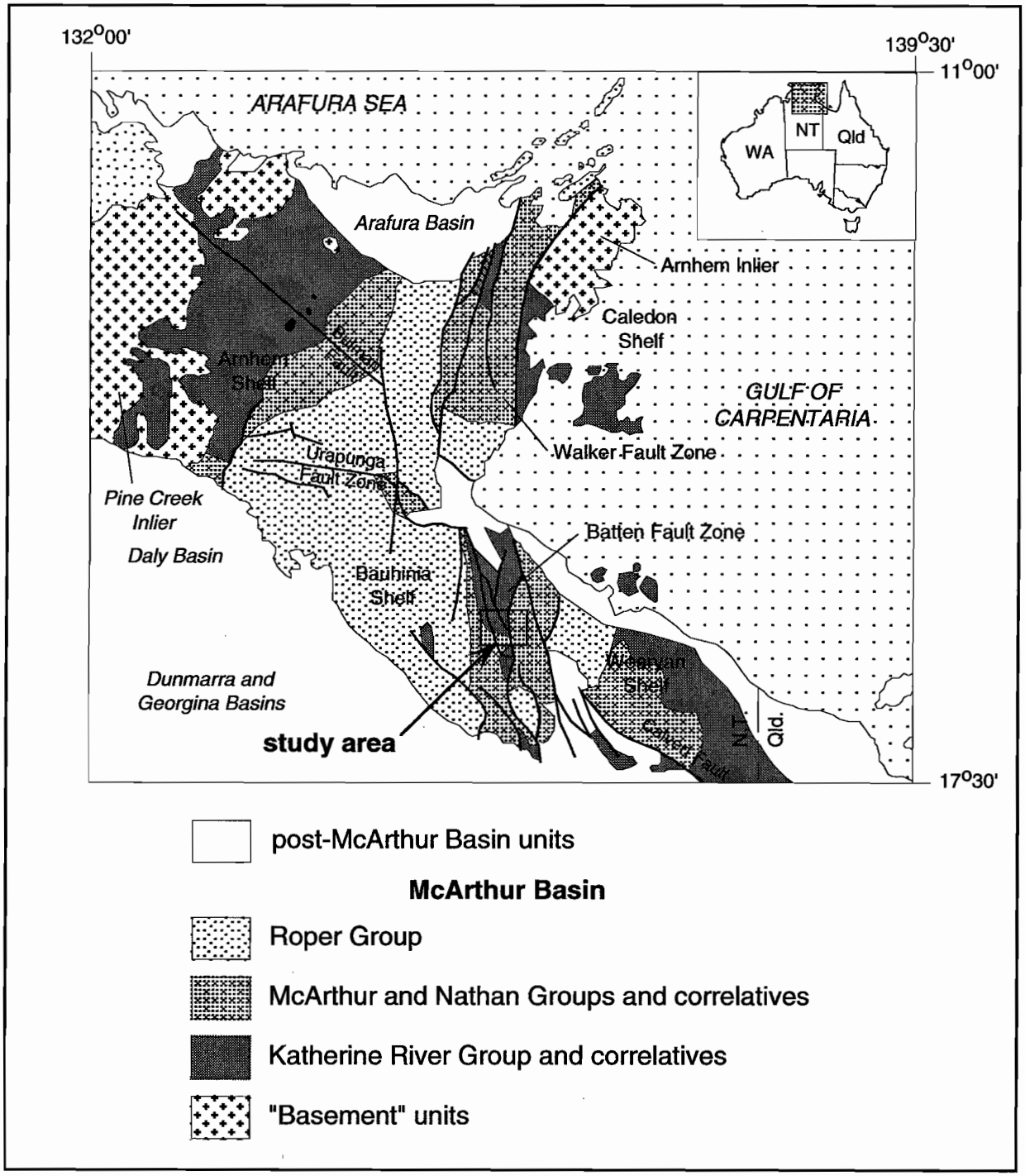

Major tectonic elements of the McArthur Basin (adapted after Pietsch et al. 1991a).

McArthur Group carbonates will act as background data in studies of mineralisation haloes around the McArthur River deposit, while also constraining models for its formation;

- criteria for distinguishing diagenetic from mineralising texture-altering processes will have direct application to exploration for mineral deposits.

Current research

Two main research bodies are currently working in the McArthur River area:

- CODES has been active over the last four years in the southern McArthur Basin with firstly a three-year program studying Proterozoic Sediment-Hosted Pb–Zn deposits, funded by AMIRA and ARC grants, and then currently a three-year extension to the original project. This PhD project forms part of the extension and its aims are tied to the Basin Analysis module of the P384A Project Outline, as well as having links with both the Deposit Halos and Brine Chemistry modules. The reader is directed to P384A Report 1 (pp. 43–46) for further details of the current project extension's aims and objectives;
- AGSO geologists as part of the NABRE project are also conducting research to attempt to correlate sedimentary sequences in the Mt Isa and McArthur Basin using sequence stratigraphic principles. Collaboration with AGSO will involve the measurement and interpretation of detailed field-sections and their incorporation within the broad-scale regional approach being adopted by this project.

Aims

The broad aims and objectives of this project are to:

- detail sedimentary facies within the upper Umbolooga Sub-group of the McArthur Group and to attempt to place these into a regional framework using sequence stratigraphic principles. Initially this will focus on the Teena Dolomite and Barney Creek Formation, hopefully expanding to also encompass the Emmerugga Dolomite and possibly the Reward Dolomite (Fig. 2);
- using the sedimentary and depositional framework provided by the above, evaluate the sequence of diagenetic processes and construct a regional diagenetic history for McArthur Group carbonates; hopefully incorporating mineralisation case-studies (both stratiform and stratabound) within the basin to provide some constraints of the age and process of their formation;
- discriminate burial diagenetic effects from possible more localised hydrothermal effects and/or ancient and modern weathering;
- combining the above, attempt to deduce the source and composition of fluids that have passed through and/or have affected McArthur Group carbonates.

Methods

Sedimentary facies analysis will be conducted primarily by the selection and mapping of several key field areas (e.g. Kilgour Gorge, Top Crossing and Weirk Waterhole). This will be combined with the detailed measurement of selected sections to obtain a better understanding of facies relationships and their extent. Mapping will be conducted using aerial photo enlargements of selected areas and sections will be measured using Abney level and Jacobs staff. As part of this project's collaboration with the AGSO NABRE project, some field sections will also be logged using a Gamma Ray Spectrometer depending on time and availability. The large amount of diamond drilling within the McArthur River area will also be utilised for the production of detailed logs as well as for sampling for later geochemical and petrographic work.

Standard carbonate and cathodoluminescence petrography will be used to detail diagenetic processes that have affected these units as well as adding in the description of sedimentary facies. Construction and correlation of a cement stratigraphy should aid in the development of a regional diagenetic history. Hopefully, by placing the mineralisation within the McArthur River area into this context, it should be possible to provide some constraints on the age and process of Pb–Zn mineralisation inherent

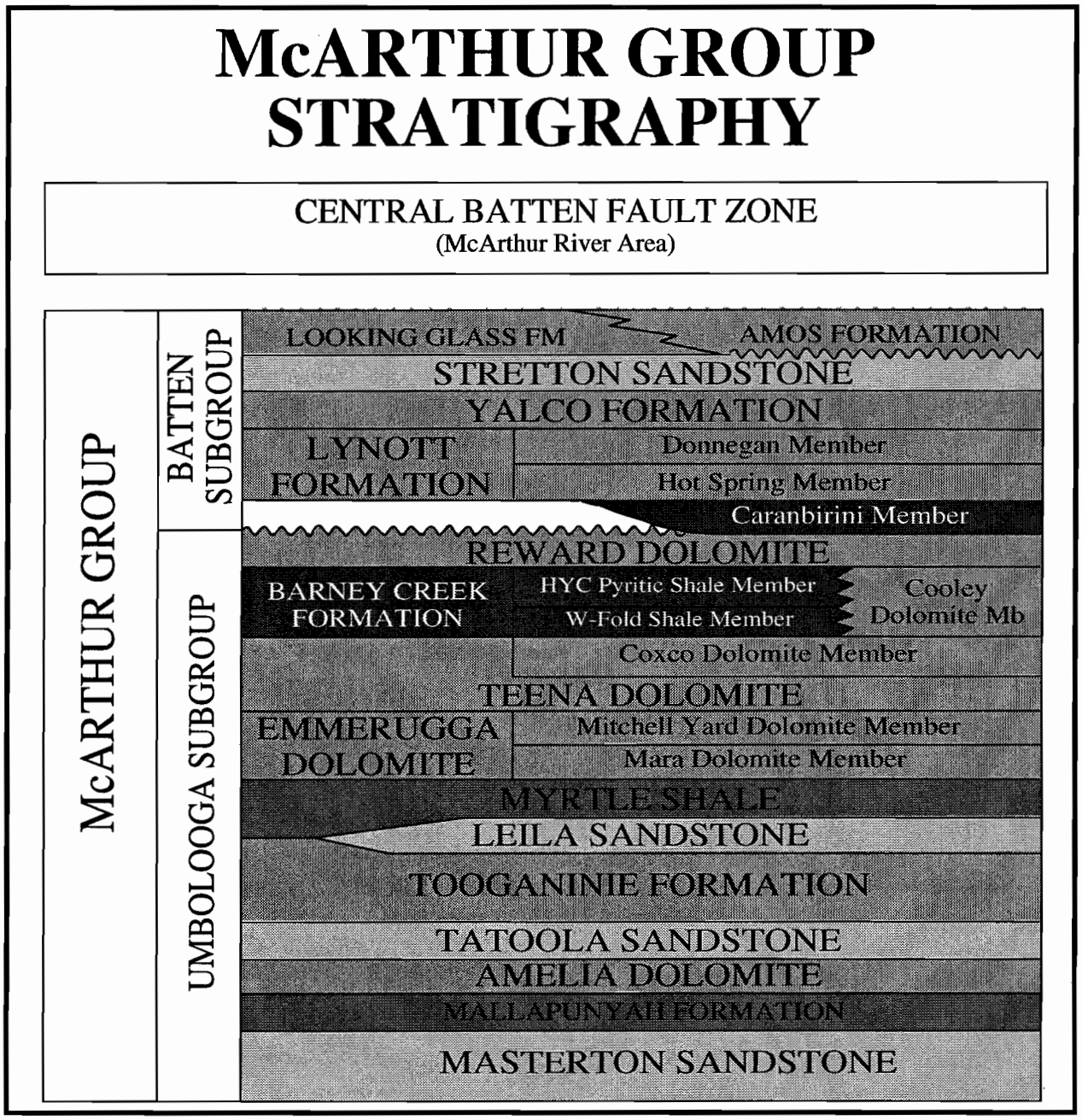

McArthur Group stratigraphy (adapted from Pietsch et al 1991a).

to this stratigraphic interval. Most of this work will be done on a standard geological microscope using a cathodoluminoscope stage for describing and photographing carbonate cements and textures. SEM imagery will also be used to aid in the documentation of samples.

Microprobe (elemental) and ICP-MS (C & O isotope) analysis of selected diagenetic cements in addition to fluid inclusion studies, will be used to document the chemistry, salinity and temperature of fluids that precipitated these cements and hopefully used to illustrate the type of fluids that have passed through and affected these carbonates.

The general approach that has been adopted for this project has been summarised as a flow diagram and included as Figure 3.

Timetable

The project commenced in March 1995 and at present, two field seasons have been completed. The first field season (1995) was primarily reconnaissance and selection of suitable mapping areas and sections for later work. Drill core logging of open-file drilling held in the NTGS core-store in Darwin was used to develop an one-dimensional stratigraphy through the upper Umbolooga Sub-group looking at characteristic facies and assessing the suitability of various formations to the diagenetic studies detailed above. The second field season (1996) was completed at the end of September and involved the mapping of two key areas (i.e. Gorge Prospect and Weirk Waterhole). In addition, numerous sections were measured to compliment this mapping as well as at other selected localities. Recently released open-file and closed file drilling along the 'east–west trend' away from HYC was logged and sampled, especially drilling from the Berjaya Prospect. The rest of 1996 and beginning of 1997 will be spent analysing data and working on petrography and geochemistry of samples collected. The 1997 field season is likely to involve the mapping, along with measurement of several sections, of the Top Crossing area. Several other areas were noted during the just-completed field season and these will be assessed over the summer to determine their suitability for further study. In addition, there is a large amount of open-file drilling that could be logged and sampled (i.e. Amelia, Mitchell Yard and Myrtle Sub-basins) and included within the study. At the completion of this final field season, there will a large amount of laboratory work (ie. geochemical and petrographic) needed on gathered samples and therefore the completion of the project and submission of the PhD thesis is projected tentatively toward mid to late 1998.

Project outcomes

The outcomes of this project will include progress reports to AMIRA sponsors and ultimately a PhD thesis. In addition a number of supporting papers will also be submitted to various geological and scientific journals. To date, two progress reports have been written and included within P384A Report 1. These are:

- Diagenetic processes in late Palaeoproterozoic McArthur Group carbonates: preliminary studies and future directions. P384A Report 1: 11;
- Carbonate–evaporite sediments in the McArthur River area: revision of middle McArthur Group lithofacies and recognition of key surfaces. P384A Report 1: 23.

A comprehensive report covering results and interpretation of work completed during the 1996 field season will be presented and included within the first P384A report of 1997.

Anticipated supporting papers

It is anticipated that several papers will be produced at the completion of this project in support of the PhD thesis. Possible topics include:

- Burial diagenesis of McArthur Group carbonates
- Radiating, acicular 'Coxco' needles — are they necessarily gypsum pseudomorphs?
- Sedimentological and diagenetic features of the Teena Dolomite and its association with the Barney Creek Formation
- Cyclicity within the Emmerugga Dolomite and

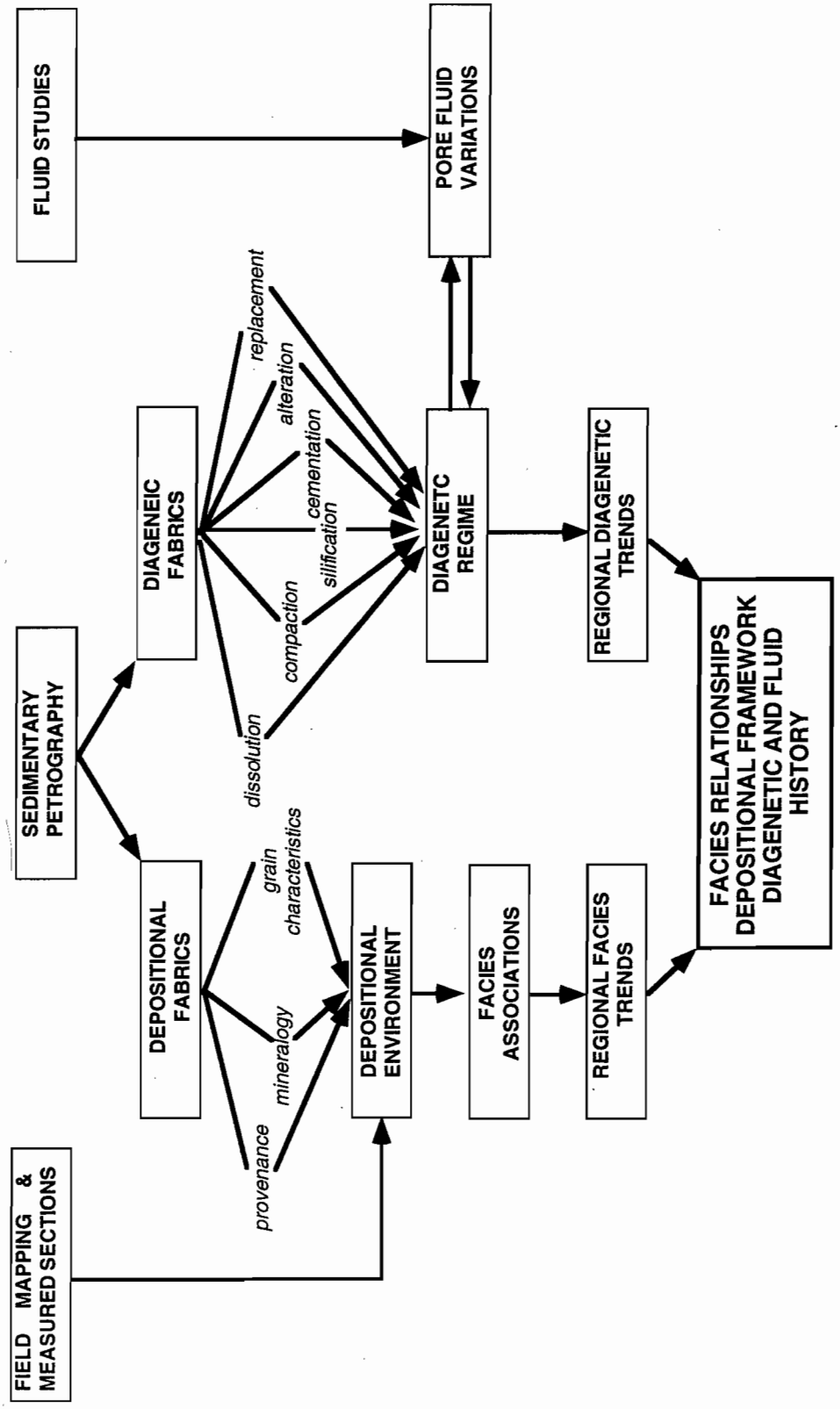

Figure 3 General approach to this study incorporating field mapping and description of measured sections with sedimentary petrology and fluid studies.

features of the Mitchell Yard Dolomite Member
- Primary dolomite or early marine dolomitisation of McArthur Group carbonates
- Timing constraints on stratabound and/or stratiform mineralisation within the McArthur Group.

References

Brown, M.C., Claxton, C.W., and Plumb, K.A., 1969. The Proterozoic Barney Creek Formation and some associated units of the McArthur Group, Northern Territory, Australia. Bureau of Mineral Resources Record 1969/145 (unpublished).

Jackson, M.J., Muir, M.D., and Plumb, K.A., 1987. Geology of the southern McArthur Basin. Bureau of Mineral Resources Bulletin 220: 173 pp.

Pietsch, B.A., Rawlings, D.J., Creaser, P.M., Kruse, P.D., Ahmad, P., Fererczi, P.A. and Findhammer, T.L.R., 1991a. Bauhinia Downs 1:250000 Geological Map Series. Northern Territory Geological Survey Explanatory Notes SE53-3.

Pietsch, B.A., Wyche, S., Rawlings, D.J., Creaser, P.M., and Findhammer, T.L.R., 1991b. McArthur River Region 1:100000 Geological Map Series. Northern Territory Geological Survey Explanatory Notes SE53-3 (6065–6165).

Primary dispersion halos associated with the Mount Novit Zn–Pb–Ag mineralisation

Peter McGoldrick
Centre for Ore Deposit and Exploration Studies, Geology Department, University of Tasmania

Summary

Gossanous ridges between 15 and 20 km south of Mt Isa are the surface expression of a pyritic interval up 25 m thick containing sporadic Zn–Pb–Ag mineralisation. The mineralised sequence is a steep west dipping, fault-bounded package of overturned lower Mount Isa Group sediments (Moondarra Siltstone) lying to the west of the Mount Isa Fault. Metamorphism has reached lower amphibolite grade and a variety of unusual rock textures are thought to reflect deformation at or near, the brittle–ductile transition.

Mineralisation is stratiform (or stratabound) disseminated to massive granular (?recrystallised) pyrite with variable amounts of sphalerite, galena, pyrrhotite and magnetite. More than 15 diamond drill holes have been drilled to test the mineralisation, with a handful of intersections exceed 10% Pb+Zn over thicknesses of more than a metre.

Three drill holes through the mineralisation at about 2 km spacing were systematically sampled to encompass the mineralised interval.

Sixty one samples were analysed for major and trace elements by XRF at the University of Tasmania and the standard set of geochemical vector parameters have been calculated. Ten samples from much lower grade (lower greenschist?) Moondarra Siltstone from diamond drill hole SA10 were also analysed.

The southernmost hole (D496) yields inconclusive results, by contrast, in drill hole F681, AI3, MnOd and Tl are anomalous for tens of metres above and below the ore positon, and in drill hole G880 for the 50 m that includes a (barren) disseminated pyrite zone correlated with mineralisation in the other two holes. None of the Mt Novit geochemical vector signatures approaches the strong response observed in samplers from the mine sequence at Mt Isa, however, patterns resemble those from other significant northern Australian deposits, suggesting the geochemical vectors are preserved during lower amphibolite grade metamorphism.

The weak geochemical vector response at Mt Novit suggests significant Zn–Pb–Ag mineralisation does not exist proximal to the known pyritic mineralisation.

Introduction

Previous work has developed a number of lithogeochemical parameters (e.g. AI, SedexAI, $MnO_{d/s}$, Tl) as useful vectors to Australian Palaeoproterozoic stratiform Zn–Pb–Ag deposits (Large and McGoldrick, 1993; Large and McGoldrick 1994; McGoldrick 1994; McGoldrick 1995a; McGoldrick 1995b). Case studies of ore grade and sub-economic mineralisation have shown these parameters to be useful discriminants in low metamorphic grade sedimentary host rocks. The Mount Novit case study, reported here, tests these parameters on a large, sub-economic, stratiform Zn–Pb–Ag deposit hosted in amphibolite-grade metasediments south of Mount Isa.

Mount Novit deposit

The Mount Novit mineralisation is a stratiform pyritic horizon up to 25 m thick within (meta) dolomitic siltstones of the lower Mount Isa Group (Moondarra Siltstone). The surface expression of the mineral-

isation is a five km strike length of gossanous ridges between 15 and 20 km south of Mount Isa mine (Fig.1). Primary mineralisation comprises coarse, often granular, massive pyrite, disseminated pyrite, with minor pyrrhotite, magnetite and siderite, and variable amounts of sphalerite and galena (Fig. 2). Fifteen cored drill holes have intersected the mineralised zone, but there is no published resource for available for Mount Novit. However, there are probably several tens of millions of tonnes of mineralisation grading better than 10 wt% Zn equivalent in several hundred million tonnes of pyritic Moondarra Siltstone. Table 1 shows the Ag and base metal grades from some representative intersections. Better grades and thicker intersections are found in the northern third of the mineralised sequence.

Host rocks

The Mount Novit host succession comprises metamorphosed dolomitic (sometimes carbonaceous) siltstones and mudstones, and is fault bounded on all sides. Early workers proposed correlations with various units in the Mount Isa Group (e.g. Russell and Cox, 1973; Russell, 1978), however, work during the 1980s by MIM geologists confirmed that they can be correlated with the upper part of the Moondarra Siltstone (lower Mount Isa Group — Mathias and Clark, 1975). At Mt Novit the Moondarra Siltstone occupies the steeply west dipping overturned limb of a faulted synform, and it have been metamorphosed to upper greenschist and lower amphibolite grades, and display a variety of textures reflecting a complex history of ductile and brittle behaviour during deformation and metamorphism (Ransom, 1991). Sedimentary laminae are well preserved in some intersections, while phyllitic and schistose rock types are present in others. Post-cleavage brecciation and flooding by calcite is also common producing what are locally termed 'birdswing' textures. Figure3 illustrates some of the diversity of host rock textures Metamorphic minerals include chlorite, biotite, tremolite, phlogopite and calcite, and possibly other carbonates (appendices in Ransom,1991). No micro-petrographic nor XRD work has been carried out during this study, but, the sketch logs depicted in Figures 4–6 illustrate some of the diversity of lithologies sampled for geochemical analysis..

Samples and geochemical database

Three drill holes through the mineralisation at about 2 km spacing were systematically sampled to encompass the mineralised interval. Schematic cross-sections and graphic logs depicting the sample locations are presented in Figures 4–6. The ore position in the northernmost hole (G880) is represented by 5–10% disseminated pyrite. Thick massive pyrite intervals are present in the other sampled holes (4 m in D496 and about 25 m in F681). The samples comprised 10–20 cm half core collected every 10–15 m in the hangingwall and footwall of

Table 1

Thickness m	Ag ppm	Pb wt%	Zn wt%	Fe wt%	Northing m (MIM grid)
4	7.2	0.7	1.0	25.6	14960
5.5	15	1.0	1.8		15900
0.9	36	1.5	3.9		16850
1.2	30	1.0	1.7		16850
14	22	1.1	2.8		
incl. 1.9	21	1.3	3.9		
1.5	48	3.3	9.1		
3.8	48	3.9	7.7		18100
4.1	100	7.6	11.6		18400

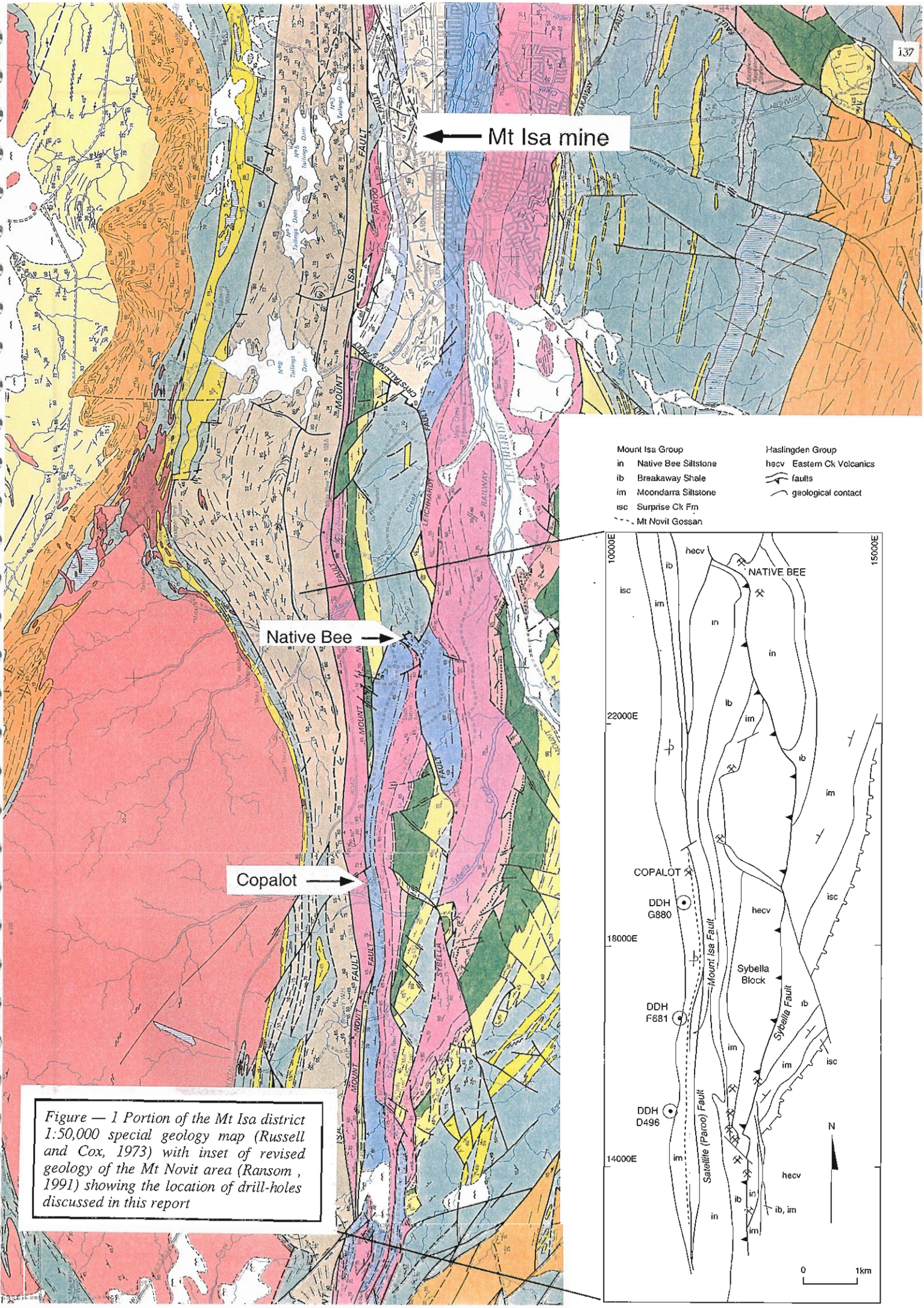

Figure — 1 Portion of the Mt Isa district 1:50,000 special geology map (Russell and Cox, 1973) with inset of revised geology of the Mt Novit area (Ransom , 1991) showing the location of drill-holes discussed in this report

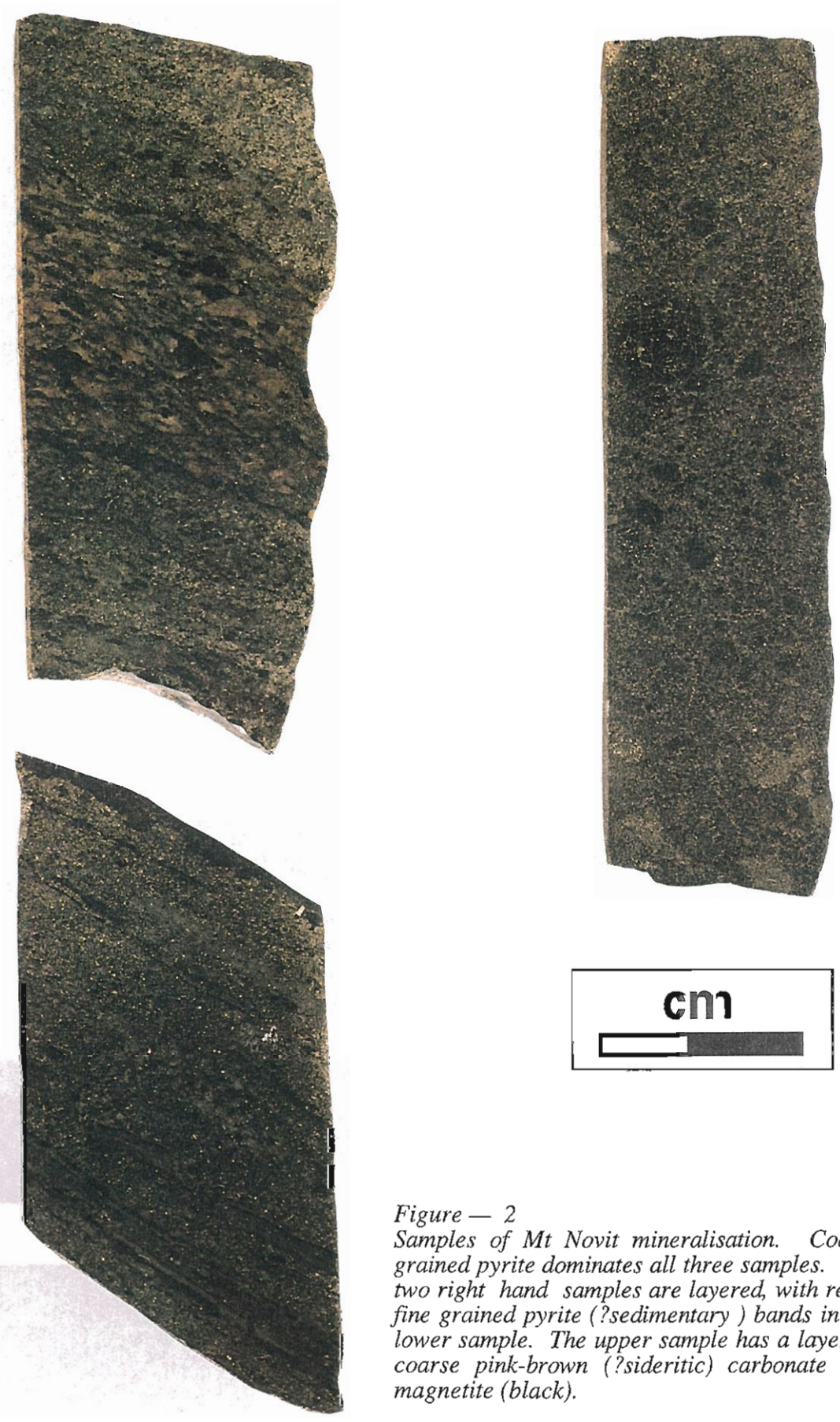

Figure — 2
Samples of Mt Novit mineralisation. Coarse grained pyrite dominates all three samples. The two right hand samples are layered, with relict fine grained pyrite (?sedimentary) bands in the lower sample. The upper sample has a layer of coarse pink-brown (?sideritic) carbonate and magnetite (black).

Figure — 3
a) Dolomitic siltstone samples from DDH SA10 338.8m & 626.6m (lower greenschist metamorphic grade)
b) Range of lithotypes in the immediate host to the Mt Novit mineralisation (upper greenschist to lower amphibolite metamorphic grade). The top left sample retains recognisable sedimentary layering, with mottling due to patches of incipient carbonate recrystallisationi. The middle sample is schistose and more pervasively recrystallised. The remaining samples have a variety of breccia and carbonate veining or flooding textures (e.g. 'birdswing' texture in centre right sample

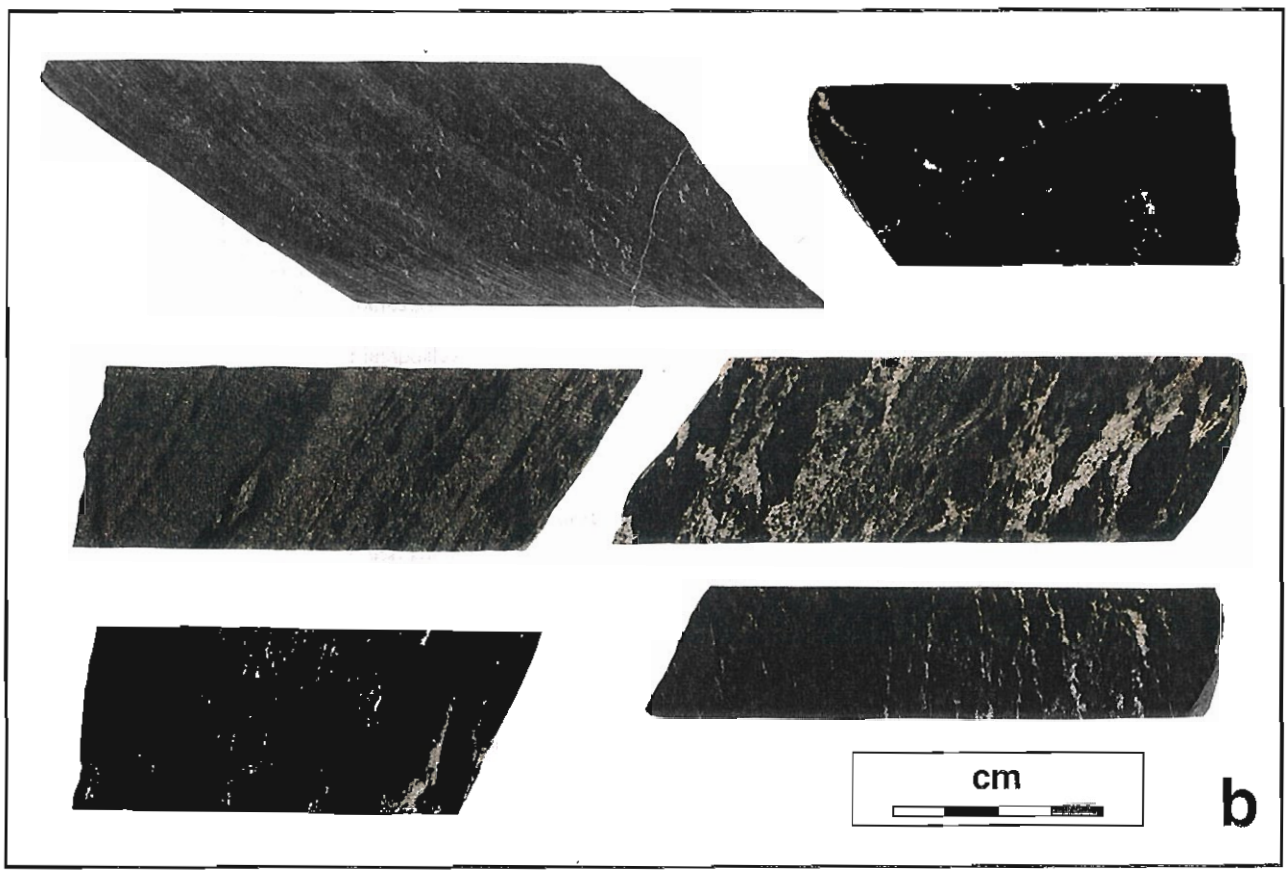

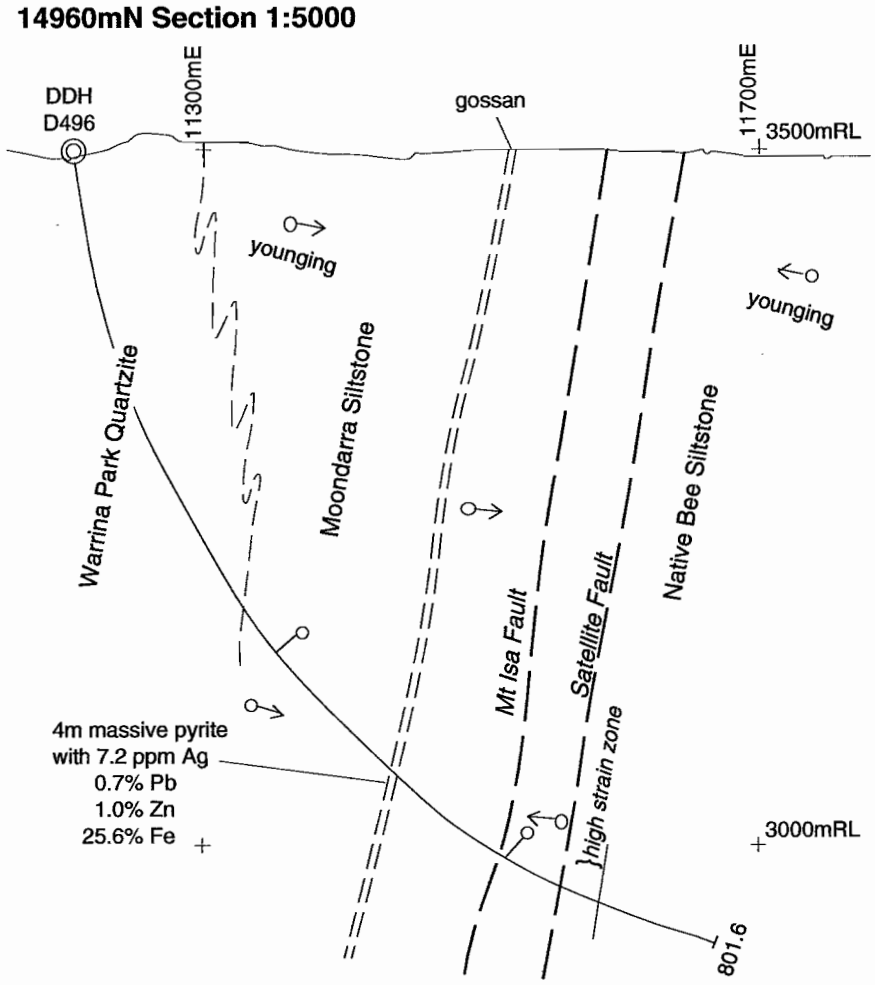

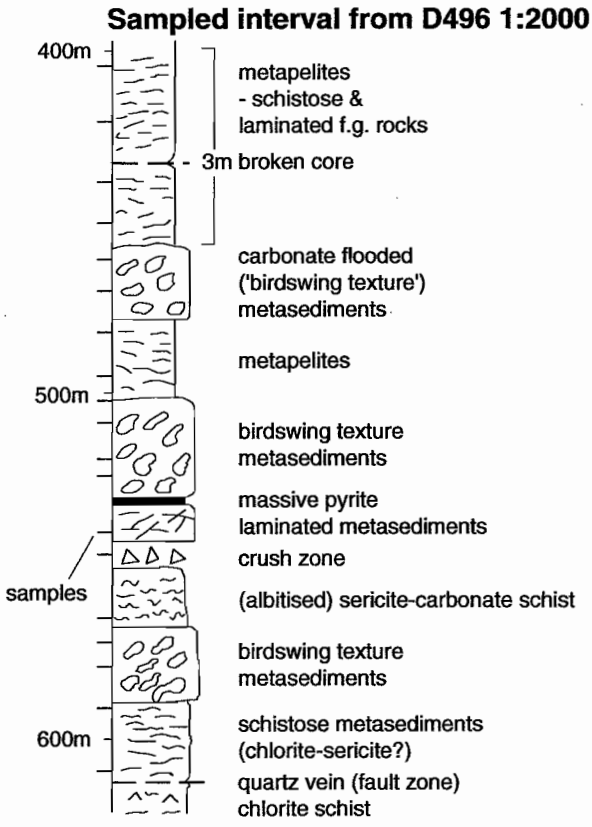

Figure 4 Schematic cross section and graphic log showing samples from DDH D496

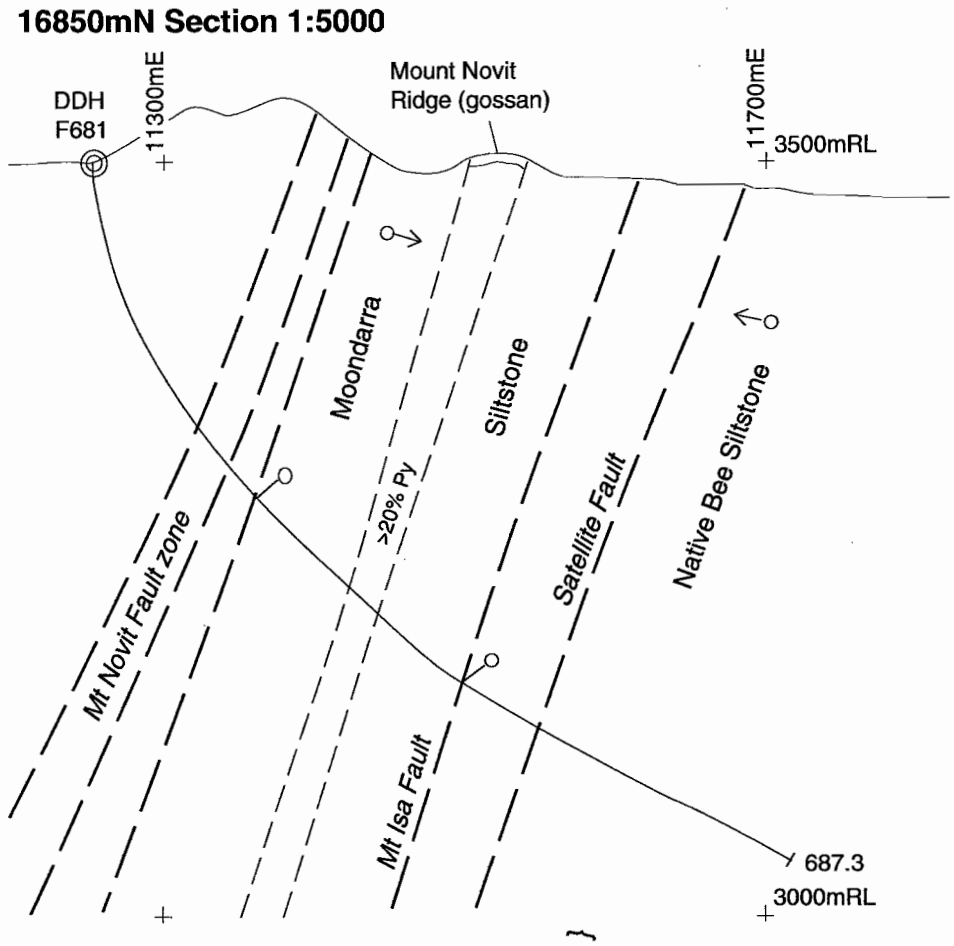

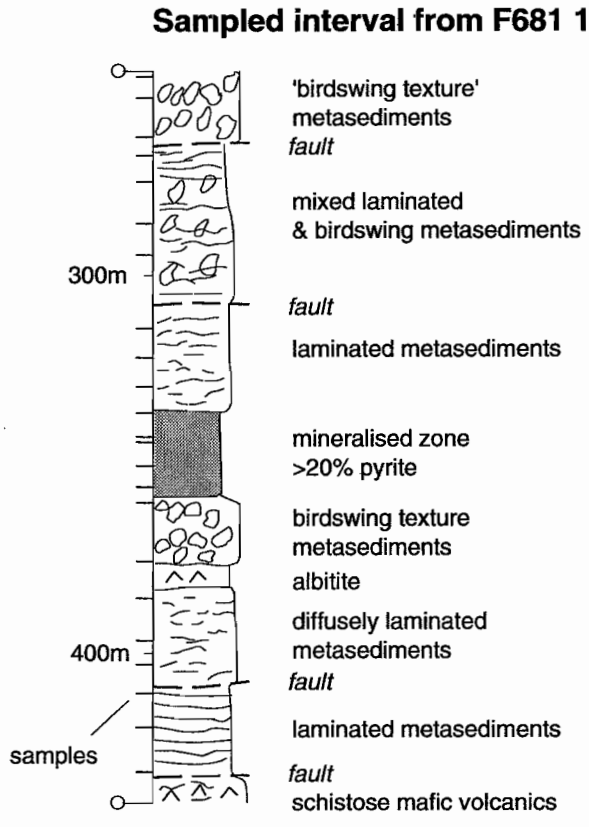

Figure 5 Schematic cross section and graphic log showing samples from DDH F681

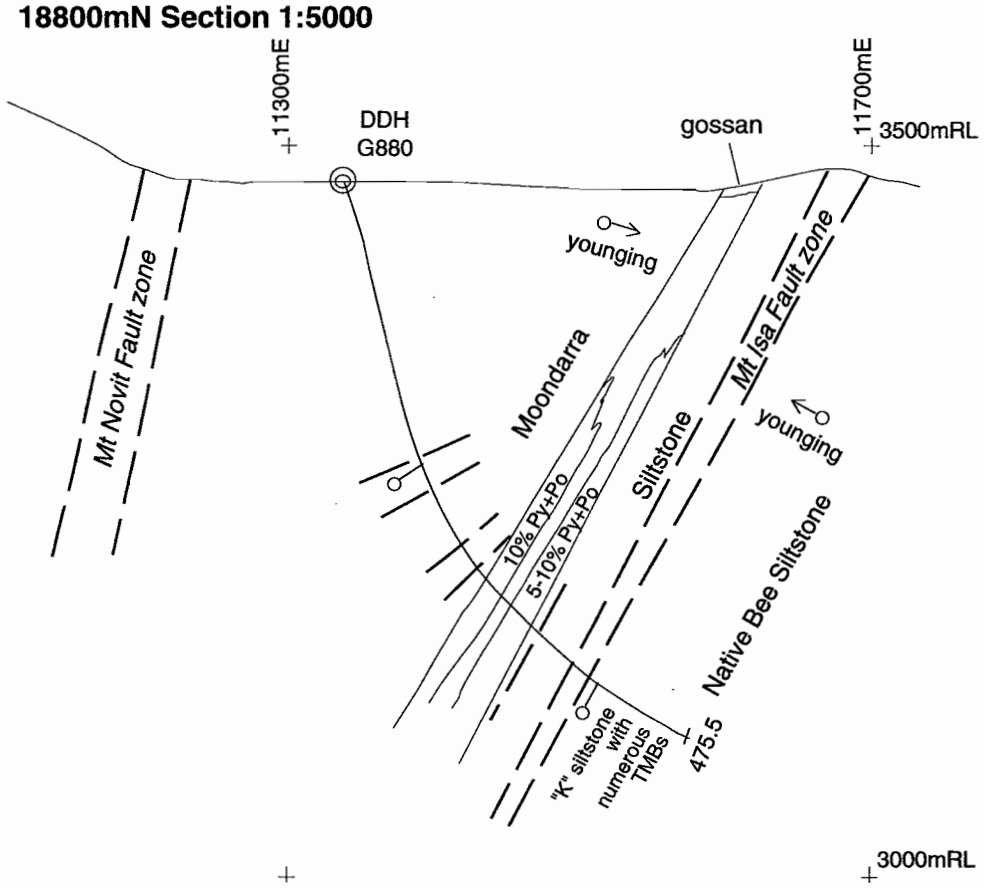

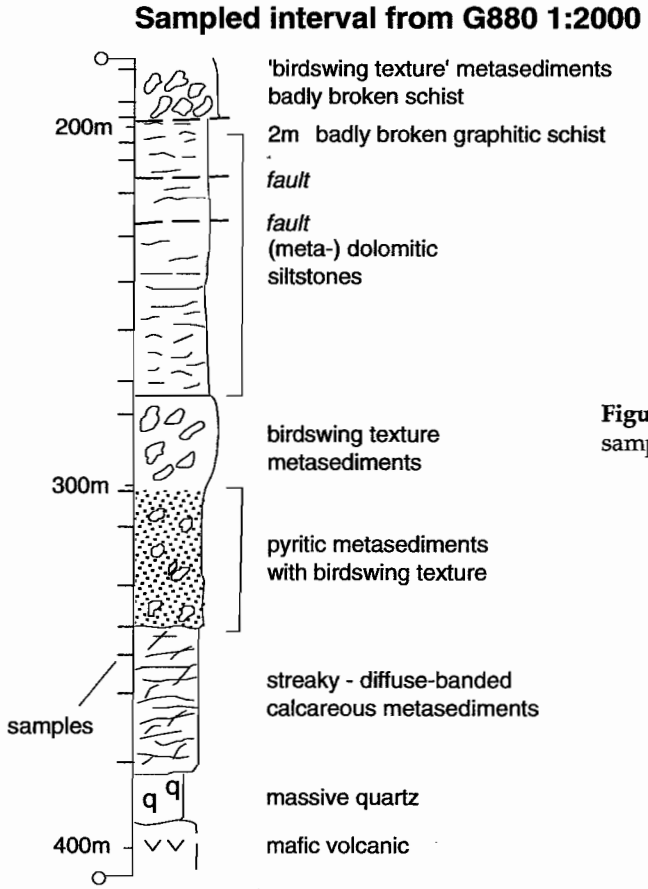

Figure 6 Schematic cross section and graphic log showing samples from DDH G880

the mineralisation, over an interval of about 200 m true stratigraphic thickness.

Sixty-one samples were analysed for major and trace elements by XRF at the University of Tasmania and the standard set of geochemical vector parameters have been calculated. A further ten samples of Moondarra Siltstone from a drill hole (SA10) in lower grade Mount Isa Group rocks north of Lake Moondarra were analysed for comparison with samples from the mineralised sequence. All the data are presented in Table 2 and are available in digital format from the author on request.

Results

Preliminary discussion

Large (1995) summarised the steps required in applying the AI and $MnO_{d/s}$ vectors in exploration. Several parameters (SedexAI, AI_3, $MnO_{d/s}$) derived from the whole rock data are compared on a series of standard plots. Thallium and Zn are considered to be useful pathfinder elements, and a trend to Fe-enrichment in carbonate, quantified as the 'Ankerite Ratio', is a vector toward mineralisation. The $MnO_{d/s}$ parameter is only applicable to samples with enough carbonate for reliable recalculation of the analyses (generally > 1wt% CO_2), hence, $MnO_{d/s}$ should not be applied to fine grained siliciclastics or argillaceous rock types. Furthermore, the main carbonate mineral in the rock must be dolomite, ankerite or siderite (not calcite or magnesite) for meaningful calculation of $MnO_{d/s}$ values. A CaO/MgO binary plot can be used to test if both these requirements are met. Figure 7 shows the CaO/MgO relationship in the Mt Novit and SA10 samples.

Pure dolomite has a CaO:MgO ratio of 1.4:1, and many of the samples analysed here plot on a linear array with CaO:MgO values of between 1.3 and 2, consistent with dolomite being the major carbonate present in these samples. Samples with lower CaO:MgO values, but lying near the linear array, probably contain a Mg-phyllosilicate phase as well as dolomite, and are still suitable for $MnO_{d/s}$ calculations, however, high-CaO — low-MgO samples probably have calcite as the main carbonate, and have therefore, been excluded from $MnO_{d/s}$ plots.

In unmetamorphosed or low grade sedimentary rocks, it is usually possible to estimate the Fe content of carbonate minerals in the rock, by making the

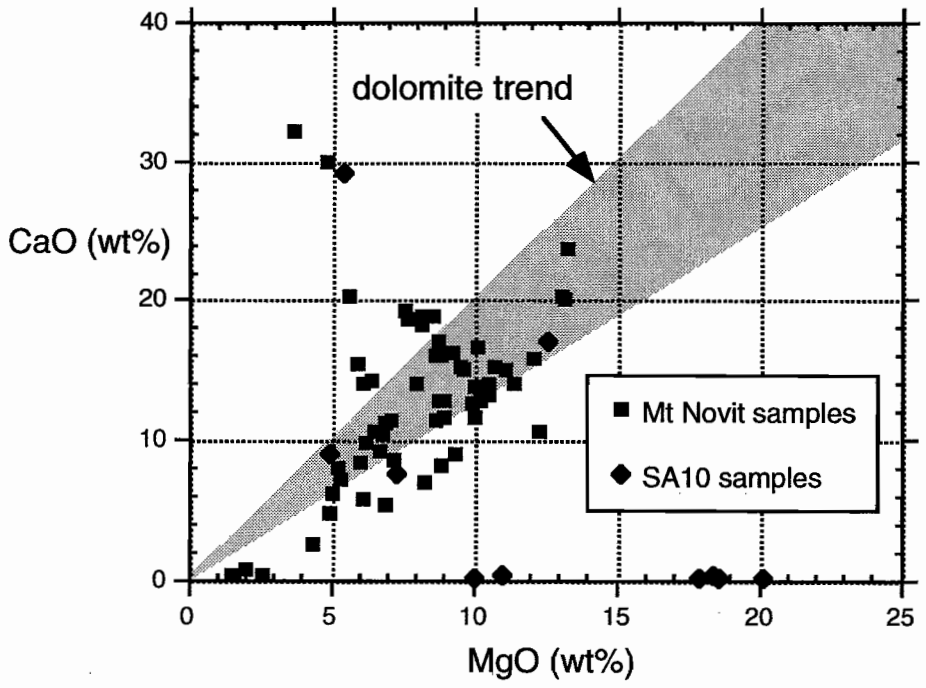

Figure 7 CaO/MgO relationship for samples from Mt Novit and DDH SA10

Table 2

Geochemical data from DDH D496 samples

DDH	depth	SiO2	TiO2	Al2O3	Fe2O3	FeO	MnO	MgO	CaO	Na2O	K2O	P2O5	Ctotal	CO2 total	loss	Total	S	Rb	Pb	As	Zn	Cu	Sr	Tl	MnOd	Al3	SedexAl
	m	wt%	wt%	wt%	wt%	wt%	wt%	wt%	wt%	wt%	wt%	wt%	wt%	wt%	wt%	wt%	wt%	ppm	ppm	ppm	ppm	ppm	ppm	ppm			
D496	403.4	65.23	0.60	11.45	5.35	4.81	0.09	4.39	2.53	0.98	3.40	0.17	1.10	4.03	5.80	100.00	1.79	140	66	19	16	31	14	<1	1.99	57	8
D496	419.6	70.27	0.70	12.78	5.46	4.91	0.01	2.64	0.28	0.15	3.99	0.21	0.49	1.80	3.04	99.99	1.42	158	16	44	13	43	12	<1	0.19	66	1
D496	438.3	73.77	0.39	12.11	3.19	2.87	0.01	2.05	0.70	0.24	3.86	0.25	1.60	5.86	4.21	100.78	1.00	126	35	106	14	552	10	<1	0.35	59	2
D496	449.4	62.27	0.38	9.91	3.00	2.70	0.09	5.33	7.27	0.08	4.12	0.14	2.93	10.74	8.10	100.69	0.37	164	14	<3	22	119	44	<1	2.44	40	24
D496	459.3	33.52	0.12	3.38	4.37	3.93	0.23	13.27	23.72	0.10	1.92	0.11	5.02	18.39	18.07	98.81	0.60	53	6	<3	9	37	53	<1	4.37	32	78
D496	468.4	47.59	0.27	7.69	2.81	2.53	0.06	10.50	13.32	0.60	3.80	0.11	3.63	13.30	13.49	100.24	0.45	117	21	30	41	22	70	<1	1.84	23	44
D496	480.6	29.35	0.09	2.25	2.95	2.65	0.15	13.14	20.05	0.11	1.66	0.08	8.43	30.89	29.57	99.42	0.29	30	7	<3	23	14	52	<1	3.99	24	66
D496	493.7	27.01	0.12	3.30	3.26	2.93	0.15	13.05	20.33	0.11	2.44	0.10	8.65	31.69	29.49	99.36	0.46	41	10	<3	15	20	64	<1	3.85	25	67
D496	499.8	45.08	0.24	7.59	3.21	2.89	0.20	12.33	10.59	0.09	3.22	0.11	4.81	17.62	16.31	98.97	0.58	121	57	8	79	8	23	1	5.53	28	35
D496	507.3	39.29	0.24	6.92	2.73	2.46	0.08	11.15	15.12	0.53	2.85	0.12	5.55	20.34	20.17	99.22	0.59	125	229	7	248	8	80	1.4	2.74	23	50
D496	517.4	43.73	0.26	7.87	3.99	3.59	0.09	10.01	11.72	0.38	2.89	0.10	5.15	18.87	17.78	98.82	0.84	125	83	25	984	14	60	3.4	2.06	31	39
D496	522.1	36.73	0.24	7.06	3.51	3.16	0.50	9.52	15.21	0.19	4.15	0.12	6.31	23.12	22.90	100.15	0.09	102	311	15	77	6	58	2.4	10.11	46	50
D496	539.2	60.90	0.27	8.02	1.63	1.47	0.11	5.25	7.98	4.53	0.21	0.15	3.48	12.75	11.62	100.68	0.58	8	4	30	9	3	23	<1	8.35	33	26
D496	544.5	69.45	0.52	15.91	0.88	0.79	0.00	1.54	0.36	5.26	2.63	0.18	1.67	6.12	3.60	100.33	0.54	122	3	20	10	<2	12	1.5	0.00	34	1
D496	554.0	58.17	0.47	13.93	3.57	3.21	0.14	4.90	4.81	3.63	3.10	0.21	1.91	7.00	7.66	100.59	0.30	125	3	3	9	12	26	<1	3.02	48	16
D496	563.8	38.69	0.21	7.22	3.01	2.71	0.23	11.37	14.10	2.16	1.72	0.10	5.98	21.91	21.40	100.21	0.39	90	4	10	13	17	33	<1	6.28	31	46
D496	570.3	42.81	0.27	7.94	3.27	2.94	0.08	8.99	12.84	1.14	2.17	0.11	5.80	21.25	20.03	99.66	0.97	86	9	13	11	5	68	1.1	2.67	29	42
D496	576.7	38.28	0.27	7.63	3.76	3.38	0.07	10.51	14.06	0.12	2.86	0.10	5.97	21.87	21.99	99.65	1.22	96	18	11	72	4	71	1.6	2.15	28	46
D496	589.1	40.10	0.29	7.74	4.24	3.82	0.10	10.20	12.93	0.23	2.88	0.11	5.57	20.41	20.12	98.97	1.79	96	13	15	22	8	71	1.5	3.42	32	43
D496	599.6	38.90	0.31	8.03	2.93	2.64	0.07	5.64	20.29	0.39	3.42	0.14	5.68	20.81	19.95	100.08	0.51	152	6	5	48	16	70	<1	2.10	37	67
D496	608.3	41.16	0.30	6.45	4.23	3.81	0.28	8.03	14.00	0.13	4.86	0.15	5.90	21.62	20.56	100.16	0.44	62	5	19	6	23	35	<1	5.24	45	46

Geochemical data for samples from DDH SA10

Drill hole	Depth	SiO2	TiO2	Al2O3	Fe2O3	FeO	MgO	CaO	MnO	Na2O	K2O	P2O5	LOI	TOTAL	H2O	CO2 (inorg)	S	As	Ba	Cr	Cu	Pb	Rb	Sr	Tl	Zn	Zr	MnOd	SedexAl	Al3
	m	wt%	wt%	wt%	wt%	wt%	wt%	wt%	wt%	wt%	wt%	wt%	wt%	wt%	wt%	wt%	wt%	ppm	ppm	ppm	ppm	ppm	ppm	ppm	ppm	ppm	ppm			
SA10	338.8	27.82	0.18	4.50	2.19	1.97	5.39	29.09	0.09	0.50	1.12	0.20	28.33	99.02	nd	27.30	0.35	4	122	27	11	18	50	161	1	35	78		35	22
SA10	451.0	32.95	0.18	4.38	3.67	3.30	12.55	17.02	0.21	0.06	1.78	0.10	25.65	98.55	nd	24.84	0.41	11	157	25	6	28	56	62	<1	13	79	0.38	30	24
SA10	626.6	47.88	0.45	11.09	4.39	3.95	7.28	7.57	0.17	0.10	7.22	0.16	12.65	98.96	nd	10.63	0.96	13	273	57	21	17	131	32	1	12	150	0.68	44	24
SA10	361.8	52.94	0.47	12.12	3.61	3.25	4.98	9.00	0.03	0.72	3.74	0.16	11.55	99.32	nd	8.98	0.55	7	337	67	12	14	172	62	2	33	155	0.10	42	17
SA10	607.6	63.73	0.49	11.27	4.78	4.30	10.00	0.19	0.01	0.04	3.62	0.14	5.34	99.60	nd	1.32	1.24	29	137	52	185	23	61	9	<1	16	192		30	17
SA10	567.0	54.40	0.42	11.23	5.74	5.16	18.52	0.23	0.01	<0.03	0.03	0.15	8.17	98.90	nd	0.92	0.79	13	<4	52	24	16	1	2	<1	18	130		22	15
SA10	589.1	71.37	0.26	7.28	5.10	4.59	10.99	0.36	0.01	<0.03	0.05	0.24	5.45	101.10	nd	0.88	1.24	12	<4	32	33	15	1	2	<1	13	76		30	20
SA10	576.5	50.87	0.48	12.02	8.01	7.21	18.38	0.24	0.01	<0.03	0.03	0.17	8.67	98.88	nd	0.70	1.90	44	<4	58	739	25	1	2	<1	17	150		28	19
SA10	397.0	53.90	0.45	11.54	7.47	6.72	17.85	0.18	0.01	<0.03	0.02	0.12	8.29	99.83	nd	0.44	0.68	16	<4	53	658	18	1	2	<1	55	177		28	19
SA10	494.8	48.72	0.55	12.78	7.78	7.00	20.11	0.15	0.01	<0.03	0.02	0.11	9.01	99.24	nd	0.26	1.15	20	<4	63	14	17	2	3	<1	31	173		26	18

Table 2

Geochemical data for DDH G880

DDH	depth	SiO2	TiO2	Al2O3	Fe2O3	FeO	MnO	MgO	CaO	Na2O	K2O	P2O5	Ctotal	CO2 total	loss	Total	S	Rb	Pb	As	Zn	Cu	Sr	Tl	MnOd	Al3	SedexAl
	m	wt%	wt%	wt%	wt%	wt%	wt%	wt%	wt%	wt%	wt%	wt%	wt%	wt%	wt%	wt%	wt%	ppm	ppm	ppm	ppm	ppm	ppm	ppm			
G880	184.3	49.07	0.40	10.11	3.12	2.81	0.08	6.45	14.15	0.57	3.10	0.18	3.18	11.65	13.11	100.32	0.35	180	38	<3	103	9	70	1.7	0.17	18	36
G880	193.5	43.47	0.31	8.36	2.83	2.55	0.26	8.73	12.76	0.51	2.39	0.12	5.54	20.30	19.94	99.69	0.66	117	72	14	498	23	45	1.2	0.62	23	37
G880	197.4	58.66	0.42	12.19	2.65	2.38	0.12	6.10	5.73	0.15	4.07	0.13	2.73	10.00	10.37	100.59	0.15	198	4	<3	25	15	32	1.2	0.64	16	37
G880	205.6	45.83	0.26	7.77	4.02	3.62	0.21	10.00	13.77	0.10	2.75	0.13	3.89	14.25	15.21	100.06	0.76	139	20	<3	24	21	55	<1	0.46	24	36
G880	209.8	60.85	0.46	12.68	2.74	2.47	0.06	6.88	5.30	0.12	5.19	0.16	1.40	5.13	6.25	100.69	0.14	203	5	<3	27	7	35	2.6	0.34	14	31
G880	219.0	38.43	0.25	6.55	2.50	2.25	0.08	8.15	18.94	0.35	3.00	0.12	5.71	20.92	21.52	99.89	0.58	96	37	14	181	14	110	<1	0.13	17	27
G880	230.9	49.11	0.39	10.97	3.38	3.04	0.05	9.31	9.07	0.40	4.84	0.13	3.09	11.32	12.52	100.17	0.78	187	30	3	106	20	61	1.4	0.17	15	28
G880	243.8	39.93	0.24	7.04	2.33	2.10	0.06	7.57	19.32	0.37	3.09	0.12	5.17	18.94	19.73	99.80	0.38	117	27	4	39	10	125	2.1	0.09	16	26
G880	256.5	30.15	0.11	2.96	0.86	0.77	0.05	3.68	32.10	0.15	1.77	0.12	7.53	27.59	27.52	99.48	0.13	48	105	<3	405	6	296	<1	0.05	16	26
G880	270.8	42.61	0.24	7.37	2.26	2.03	0.06	8.89	16.05	0.39	3.77	0.11	4.97	18.21	18.32	100.07	0.34	141	21	16	40	9	87	<1	0.11	14	23
G880	280.0	41.71	0.21	5.96	1.64	1.48	0.08	8.15	18.25	0.72	2.47	0.11	6.42	23.52	21.65	100.95	0.29	92	78	<3	106	4	101	1.3	0.13	14	22
G880	295.8	41.84	0.25	7.43	16.03	14.42	0.09	5.04	6.13	0.03	3.56	0.12	3.13	11.47	22.12	102.62	10.67	124	47	59	17	69	25	7.7	0.45	55	75
G880	301.5	36.66	0.23	6.83	2.95	2.65	0.37	10.68	15.25	1.88	2.32	0.12	5.76	21.11	22.51	99.80	0.27	73	12	9	29	281	31	1.2	0.74	27	37
G880	311.2	44.39	0.33	9.77	5.99	5.39	0.42	6.77	10.44	0.12	5.08	0.11	3.95	14.47	18.13	101.52	1.02	176	14	<3	20	9	29	5.1	1.22	37	59
G880	327.5	45.15	0.29	8.77	5.52	4.97	0.27	6.51	10.52	5.11	0.21	0.13	4.49	16.45	19.27	101.73	2.25	15	16	34	12	30	19	1.7	0.78	33	54
G880	339.0	42.61	0.23	6.88	7.12	6.41	0.37	6.91	11.24	3.87	0.31	0.11	4.75	17.40	22.30	101.95	3.79	20	175	57	18	3	19	2.7	1.00	42	59
G880	346.6	45.16	0.36	9.36	3.25	2.92	0.13	7.14	11.34	2.14	3.88	0.12	4.63	16.96	16.78	99.64	0.71	116	57	8	20	15	35	1.6	0.35	20	37
G880	357.5	49.26	0.35	11.32	3.73	3.36	0.27	8.82	8.12	2.81	2.94	0.11	2.98	10.92	12.76	100.49	0.26	140	2	<3	4	12	34	<1	1.01	23	41
G880	369.6	44.86	0.29	8.90	3.17	2.85	0.98	8.97	11.59	1.54	2.32	0.12	4.52	16.56	17.88	100.64	0.11	91	3	<3	9	8	77	<1	2.57	41	59
G880	375.1	49.68	0.35	10.50	4.27	3.84	0.19	7.23	8.55	0.64	3.29	0.12	3.74	13.70	15.72	100.53	0.19	145	<1.5	14	19	19	72	<1	0.68	24	44

Geochemical data from DDH F681 samples

DDH	depth	SiO2	TiO2	Al2O3	Fe2O3	FeO	MnO	MgO	CaO	Na2O	K2O	P2O5	Ctotal	CO2 total	loss	Total	S	Rb	Pb	As	Zn	Cu	Sr	Tl	MnOd	Al3	SedexAl
	m	wt%	wt%	wt%	wt%	wt%	wt%	wt%	wt%	wt%	wt%	wt%	wt%	wt%	wt%	wt%	wt%	ppm	ppm	ppm	ppm	ppm	ppm	ppm			
F681	811.0	50.37	0.41	10.17	3.08	2.77	0.09	6.17	14.03	0.67	3.41	0.14	3.06	11.21	11.59	100.13	0.40	141	9	<3	18	35	80	<1	0.20	18	37
F681	827.0	46.91	0.40	10.28	3.39	3.05	0.10	5.97	15.55	0.56	3.90	0.14	3.44	12.60	12.94	100.14	0.47	175	9	<3	22	17	64	<1	0.20	20	40
F681	861.0	40.65	0.29	7.82	4.14	3.73	0.12	9.91	12.73	0.13	2.75	0.14	5.31	19.46	20.43	99.11	1.08	95	5	32	18	160	50	1.1	0.29	22	33
F681	878.0	74.70	0.37	11.95	2.17	1.95	0.01	1.63	0.33	1.25	3.40	0.19	2.34	8.57	4.34	100.34	0.21	142	32	<3	61	11	25	<1	0.92	13	56
F681	903.0	50.78	0.39	12.18	3.92	3.53	0.29	8.25	6.96	1.96	3.76	0.11	2.70	9.89	11.43	100.03	0.36	167	<1.5	<3	14	2	35	3.2	1.27	24	44
F681	940.5	41.38	0.23	6.20	2.14	1.93	0.07	8.77	17.08	0.24	3.19	0.11	5.38	19.71	20.46	99.88	0.37	103	19	<3	18	11	108	1.2	0.12	15	23
F681	968.0	39.30	0.23	6.29	2.19	1.97	0.06	8.53	18.92	0.41	2.21	0.12	5.62	20.59	21.66	99.93	0.33	109	65	<3	48	10	146	<1	0.10	15	23
F681	990.0	39.29	0.28	7.63	2.36	2.12	0.05	7.67	18.66	0.35	2.93	0.13	5.78	21.18	20.55	99.91	0.53	121	20	5	147	11	121	1.3	0.08	15	25
F681	1034.0	36.55	0.20	5.78	2.16	1.94	0.12	12.13	15.77	0.13	3.19	0.10	6.30	23.08	23.83	99.97	0.28	95	15	<3	28	<2	58	2.7	0.23	15	21
F681	1060.0	43.85	0.29	8.42	9.74	8.76	0.16	6.07	8.48	0.06	4.33	0.10	3.46	12.68	20.27	101.74	5.87	133	47	96	15	39	33	9.9	0.57	42	63
F681	1086.0	42.51	0.28	7.76	5.61	5.05	0.21	8.65	11.41	0.08	3.60	0.10	4.69	17.18	20.91	101.10	2.40	121	65	40	26	16	37	8.7	0.56	30	45
F681	1190.0	46.89	0.30	8.89	6.28	5.65	0.32	6.25	9.85	0.13	4.75	0.12	4.26	15.61	14.84	98.64	1.75	155	54	6	137	13	32	16.6	0.99	37	59
F681	1200.0	29.33	0.18	4.90	11.55	10.39	0.87	8.64	16.01	0.08	2.25	0.13	6.44	23.60	27.91	101.83	2.78	80	34	17	57	28	36	4.7	1.65	59	69
F681	1237.0	48.21	0.36	10.96	4.20	3.78	0.11	6.69	9.18	0.11	5.55	0.12	3.77	13.81	14.96	100.45	0.96	188	24	10	21	19	23	5.8	0.36	22	42
F681	1270.0	36.50	0.23	7.73	2.93	2.64	0.22	9.63	15.10	2.81	2.43	0.10	6.00	21.98	22.10	99.80	0.38	48	3	23	4	<2	30	1	0.44	22	33
F681	1309.0	73.50	0.38	12.64	1.91	1.72	0.01	1.52	0.29	0.20	4.39	0.18	2.62	9.60	4.95	99.97	0.28	160	10	<3	12	15	13	<1	1.05	11	54
F681	1330.0	45.20	0.31	9.18	3.75	3.37	0.78	8.92	11.53	1.20	3.03	0.13	3.87	14.18	15.76	99.79	0.21	144	<1.5	<3	25	<2	77	1.7	2.06	38	56
F681	1355.0	36.56	0.20	5.79	2.92	2.63	0.13	10.17	16.61	0.41	2.86	0.10	6.42	23.52	24.22	99.97	0.34	74	8	7	18	10	63	1.5	0.24	20	28
F681	1386.0	38.35	0.26	7.39	2.31	2.08	0.07	9.25	16.33	0.65	2.49	0.12	6.00	21.98	22.67	99.89	0.33	96	4	5	19	11	88	1.7	0.13	14	23
F681	1426.0	30.92	0.11	2.73	1.16	1.04	0.06	4.84	29.96	0.11	1.74	0.12	7.61	27.88	27.91	99.66	0.17	57	31	5	203	6	296	2.5	0.06	18	25

simple assumption that Fe is present in only common sulfide minerals and carbonates. Hence, once Fe in sulfides is accounted for the remaining Fe can be assigned to carbonate. It is then quite simple to determine if ferroan dolomite, ankerite or siderite is present without recourse to XRD or microprobe analysis (Large, this volume CHECK THIS). Unfortunately, the common occurrence of ferroan silicate minerals (e.g. biotite, phlogopite, chlorite and tremolite–actinolite) in the Mt Novit metasediments, precludes using whole geochemical data to gauge Fe content of carbonates in the Mt Novit samples. For the purpose of discussion and plotting samples with less than about 1wt% CaO are assumed to be 'shales', or have a shaley (argillaceous) precursor lithology; other samples are carbonate-bearing.

Zinc, SedexAl, Al_3 and MnO_d cross-plots

Figure 8 displays crossplots showing Zn, Al and (for 'dolomitic' samples) MnO_d for the Mt Novit and SA10 samples. None of the SA10 samples have anomalous Zn or AI_3 values, and only three SA10 samples have enough dolomite for meaningful MnO_d calculations, but none are anomalous. About a dozen of the Mt Novit samples have anomalous AI_3 and MnO_d values with one sample from F681 plotting in the "Prospectivity 2" box of the AI_3 MnO_d plot.

Down-hole plots

Figures 9–11 show the variation in Zn, SedexAI, AI3, MnOd (for 'dolomitic' samples, and Tl with distance down-hole, for the three Mt Novit holes. The median values for the SA10 samples are plotted to give an indication of 'background' values for the Moondarra Siltstone. Samples from D496 have inconclusive down-hole patterns, with anomalous Zn and Tl in samples up to 50 m into the hanging wall of the mineralisation. Two high MnOd values bracket the mineralisation. Drill-hole F681 has a stronger response, with a combination of high AI3, MnO_d and Tl for about 100 m into the hanging wall and 30 m into the footwall. Zinc values are elevated in two samples from just below the mineralisation. The hanging wall response in G880 is poor for all parameters, while the pyritic interval correlating to mineralisation in the other holes has a few samples with anomalous AI3, MnO_d and Tl in several samples. The Zn levels are uniformly low, except for a couple of samples well into the hang wall.

Comparison with the Mine Sequence at Mount Isa

Figures 12 and 13 display the data from the 7402 cross-cut from underground at Isa Mine. These samples are barren interore beds from a 250 m interval of Urquhart Shale containing Zn–Pb–Ag orebodies numbers 5 to 14/30. These results have been discussed previously by (McGoldrick, 1994). The Mt Isa samples come from a similar stratigraphic thickness to the Mt Novit samples, but with fewer samples. It is clear from Figures 12 and 13 that the Isa Mine samples are anomalous in all the vector parameters discussed here, and patterns are markedly different to those observed from the Mt Novit samples.

Discussion

Taken in isoloation the Mt Novit data are mildly encouraging, as they show similar, but weaker, patterns to the large northern Australian deposits documented previously (various reports, AMIRA P384). This suggests that the vector parameters survive amphibolite-grade metamorphism and that the sampling protocol used in lower grade sequences can be used in higher grade terrains. The levels and spatial distribution of vector parameters most closely resemble those from Walford Creek (McGoldrick, 1995a). The size of the Mt Novit pyritic mineralisation, and contained base metal resource are probably quite similar to Walford Creek, and, although the textural and fluid inclusion evidence used by (Rohrlach et al., 1996) to support a syn-diagentic origin for Walford Creek is unlikely to survive the metamorphism experienced by Mt Novit, it is possible to speculate that Mt Novit has a similar origin to Walford Creek.

In comparison to the strong response from the barren inter ore sediments from Mt Isa, the Mt Novit vector geochemical signature is subdued, and is considered good empirical evidence that a Mt Isa size Zn–Pb–Ag resource is unlikely to exists proximal to the Mt Novit pyrite mineralization.

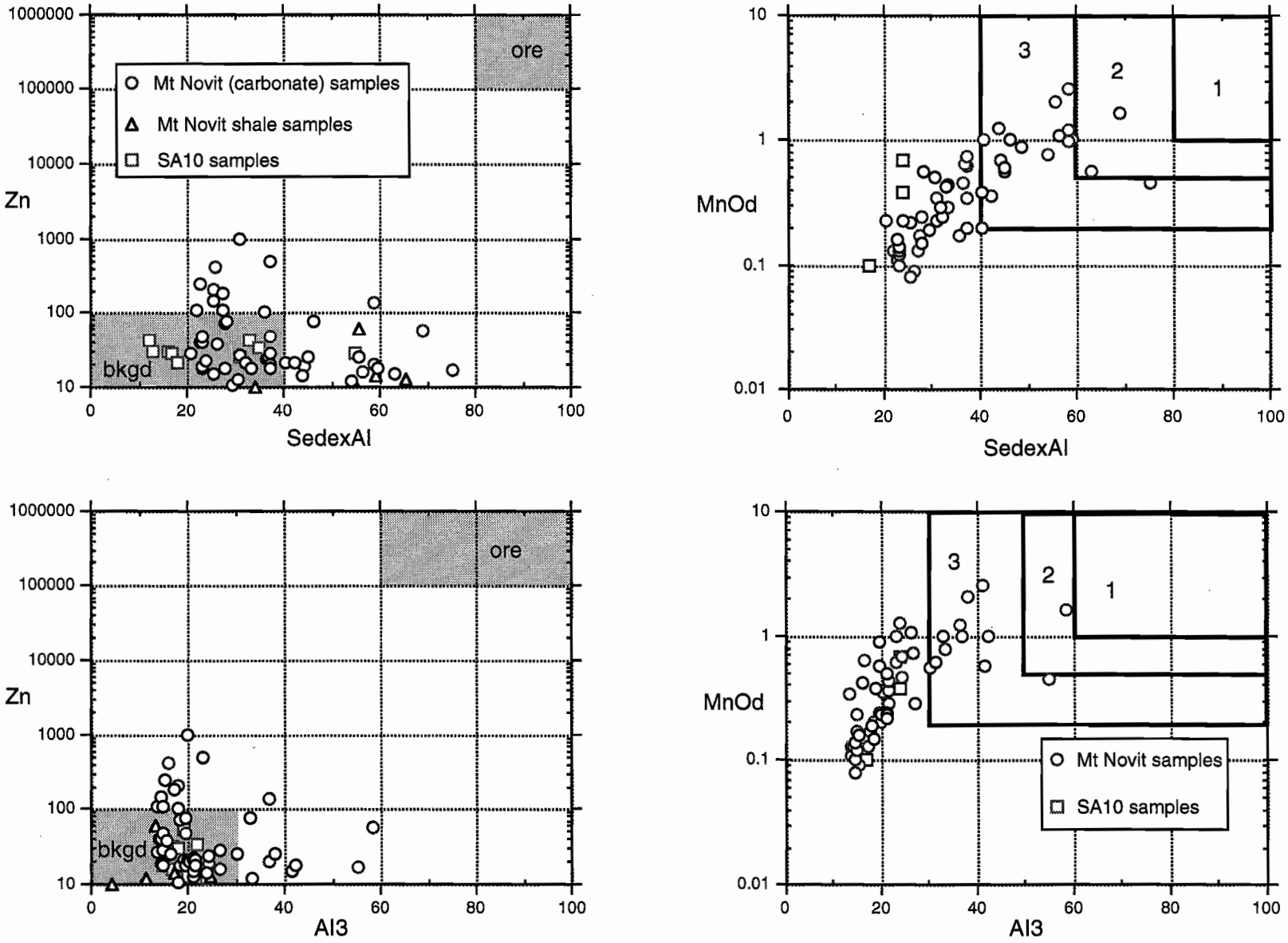

Figure 8 Zinc, SedexAI, AI3 and MnOd relationships for Mt Novit and SA10 samples (note: low carbonate samples have been excluded from MnOd plots)

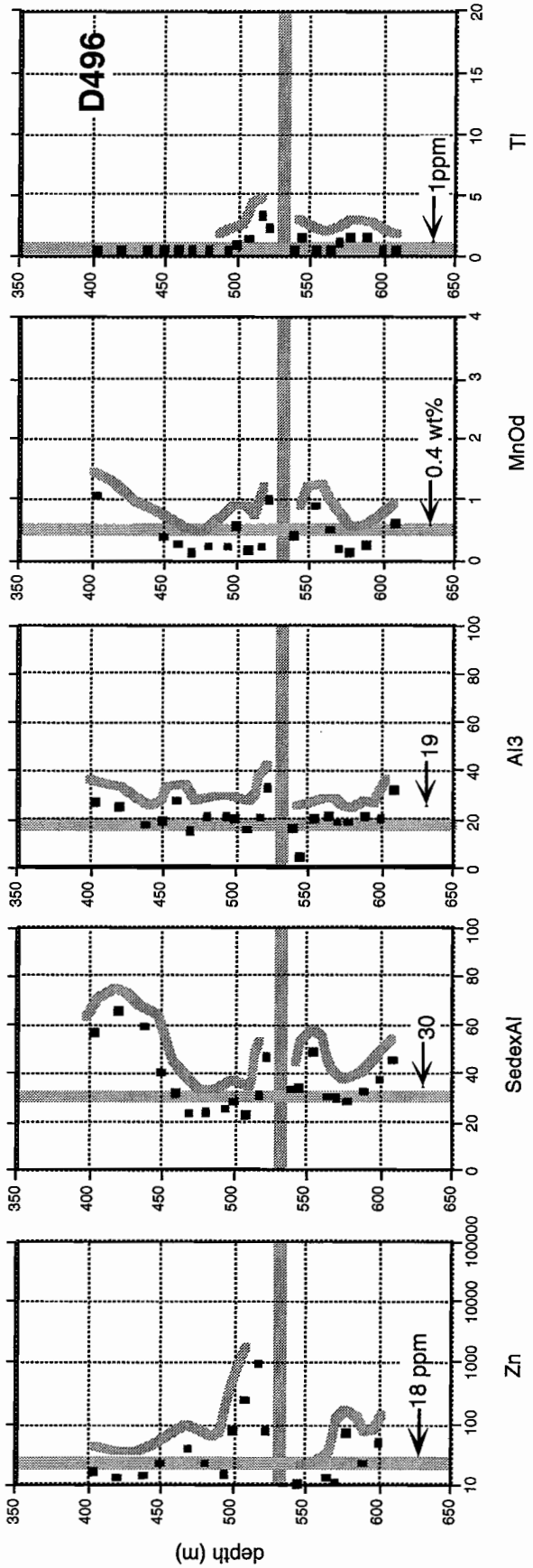

Figure 9 Down-hole variation in Zn, SedexAl, Al3, MnOd and Tl for DDH D496

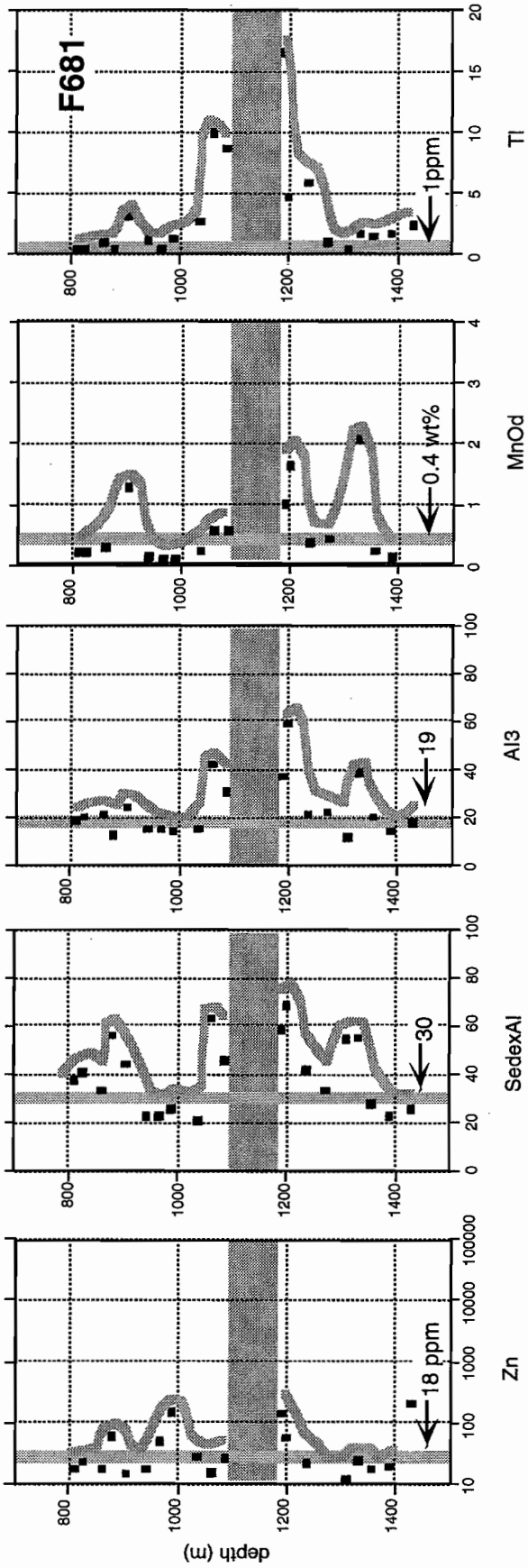

Figure 10 Down-hole variation in Zn, SedexAI, AI3, MnOd and Tl for DDH F681

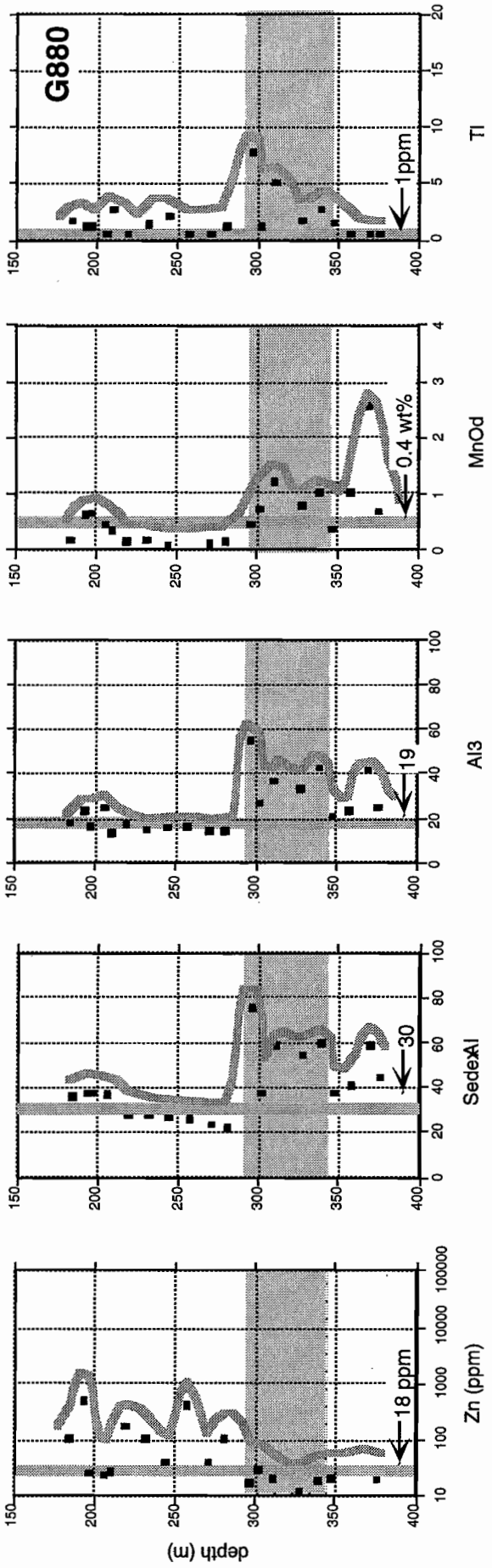

Figure 11 Down-hole variation in Zn, SedexAl, Al3, MnOd and Tl for DDH G880

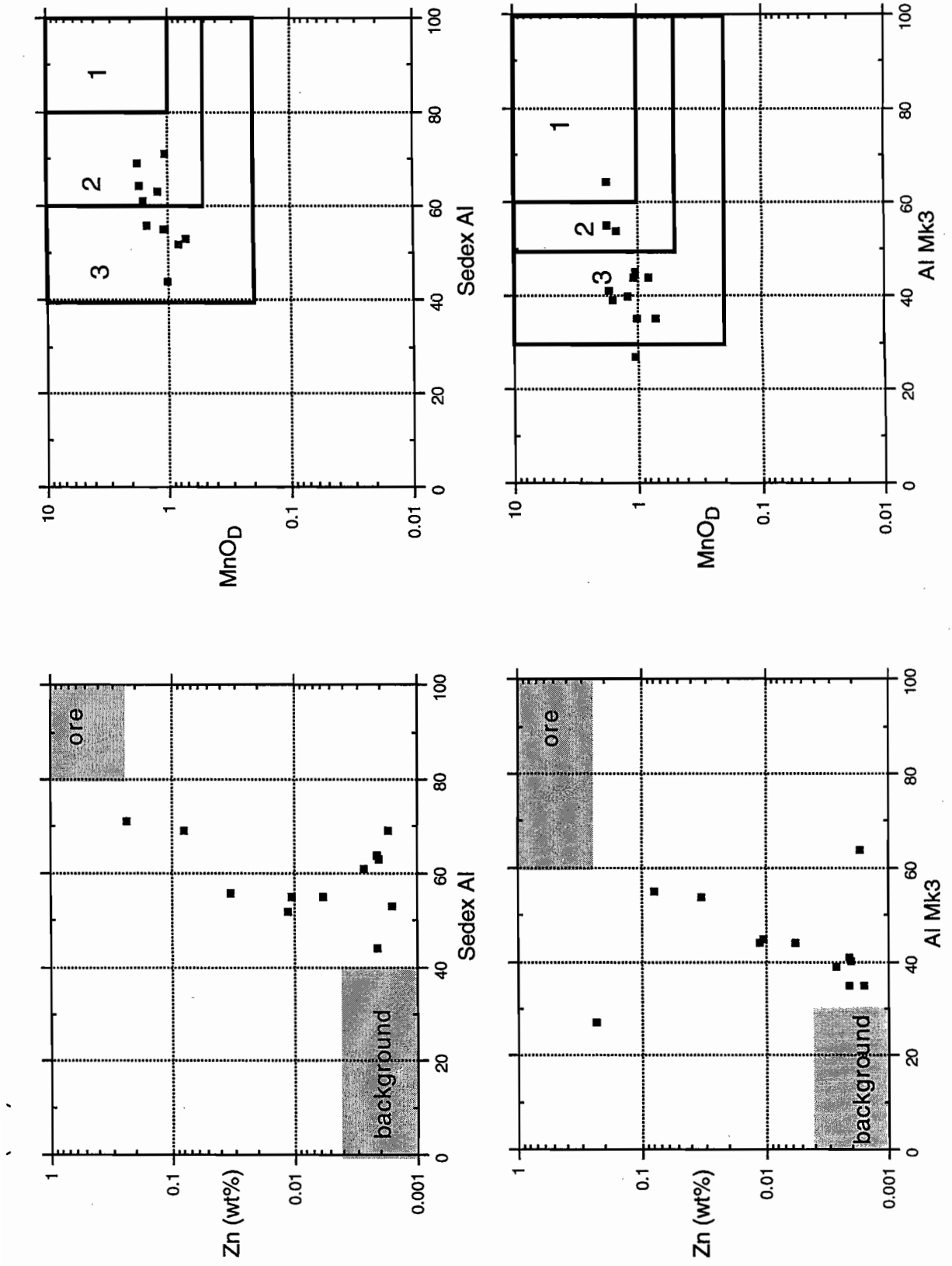

Figure 12 Zinc, SedexAI, AI3 and MnOd relationships for unmineralised siltstone samples from the 7402 cross-cut (5 to 14/30 Zn-Pb-Ag orebody sequence) at Mt Isa mine

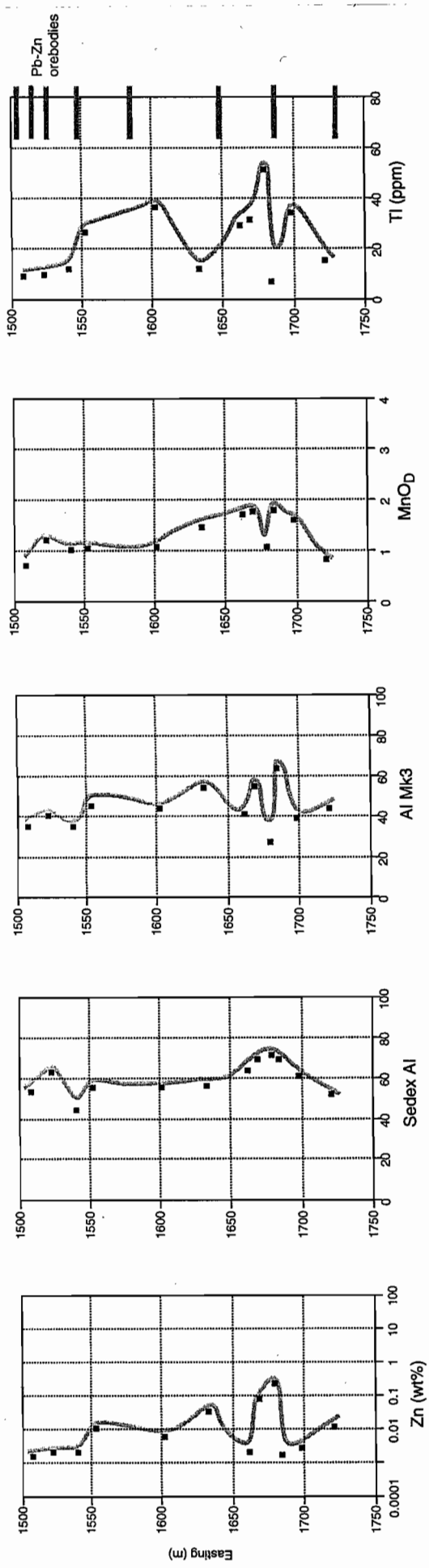

Figure 13 Stratigraphic variation in Zn, SedexAl, Al3, MnOd and Tl for unmineralised siltstone samples from the 7402 cross-cut (5 to 14/30 Zn-Pb-Ag orebody sequence) at Mt Isa mine

Summary and Conclusions

Three drill holes through the Mt Novit mineralisation, and a drill hole through unmineralised Moondarra Siltstone have been sampled for whole rock geochemical analysis.

Major and trace element data, and several vector parameters from seventy one samples have been presented on tables and as a series of standard plots, and results compared to a data set from the Mt Isa mine sequence.

The Mount Novit data indicate that the parameters useful for vectoring deposits hosted in low metamorphic grade sedimentary can be used in higher grade rocks.

The vector geochemical response at Mt Novit is subdued and resembles the response from similar sized (subeconomic) base metal mineralised pyrite lenses at Walford Creek.

It is unlikely that significant Zn–Pb–Ag mineralisation occurs proximal to the Mt Novit pyrite mineralisation.

References

Large, R.R. and McGoldrick, P.J., 1993. Deposit Halos 5. Primary geochemical halos related to Proterozoic sediment hosted Pb–Zn deposits and applications to exploration: CODES AMIRA/ARC Project P384 — Proterozoic sediment-hosted base metal deposits. Report No. 3: 63–126.

Large, R.R. and McGoldrick, P.J., 1994. Refinement of the Sedex Alteration Index and MnOD vectors: CODES AMIRA/ARC Project P384 — Proterozoic sediment-hosted base metal deposits. Report No. 5: 1–17.

Mathias, B.V. and Clark, G.J., 1975. The Mount Isa copper and silver–lead–zinc orebodies - Isa and Hilton mines. In Knight, C.L. (Ed.): *ECONOMIC GEOLOGY OF AUSTRALIA AND PAPUA NEW GUINEA*. Australasian Institute of Mining and Metallurgy: 351–371.

McGoldrick, P.J., 1994. Application of the Alteration Index and MnOD to the Mount Isa and Hilton zinc–lead–silver deposits: CODES AMIRA/ARC Project P384 — Proterozoic sediment-hosted base metal deposits Report No. 7: 115–140.

McGoldrick, P.J., 1995b. The Alteration Index and MnOD at Kamarga (re-visited): new geochemical data: , AMIRA, p. 319–332.

McGoldrick, P.J., 1995a. Geochemical vectors to stratiform sediment-hosted base metal deposits at the Walford Creek prospect, northwestern Queensland: , AMIRA: 303–318.

Ransom, P.W., 1991, 1990. Drilling in the Mount Novit and Cluny Area, Carpentaria Exploration Company Pty Ltd, Technical Report

Rohrlach, B., Fu, M. and Clarke, J., 1996. The geology and paragenesis of the Walford Creeek Zn–Pb–Cu–Ag prospect: MIC '96: 99–103.

Russell, R.E., 1978. Mt Novit prospect, Mt Isa: 3rd Australian Geological Convention Abstracts: 31.

Russell and Cox, 1973. Geological Map of the Mount Isa District 1:50,000, 2nd edn.